Changes in connectivity, structure and function following damage to the primary visual cortex

Dr Sara Ajina

Senior Scholar, Hertford College

Thesis for the degree of
Doctor of Philosophy (D.Phil.)

University of Oxford

Hilary Term, 2015

Abstract

Changes in connectivity, structure and function following damage to the primary visual cortex

Thesis for the degree: Doctor of Philosophy (D.Phil.)

Dr Sara Ajina
Hertford College
Hilary Term, 2015

Residual vision, or blindsight, following damage to the primary visual cortex was first identified almost a century ago. However, the mechanism and pathways underlying this ability, as well as the extent of visual function, remain unclear and are a continuing source of speculation. The work presented here goes some way to try to address these questions, investigating 18 patients with V1 damage and homonymous visual field loss acquired in adulthood. Six experimental chapters explore the extent and potential for visual function after V1 damage, and apply novel neuroimaging paradigms and techniques to try to uncover the mechanisms and pathways that might be involved.

A combination of psychophysics, functional and structural MRI was used to investigate responses to blind field stimulation in the dorsal and ventral streams. In addition, diffusion MRI tractography was performed and related to psychophysical performance, so that the three main pathways implicated in blindsight could be evaluated. Lastly, a small rehabilitation study was carried out to assess the effect of training in the blind hemifield, and to investigate whether there is any transfer of learning between the dorsal and ventral visual streams.

The results from this work reinforce the suggestion that blindsight may be more common than was first thought, and may extend across a number of characteristics involving both visual streams. It is also suggested that visual function need not be completely unconscious, but that certain salient stimuli can elicit both non-visual and crude visual experience. The use of parametric functional imaging paradigms has enabled a number of properties of non-striate inputs to the extrastriate cortex to be revealed. Together with tractography, this points to an important role for the ipsilateral lateral geniculate nucleus in blindsight function. It is hoped that future work will build upon this, and that it may be possible to target these residual pathways in the rehabilitation of patients with V1 damage.

Contents

Acknowledgements

There are many people I would like to thank for their help in carrying out this work. In particular I am extremely grateful for the input, guidance and support from my supervisors Holly Bridge and Chris Kennard. It has been an absolute pleasure to work with them both, and I am certain that I could not have carried out this work in a better environment.

This work would also not have been possible with out the help of Alex Leff, Alidz Pambakian, Susie Mollan and Enrico Flossmann in sourcing patients. I am extremely grateful, and to all the patients who travelled many miles to take part in this research.

In the John Radcliffe Hospital, I would like to thank the Stroke and Optometry departments for also helping me to source patients and measure visual fields. I am especially grateful to Caroline Dodridge, Charles Cottriall, Patsy Terry, and Rachel Teal. I also want to thank our lead radiographer, Mike Sanders, for his on-going help, patience and good humour, and Stephen Hicks for helping to set up the eye-tracker for my psychophysics experiments.

I have been extremely fortunate to be involved in two very exciting collaborations, which I hope to continue. I would like to thank Arash Sahraie for providing me with his visual field training protocol and equipment to undertake my rehabilitation study, and for his thoughtful and beneficial comments on my work. I am also hugely grateful to Brian Wandell and the Vista lab, who looked after me during my visit to Stanford and assisted me with DTI pre-processing and analysis. Special thanks to Franco Pestilli, who was always eager to help me – even when he was getting married the next day!

Lastly I want to thank Geraint Rees for his continuing support and encouragement, both in science and writing papers, and on my gradual progress towards an academic career. Thank you for inspiring me to pursue this route of study.

Abbreviations

2-AFC	Two-alternate forced choice questioning
AC-PC	Anterior commissure – posterior commissure
ANOVA	Analysis of variance
BET	Brain extraction tool
BOLD	Blood-oxygenation-level-dependent
C_{50}	Neurophysiological response reaches half their maximum
CaMK2	Calcium/calmodulin-dependent protein kinase II
C_{DT}	Contrast detection threshold
Contra	Contralateral
COPE	Contrast of parameter estimate
CSD	Constrained spherical deconvolution
df	Degrees of freedom
DTI	Diffusion tensor imaging
EEG	Electroencephalography
EPI	Echo-planar imaging
ERP	Event-related potential
FA	Fractional anisotropy
FFA	Fusiform face area
FLIRT	FMRIB's linear registration tool
fMRI	Functional MRI
FMRIB	Oxford centre for functional MRI of the brain
FNIRT	FMRIB's non-linear registration tool
FSL	FMRIB's software library, www.fmrib.ox.ac.uk/fsl
FST	Fundus of the superior temporal area

FWHM	Full width at half maximum
GLM	General linear model
HVFD	Homonymous visual field deficit
hMT+	Human equivalent of motion areas MT and MST
HRF	Haemodynamic response function
Ipsi	Ipsilateral
K-channel	Koniocellular channel
LGN	Lateral geniculate nucleus
LHF	Left hemifield
LOC	Lateral occipital cortex
LUQ	Left upper quadrant
M-channel	Magnocellular channel
MD	Mean diffusivity
MEG	Magnetoencephalography
MNI	Montreal Neurological institute
MPRAGE	Magnetization-prepared rapid acquisition with gradient echo
MST	Medial superior temporal area
MT	Middle temporal area
NHS	National health service
NifTI	Neuroimaging Informatics Technology Initiative
OFA	Occipital face area
OFG	Occipital fusiform gyrus
P-channel	Parvocellular channel
PPA	Parahippocampal place area
PPV	Positive predictive value
RHF	Right hemifield

ROI	Region of interest
RUQ	Right upper quadrant
S-cones	Short-wavelength sensitive cones
SC	Superior colliculus
SNR	Signal-to-noise ratio
SPM	Statistical parametric mapping software
TE	Echo time
TMS	Transcranial magnetic stimulation
TR	Repetition time
V1	Primary visual cortex (striate cortex)
VISTALab	Stanford Vision and Imaging Science and Technology software
VRT	Visual field restitution therapy

Chapter 1

General Introduction

1.1 Structure of the visual system, and patterns of homonymous visual field loss

The principal visual pathway connecting the retina to the primary visual cortex (V1) is the retino-geniculo-striate pathway. Approximately 90% of all retinal ganglion cells project to the lateral geniculate nucleus, with a similar proportion of geniculate axons reaching V1 – thus accounting for its description as the primary visual centre in the brain (Perry et al., 1984; Hubel and Wiesel, 1968; 1972).

The representation of the visual field in the retina retains its topography as it is mapped onto the cerebral cortex. It is therefore useful to consider it as composed of four segments: nasal and temporal, and upper and lower (Zeki, 1993). The nasal retina views the temporal field, and the temporal retina views the nasal field. Therefore each hemifield represents a combination of visual signals from the nasal retina in one eye and the temporal retina in the other.

The most sensitive portion of the retina, the fovea, spans the central 1 degree of the visual field. This corresponds to the fixation point of the eye, from which the position of peripheral stimuli are described. This is different from the macula, which covers the central 5 degrees of the visual field and corresponds to the occipital pole. This region is somewhat unique as it is served by a dual blood supply from the posterior and middle cerebral arteries. In situations of vascular damage, the occipital pole is often spared, leading to a pattern of macular sparing in which the central few degrees of vision remain intact.

1.1.1 Optic tract and lateral geniculate nucleus

Impulses leave the retina via the optic nerve, whose fibres demonstrate a high degree of spatial organisation. These reach the optic chiasm, located in the midline of the brain just superior to the pituitary stalk (see Figure 1). It is at this point that axons from the nasal portion of the retina decussate to the opposite hemisphere. This pattern of selective crossing ensures that beyond this point in the visual pathway, retinal information refers only to the contralateral visual hemifield.

Beyond the optic chiasm, axons connect via the optic tract to the lateral geniculate nucleus (LGN), a subdivision of the subcortical thalamus. Because of the crossed fibres, selective damage to this region results in a homonymous hemianopia (Figure 1A). ‘Homonymous’ refers to the fact that the same portion of visual field is affected in both eyes. The most frequent cause of damage here includes vascular aneurysms, craniopharyngiomas, and pituitary tumours, with visual field loss partial or complete, depending upon the extent of damage.

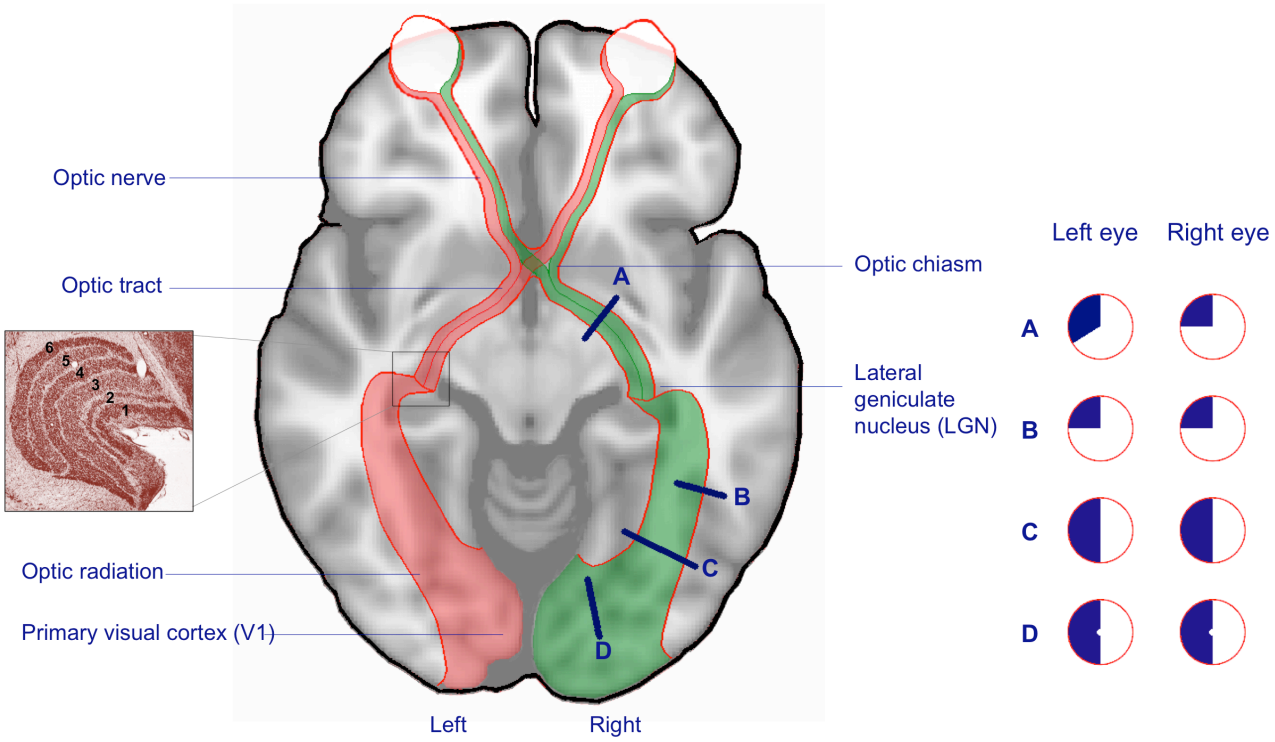

Figure 1. The primary visual pathway and patterns of field loss. An illustration of the connections from the retina to the cerebral cortex, transmitting the left visual hemifield in green, and right hemifield in red. The inset to the left shows the multi-layered lateral geniculate nucleus (LGN). Lesion locations and their corresponding visual field deficits are shown on the right. A: optic tract lesions result in incongruous hemianopic defects; B, C: lesions of the optic radiation result in either homonymous quadrantanopia or hemianopia depending on the extent and location of the lesion (upper quadrant, temporal lobe; lower quadrant, parietal lobe); D: lesions of the striate cortex produce a homonymous hemianopia, sometimes with macular sparing, particularly with vascular disturbances.

The LGN receives retinal input from the contralateral visual hemifield in both eyes, and is also highly organised. Inputs from each eye remain segregated according to its laminar structure. Fibres from the ipsilateral eye terminate in layers 2, 3, and 5 whilst those from the contralateral eye terminate in layers 1, 4, and 6 (see Figure 1). The LGN also demonstrates a functional subdivision of neuronal cell types. Its upper four layers contain neurons with small cell bodies termed parvocellular (P) neurons, whilst the lower two layers have much larger cell bodies, termed magnocellular (M). In between are so-called interlaminar zones, which are suggested to contain a high

proportion of koniocellular (K) neurons, equivalent in number to M-neurons in the lower layers (Hendry and Yoshioka, 1994).

1.1.2 Optic radiation

Geniculate cell axons travel via the optic radiation to the visual cortex, with the majority of neurons terminating in V1. As geniculo-striate fibres leave the LGN, ventral fibres subserving the superior visual field pass anteriorly around the temporal horn of the lateral ventricle to form Meyer's loop. Lesions here usually result in congruous, wedge-shaped homonymous field deficits, mostly affecting the superior quadrant as they pass through the temporal lobe (Figure 1B). Less frequently, larger lesions can result in a complete homonymous hemianopia with macular splitting (Figure 1C). Damage is most frequently caused by vascular occlusion, tumour, or abscess. This region is also particularly susceptible to axonal injury during anterior temporal lobe resection for intractable epilepsy, causing post-operative visual field loss in 15% of cases (Powell et al., 2005).

In the parietal lobe, damage to the optic radiation tends to elicit a predominantly lower visual field loss. This may be associated with visual inattention or neglect if it restricted to the right hemisphere. In visual neglect, a stimulus in the contralateral visual field may be perceived normally, but if an identical object is presented simultaneously in the ipsilateral visual field, the image in the contralateral field may appear to disappear.

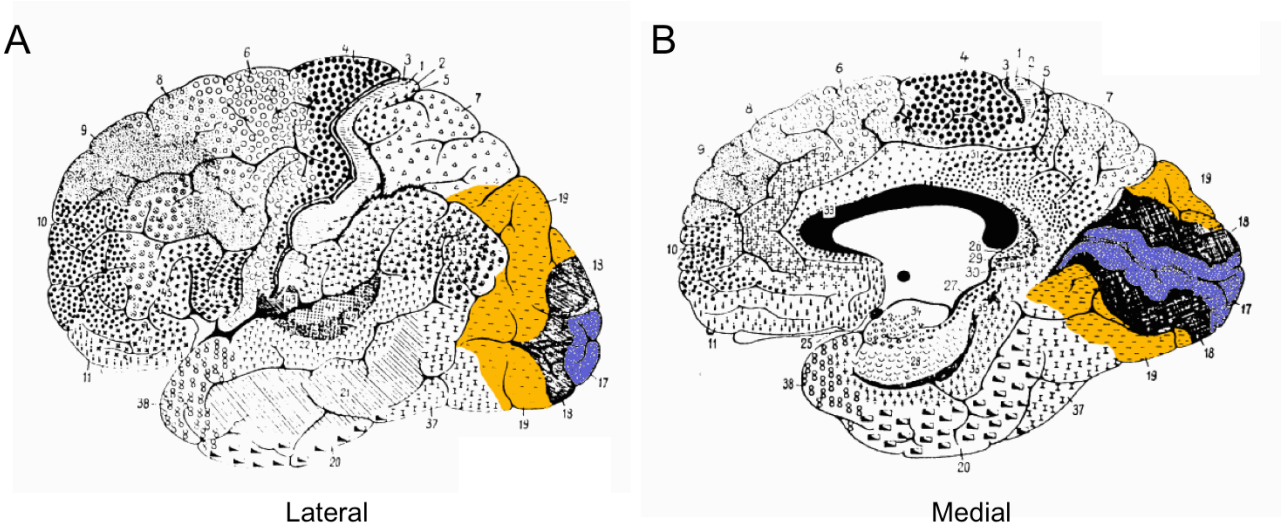

Figure 2. Brodmann's areas, highlighting the visual cortices. Brodmann originally defined and numbered these regions of the brain according to their cytoarchitectural organization using Nissl staining. These were numbered according to the sequence in which they were studied. Brodmann area 17, in blue, corresponds to the primary visual cortex (V1). Areas 18 (black hatched) and 19 (yellow) correspond to the extrastriate cortex or visual association areas. Brodmann's area 18 shows a vague correspondence with visual area V2, although this is not a clear association (Dougherty et al., 2003). Area 19 is reputed to contain regions of the visual areas consistent with V3, V4, V5/hMT+, and V6.

1.1.3 Occipital lobe

The primary visual cortex, corresponding to Brodmann's area 17, is the major recipient of geniculate input from the same hemisphere (Figure 2). Much of this region is located within a medial sulcus in the occipital lobe, known as the calcarine sulcus. It is also possible to identify V1 by its characteristic myelination pattern. The Stria of Gennari is visible under light microscope, and accounts for its alternate title of striate cortex (Gennari, 1782). Inputs here possess a high degree of order and segregation, with P-channel projections largely terminating in layer 4Cβ, and 4Cα for the M-channel. Numerically, V1 neurons receive considerably greater input from relay neurons of the P-variety (Peters et al., 1994). It is also suggested that K-channel projections specifically target the colour-sensitive cytochrome oxidase rich blobs of V1 (Livingstone and Hubel, 1982; Fitzpatrick et al., 1983).

Occipital lesions tend to be caused by infarction, trauma, or tumour, and produce homonymous congruent field defects. The principal features of deficits here, which help distinguish them from the anterior optic radiation, are the presence of macular sparing and the greater likelihood that they will be complete – see Figure 1D**.** This pattern, however, depends very much on the size and pattern of cortical damage. In the striate cortex, the superior bank of the calcarine represents the lower half of the visual field, whilst the inferior bank represents the upper visual field. In most cases, however, where damage is ischaemic, the hemianopic field is split along the vertical meridian through the fixation point (macular splitting).

Extrastriate, or 'visual association areas' in the occipital lobe receive a dominant input from V1, but are also known to receive direct subcortical input as well as extensive intrinsic connections (Benevento and Yoshida, 1981; Adams et al., 2000). These regions include areas V2 – V6, and tend to support more complex processing in the visual hierarchy. In particular, visual information is believed to follow two streams from V1, one is more ventral and involved in perceptual representation, 'what', and the other dorsal stream is involved in the visuomotor control of action (Goodale and Milner, 1992), with interaction between the two. The ventral stream consists of projections from V1 to the inferotemporal cortex via a number of routes involving areas V2, ventral portion of V3, V4 and TEO in the temporal lobe (Ungerleider and Mishkin, 1982). In particular, there appears to be progressively detailed coding of visual features moving from V1 up through the hierarchy (Milner and Goodale, 1995). Increased specificity is even more pronounced in the inferotemporal cortex, where neurons demonstrate selectivity for specific figural stimulus properties (Gross, 1992). There are even examples of ventral cortical areas

involved in category-specific processing related to specific shapes and forms such as faces or objects (Kanwisher et al., 1997; Epstein and Kanwisher, 1998).

In comparison, the dorsal stream includes connections from V1 to higher-level visual areas in the posterior parietal cortex via a number of routes. These include projections to the motion area, MT, and subsequently MST (the combination of which equates to hMT+ in humans) and FST. Additional inputs are also likely to come from V2 and V3, as well as from the opposite hemisphere to MST where neuronal receptive fields cross the vertical meridian to span the ipsilateral field (Tanaka et al., 1986; Huk et al., 2002). The magnocellular channel normally dominates motion area MT responses, where it contributes to a number of characteristic responses (Maunsell et al., 1990). Both ventral and dorsal regions also receive direct geniculate (Fries, 1981; Cowey and Stoerig, 1989; Schmid et al., 2010) and extrageniculate subcortical inputs from the superior colliculus via the medial pulvinar (Benevento and Davis, 1977; Benevento and Standage, 1983; Adams et al., 2000), although the roles of such alternative pathways remain less clearly understood.

1.2 Natural history of homonymous visual field loss

It is widely recognised that stroke is the most frequent cause of homonymous visual field deficits, with an estimation that between 40-86% of isolated cases are caused by posterior circulation ischaemia (Smith 1962; Fujino 1986; Trobe 1973; Zhang 2006a). Other common aetiologies include traumatic brain injury, tumour (each <15%), and

less frequently brain surgery and demyelination (Zhang et al., 2006a), with causative lesions most commonly in the occipital lobes (45%) and optic radiations (32.2%).

In the UK alone there are approximately 150,000 new cases of stroke a year, with between 8-26% left with persistent hemianopia (Gilhotra et al. 2002; Gray et al. 1989), which may be closer to 30% acutely (Haerer, 1973). Figures vary quite extensively, however, with variable population demographics, measurement techniques, and reporting biases.

Stroke is also considered to be the most common cause of disability in adults (Hankey, 1999), and is likely to increase in the future with an aging population. Importantly, visual field loss in such patients is associated with an adverse functional prognosis, including likelihood of discharge home (Schlegel et al., 2003), decreased mobility and survival (Haerer, 1973; Gray et al., 1989). Functionally, it can impair day-to-day activities including driving, reading and obstacle avoidance, reduce participation in social activities and quality of life (Trauzettel-Klosinski, 2011). At the other end of the spectrum, visual field deficits often go unreported, perhaps overlooked or under-prioritised by clinicians, or because patients learn to compensate for their deficit (Zhang et al., 2006a; Gilhotra et al., 2002).

1.2.1 Early recovery

There has been some debate about how quickly recovery of visual field loss occurs after brain injury, with reports varying from two weeks (Gray et al., 1989) to one year (Trauzettel-Klosinski, 2005). Zhang et al. (2006b) reviewed the medical records of

254 consecutive patients with a range of aetiologies over 15-years, and performed a regression analysis to determine the probability of improvement (reduction in field loss of more than 10° horizontally or 15° vertically) as a function of time after injury. Although this was not prospective and follow-up varied between patients, they suggested that at one month there was a 50-60% chance of recovery, falling to around 20% at 6 months. They continued to see a similar improvement beyond 6 months, although changes were attributed to improvement in the underlying disease (such as demyelinating disease or tumour) or cognitive ability to undergo testing. No cases with stable brain disease such as stroke continued to improve beyond 6 months, with most improvement occurring within 3 months. These results are consistent with prospective stroke studies (Tiel and Kolmel 1991; Gray et al. 1989; Celebisoy et al., 2011), which also report that improvement tends to occur in peripheral zones, with the worst prognosis associated with striate cortex involvement and greater lesion size. Neuroimaging studies suggest that visual improvements over this period may be associated with a return in ipsilesional V1 activity, and perhaps even a restoration of tract integrity in the ipsilesional optic radiation (Raposo et al., 2011; Polonara et al., 2011). Whether a similar mechanism may underlie improvements in performance following rehabilitation in the chronic phase is unlikely, but remains relatively unexplored (Sahraie et al., 2008; Huxlin et al., 2009).

1.2.2 Residual function and spontaneous functional adaptation

In the chronic phase after injury, visual field loss appears to become more static, and it is this stage that is most difficult to treat. Numerous studies have suggested that

during this chronic phase, patients may adopt compensatory eye movement strategies to assist with their deficit (Pambakian et al., 2000; Zihl 1995). Whilst healthy controls fixate mostly on central targets, hemianopes paradoxically fixate longer on targets in the blind hemifield, shifting it into view (Ishiai et al., 1987). This has been shown in a number of different tasks such as viewing images of real scenes (Pambakian et al., 2000), and whilst assembling wooden models (Martin et al., 2007) – although in the latter this was not seen in every participant.

Hemianopic patients may also adopt strategies for refixating between targets (Meienberg et al., 1981), for example performing a number of increasing hypometric saccades (stairstep) before finding the target or overshooting by a few degrees together with a short, corrective saccade to foveate the target. These mechanisms, however, are not ideal as an increased number of refixations, together with somewhat disorganised scanning leads to longer search times and possible omission of relevant objects (Zihl 1995). More recent research suggests that which gaze strategies are employed vary according to lesion site, and as a function of task demand (Hardiess et al., 2010).

1.3 Blindsight

Blindsight refers to the observation that certain stimuli within the blind visual field of patients with V1 damage can undergo processing and influence behaviour despite the individual often being completely unaware of their presence (Weiskrantz et al., 1974). It suggests that even in the chronic phase, when standard perimetry demonstrates complete visual field loss, certain aspects of visual processing such as motion or contrast detection may be retained. This can be identified using a number

of different approaches, such as forced-choice questioning (Azzopardi and Cowey, 1997), saccadic eye movements (Barbur et al., 1988) or obstacle avoidance (Streimer et al., 2009).

The residual function associated with blindsight is classically defined as unconscious, however this is a source of some debate as awareness can vary between participants or in response to certain manipulations (see Weiskrantz 2004 for review). Another early criticism of blindsight research was that it could be attributed to surviving 'islands' of V1 (Fendrich et al., 1992), however there is now substantial evidence to the contrary (Stoerig et al., 1998). Indeed, stimuli with specific spatio-temporal properties appear to be particularly effective at eliciting blindsight, with this ability perhaps even present in the majority of patients with V1 damage (Sahraie et al., 2008).

Three main pathways have been suggested to underlie blindsight, with evidence in support of each (Figure 3). One involves subcortical projections from the retina to the superior colliculus and pulvinar, which then project to other visual cortical areas bypassing damaged V1 (Feinberg et al., 1978; Rodman et al., 1989; Kato et al., 2011). The second projects directly from surviving LGN neurons to the extrastriate cortex (Cowey and Stoerig, 1989; Schmid et al., 2010). A third pathway might represent a plasticity phenomenon, and involves connections between the extrastriate cortex in the damaged hemisphere and the opposite intact side. This includes direct connections between hMT+ bilaterally, or with subcortical structures in the intact hemisphere (Leh et al. 2006, Bridge et al., 2008; Silvanto et al., 2009). The question of whether blindsight reflects intact residual pathways or an ability of the human cortex

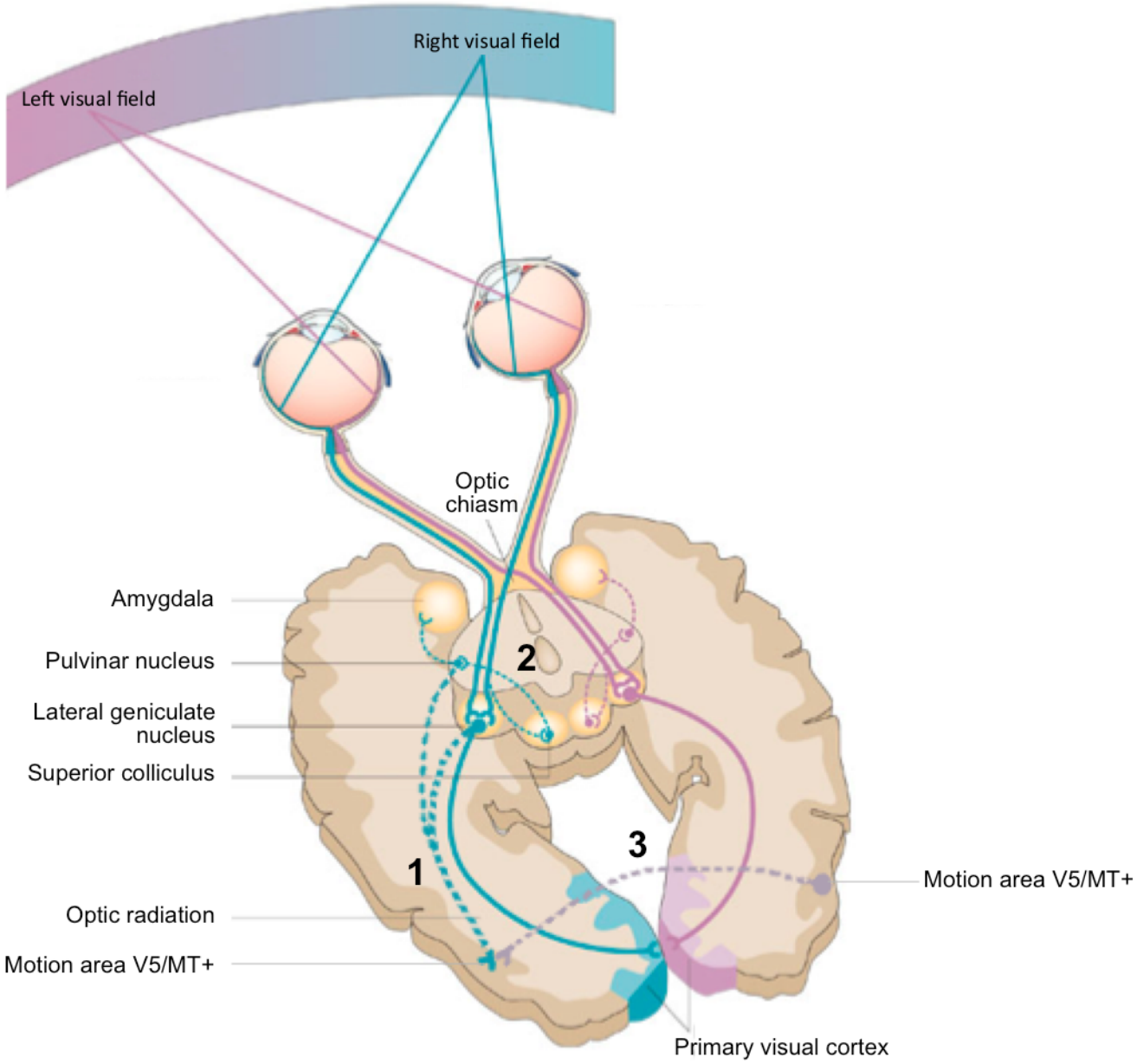

Figure 3. Alternate visual pathways, suggested to be involved in blindsight. A number of different structures and pathways are implicated in blindsight, or residual visual processing after V1 damage. This diagram illustrates the three main proposed routes, which will be assessed using diffusion MRI tractography in Chapter 7. **(1)** A direct connection between the lateral geniculate nucleus (LGN) and extrastriate cortex, hMT+. **(2)** A distinct subcortical pathway from the superior colliculus to the extrastriate cortex via the inferior pulvinar. **(3)** Interhemispheric connections from the undamaged hemisphere, connecting V5/hMT+ bilaterally via the corpus callosum.

to reorganise following injury remains unanswered, but has important implications for rehabilitation.

1.4 Neuroimaging of residual vision after V1 damage

Functional MRI (fMRI) in patients with hemianopia is important not only to further our understanding of blindsight, plasticity, and recovery after brain injury, but also to increase our understanding of the visual system. To date, fMRI and related imaging techniques have been used numerous times to investigate patients with V1 damage. Their results are arguably most consistent for high contrast motion in the blind hemifield, which can elicit significant activation in motion area hMT+ (Barbur et al., 1993; Holliday et al., 1997; Zeki and ffytche, 1998; Goebel et al., 2001; Schoenfeld et al., 2002; Morland et al., 2004). However, there are inconsistencies concerning which hemisphere is activated. Also, all of these studies have focused on the presence or absence of activity, rather than measuring responses to the parametric alteration of stimulus properties. This alternative technique is more challenging to undertake, but could help reveal the physiological characteristics of residual visual responses. In turn, this could help advance our understanding of non-striate visual pathways in blindsight.

Affective blindsight is the non-conscious recognition of emotional stimuli in the absence of primary visual cortex, and de Gelder and colleagues have made considerable advances in this field (e.g. de Gelder et al., 1999). In particular, neuroimaging has implicated the amygdala as playing an important role in visual

responses. It shows selective activation for emotional faces (Morris et al., 2001; Pegna et al., 2005), directed versus averted gaze (Burra et al., 2013), and even whole-body emotional actions (Van den Stock et al., 2011). The amygdala also demonstrates increased connectivity with the pulvinar and superior colliculus compared to healthy controls (Tamietto et al., 2012).

Despite certain limitations, diffusion-weighted MRI offers a unique method to explore non-invasively the organization of white matter in the living human brain. A small number of studies have employed this technique using probabilistic tractography after V1 damage, but have differed in their principal findings. Leh et al. (2006) suggested that blindsight patients show unique interhemispheric connections between the superior colliculus and visual, parietal, and prefrontal areas, which are not present in blindsight negative patients or healthy controls. Bridge et al. (2008) used similar techniques in a well-described blindsight patient, GY. They also found connections that were considerably stronger than in healthy controls. However, they involved the extrastriate cortex bilaterally, and contralesional LGN. Both studies should also be interpreted with the caveat that the original brain damage occurred early in life, when it is suggested that plasticity is more viable. In adult-onset cortical blindness, crossing connections appear to be less important (De Gelder et al., 2008). Ipsilateral geniculo-extrastriate pathways are instead implicated, and are also present in GY and healthy controls (Bridge et al., 2010, Bridge et al., 2008). There are many reasons why different pathways may be implicated in different studies, and more homogenous, group studies may prove particularly beneficial.

1.5 Synopsis and overview of experimental chapters

This series of six experimental chapters are designed to explore the extent and potential for visual function after V1 damage in adulthood, and to use novel neuroimaging techniques to try to uncover the mechanisms and pathways that may be involved. This will advance our understanding of the normal role of V1 and, in particular, the properties of non-striate inputs to the extrastriate cortex that cannot otherwise be measured. Ultimately, it is hoped that this will provide a more effective target for rehabilitation in patients with V1 damage.

Chapter 3. Abnormal contrast saturation in hMT+

Residual vision, or blindsight, following V1 damage is particularly robust for high contrast, moving stimuli. This is somewhat incongruous with our understanding of normal hMT+ sensitivity to contrast, where early saturation means that even low contrast levels elicit neural activation close to ceiling, attributed to a dominant input from the magnocellular layers of the LGN. The first experimental chapter seeks to investigate this discrepancy by measuring psychophysical and neural responses to increasing luminance contrast in patients with V1 damage with functional MRI. By comparing responses during blind field stimulation to hMT+ and V1 activity in the sighted field and a group of age-matched controls, this discrepancy should be directly addressed. Furthermore, by revealing the physiological properties of residual hMT+ it may be possible to speculate on the pathways underlying these responses, and how they may relate to behavioural performance.

Chapter 4. hMT+ response to global motion in the absence of V1 resembles early visual cortex

Motion area hMT+ shows a variety of characteristic visual responses, which are heavily influenced by its rich connectivity with V1. Of these, the response to global motion coherence is particularly well described. However, very little is known about alternative inputs to hMT+ and how they may drive and influence its activity. Using fMRI, this chapter investigates the response of hMT+ to increasing the proportion of coherent motion in patients with unilateral V1 damage and a group of healthy age-matched controls. The purpose is to reveal how hMT+ responds to global motion when the dominant input from V1 is silenced. Furthermore, the chapter will evaluate whether non-striate input may contribute to normal hMT+ activity in the intact visual system, thus having direct implication for current models of the visual cortex.

Chapter 5. The presence or absence of blindsight affects sensitivity of hMT+ to speed of motion

The response of hMT+ to increasing stimulus speed is also well described, and is often depicted as an inverted-U pattern. However, it remains unclear whether this reflects intrinsic properties of hMT+ neurons, or relates to the characteristics of pathways underlying these responses. One prevailing theory is that slow motion is mediated via V1, and should therefore not be possible when V1 is damaged. This chapter seeks to address this controversial theory by measuring behavioural performance and hMT+ response to increasing speed for the first time in patients with V1 damage. A relatively large group of patients are recruited so that fMRI

activity can be compared according to the presence or absence of blindsight function. This will advance our understanding of the mechanisms underlying hMT+ sensitivity to speed, and the importance of different pathways in residual function after V1 damage.

Chapter 6. Category-specific visual processing in the ventral stream

Ventral stream processing after V1 damage is a relatively neglected area of study. This is likely to reflect the fact that blindsight performance and neuroimaging responses for ventral stimuli are notoriously difficult to elicit. Despite this, research in non-human primates suggests that numerous non-striate pathways carry visual information to the ventral visual cortex. This chapter employs psychophysics and a prolonged fMRI design to explore category-specific processing for faces and places in a large group of patients with V1 damage. The purpose of the study is to determine whether category-specific ventral processing is possible after V1 damage, to consider how it may occur, and how common it might be.

Chapter 7. Diffusion MRI tractography: Connectivity of the extrastriate cortex underlying blindsight

Three main pathways are suggested to underlie blindsight, with evidence in support of each (see Figure 3). These include ipsilateral extrastriate connections to the LGN, connections with the superior colliculus and pulvinar, and interhemispheric connections that appear stronger than healthy controls. This chapter seeks to resolve this fundamental question by employing diffusion MRI tractography in a large group of patients with unilateral V1 damage sustained in adulthood. In particular, patients

are assessed for the presence or absence of blindsight function so that the existence, strength, and integrity of these three pathways can be compared in blindsight positive and negative patients, as well as healthy controls. This will help to establish whether a single pathway is common and specific to patients with blindsight, and will also address the prevailing question of whether blindsight may reflect a plasticity phenomenon.

Chapter 8. Visual field rehabilitation with motion stimuli transfers learning to the ventral stream

Rehabilitation strategies that target residual visual processing in the blind hemifield undergo criticism for several reasons, including a failure to adequately control eye movements, the non-transferability across stimulus properties, and the fact that blindsight is, by definition, an unconscious phenomenon. Recent work suggests, however, that these criticisms may no longer be valid. This final experimental chapter assesses the effect of three months of blindsight training on four patients with chronic V1 damage, using a motion stimulus with spatial and temporal properties that are particularly effective for blindsight. By measuring a number of distinct stimulus categories and parameters before and after training, this study seeks to specifically address the question of transferability across modalities, including any possible crossover between the dorsal and ventral visual streams.

Chapter 2

General Methods

2.1 Participants

Patients were recruited from ophthalmological or stroke services in five UK NHS centres. Testing was performed at the John Radcliffe Hospital, Oxford. All patients had sustained unilateral damage to the primary visual cortex (V1), causing homonymous visual field loss recorded by Humphrey Perimetry. Wherever possible perimetry was carried out at the John Radcliffe Hospital eye clinic, otherwise it was performed at the referring hospital. Cases with additional visual impairment or additional neurological disease were excluded from participation. Healthy, age-matched controls all had normal or corrected-to-normal visual acuity and no history of neurological disease. Written consent was obtained from all participants. Ethical approval was provided by the Oxford Research Ethics Committee (Ref B 08/H0605/156).

2.2 Stimuli

Stimuli were generated using MATLAB (Mathworks) and the Psychophysics Toolbox (Brainard et al., 1997; Kleiner et al., 2007). Images were displayed on a uniform grey background. Stimulus location was restricted to the scotoma in patients, a minimum

of 2.5 deg from fixation. In age-matched controls, we also matched the stimulus size and position to our patient group. Individual cases were paired to controls, with stimulus size and position replicated.

2.3 Psychophysical Experiments

2.3.1 General procedure

Psychophysical testing was conducted outside the MRI scanner on the same day as scanning, using a 60Hz cathode ray tube monitor at a distance of 68 cm. Fixation was recorded throughout with an Eyelink 1000 eye tracker (SR Research Limited, Ontario, Canada), and any trials with eye position more than 1 degree from fixation were excluded from analysis – see Chapter 3: Figure 2b for examples. Participants were reminded to maintain fixation, with the investigator observing this in real-time. Anyone making even a small eye movement into their damaged hemifield was given specific instruction not to do so, and it was explained that these data would have to be discarded.

2.3.1.1 2-AFC Temporal Detection

Participants were asked to indicate whether a stimulus appeared in the first or second time-interval (Chapter 3: Figure 2a), using a two-alternate forced choice paradigm (2-AFC). If they saw nothing, they were instructed to guess. Onset of each interval was indicated by a 500ms auditory tone, 300Hz marking onset of the first interval, and 1200Hz for the second. Visual stimuli appeared for 500 ms with jittered

onset while the participant fixated on a central black cross. The allocated interval (first or second) was generated at random.

2.3.1.2 2-AFC Discrimination

Patients were asked to indicate which of two stimulus characteristics were correct, e.g. motion direction was horizontal or vertical (Chapter 5). If patients saw nothing, they were instructed to guess. Visual stimuli appeared for 500 ms with jittered onset, whilst the participant fixated on a central black cross.

2.3.2 Blindsight assessment

The presence or absence of blindsight or residual visual function was determined separately for each experiment. This was defined as achieving either an average score, or a score for individual conditions that was significantly above chance, using a statistical threshold of $p < 0.05$ and a cumulative binomial distribution. The primary outcome used for psychophysics was visual performance rather than a dissociation between awareness and performance, which is associated with a more classical definition of blindsight (see Chapter 9.2.1 for a discussion around this issue, and the limitations of this current classification). A proportion of patients did, however, provide confidence ratings on a trial-by-trial basis for their 2-AFC decisions, ranging from 1 (complete guess) – 10 (certain). All patients were also asked to provide a description of the blind-field stimulus to the experimenter, which was noted down for each experiment.

2.4 MRI procedure

Scanning took place in a 3T Siemens Verio MRI scanner at the Functional Magnetic Resonance Imaging Centre of the Brain (FMRIB, University of Oxford), using a 32-channel head-coil.

A high-resolution (1 mm x 1 mm x 1 mm voxels) whole head T1-weighted MPRAGE anatomical image (TE = 4.68ms, TR = 2040ms, field of view = 200 mm, flip angle = 8 deg) was acquired for all patients.

2.4.1 fMRI procedure

Stimuli during scanning were presented on a 1280 x 1040 resolution monitor at the back of the MRI scanner bore. Participants viewed stimuli via a double mirror mounted on the head coil. When in position, the screen subtended a visual angle of 23^{o} x 13^{o}. Throughout all experiments (during condition and rest blocks), participants performed a task to maintain fixation by pressing a button every time a central fixation cross changed color from black to red (see Figure 3c, Chapter 3). Color changes occurred at random lasting 300ms duration, and participants were instructed at the start to try not to miss any red crosses. It was emphasized that they must try to maintain fixation throughout, and avoid moving their eyes around the screen. An EyeLink 1000 eye tracker (SR Research Limited, Ontario, Canada) was used to confirm central fixation by recording eye position (see Section 2.4.4 below).

2.4.2 fMRI acquisition and pre-processing

The same basic scanning parameters were used for all fMRI Experiments in Chapters 3 - 6. At the start of each sequence, magnetization was allowed to reach a steady state by discarding the first five volumes, an automated feature of the scanner. EPI sequences were T2*-weighted, covering 34 sequential 3 mm slices. Repetition time (TR) = 2,000 ms, echo time (TE) = 30 ms, field of view (FOV) = 192 mm. The number of volumes and runs for each EPI sequence were specific for each Experiment, and are described in the Methods sections of Chapters 3-6.

A field map was also acquired for each fMRI experiment. This had dual echo-time images (TE1 = 5.19 ms, TE2 = 7.65 ms, whole brain coverage, voxel size 2 mm × 2 mm × 2 mm) covering the same field of view as the experimental EPI.

Preprocessing and statistical analyses were carried out using tools from FSL (FMRIB's Software Library, www.fmrib.ox.ac.uk/fsl). Non-brain tissue was excluded from analysis using the Brain Extraction Tool (BET; Smith, 2002), motion correction was carried out using MCFLIRT (Jenkinson et al., 2002), images were corrected for distortion using field maps, spatial smoothing used a Gaussian kernel of FWHM 5mm, and high-pass temporal filtering (Gaussian-weighted least-squares straight line fitting, with sigma = 13.0 s) was employed. Functional images were registered to high-resolution structural scans using FLIRT (Jenkinson and Smith, 2001), and to a standard MNI brain template using FLIRT and FNIRT (Andersson et al., 2007).

2.4.3 fMRI analysis

Functional images were registered to high-resolution scans and the MNI brain template, as described above. All activation coordinates are reported in MNI space, and region identification was determined using the FSLview atlas. It is worth noting that this procedure was useful for displaying group results on canonical brain images, and for model fitting. All graphs, signal change calculations, and correlation statistics were calculated using data from participants' native space.

2.4.3.1 Regions of interest

hMT+ masks were derived from anatomically defined probabilistic maps (Juelich atlas implemented in FSL, Malikovic et al., 2007), non-linearly transformed into functional space for both patients and controls to ensure consistency between participant groups. V1 masks in controls, and in the intact hemisphere of patients were functionally defined for each participant so that they corresponded to stimulated regions of calcarine cortex.

2.4.3.2 Region of interest analysis

This was carried out in the same way for all fMRI chapters. Each experimental condition (e.g. left hemifield, 1% contrast) was entered into the general linear model (GLM) as a separate explanatory variable, and was contrasted against the baseline fixation task to generate contrast of parameter estimates (COPEs) for each condition in every voxel. Signal change was then extracted from regions of interest within functional-space for each individual. The percentage signal change was calculated by

scaling the COPE by the peak-peak height of the regressor, and dividing by the mean over time. These measures were averaged across participants to generate group plots for signal change as a function of the condition under investigation, and were used in all correlation and regression analyses.

Pearson correlation analyses were used to compare patterns of activation with the condition of interest across ROIs, and between patients and controls. When comparing activity in the same participants, paired correlation analyses were performed. All tests were 2-tailed unless otherwise stated.

2.4.4 Eye Movements

Eye movements during fMRI can be a legitimate concern when considering results for visual stimulation inside a scotoma. Chapter 6 (Face/Place) employed a particularly stringent set of criteria, discussed there in detail. For Chapters 3 – 5, three lines of evidence suggest that this was not a problem and could not have accounted for the results. Firstly, concurrent eye movement data was collected on almost all patients (86.2% across all experiments) using an eye tracker positioned at the base of the MRI bore. The majority of these patients underwent successful eye-tracker calibration, with accurate data throughout fMRI runs. For those patients, the total number of eye movements recorded ranged from 0 - 12, defined as a movement of 2 degrees or more towards the scotoma. This accounted for < 0.6% of the scan duration i.e. < 0.3% of the blind conditions, making any contribution likely to be negligible. To confirm this, when scanner volumes corresponding to eye movements were regressed out of analyses, the results remained unchanged. For certain patients, there was a difficulty

with calibration due to their dense field loss (affecting 28% of eye-tracked scans). In this situation, direct visualization of the pupil was used via video recording to observe any overt eye movements during the experiment.

Second, all participants performed over 90% on a concurrent behavioural task requiring fixation throughout the experiment. Brief colour changes of the fixation cross (300ms duration) occurred at frequent and random intervals, and participants were given a window of 1 s to press a button connected to the stimulus computer via a parallel port, being specifically instructed not to miss any red crosses or move their eyes around the screen. In addition, before the fMRI scan all participants took part in behavioural testing lasting at least 60 minutes, focused on their damaged region of vision. Participants became very experienced at maintaining fixation during this assessment. Anyone making even a small eye movement into their damaged hemifield was given specific training not to do so, and it was explained that their data could not be used if this was the case.

Finally, the results from Chapter 3 and 4 show a difference in fMRI patterns in patients compared to healthy controls and their own intact hemisphere. If eye movements were made, one would expect to see a response in hMT+ that matched that for the sighted hemifield, which was not the case. This suggests that eye position cannot account for the findings.

Chapter 3

Abnormal contrast saturation in hMT+ after V1 damage

3.1 Abstract

When V1 is damaged, residual vision is most robust for high contrast, moving stimuli. This is somewhat incongruous with our understanding of normal hMT+ sensitivity to contrast, where early saturation means that even low contrast levels elicit neural activation close to ceiling, attributed to a dominant input from the magnocellular layers of the lateral geniculate nucleus (LGN). This study sought to investigate this discrepancy by measuring behavioural and neural responses to increasing contrast in patients with V1 damage. Eight patients underwent behavioural testing and functional MRI to record contrast sensitivity in hMT+ of their damaged hemisphere, using Gabor stimuli with a spatial frequency of 1 cycle/degree. The responses from the blind field were compared to hMT+ and V1 responses for the sighted field of patients and a group of age-matched controls. Unlike hMT+, responses in V1 do not normally show early saturation with increasing contrast, reflecting a dominant parvocellular channel input. Across all patients, the response of hMT+ to the blind hemifield no longer showed an early saturation, but increased linearly with contrast

in a pattern similar to V1 in sighted controls. This suggests that a distinct input channel to normal dominates hMT+ responses in patients. Given the spatiotemporal parameters of the stimuli used, this could be consistent with known subcortical projections to hMT+ from the koniocellular layers of the LGN.

3.2 Introduction

It is well established that residual vision, or blindsight, following damage to V1 is most consistent for moving and high luminance contrast stimuli (Riddoch, 1917; Weiskrantz et al., 1974; Zihl and Von Cramon, 1980), with the human motion area, hMT+, frequently implicated in functional imaging studies of cortical blindness (Zeki and Ffytche, 1998; Goebel et al., 2001; Schoenfeld et al., 2002; Nelles et al., 2002; Bridge et al., 2010). Such observations are somewhat incongruous with our understanding of normal hMT+ sensitivity to luminance contrast, where a dominant magnocellular input conveys early saturation such that even very low levels of contrast elicit significant activation above baseline (Tootell et al., 1995). Although receptive field summation is likely to contribute to this effect, high contrast sensitivity is a feature of all stages of the M-channel, including M-neurons in the lateral geniculate nucleus (Derrington and Lennie, 1984). The implication is that blindsight function may be mediated by different pathways to hMT+, and that by understanding their different characteristics, it may be possible to uncover which pathways are involved.

Several visual pathways are implicated in blindsight, with diffusion-weighted tractography studies (DTI) demonstrating geniculo-extrastriate, cortico-cortical, and tecto-cortical pathways (Bridge et al., 2008; Leh et al., 2006). However, the ability to use DTI to track between two brain regions does not provide information about function. Furthermore, it is not yet possible to perform human DTI at sufficient resolution to distinguish divisions of pathways into subtypes such as the M, P or K-channels. In contrast, by exploiting the known properties of these different channels, fMRI and psychophysics can be used to investigate the physiological properties of residual hMT+ neurons when V1 is damaged. By comparing these responses to normal hMT+ and V1 activity it can be determined whether contrast sensitivity in hMT+ of patients reflects normal M-driven responses or is better described by response properties of P- or K-pathways.

It is also possible to measure behavioural performance for stimuli presented to the blind hemifield, to determine how neural activity relates to blindsight experience, a relatively neglected issue (Zeki and ffytche, 1998; Sahraie et al., 1997). In particular, it may be possible to evaluate whether hMT+ activity correlates more strongly with the basic image properties of a stimulus, or with the perceptual experience associated with its detection (Panagiotaropoulos et al., 2012), and to consider how these two components may both be reflected in BOLD signal changes.

These questions were investigated using fMRI in eight patients with unilateral damage to primary visual cortex. To anticipate the findings, it was found that the pattern of BOLD signal changes evoked by different levels of contrast in ipsilesional hMT+ did not saturate at low contrast as predicted by input from the M-pathway.

Rather there was a linear response to increasing contrast that was very similar to the response pattern in control V1. Given the known subcortical projections from koniocellular layers of the lateral geniculate nucleus to hMT+, and the stimulus parameters used in this study, it is proposed that BOLD responses in hMT+ may be driven predominantly by the K-pathway in the absence of V1.

3.3 Methods

3.3.1 Participants

Eight patients (three female) took part in the study. Pathological changes had been caused by posterior circulation stroke in seven patients, and by benign tumour resection in one patient, at least 6 months previously – see Table 1 for details, and Figure 1b for example axial and sagittal images from two patients. Average age at the time of participation was 49.6 years ±15.0 S.D., average time after pathology onset 42.5 months (range 6-156 months) Eight age-matched, healthy participants (53.6 ±12.2 S.D years of age, three female) served as controls.

3.3.2 Stimuli

Visual stimuli consisted of a drifting achromatic Gabor patch, i.e. a grating that was drifting within a stationary envelope, of 5^{o} or 8^{o} diameter, displayed on a uniform grey background; temporal frequency 10Hz, spatial frequency 1.3 cycles/^{o}. Five contrast levels were used: 1%, 5%, 10%, 50%, and 100%, with stimulus location restricted to the scotoma and its corresponding location in the sighted hemifield in

patients, a minimum of 3° from fixation (see Figure 1a for schematic representation of stimulus location in two patients). The two stimulus sizes (5° or 8°) were selected according to the size of the patient's visual field deficit. The smaller 5° diameter stimulus was used in patients with quadrantanopia or more peripheral visual field deficits. The orientation of drift during each trial/fMRI presentation was randomly allocated between two orthogonal directions: 45° or 135°.

Patient	Sex	Age (years)	Pathology	Time since pathology (months)	HVFD
P1	F	67	Right occipito/temporal haemorrhage	6	LUQ
P2	F	38	Right occipital tumour resection	36	LHH
P3	M	69	Right occipital infarct	16	LUQ
P4	M	55	Left occipital and cerebellar infarct	18	RHH
P5	F	42	Left occipital infarct	6	RHH
P6	M	36	Left occipital infarct	6	RHH
P7	M	60	Left occipital infarct	96	RLQ
P8	M	30	Left occipital infarct	156	RHH

Table 1. Clinical details for eight patients with unilateral striate cortex damage and homonymous visual field deficits (HFVD), who participated in this study. LUQ = left upper quadrant, RLQ = right lower quadrant, RHH = right homonymous hemianopia, LHH = left homonymous hemianopia, F = female, M = male.

3.3.3 Psychophysics

Psychophysical testing was based on a 2-AFC temporal detection task (see General Methods, and Figure 2a for illustration). In a subgroup of four patients, confidence ratings were also collected for each trial, using a scale of 1-10. It was explained that a rating of 10 was to be used if they were absolutely certain, whilst 1 was for a complete guess. Stimulus contrast was altered parametrically between the five levels

at random, with 20 trials per condition. Participants additionally performed a run of control testing, with stimuli presented to the equivalent location in their sighted visual field. The presence or absence of blindsight was assessed according to the criteria described in the General Methods.

Patients were also asked to describe the stimulus presented to their blind field. This was carried out after three blocks of testing, i.e. after all five contrast levels had been tested three times in the blind field, but before the sighted hemifield had been tested. Patients were encouraged to be as detailed as possible with their description, which was noted down by the experimenter. No feedback was given on the accuracy of their description.

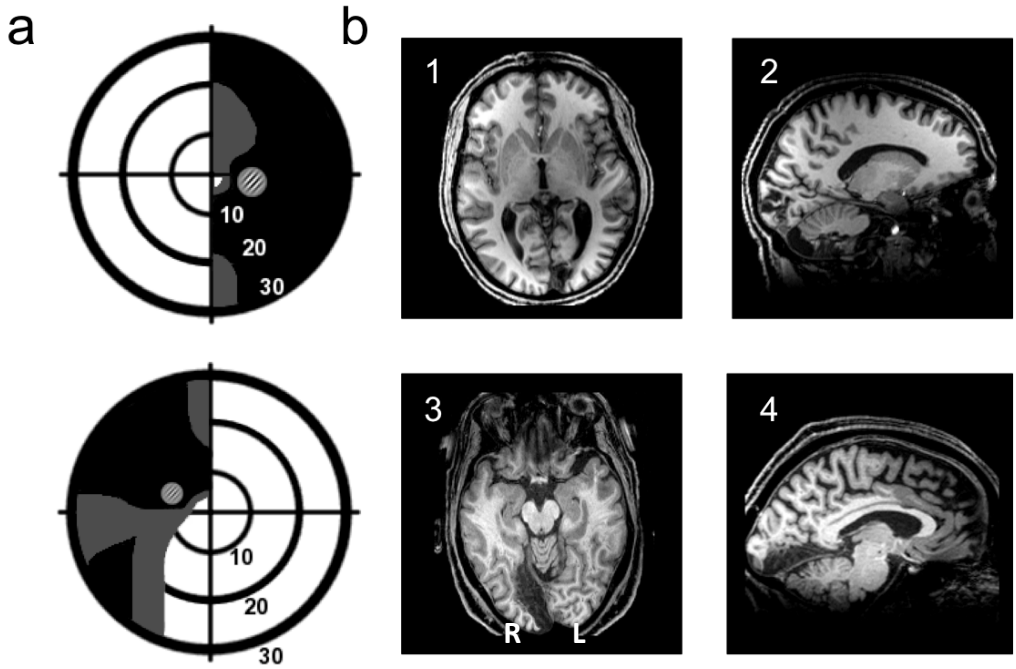

Figure 1. Example visual field deficits and structural MRI scans for two patients, P4 (upper) and P3 (lower). **(a)** Humphrey visual fields drawn schematically, with the location of the target stimulus superimposed. Dense visual field loss is shown in black (< 0.5%) and partial loss in grey (< 2%). Concentric rings represent increments in retinal position of 10 degrees, spanning the central 30 degrees. **(b)** MPRAGE T1 structural, representative axial and sagittal slices demonstrating lesion location. Radiological convention.

3.3.4 fMRI procedure

The same five contrast levels were presented separately to each hemifield representing a 10-condition block design, with equivalent diameter and screen position to that used in behavioural testing (see Figure 3a for illustration). For each block, a Gabor of the same luminance contrast appeared eight times with 2 s duration and inter-stimulus interval of 500 ms. A 10 s 'rest' period followed each 20 s block, during which time the fixation task continued, but there were no stimulus presentations. There were three runs in total, each lasting 300 s.

3.3.5 fMRI acquisition and pre-processing

456 functional volumes were acquired in a single session, duration 15 min. For parameter and pre-processing details, please see General Methods (Chapter 2).

3.3.6 fMRI analysis

3.3.6.1 Regions of interest

Anatomical hMT+ and functional V1 masks were derived according to the procedure in the General Methods. In native space, average hMT+ ROI volume was 87.3 ±30.8 voxels in patients, 99.6 ±14.3 voxels in controls. Average V1 ROI volume was 38.5 ±37.9 voxels in patients (undamaged hemisphere) and 23.7 ±20.1 voxels in controls (averaged across hemispheres), the small volume reflective of the small 5^{o} or 8^{o} diameter stimulus used.

Each of the 10 fMRI conditions (e.g. left hemifield, 1% contrast) were entered into the general linear model (GLM) as separate explanatory variables. Please see General

Methods (Chapter 2) for details. All graphs, signal change calculations, and correlation statistics were calculated for each condition relative to baseline, using data from participants' native space. Baseline refers to the rest blocks of 10 s duration, occurring after each condition block.

3.3.6.2 Whole brain GLM group analysis

Group analyses were also performed to look for brain regions showing significant activation during blind hemifield stimulation. For this purpose it was necessary to align patient brains to a uniform pathological template, with lesions located in the same 'left' hemisphere, corresponding to a 'right-sided' visual deficit. This required that the structural and functional images of three patients (P1, P2, P3) were flipped in the horizontal plane. All activation coordinates are reported in MNI space, and z statistic images are displayed on mean structural images for the group, transformed to standard space. Mixed effects analyses were carried out for each hemifield separately, in control and patient groups. A statistical threshold of $p < 0.001$ uncorrected was used to test for significance within V1 and extrastriate cortex, for which there were *a priori* hypotheses. Elsewhere correction for multiple comparisons was made using a cluster threshold of $p < 0.05$ unless otherwise stated.

3.3.6.3 Whole brain parametric group analysis

A parametric group analysis was also performed to assess the specificity of different relationships between fMRI signal change and stimulus contrast throughout the whole brain. The same technique and statistical analyses were used as for the whole brain GLM analysis, except that normalized integers representing linear and logarithmic models were entered as weights into a group GLM, along with the contrast of parameter estimate (Chapter 2.4.3.2) for each condition versus baseline

fixation for all participants.

3.3.6.4 Whole brain behavioural group analysis

A similar technique was also used to look for brain regions demonstrating a direct relationship between fMRI signal change and behavioural 2-AFC performance. Only patients showing significant detection above chance were included in this analysis. This was defined as achieving an average score above chance, using a statistical threshold of $p < 0.01$ and a cumulative binomial distribution. This criterion led to the exclusion of one participant from analysis (P3). Individual detection scores for each contrast level in the 7 remaining patients were normalized and entered as weights into a higher-level general linear model, along with the corresponding contrast of parameter estimate for the blind hemifield condition. Fixed effects analyses were carried out, for the blind hemifield only.

3.4 Results

Of the eight participants with V1 damage, seven performed significantly above chance at detecting a drifting achromatic Gabor within their blind field of vision (Figure 2c). Blindsight performance showed a clear positive relationship with stimulus contrast, which was best described by a logarithmic relationship, i.e. a linear relationship with log contrast, as seen in Figure 2d ($R^2 = 0.98$, $F = 9.7$ log versus linear regression, $p = 0.05$). Throughout all experiments, trials with eye movements were discarded from analysis (see Figure 2b for example eye-tracker data over three trials. Overall, significant deviation from fixation constituted 1.88% of all trials, which were discarded. Participants performed an identical task for stimuli presented to their sighted hemifield, with average detection performance 98.3%

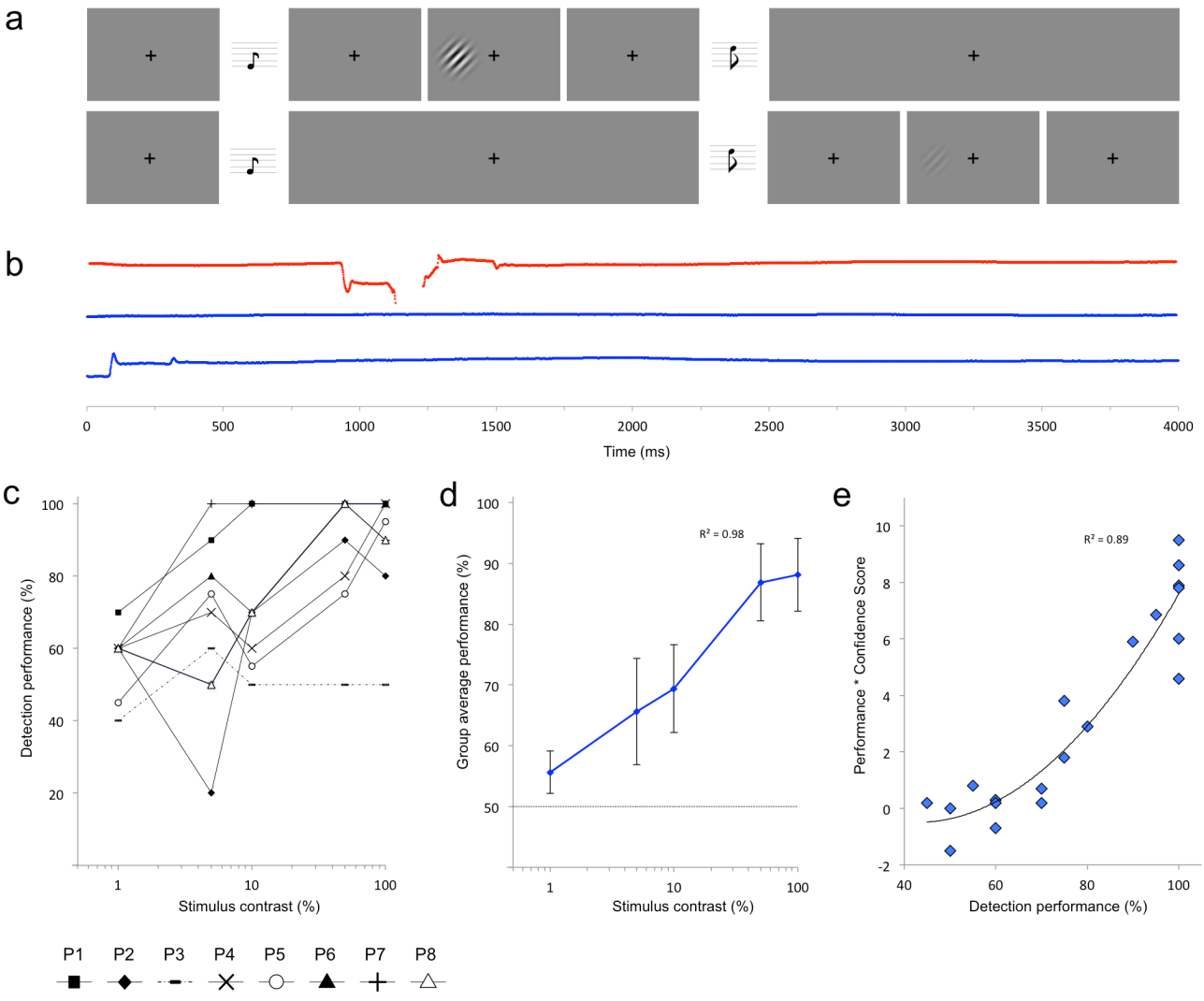

Figure 2. Behavioural protocol and results for all patients. (a) Schematic of the 2-AFC detection procedure. Participants fixate on a central cross, with the onset of each 1500ms interval alerted by a low (interval 1) or high pitch (interval 2) tone. The stimulus can appear in either interval, for a period of 500ms. At the end of the trial, participants are instructed to decide which interval the stimulus appeared, with a subset of patients also asked to rate the confidence of this response. **(b)** Throughout the experiment, fixation was recorded with eye-tracking. Example data over three trials are displayed here, the y-axis representing horizontal gaze position on the screen. Any trials containing eye movements greater than 1 degree towards the stimulus were excluded from analysis (red plot), blue plots represent adequate fixation. **(c)** Individual 2-AFC detection performance for all individuals. The individual at chance (P3, dotted line) is clearly distinct from other patients. **(d)** Average group performance, error bars representing standard error of the mean. Detection exhibits a logarithmic relationship with contrast (R^2 = 0.98). **(e)** Individual confidence ratings for four patients were multiplied by trial performance (correct +1, incorrect -1) to generate a y-score reflecting both these measures, plotted here against detection performance. The relationship is best described as a non-linear curve, with confidence increasing the most for higher performance scores (R^2 = 0.89).

±1.4% S.D., and no significant difference across contrast levels, including the 1% contrast condition.

3.4.1 Optimal performance is associated with a greater increase in confidence

Descriptions of stimuli in the blind field varied considerably, with some patients stating that their responses were almost exclusively guesses (P2), or that they were aware of something, but were unable to describe it at all (P7). Another patient reported, on occasions, being able to see "s*omething fuzzy/murky, but nothing distinct*" (P4). Two patients described seeing movement of some sort, with one unable to appreciate any detail (P8), whilst the other thought that images were black (P5). Another patient interestingly described their experience as "*like an after-image, with dancing colours*" (P6), and was able to point to the position on the screen where the stimulus appeared. The most detailed report was of seeing "*grey clouds*" which became "*more bold*" at times (P1).

All four patients tested for confidence showed greater confidence for correctly identified versus incorrect trials, however there was wide inter-subject variability in their ratings. P1: 7.5 vs. 2.6, P4: 2.6 vs. 1, P5: 4.3 vs. 1.4, P6: 5.1 vs. 3.4. On average, patients mostly used confidence ratings under 5 for correct responses. However, this increased considerably for stimuli at 100% contrast (mean confidence score 7.0). Individual 2-AFC performance correlated well with confidence ratings, with the relationship best described by a non-linear curve (see Figure 2e), such that confidence increased the most for higher performance scores.

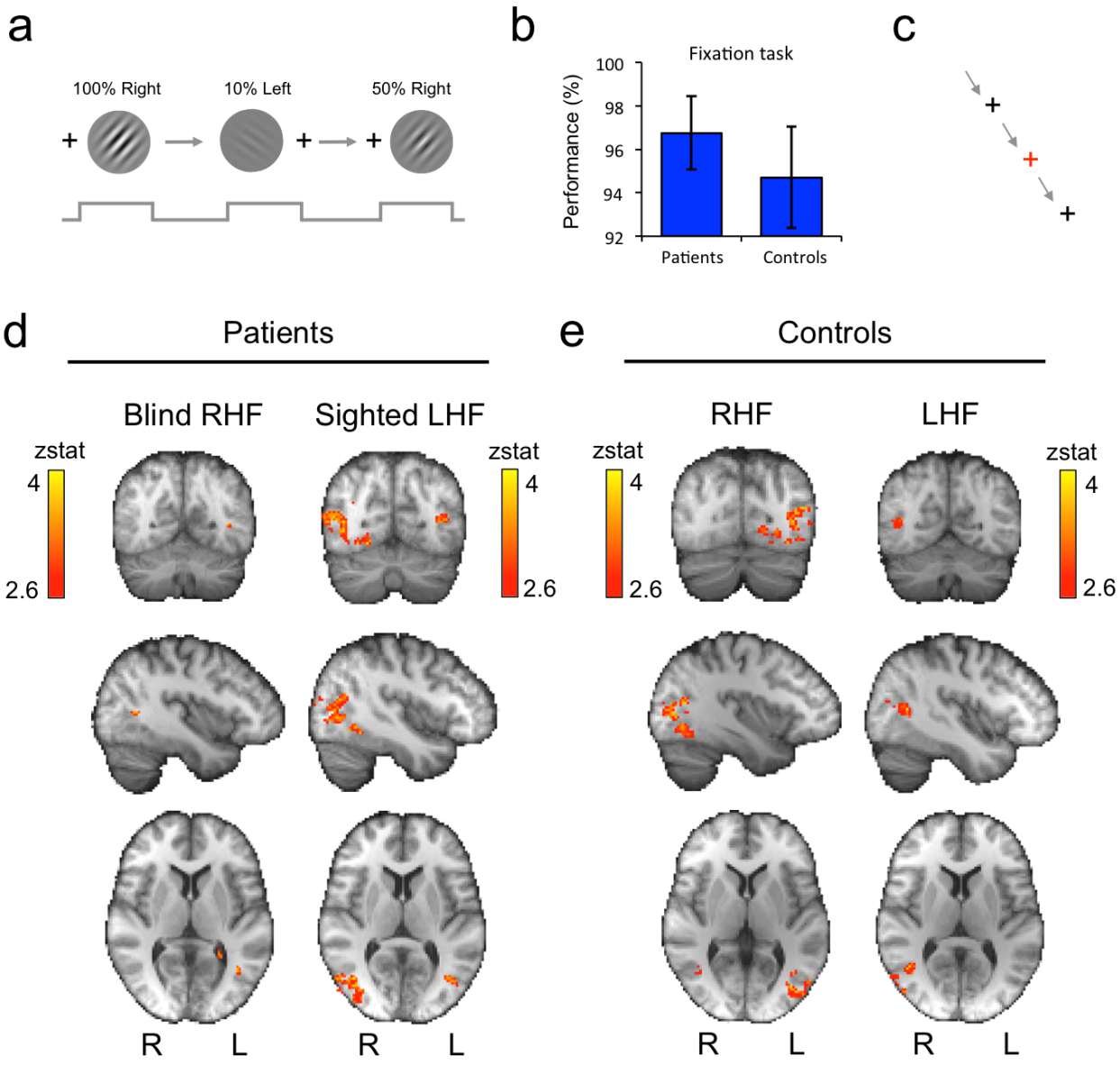

Figure 3. **fMRI procedure and activation results for high contrast motion. (a)** Simple block design displays a drifting Gabor to the 'blind' portion of visual field, or its equivalent location in the sighted hemifield during 20s blocks. Stimulus contrast is altered at random for each block across five contrast levels, representing 10 conditions. **(b)** A fixation task requires participants to press a button every time the fixation cross changes colour to red **(c)**. Performance is plotted for both groups, error bars representing standard error of the mean. **(d)** Thresholded activation maps for 100% contrast stimulation versus baseline fixation, comparing the blind (left column) and sighted (right column) hemifields of patients. **(e)** Equivalent results in control participants. Mixed effects analysis, $p < 0.001$ uncorrected for *a priori* regions of interest, elsewhere cluster corrected, $p < 0.05$, results displayed on average high resolution structural in MNI space. RHF = right hemifield, LHF = left hemifield.

3.4.2 hMT+ responds to high contrast motion in the blind hemifield

A group-level analysis was performed to measure the effect on BOLD signal change for a high-contrast drifting Gabor (100% contrast) presented within the blind visual field of patients, compared to baseline fixation. This was compared to stimulation of the opposite, sighted hemifield (Figure 3d), as well as a group of age-matched controls (Figure 3e). As expected, controls showed significant activation throughout contra-lateral visual cortex, with peak activation in hMT+ on the right (z = 4.0, MNI coordinates: 46,-60,8) and areas V4 and hMT+ on the left (z = 4.6, MNI coordinates: -30,-70,-14; z = 4.3, MNI coordinates: -40,-78,8). Patients showed a similar pattern for their sighted hemifield, although demonstrating a slightly greater degree of ipsilateral hMT+ activation (i.e. in the ipsilesional hemisphere) compared to controls (Figure 3d, right column). For stimulation of the blind hemifield (Figure 3d, left column), a small region in contralateral hMT+ (ipsilesional) demonstrated significant activation above baseline (peak z = 3.6, MNI coordinates: -40,-62,6, $p < 0.001$). No significant activity was seen in early visual cortex (where lesions are located), or the intact hemisphere.

3.4.3 Blind hMT+ contrast-response resembles healthy V1

Responses to increasing contrast in control participants are shown in Figure 4a and 4b. As expected, contralateral hMT+ (Figure 4a) showed a large initial increase in signal change for low levels of contrast, with activity remaining fairly constant despite subsequent increases in contrast. This is best described by a logarithmic curve, i.e. a linear relationship with log contrast, although this does not fully reflect the steep initial rise in signal change between stimuli of 1% and 5% contrast. A similar response function was seen in contralateral hMT+ for the sighted hemifield of patients (Figure 4c). In contralateral V1 of controls (Figure 4b), there

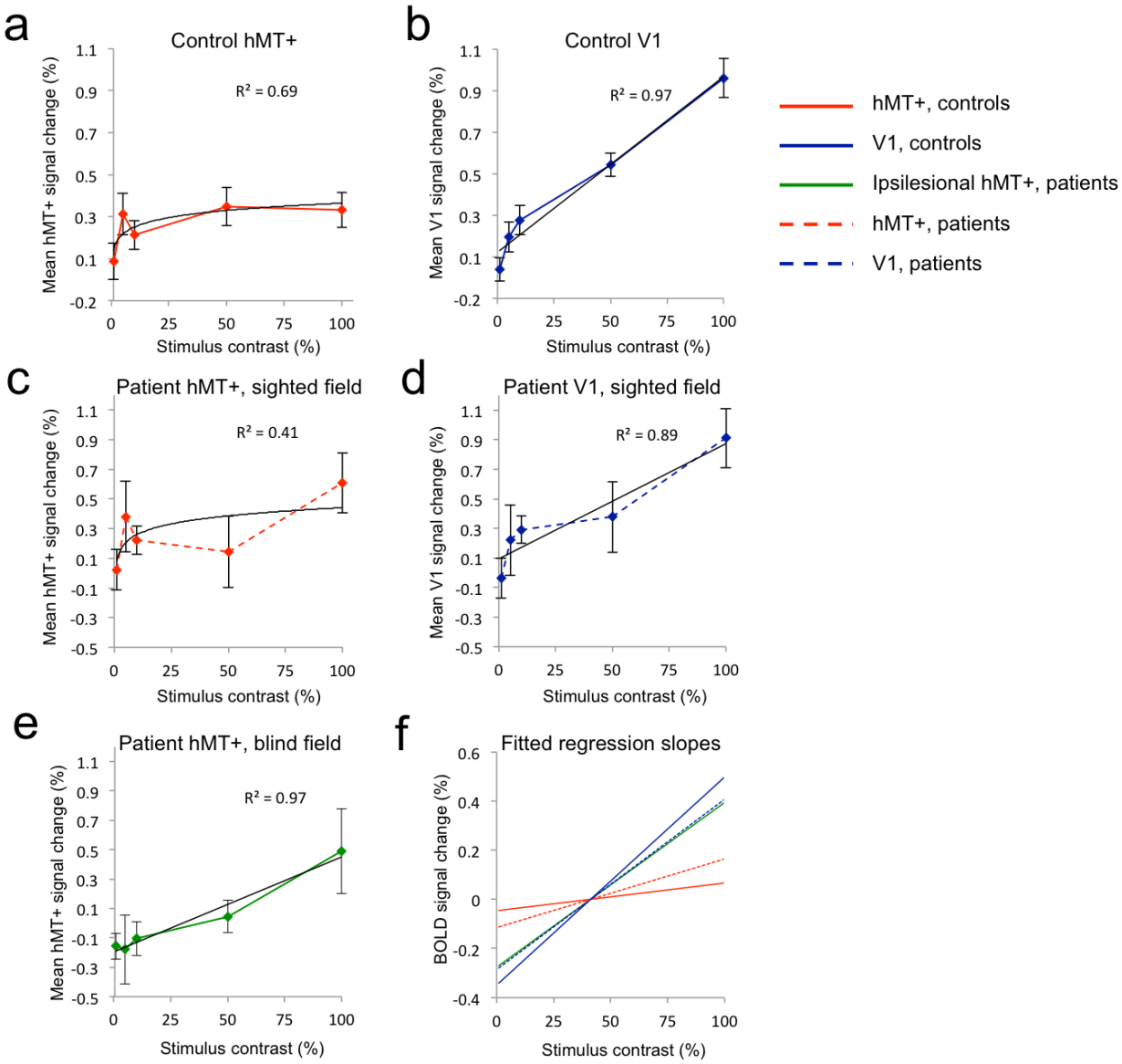

Figure 4. Group plots of signal change versus stimulus contrast within V1 (blue) or hMT+ (red) regions of interest. (a) Control group hMT+ shows an early saturation at low levels of contrast, described by a logarithmic response – i.e. a linear relationship with log contrast, depicted here on a linear scale to allow easier comparison to V1 patterns. **(b)** Control V1 shows a much stronger linear component, with signal change continuing to increase with each rise in stimulus contrast. **(c)** Sighted hMT+ response in patients shows high signal change at 5% and 10% contrast. **(d)** Sighted V1 in patients undamaged hemisphere, similar to controls, shows a predominantly linear relationship with increasing contrast. **(e)** Ipsilesional hMT+ in patients is also best described by a linear relationship with contrast. **(f)** Normalized linear regression lines between 5% - 100% contrast capture the early plateau of activity in normal hMT+ responses. hMT+ in controls (red) and the sighted hemifield of patients (dotted red) both show shallow increases in signal change representative of this early saturation in activity. Conversely, V1 of controls (blue) and the intact hemisphere of patients (dotted blue) show a comparable, steeper gradient that is notably similar to the regression line for hMT+ during blind field stimulation in patients (green). Error bars represent standard error of the mean.

was a linear relationship between signal change and stimulus contrast, with a very similar pattern for the sighted hemifield of patients (Figure 4d), also best described by a linear function.

For stimulation of the blind hemifield (Figure 4e), signal change in hMT+ generally increased as stimulus contrast was increased, and this relationship was also best described by a linear regression ($R^2 = 0.97$). A shallow gradient of the regression lines fit across 5 – 100% contrast should reflect the early plateau of activity seen in normal hMT+. In contrast, in V1, where signal change continues to increase with stimulus contrast, the gradient will be steeper. Indeed in controls and the sighted hemifield of patients, there was a shallow increase in signal change in hMT+, representative of early saturation in activity (Figure 4f). Conversely, V1 of controls and the intact hemisphere of patients showed a steeper gradient, notably similar to the regression line for hMT+ during blind field stimulation in patients.

Additionally, it was evaluated how well activity patterns in hMT+ during blind hemifield stimulation correlated with either sighted hMT+ activity (Figure 5d), or intact V1 in patients (Figure 5c), or the equivalent regions in controls (Figure 5a and b). The data for paired within-participant analyses was normalized for each participant, to reduce the impact of any between-subject differences on skewing the correlation. There was a significant correlation between blind field-stimulated hMT+ activity and intact V1 responses to the sighted field, ($r = 0.31$, $p = 0.05$), but not with sighted hMT+ response in the undamaged hemisphere ($r = 0.19$, $p = 0.24$). Similarly, blind hMT+ activity shows a significant correlation with V1 activity in controls (Figure 5a, $r = 0.94$, $p = 0.01$), but not with control hMT+ responses ($r = 0.68$, $p = 0.2$, Figure 5b).

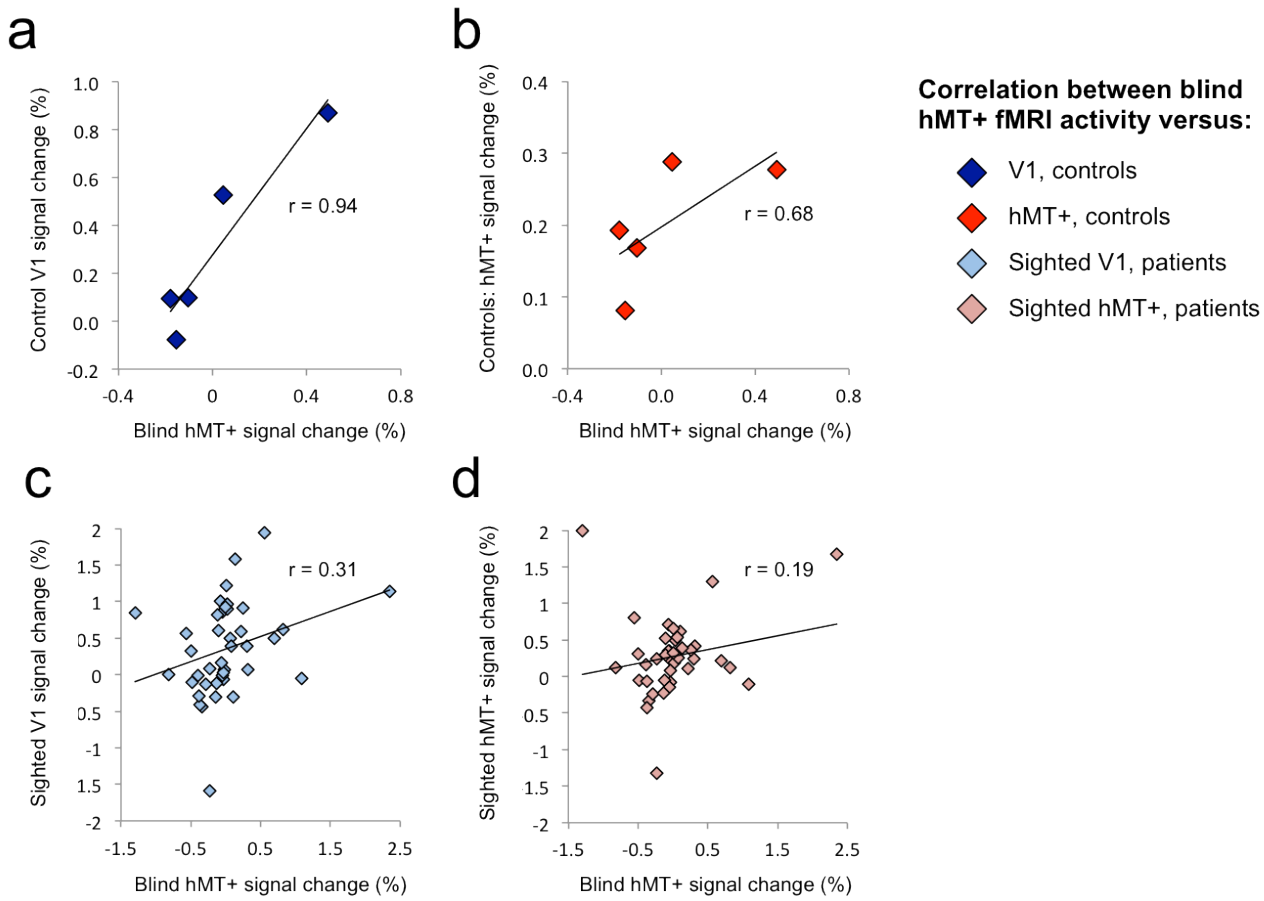

Figure 5. Correlations between hMT+ activity in patients during blind field stimulation versus sighted responses in V1 and hMT+ of patients and controls. (a) Average hMT+ signal change during blind hemifield stimulation in patients correlates well with contrast-related activity in V1 of control participants, but not with control hMT+ responses **(b)**. **(c)** Blind hMT+ activity also correlates with V1 responses to the sighted hemifield in patients' intact hemisphere. This remains significant when the three most distant outliers are excluded from analysis, r = 0.35, p = 0.03. **(d)** There is no significant correlation with contrast-related hMT+ responses to patients' sighted hemifield, which remains unchanged when the three most prominent outliers are excluded (r = 0.19, p = 0.26). The data for **(c)** and **(d)** was normalized for each participant, to reduce the impact of any between-subject differences skewing the correlation.

3.4.4 Blind hMT+ shows activity according to a linear, not logarithmic model

To determine brain regions in which the activation patterns followed either a logarithmic or linear relationship with increasing stimulus contrast, a higher-level group analysis was performed. Employing a whole brain parametric approach does not require predetermined regions of interest and thus can identify brain areas

where activation patterns relate significantly to the hypothesized relationships. Furthermore, this approach can quantify the sensitivity and specificity of such models to regional patterns of activity in both participant groups.

In control participants the linear model showed a significant fit with activation patterns in a specific region of contralateral V1, V4, and to a lesser extent

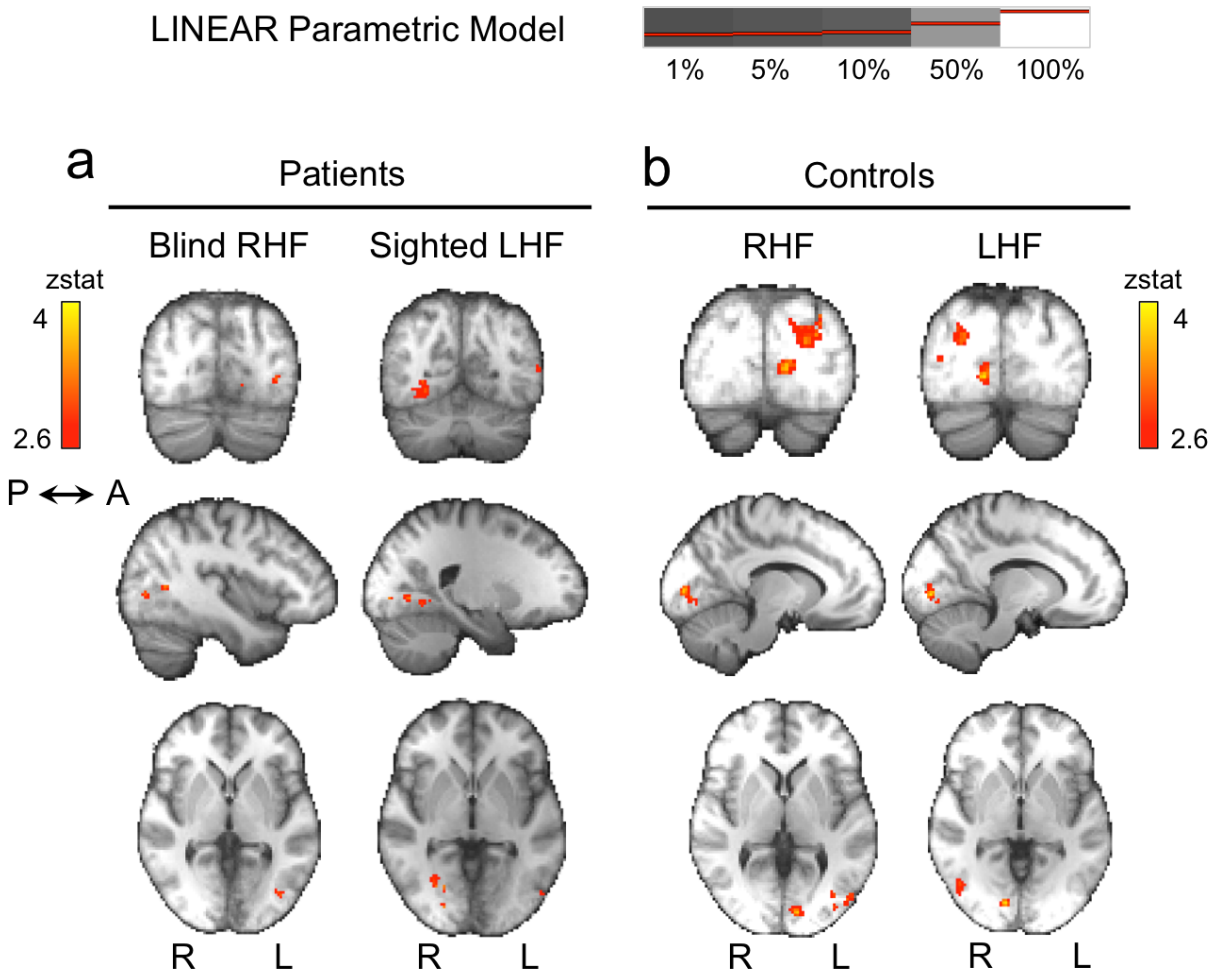

Figure 6. Cortical regions demonstrating a significant linear relationship with stimulus contrast. (a) In patients, only contralateral hMT+ shows significant activity according to this model during blind hemifield stimulation. For the sighted hemifield (right column), and control participants **(b)** there is a significant linear relationship with contrast in contralateral V1, V4 and to a lesser extent hMT+. Mixed effects analysis, $p < 0.001$ uncorrected for *a priori* regions of interest, elsewhere cluster corrected, $p < 0.05$. Results displayed on average high resolution structural in MNI space. RHF = right hemifield, LHF = left hemifield.

Controls	**x**	**y**	**z**	**z-stat**		**x**	**y**	**z**	**zstat**
Right hemifield					Left hemifield				
Linear Model					*Linear Model*				
Left V4 (occipital fusiform gyrus, OFG)	-24	-78	-8	4.5	Right V1	12	-82	-2	3.8
Left V1	-10	-88	2	3.7	**Right hMT+**	**46**	**-66**	**8**	**3.5**
Left hMT+	**-44**	**-78**	**8**	**3.4**	Right LOC, superior division	26	-84	18	3.5
Left LOC, superior division	-20	-88	16	3.4					
Logarithmic Model					*Logarithmic Model*				
Left V4 (OFG)	-24	-68	-16	4.1	**Right hMT+**	**46**	**-66**	**6**	**3.6**
Left hMT+	**-36**	**-72**	**8**	**3.6**	V1/V2 boundary	12	-80	0	3.3
Patients	**x**	**y**	**z**	**z-stat**		**x**	**y**	**z**	**zstat**
Blind right hemifield					Sighted left hemifield				
Linear Model					*Linear Model*				
Left hMT+	**-40**	**-62**	**6**	**3.2**	Right V1	22	-84	-2	3.3
					Right optic radiation/ V1 boundary	30	-62	0	3.4
					Right V4 (OFG)	28	-66	-8	3.2
					Left hMT+	**-46**	**-72**	**4**	**3.1**
Logarithmic Model					*Logarithmic Model*				
No significant activity					Right paracingulate gyrus	2	32	40	4.1
					Left hMT+	**-40**	**-70**	**14**	**3.9**
					Right hMT+	**48**	**-64**	**16**	**3.6**

Table 2. Cortical regions demonstrating a significant linear or logarithmic relationship with stimulus contrast. Only the most significant peak within each region of activation is reported, with its corresponding MNI coordinates and z-statistic. A statistical threshold of $p < 0.001$ uncorrected was used for a priori regions of interest, elsewhere correction for multiple comparisons was made with a cluster threshold of $p < 0.05$, mixed effects analysis.

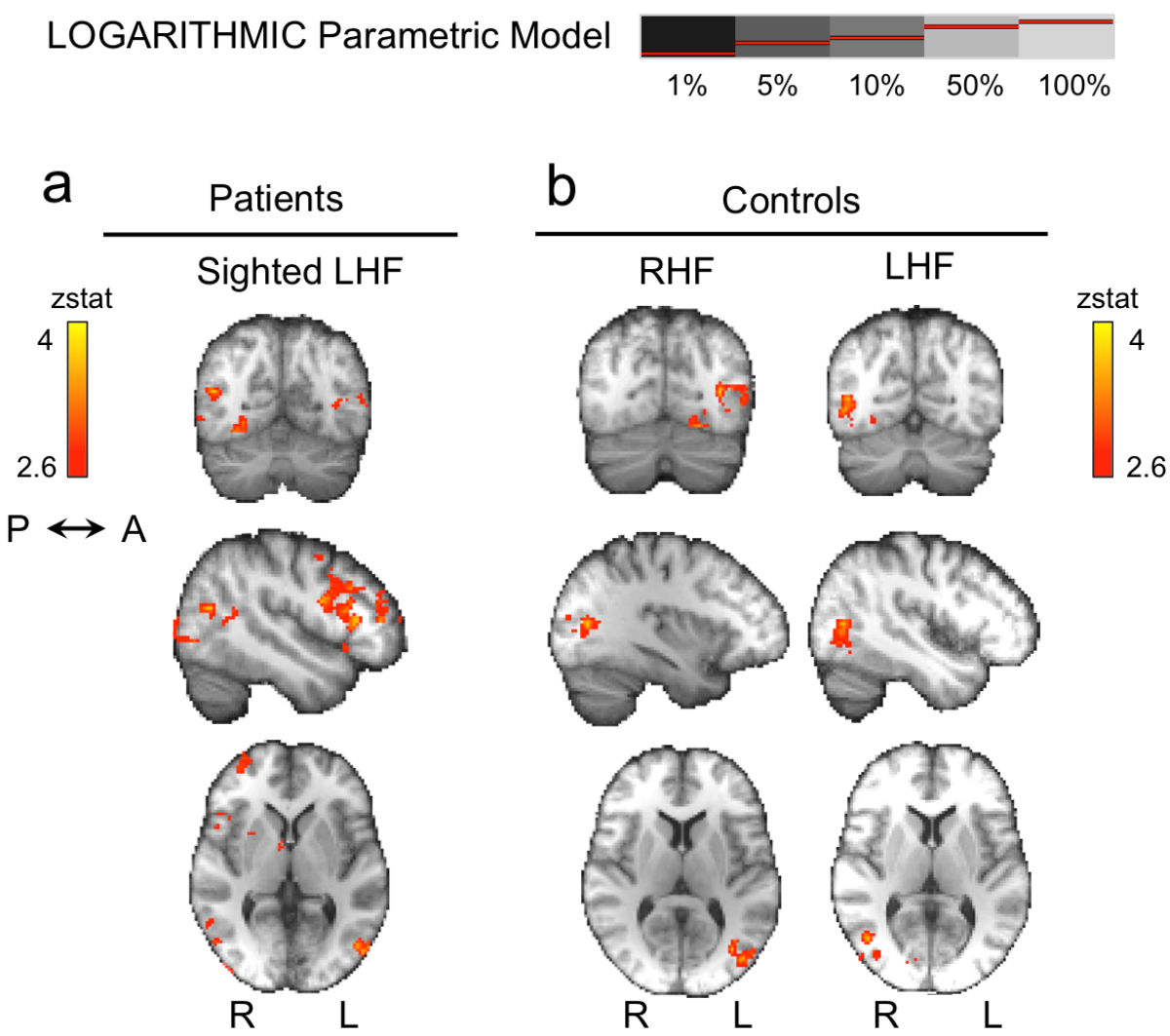

Figure 7. Cortical regions demonstrating a significant logarithmic relationship with stimulus contrast. (a) In patients, no regions respond logarithmically to contrast in the blind hemifield. In the sighted hemifield and in controls **(b)** there is a significant logarithmic relationship with contrast in hMT+ and V4, see Table 2 for details. Mixed effects analysis, $p < 0.001$ uncorrected for *a priori* regions of interest, elsewhere cluster corrected, $p < 0.05$. Results displayed on average high resolution structural in MNI space. RHF = right hemifield, LHF = left hemifield.

contralateral hMT+ (Table 2, Figure 6b; Amunts et al., 2000; Rottschy et al., 2007; Malikovic et al., 2007). A similar pattern was seen for the sighted 'left' hemifield of patients (Figure 6a, right column). For the blind hemifield, the only brain region showing a significant fit according to the linear model was in left hMT+ in the damaged hemisphere, with a similar z-statistic to intact V1 during sighted hemifield stimulation (Table 2, Figure 6a left column).

For the sighted hemifield in patients, there was a significant fit with the logarithmic model in regions corresponding to hMT+ bilaterally, as well as the right paracingulate gyrus (see Table 2 for full details, Figure 7a for representative brain slices). In controls, contralateral hMT+ also showed activity according to this model (Figure 7b), as well as left V4 (during right hemifield stimulation) and an area at the border of right V1 and V2 (left hemifield stimulation, see Table 2). For blind hemifield stimulation, no brain regions showed activity with a logarithmic relationship to stimulus contrast.

3.4.5 Is stimulus contrast or blindsight performance a better predictor of hMT+ activity?

It is clear that blindsight performance and fMRI activity in contralateral hMT+ both relate in some way to the strength of stimulus contrast inside the blind hemifield. What is not clear is how hMT+ activity specifically relates to 2-AFC performance, and indeed whether it is the low-level features of stimulation inside the blind hemifield (i.e. stimulus contrast) or the ability for patients to detect a stimulus that is the stronger indicator of hMT+ activity.

Across all participants, hMT+ activity showed a weak, yet significant logarithmic relationship with blindsight performance (Figure 8a, $r = 0.35$, $p = 0.03$). The contribution of stimulus contrast can be appreciated using colour-scaling, with an anticipated clustering of higher contrast stimuli towards the upper end of the performance axis. A comparable analysis (Figure 8b) reiterates that hMT+ activity

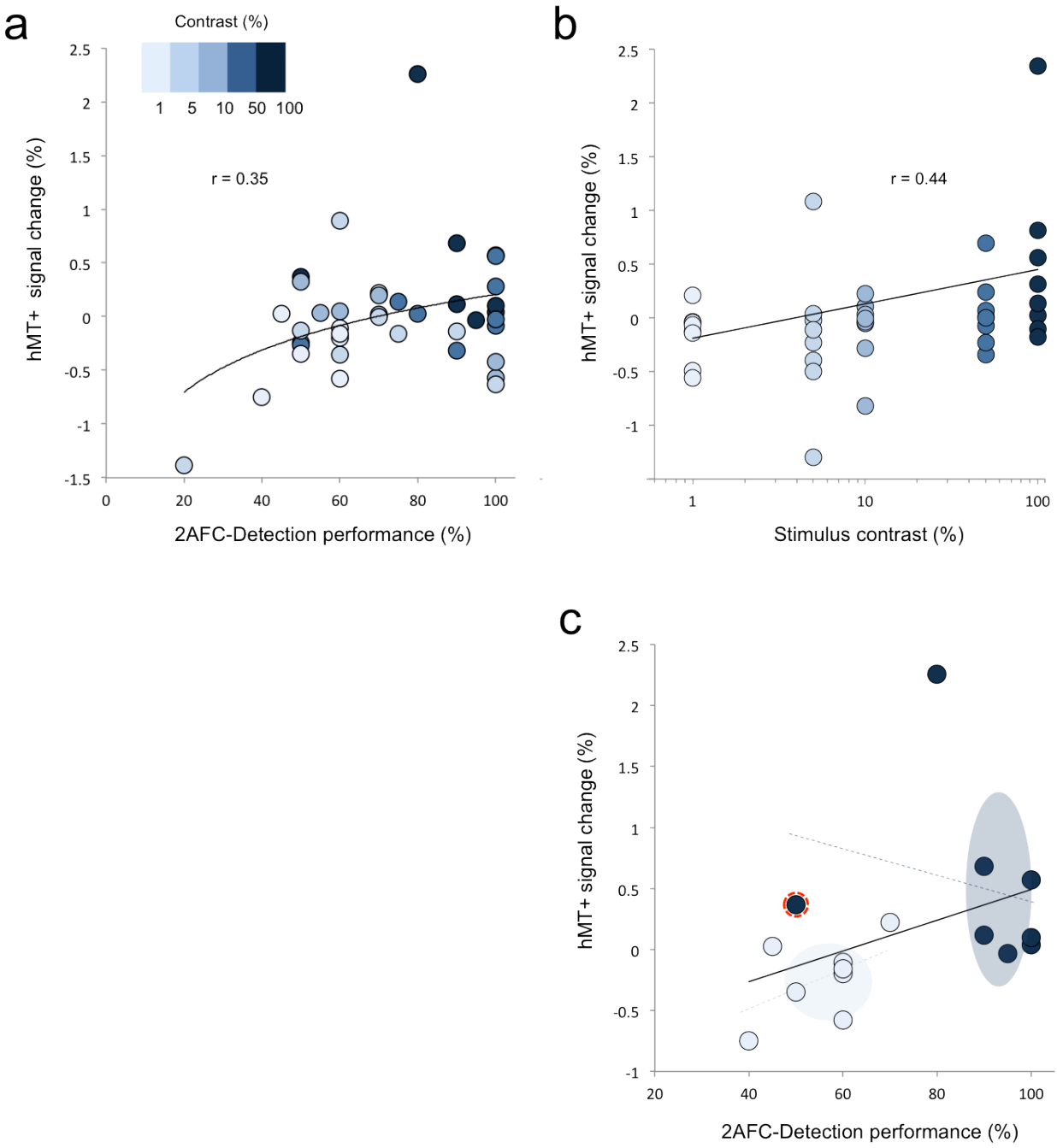

Figure 8. The relative influence of contrast and detection performance on hMT+ activity in patients. (a) hMT+ shows a significant logarithmic relationship with blindsight performance across all patients, with the contribution of stimulus contrast appreciated using a colour scale. **(b)** As previously shown, hMT+ shows a linear relationship with stimulus contrast. **(c)** Results for only 1% and 100% contrast from (a) are replotted here. The overall trend line is shown (black line, r = 0.4), as well as individual trend lines for both contrast levels (dotted coloured lines). Similar analyses were also carried out for 5%, 10% and 50% contrast (data not shown). There is clear clustering according to contrast in both the x (performance) and y (signal change) planes, illustrated by coloured ellipses representing the mean and standard deviation at each contrast level. The data-point highlighted in red demonstrates a distinct contrast-fMRI-performance relationship, which corresponds to results for the blindsight negative patient, P3.

related linearly to contrast, exhibiting a stronger correlation coefficient ($r = 0.44$, $p = 0.004$).

It is possible to completely remove stimulus contrast as a confound by examining how performance relates to hMT+ activity within identical contrast conditions (Figure 8c). No contrast levels showed a significant linear relationship between hMT+ activity and performance, with coefficients ranging from -0.74 to 0.56, and the strongest positive correlation for stimuli of 1% contrast ($p = 0.2$; Figure 8c, pale blue). Interestingly, the patient without blindsight (P3) showed relatively high signal change at 100% contrast despite poor behavioural performance (Figure 8c, red circle). From this it may be tempting to infer that fMRI activity can be driven by stimulus attributes, even in the absence of blindsight. However, significant noise in his fMRI responses make this difficult to assess in the absence of further blindsight negative patients.

3.4.6 Neural correlates of blindsight performance

Although hMT+ clearly has an important role in the perception of visual motion, it is also worth considering whether blindsight performance may reflect activity in distinct brain regions that had not been detected from analyses so far. A group analysis revealed only small regions in the ventral portion of the anterior cingulate cortex and right amygdala that showed a significant linear relationship with behavioural 2-AFC performance, but did not survive cluster correction ($p < 0.001$ uncorrected, peak $z = 3.3$, MNI: -6,32,-12; $z = 3.3$, MNI: 28,-4,-16). Thus, there were no reliable linear correlates of blindsight performance, including the visual cortex.

3.5 Discussion

These results show that after V1 is damaged, hMT+ responses to stimulus contrast are changed, with responses now increasing linearly with contrast in a pattern very similar to that seen in the healthy V1 of controls. V1 is therefore essential for the marked contrast-sensitivity and early saturation that is typical of normal hMT+ responses. This is largely attributed to its dominant input from the magnocellular (M) pathway, which is likely to pass through V1 before projecting to the extrastriate cortex. Visual signals must therefore reach hMT+ via alternative channels in patients with V1 damage. By considering the different properties of these pathways, it may be possible to uncover which is involved.

3.5.1 Blindsight performance and hMT+ activity in patients is not consistent with the M- or P- channel

The vast majority of neuronal responses in MT are from the M-channel, whilst a greater proportion of V1 neurons show responses of the parvocellular (P) variety (Maunsell et al., 1990; Movshon and Newsome, 1996). Typical responses reach half their maximum (C_{50}) around levels of 30% contrast in the P-channel, compared to <10% for the M-channel in V1 (Tootell et al., 1988; Hawken and Parker, 1984), with slightly greater sensitivity in MT M-neurons, perhaps reflecting further receptive field summation (Sclar et al., 1990). Human imaging studies produce similar results where C_{50} is close to 1% in hMT+ and 15% in V1 (Tootell et al., 1995). This is consistent with the control data presented here where C_{50} is around 2% in hMT+ and 35% in V1, although stimulus size and eccentricity affect the exact values (Sclar et al., 1990). The

V1 estimate here becomes closer to the earlier study (C_{50} = 25%) if an equivalent method of normalization is adopted, and the results are extrapolated for their smaller contrast range (1.6% - 82%).

fMRI responses in healthy controls are very different to the blind hemifield of patients. Equivalent C_{50} in hMT+ of patients is 55%, with average contrast detection threshold (C_{DT}) of 26%. This is the average contrast level above which each patient has scored significantly above chance ($p < 0.05$) using a cumulative binomial distribution. Even if one were to account for a loss of receptive field summation due to V1 damage and compare results to the LGN or normal V1, there are still clear differences. One would expect any M-driven responses to be considerably more sensitive to contrast.

P-cells have a C_{50} more comparable to the current results, but show a number of stimulus preferences that do not fit with our understanding of blindsight function. Considerable work has gone into identifying the optimal characteristics for visual stimuli to influence responses after V1 damage (Barbur et al., 1980; Sahraie et al., 2003; Sahraie et al., 2008). This led to the somewhat controversial suggestion that blindsight may be more common than first considered, and was an important consideration when selecting stimulus parameters for this study.

In particular, blindsight performance is optimal for low spatial frequencies around 1cycle/deg (Sahraie et al., 2003) and intermediate temporal frequencies 10-20Hz (Sahraie et al., 2008). Whilst not specifically assessed here, 7 out of 8 patients achieved over 80% at 2-AFC performance and elicited significant hMT+ activity using

stimulus parameters of 1.3cycle/deg and 10Hz that differ from typical P-channel preferences (Foster et al., 1985; Sclar et al., 1990; Derrington and Lennie; 1984).

Thus, in trying to evaluate which processing stream may drive blindsight performance and fMRI activity, certain features of the data are consistent with both the M- and P-channels. However, discrepancies with either the contrast sensitivity or the spatiotemporal properties of these streams make this difficult to reconcile. This may not be surprising if one considers the anatomy of these pathways, and the likelihood that both pass through V1 before reaching hMT+ (Hubel and Wiesel, 1972).

3.5.2 The K-channel could explain the results, and may reflect a network of heterogeneous pathways

The koniocellular (K) LGN neurons are equivalent in number to M-neurons, and primarily located in the interlaminar portions of the LGN (Hendry and Reid, 2000). K-neurons are often attributed to transmitting short-wavelength sensitive opponent signals from S-cones via blue-on retinal ganglion cells to cytochrome oxidase rich blobs in V1 (Livingstone and Hubel, 1982; Fitzpatrick et al., 1983). However, the presence of K-cells in nocturnal species lacking S-cones (Shostak et al., 2002), and the fact that only 25% of interlaminar neurons respond to blue-on signals in diurnal primates (White, 1998) suggests a heterogeneous population that may serve distinct roles (Rodman et al., 2001).

K-cells show a range of contrast sensitivities, more comparable to the P-channel (C_{50} 10-60%), while spatial and temporal frequency preferences are similar to M-cells (Xu

et al., 2001), particularly in koniocellular populations that are not driven by blue-on signals.

A role for K-cells has also been suggested in direct geniculate-extrastriate projections. In particular, there is increasing support for direct pathways to MT, with connections often demonstrating K-channel features such as interlaminar predominance and/or characteristic immunostaining (Fries 1981; Rodman 2001; Sincich 2004). Sincich et al. report that 70% of MT-projecting neurons in the macaque LGN are interlaminar and 63% (including M and P layers) koniocellular – defined by their neurochemical profile. The LGN-MT projection is therefore "K and intercalated-dominant", although not exclusively one or the other. A substantial number of intercalated K-cells also do not project directly to MT, but may include recipients of S-cone signals projecting to V1 (Jayakumar et al., 2013).

This supports the view of a heterogeneous K population possessing distinct responses, functions, and innervations (Hendry and Reid, 2000; Szmajda et al., 2008; Warner et al., 2010). It also represents a potential pathway for blindsight function, with preference for low spatial frequency, high temporal frequency, and contrast sensitivity more akin to the P-channel.

3.5.3 Intact hemisphere responses for the sighted field are largely normal

The similarity between blind hMT+ and normal V1 responses (but not normal hMT+) remained consistent irrespective of whether comparing to controls or to the intact

hemisphere and visual field of patients. Nevertheless, using patients as their own controls can be problematic, as a number of studies have identified impairments in the intact visual field of patients with hemianopia (e.g. Rizzo and Robin, 1996). This includes impairments in contrast sensitivity (Hess and Pointer, 1989), as well as more complex procedures such as perceptual grouping (Schadow et al., 2009). One explanation offered for these findings is an impairment of interhemispheric transfer, which may play a part in normal visual function (Rizzo and Robin, 1996; Perez et al., 2013). Although the patients all performed at ceiling for detection of 1% contrast in their intact visual field, slight differences in fMRI responses compared to controls could reflect impairments in this mechanism. However, the importance of scotoma size (and thus probably lesion size) on the degree of impairment, and the lack of any difference when comparing retinotopically equivalent responses to non-equivalent regions in a large group of quadrantanopes (Bola et al., 2013) suggest a more global effect that may reflect additional regions of cortical damage.

3.5.4 hMT+ activity may reflect retinal and perceptual experience

When evaluating whether blindsight performance or stimulus contrast were stronger predictors of fMRI hMT+ activity, the evidence weighed in favour of the low-level features. This may be surprising as hMT+ activity is often closely linked to perception rather than physical attributes (Zeki et al., 1993; Heeger et al., 1999). Indeed, a potential criticism could be that behaviour was not measured during fMRI acquisition, which would have dramatically increased scan time. Instead, stimuli were matched as closely as possible for size, position and luminance between both paradigms.

Normal contrast detection is likely to reflect a change in hMT+ signal that is at, or very close to, baseline. A similar mechanism may occur in blindsight patients, where the 95% confidence interval for contrast detection-threshold (C_{DT}) corresponds to a range that spans the zero baseline for hMT+ signal change. At a cellular level, MT neurons continue, or even increase spiking in the presence of non-conscious motion during binocular suppression (Panagiotaropoulos et al., 2012). Indeed, responses of some cells appear to reflect perceptual experience whilst those of others are dictated by retinal input (Logothetis and Schall, 1989), and this appears to be somewhat dynamic (Maier et al., 2007). fMRI reflects a heterogeneous neuronal population that may incorporate both retinal and perceptually driven responses. It is possible that activation above baseline in hMT+ reflects a significant component of perceptually driven neurons, which is sufficient to generate some sort of perceptual experience facilitating detection. This could account for the steep increase then plateau in 2-AFC performance with increasing contrast. It is, however, further complicated by the fact that these patients do not experience true conscious vision, but show variability in awareness that merits further investigation.

3.5.5 Conclusions

In conclusion, patients with V1 damage showed a linearly increasing response in hMT+ to increasing contrast. This pattern was more similar to V1 in sighted participants than the typical early saturating response of hMT+. Such response patterns are not consistent with a residual M-channel, but could be explained by input from an intact koniocellular or parvocellular pathway. In particular, this would

be in keeping with anatomical descriptions and spatiotemporal properties of the K-channel.

Chapter 4

hMT+ response to global motion in the absence of V1 resembles early visual cortex

4.1 Abstract

Motion area hMT+ shows a variety of characteristic visual responses, often linked to perception, which are heavily influenced by its rich connectivity with the primary visual cortex (V1). This human motion area also receives a number of inputs from other visual regions, including direct subcortical connections and callosal connections with the contralateral hemisphere. Very little is currently known about such alternative inputs to hMT+ and how they may drive and influence its activity. Using functional magnetic resonance imaging, the response of human hMT+ to increasing the proportion of coherent motion was measured in seven patients with unilateral V1 damage acquired during adulthood, and a group of healthy age-matched controls. When V1 was damaged, the typical hMT+ response to increasing coherence was lost. Rather, hMT+ in patients showed a negative trend with coherence that was very similar to coherence-related activity in V1 of healthy controls. This shift to a response-pattern more typical of early visual cortex suggests that in the absence of V1, hMT+ activity may be shaped by similar direct subcortical input. This is likely to reflect intact residual pathways rather than a change in

connectivity, and has important implications for blindsight function. It also confirms predictions that V1 is critically involved in normal hMT+ global motion processing, consistent with a convergent model of V1 input to hMT+. Historically, most attempts to model cortical visual responses do not consider the contribution of direct subcortical inputs that may bypass striate cortex, such as input to hMT+. This study has shown that the signal change driven by these non-striate pathways can be measured, and suggests that models of the intact visual system may benefit from considering their contribution.

4.2 Introduction

A major unsolved problem in our understanding of the human cortex is uncovering the influence of weaker pathways, which may be overshadowed by activity derived from more dominant inputs. By completely removing the influence of these driving cortical areas, the remaining innervations and responses can be studied. In the visual system, the primary visual cortex (V1) has neurons with small receptive fields that are modulated by multiple stimulus characteristics. Areas higher in the visual hierarchy tend to have larger receptive fields, but show increasing stimulus preference. This finding is supported by human studies using population receptive field mapping (Dumoulin and Wandell, 2008; Amano et al., 2009), and is consistent with a feed-forward model of converging V1 signals (Simoncelli and Heeger, 1998; Rust et al., 2006; Wang et al., 2012). However, it is likely that hMT+ also possesses direct connections to other cortical and subcortical brain regions. How these alternate inputs are organized and influence hMT+ responses remains unknown, yet is essential to understand when developing complete models of the human visual system. Here this question is addressed by investigating the response of human motion

area hMT+ following unilateral V1 damage.

In the intact human visual system, blood-oxygenation-level-dependent (BOLD) signals in motion area hMT+ increase with increasing global coherence (Rees et al., 2000; Braddick et al., 2001). This is consistent with neurophysiological reports in non-human primates, which show not only that the middle temporal area (MT) is essential for global motion perception (Newsome and Paré, 1988), but that neuronal responses in macaque MT and MST (medial superior temporal area) are approximately linearly proportional to coherence (Britten et al., 1993; Heuer and Britten, 2007). In fact, findings in the opposite direction have also been reported in human studies (McKeefry et al., 1997; Smith et al., 2006; Harrison et al., 2007), making an underlying mechanism more difficult to discern and still somewhat unresolved. Despite helpful computational models in the macaque (Rust et al., 2006), attempts to model changes in the BOLD responses remain challenging (Hallum et al., 2011; Kay et al., 2013). Early visual cortical areas, particularly V1, tend to exhibit a negative response to increasing coherence of moving dots, although this has not been as clearly demonstrated as for hMT+ and studies have also generated mixed results (Rees et al., 2000; Handel et al., 2007; Costagli et al., 2014).

One possible explanation for the differing responses in these two regions, and in different imaging studies, is the organization of V1 input onto hMT+ neurons, which may result in summation of coherent, and suppression of non-coherent motion signals. Where this is not possible or insufficient due to an extremely sparse display, the hMT+ response would not get boosted with increasing coherence and may resemble responses in early visual cortex (Harrison et al., 2007).

The influence of both striate and non-striate inputs on hMT+ responses can be assessed, by comparing neural activity in the visual cortex of patients where V1 has been unilaterally destroyed to healthy controls where both hemispheres are intact. When V1 is damaged, the response to motion coherence may be determined by interhemispheric interaction or by direct subcortical input to hMT+. Extensive research shows that certain aspects of visual information may still undergo processing and influence behaviour even without subjective awareness (Weiskrantz et al., 1974; Leopold, 2012). A number of potential pathways to extrastriate cortex have been postulated, including direct subcortical connections via pulvinar or lateral geniculate nucleus (Sincich et al., 2004; Schmid et al., 2010), as well as callosal connections with the contralateral hemisphere (Bridge et al., 2008).

Functional magnetic resonance imaging (fMRI) was used to investigate the effect of changing motion coherence on human hMT+ responses in patients with unilateral damage to V1. By comparing responses in patients elicited by stimulation of the blind field to both those found in the sighted field, and with healthy control participants, I sought to uncover the influence of inputs to hMT+ that are not normally detectable, and to confirm the role of early visual cortex in normal hMT+ responses. We predicted that unilateral V1 damage would lead to abolition of the increasing response with coherence in hMT+ of the damaged hemisphere. Instead, a dominant direct subcortical input to hMT+ should cause coherence-related responses that resemble patterns in V1.

4.3 Methods

4.3.1 Participants

Seven patients were recruited with posterior circulation stroke (n = 5), or benign tumour resection (n = 2), at least 6 months previously (range: 6 – 252 months post-lesion, ages 38 – 76). See Figure 1 for radiology and visual field schemata in all patients. Six age-matched participants (ages 25 – 68) were recruited as controls.

4.3.2 Lesion details

Lesion volumes, shown in Table 1, were estimated by creating lesion masks from patients' T1-weighted structural scans. The distribution and extent of damage was also estimated by transforming lobar and subcortical masks from the MNI and Juelich structural atlases to individual structural space using non-linear transformation. Any region of overlap between the lesion and lobe masks was measured and quantified as a percentage of the total lobe volume. The subcortical mask incorporated the thalamus (including lateral geniculate nucleus and pulvinar), striatum, and superior colliculi, with an approximate unilateral volume of 50,000mm^3. No patients showed any notable involvement of these structures in their lesions (Table 1, column 3).

The majority of patients with lesions affecting less than 20% of the occipital lobe had some small area of V1 sparing. This usually corresponded to the occipital pole, or a region of cortex far anteriorly. These regions would in turn be associated with visual field preservation at the very centre of vision, so called 'macular sparing', or in the far

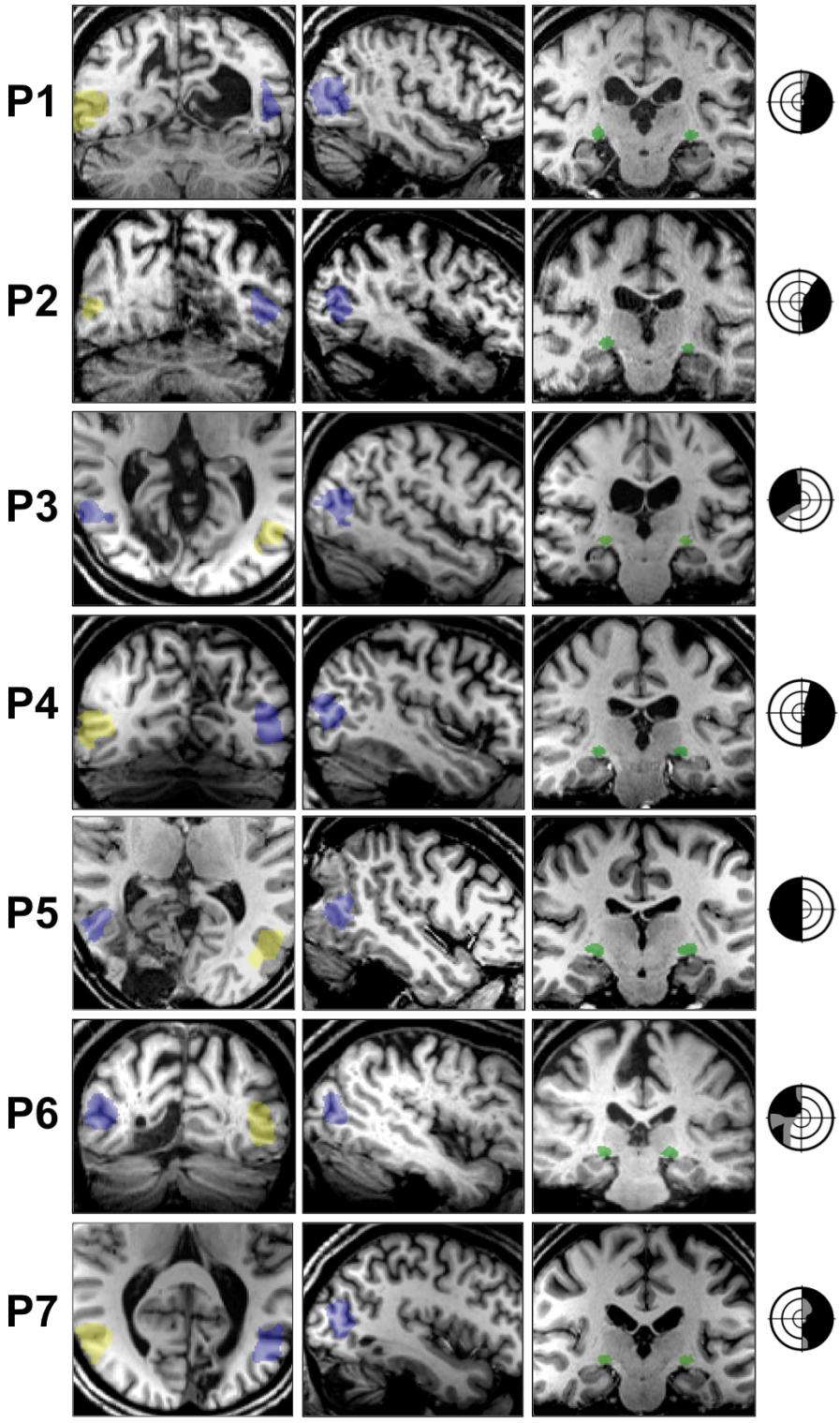

Figure 1. Patient neuroimaging and visual field deficits. hMT+ masks are overlaid on example coronal or axial (left column) and sagittal (middle column) T1-weighted slices for all seven patients (radiological convention). Ipsilesional hMT+ is shown in blue, contralesional in yellow. Coronal slices (right column) also demonstrate the intact lateral geniculate nucleus in green. The lateral geniculate nucleus was identifiable by manual inspection of the anatomical T1-weighted images (Horton et al., 1990), with a radiological brain atlas to aid identification. Visual field deficits are adapted from 30:2 threshold Humphrey visual field perimetry reports, and show dense visual field loss in black (< 0.5%) and partial loss in grey (< 2%). Stimulus location was always restricted to a region of dense visual field loss. Concentric rings represent increments in retinal position of 10 degrees, spanning the central 30 degrees.

periphery. All patients had stimuli presented to their dense region of field loss, which would not be supported by the regions of V1 sparing that were observed radiologically.

No patients showed specific damage to either the lateral geniculate nucleus, or to extrastriate region hMT+ in the damaged hemisphere. Figure 1 identifies these regions in all patients, and also suggests that the underlying white matter supporting hMT+ should be largely intact.

Patient	Total lesion volume	Occipital damage	Subcortical damage
P1	30,066 mm^3	38.48 %	0.00 %
P2	20,224 mm^3	15.56 %	0.00 %
P3	7080 mm^3	8.23 %	0.01 %
P4	8752 mm^3	9.22 %	0.00 %
P5	28,736 mm^3	33.33 %	0.00 %
P6	15,000 mm^3	14.63 %	0.00 %
P7	16,432 mm^3	15.79 %	0.10 %

Table 1. Patient lesion size and extent. No cases showed additional damage to the frontal, parietal, or temporal lobes. P7 did show evidence of additional left cerebellar hemisphere involvement, visible in Figure 1.

4.3.3 Stimuli and procedure

Stimuli consisted of an aperture of 5^o or 8^o diameter, displayed on a uniform grey background. Apertures contained moving black dots at an average density of 8 dots/^{o2}, moving at 5^o/s. Each dot was 0.075^o in diameter, and had a lifetime of 12 frames so it was not possible to infer global direction by tracking individual dots (Figure 2A).

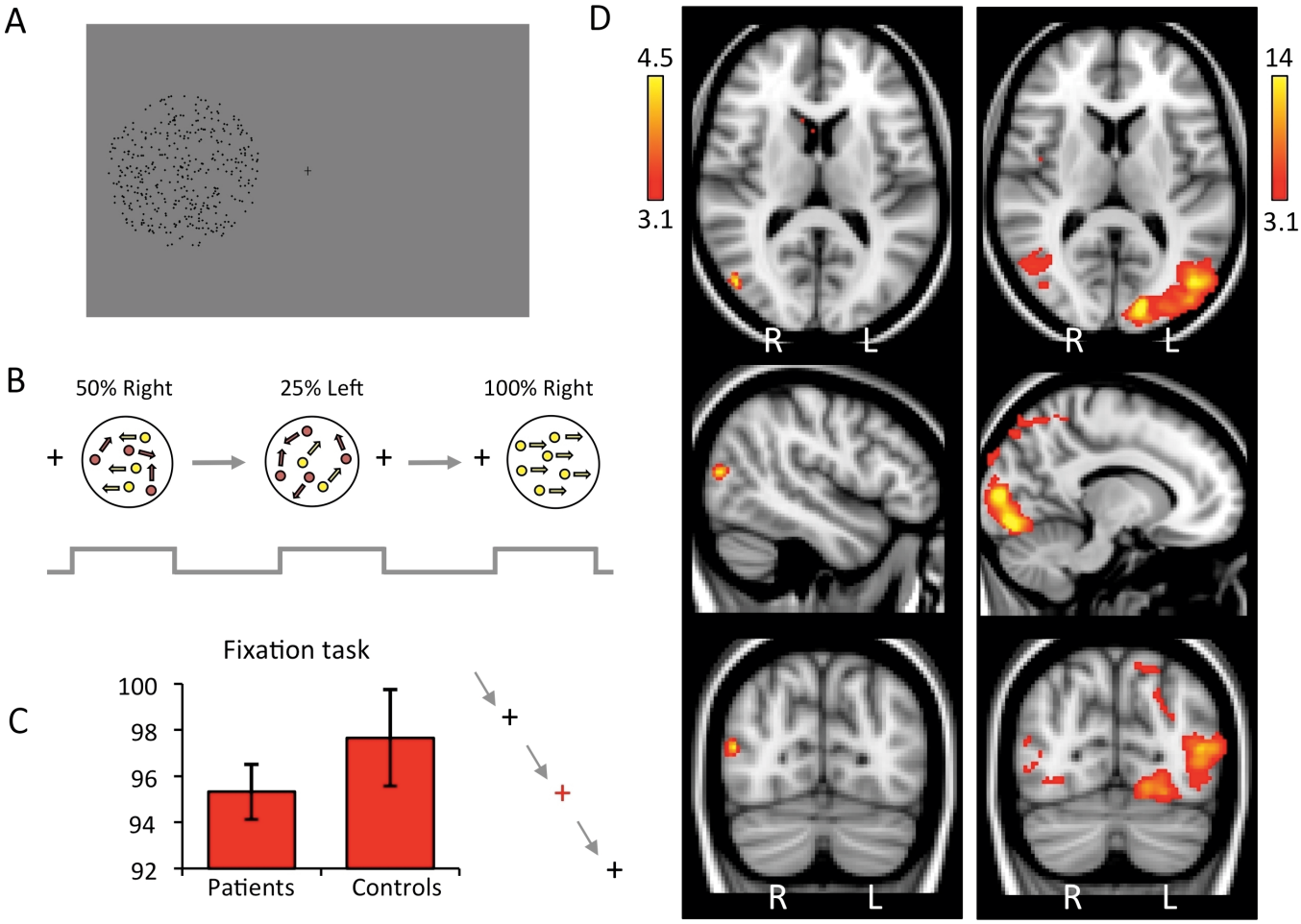

Figure 2. Experimental design, and average cortical response to visual motion in patients. (A) Experimental stimulus. Participants viewed an aperture containing moving black dots at 8 dots/^{o2} on a grey background, at least 2.5^{o} from fixation. **(B)** The stimulus was presented to each hemifield separately at six coherence levels, with a random sequence 12-block design: 0%, 12.5%, 25%, 50%, 75%, 100%. **(C)** During stimulus presentation, participants were asked to perform a simple task to detect colour changes at fixation. Median performance is shown here for patient and control groups, error bars represent standard error of the mean. All participants scored over 90% on this task. **(D)** Thresholded activation maps across all coherence levels, comparing the blind and sighted hemifields of patients. Left column: Blind 'left' hemifield stimulation. Peak zstat = 4.46, MNI coordinates: [48, −74, 14]. Right column: Patients sighted 'right' hemifield. Peak zstat = 18.4, MNI coordinates: [−14, −90, 6]. Fixed effects analysis, $p < 0.001$ uncorrected in V1 and extrastriate cortex (cluster extent threshold >10 voxels), elsewhere cluster correction threshold $p < 0.01$, results displayed on MNI standard brain.

Coherence levels were set at 0%, 12.5%, 25%, 50%, 75% and 100% for each hemifield, representing a twelve-condition block-design (Figure 2B). In each block the aperture

appeared for 16s, during which time global motion direction was changed every two seconds (8 directions: 45°, 90°, 135°, 180°, 225°, 270°, 315°, 360°). A 10s rest period followed each block. There were four runs in total, each lasting 312s.

4.3.4 fMRI acquisition and pre-processing

630 functional volumes were acquired in one single session, duration 21 min. See General Methods (Chapter 2) for detailed parameters and pre-processing methods.

4.3.5 fMRI analysis

For group analyses it was necessary to align patient brains to a uniform pathological template. Consequently, patients with lesions in the left occipital lobe (n = 4) had their structural and functional images flipped in the horizontal plane for subsequent stages of analysis. This meant that as a group (n = 7), all patients had sustained damage to the same 'right' hemisphere, corresponding to a visual field deficit on the left side of space.

4.3.5.1 Regions of Interest

In native space, average right hMT+ volume (anatomically defined) was 107 ±8.5 voxels in patients, 111 ±11.3 voxels in controls. Left hMT+ was 102 ±11.3 voxels in patients, 106 ±18.9 voxels in controls (see Figure 1). Average V1 ROI volume (functional defined) was 61 ±62.2 voxels in patients (undamaged hemisphere), and 108 ±73.9 voxels in controls.

To measure the effect of motion coherence on BOLD activation, a data-driven model was felt to be most sensitive to any differences between patients and controls. Each of the 12 fMRI conditions were entered into the general linear model (GLM) as separate

explanatory variables (see General Methods, Chapter 2 for further details). All graphs, signal change calculations, and correlation statistics were therefore calculated for each condition relative to baseline, using data from participants' native space. An additional analysis was performed to measure average BOLD response across all coherence levels for each hemifield separately.

4.3.5.2 Model Fitting

For model fitting, signal change in contralateral hMT+ and V1 ROIs in controls were averaged and normalized, such that the sum of all points was equal to zero. Integer values representing points along these curves were then entered as weights into a higher-level general linear model, along with contrast images for all participants. Fixed-effects analyses were carried out for each hemifield separately, in control and patient groups. In the patient group, this analysis was repeated using a mixed effects model to determine whether individual outliers may have skewed the results. A statistical threshold of $p < 0.001$ uncorrected (cluster extent threshold > 10 voxels) was used to test for significance within V1 and extrastriate cortex, for which there were a priori hypotheses. Elsewhere correction for multiple comparisons was made using a cluster threshold of $p < 0.01$. For this purpose, anatomically-defined probabilistic maps (Juelich atlas implemented in FSL) were used to define these regions of interest (bilateral V1 and extrastriate cortex including V2 – V5/hMT+), total volume = 15,800 mm^3.

4.4 Results

4.4.1 Motion in the blind hemifield elicits significant contralateral cortical activation

To quantify responses to visual motion, activation (averaged across coherence levels) relative to baseline fixation was measured for patients and controls. Control participants showed extensive activation throughout the visual cortices (not shown). This pattern was similar to stimulation of the sighted hemifield of patients (Figure 2D, right side), with activity in V1 and hMT+ contralateral to the stimulus, in addition to ipsilateral hMT+ activity. When the blind field was stimulated, no discernable activity was seen in early visual cortices. There was, however, significant activation of contralateral hMT+ (Figure 2D left column), albeit to a considerably reduced spatial extent and percentage signal change compared to the sighted hemifield. The absence of significant activation in ipsilateral hMT+ or ipsilateral V1, suggests few, if any, eye movements towards the stimuli.

4.4.2 Contralateral hMT+ shows an unusual pattern of activity during blind hemifield stimulation

Since V1 and hMT+ exhibit different patterns of response to motion coherence (Braddick et al., 2001; Handel et al., 2007; Costagli et al., 2014), the percentage BOLD signal change was extracted at each coherence level within regions of interest corresponding to these two visual areas.

In controls and in the sighted hemifield of patients, activity in contralateral hMT+ showed a significant positive relationship with motion coherence, $r = 0.44$ (controls, $p < 0.001$), and $r = 0.33$ (patients, $p = 0.03$). This was very much as expected from previous research into motion coherence (Rees et al., 2000). However the relationship was not strictly linear, and followed a sigmoid-pattern that was consistent across participants, with strong correlation between the two groups ($r = 0.91$, $p = 0.01$). Figure 3A (upper row) shows the pattern of response in hMT+ in controls and patients to contralateral stimulation.

When the blind hemifield of patients was stimulated, activity in contralateral hMT+ no longer showed a positive relationship with increasing coherence. Instead there was a non-significant negative trend ($r = -0.22$, $p = 0.16$, see Figure 3A). The slope of this fitted regression line differed significantly from that fit to the (positive) pattern in the sighted field ($z = 2.5$, $p = 0.01$). This was fairly consistent across participants, and showed no correlation with 'normal' hMT+ activity patterns in controls ($r = -0.02$, $p = 0.95$) or patients own sighted hemifield ($r = -0.13$, $p = 0.4$).

4.4.3 Ipsilateral hMT+ response for the sighted hemifield is intact despite V1 damage in the same hemisphere

Some hMT+ neurons, particularly those in MST (Huk et al., 2002) have large receptive fields that cross the vertical meridian into ipsilateral visual space. Indeed, some studies on patients with V1 damage have indicated enhanced ipsilateral representation in the damaged hemisphere (Nelles et al., 2002; Nelles et al., 2007). Determining the response of hMT+ in the damaged hemisphere raises an important question about whether the altered pattern to motion coherence is an inherent property of that area. An ipsilateral response for the

sighted hemifield is likely to be processed by the intact V1, and propagated across the corpus callosum to the damaged hemisphere. The input would, therefore, receive processing beyond that in subcortical regions.

In controls, where response to coherence in the ipsilateral hemisphere has not been systematically investigated in the past, a positive sigmoid relationship was found in hMT+, similar to that seen on the contralateral side $r = 0.23$ ($p = 0.048$, Figure 3A lower row). As expected, the amplitude of signal was generally lower than contralateral responses. Furthermore, the peak signal in left hMT+ was slightly anterior to that with contralateral stimulation (ipsi: −44, −70, 6 vs. contra: −40, −74, 6), which may be indicative of the slightly anterior location of human MST relative to MT (Smith et al., 2006).

The same positive sigmoid pattern was also present in the sighted field of patients, where ipsilateral hMT+ activity (which was still intact) appeared unaffected by the presence of damage to V1 within the same hemisphere ($r = 0.53$, $p < 0.001$, Figure 3A lower row), and correlated highly with ipsilateral activity in the control group ($r = 0.93$, $p = 0.007$). Notably, this positive linear component was significantly different from the negative trend fit to the same ROI during stimulation of the blind hemifield ($z = 3.4$, $p < 0.001$). This implies that it is the input to hMT+ that is critical in driving its response pattern. In this case, input most likely comes from the healthy hemisphere, perhaps via interhemispheric callosal connections (which likely involves healthy V1).

4.4.4 Ipsilateral hMT+ response for the blind hemifield appears abnormal

For the blind hemifield of patients, I was interested in whether activity in ipsilateral hMT+ more closely resembled healthy positive sigmoid patterns, or the negative trend seen in contralateral hMT+. This would allow us to infer specifically whether V1 in the opposite hemisphere was involved in driving ipsilateral hMT+ response patterns. In fact, ipsilateral hMT+ activity remained very close to baseline across all coherence levels (Figure 3A), and showed neither a positive nor negative trend with increasing coherence ($r = -0.005$). The lack of any significant response may indicate that (intact) contralateral V1 is critical for ipsilateral hMT+ patterns, however this cannot be confidently stated based on the current data.

4.4.5 Parametric analysis using a data-driven V5 model does not fit hMT+ activity in the blind hemisphere

The normalized mean signal change at each coherence level within hMT+ of control participants was used to generate a data-driven model summarizing the relationship between activation and coherence in contralateral hMT+ of the healthy control brain, illustrated in Figure 3B. Obviously since the model was generated from hMT+, a significant response in this area must follow. However this method allows us to both quantify the specificity of this response pattern, and test for similar patterns in independent data from patients. The model was utilized as the basis for a parametric general linear model analysis in both groups, carried out separately for each stimulated hemifield. Individual contrasts of parameter estimates for each participant (for example 100% coherence versus baseline) were entered, with explanatory variables weighted according to the model being tested. Additional explanatory variables representing the average response for each participant across conditions were included as regressors of no interest.

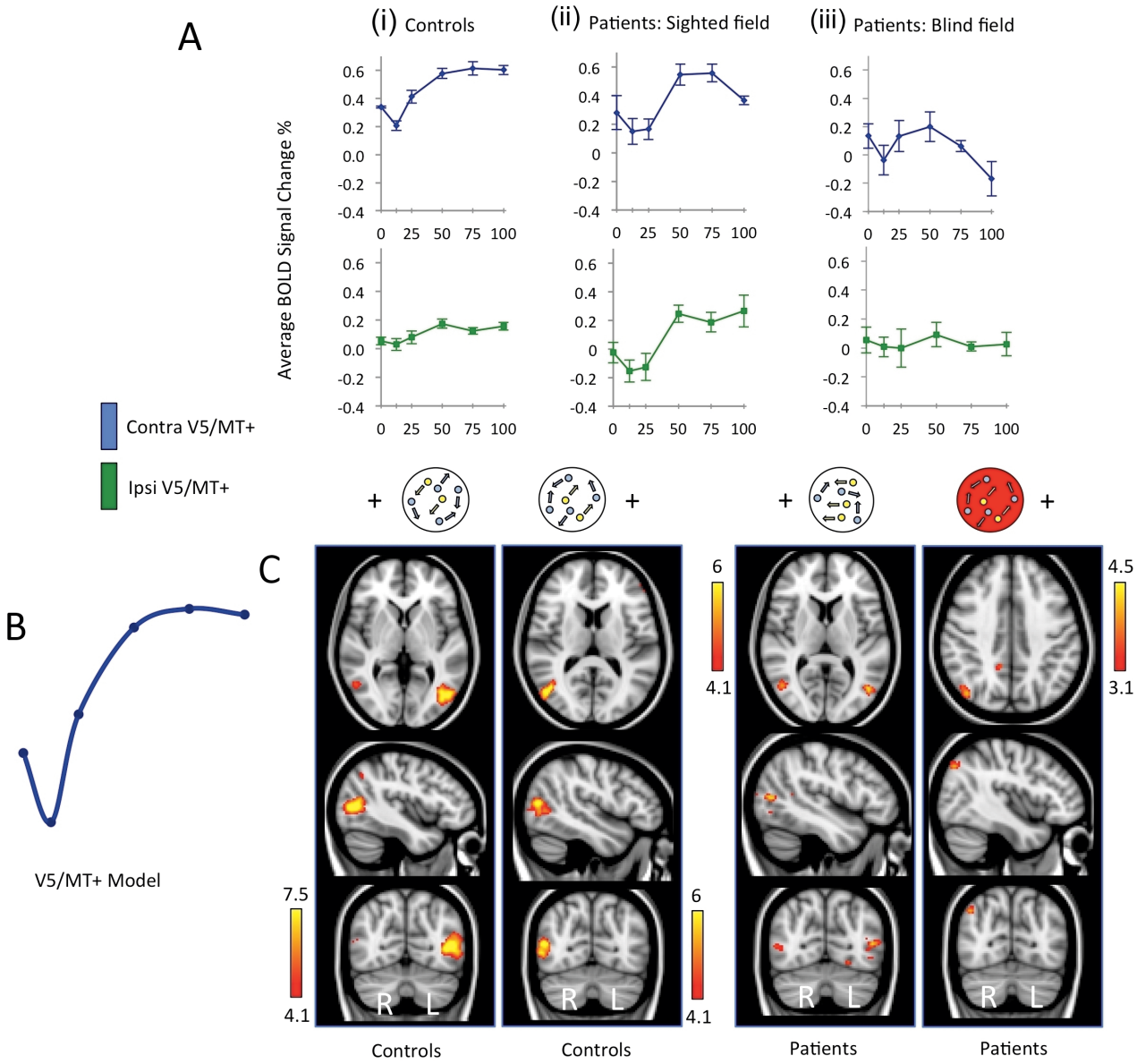

Figure 3. hMT+ response to motion coherence in patients and controls. (A) Graphs show average % BOLD signal change in anatomically-defined hMT+ ROIs as a function of coherence for controls (i), patients' sighted hemifield (ii), and patients' blind hemifield (iii). Blue lines represent contralateral hMT+ signal change, green represent ipsilateral. Error bars display normalized standard error of mean. **(B)** Schematic depiction of the demeaned data-driven hMT+ model for fMRI response to motion coherence. **(C)** Thresholded activation maps in controls and patients, highlighting regions with a significant relationship with coherence according to the V5 model in (B). Results for each hemifield are shown separately. The red aperture signifies results for the blind hemifield. Fixed-effects analysis, corrected cluster threshold $p < 0.05$, pre-threshold masking applied to V1 and extrastriate cortex.

Figure 3C indicates the regions showing significant activation that follows the sigmoidal shape. The left panel shows the response in control participants who have significant activity in contralateral hMT+ (and ipsilateral in the case of right hemifield stimulation, see Table 2 for details). In addition, significant activity was identified in medial and lateral regions of the frontal pole (Table 2). The right panel indicates significant regions of activity in patients. When the stimulus is in the sighted field, activation in bilateral hMT+ fit well with the control model ($p < 0.0001$). However, for the blind 'left' hemifield, no activity corresponding to this model was seen in hMT+ or early visual cortex. This remained the case even when a more liberal statistical threshold of $z = 2.3$ was used. Instead, two small clusters were identified in right inferior parietal lobule (IPL) and right posterior cingulate gyrus (Figure 3C, Table 2), perhaps reflective of the more downstream position of the IPL in the dorsal visual stream (Ungerleider and Mishkin, 1982). This suggests that the response pattern to changing coherence in hMT+ of patients has a different pattern to healthy hMT+. When V1 is damaged, the input underlying responses in this area may come directly from subcortical regions (Sincich et al., 2004). We therefore also compared the response pattern in patients to V1 responses in control participants, where substantial input comes direct from the thalamus.

4.4.6 Healthy V1 shows a characteristic response to coherence, which is highly correlated to contralateral hMT+ in patients

The motion stimulus significantly activated contralateral V1 in controls and in the sighted hemisphere of patients. Response magnitude as a function of coherence in control participants, quantified by percent change in BOLD signal, is shown in Figure 4A. The left graph indicates a weak negative correlation overall ($r = -0.12$), with a significant decrease in signal change in the coherent condition compared to random motion (paired $t = 3.4$, $p =$

CONTROLS	x	y	z	z-stat		x	y	z	z-stat
hMT+ Model: LHF					**hMT+ Model: RHF**				
Right hMT+	50	-70	12	6.67	Left hMT+	-42	-68	6	10.31
Left frontal pole	-50	38	10	4.19	Right hMT+	54	-60	2	5.32
					Left frontal pole	-4	58	18	4.69
V1 Model: LHF					**V1 Model: RHF**				
Right V1	6	-92	2	4.51	Left V1	-18	-66	6	4.01
Right inferior parietal lobule	50	-66	30	4.21	Left insula	-36	-22	-2	4.10
					Right lingual gyrus	14	-54	0	4.20
PATIENTS	**x**	**y**	**z**	**z-stat**		**x**	**y**	**z**	**z-stat**
hMT+ Model: Blind LHF					**hMT+ Model: Sighted RHF**				
Right inferior parietal lobule	42	-72	40	4.16	Left hMT+	-46	-70	8	5.80
Right posterior cingulate gyrus	12	-46	36	3.79	Right hMT+	50	-64	6	5.63
V1 Model: Blind LHF					**V1 Model: Sighted RHF**				
Right hMT+	54	-68	12	3.82	Left inferior parietal lobule	-42	-60	42	3.66
					Left precuneus	-10	-58	40	3.57

Table 2. MNI coordinates and z-statistics for brain areas demonstrating a significant relationship with motion coherence, according to the hMT+ or V1 models. Only the most significant peak within each area of activation is reported. A statistical threshold of $p < 0.001$, uncorrected for multiple comparisons, was used within V1 and extrastriate cortex (cluster extent threshold >10 voxels). Elsewhere correction for multiple comparisons was made with a cluster threshold of $p < 0.01$, fixed-effects analysis.

0.006). This relationship again appeared non-linear, with a nadir in activity for coherence levels of 12.5%.

In patients, this pattern of negative association with coherence seen in control V1 was also present in hMT+ on the side without functioning V1. There was a strong and significant correlation between control participant V1 activity and the pattern of activity in hMT+ on the lesion side during blind hemifield stimulation ($r = 0.98$, $p < 0.001$). This relationship is shown in Figure 4B and is in stark contrast to the absence of any correlation with normal hMT+ patterns.

4.4.7 Parametric analysis using a data-driven V1 model fits hMT+ activity in the blind hemisphere

Using an analogous method to that illustrated in Figure 3, a normalized V1-data driven model was generated from contralateral V1 responses in control participants, and applied to both control and patient groups (Figure 4C). This V1 model shows an initial dip similar to the hMT+ model, but then shows a considerable decrease with higher coherence levels. In control participants no regions of extrastriate cortex showed activity conforming to the V1 model. However, there was such activation in the left insula, which has previously been shown to exhibit a negative linear relationship with motion coherence (Rees et al., 2000), and right inferior parietal lobule (Table 2).

When the V1 model was applied to the blind field of patients, the only occipital area conforming to this pattern was contralateral cortex corresponding to hMT+ ($z = 3.82$, $p < 0.001$ uncorrected. See Figure 4C, and Table 2 for coordinates). No other region showed a significant association with this model. This finding remained significant when analysed

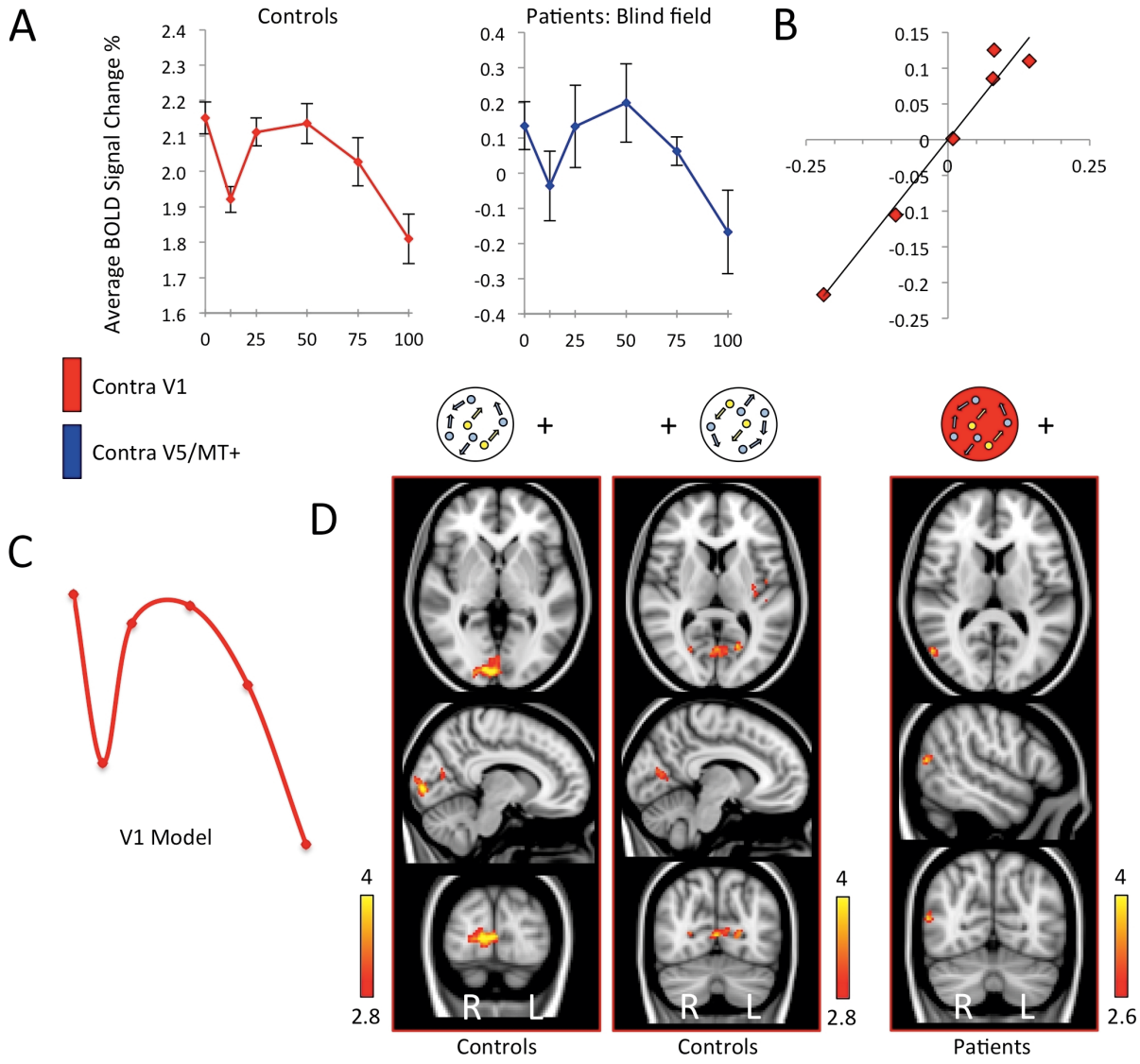

Figure 4. V1 response to motion coherence in controls, and the cortical regions active according to this V1 model in patients and controls. (A) Average % BOLD signal change as a function of stimulus coherence. The left graph (red) shows the response pattern in contralateral V1 of control subjects, averaged across hemispheres. The right graph (blue) shows the activation in hMT+ of the blind hemisphere in patients. Error bars represent normalized standard error of the mean. **(B)** Correlation of normalized signal change in contralateral hMT+ for patients blind hemifield, versus contralateral V1 activation in healthy controls, $r = 0.98$, $p < 0.01$. **(C)** Schematic of demeaned data-driven V1 model from control subjects for fMRI response to motion coherence. **(D)** Active brain regions showing a significant relationship with motion coherence according to the V1 model in (C). Results for each hemifield are shown separately for controls, and patients' blind hemifield (highlighted by the red aperture). Fixed-effects analysis, corrected cluster threshold $p < 0.05$, pre-threshold masking applied to V1 and extrastriate cortex.

using a mixed effect model ($z = 3.52$, $p < 0.001$), implying the result to be robust across the patient group.

4.4.8 A weighted-linear model can accurately predict hMT+ response

Finally, I had also predicted that weaker non-striate projections to hMT+ may normally contribute to average neuronal responses, but are likely to be overshadowed by the much greater input from V1. This study has now revealed that when V1 is absent due to damage in adulthood, hMT+ responds in a pattern typical of (normal) early visual cortex. According to the prediction, this pattern of activity should also contribute to average hMT+ responses in healthy control subjects, who also possess a direct subcortical connection, but whose activity is normally dominated by input from V1. Indeed, I was able to generate a highly predictive model of control hMT+ BOLD response patterns by simply taking a linear combination of:

(1) A direct linear relationship between signal change and coherence, as predicted from studies measuring neuronal electrophysiology responses in MT.
(2) The average response pattern in patient hMT+ when V1 is damaged (postulated to reflect direct, residual subcortical input).

Using this model, it is possible to account for 98% of the variance in control hMT+ fMRI signal change (see Figure 5). This equation can also be rearranged to model the abnormal hMT+ responses in patients, defined by a loss of the positive linear component in control hMT+ responses, which also accurately predicts the data ($R^2 = 0.93$), or indeed the positive linear component itself ($R^2 = 0.98$).

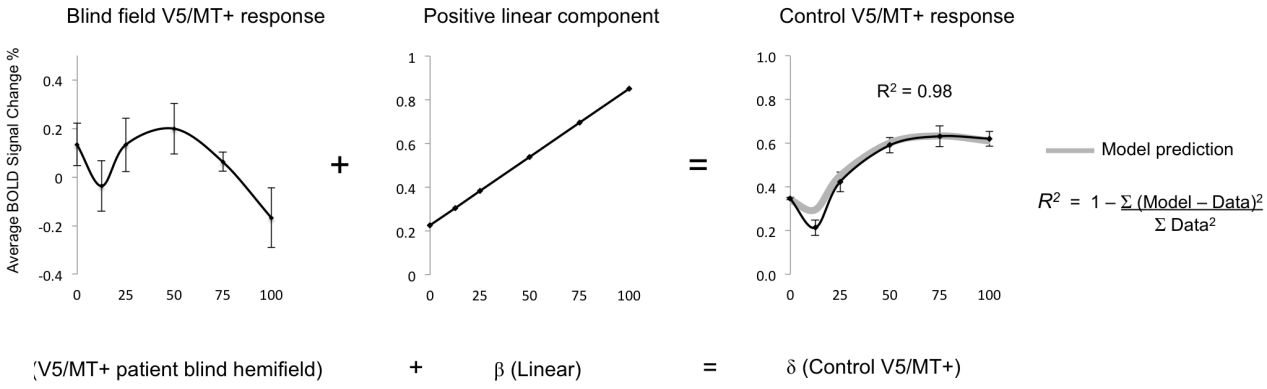

Figure 5. Activity in hMT+ can be accurately predicted from a weighted-linear model. hMT+ activity in patients during blind hemifield stimulation can be combined with a simple positive linear component to predict BOLD signal change in hMT+ of controls to a high degree of precision. Relative weightings are signified here by α, β, and δ symbols.

BOLD signal is an indirect measure of neural activity that reflects a population average and is likely to combine signals even at the level of a single voxel. Separately driven signals within the same region of interest may be embedded in average BOLD responses, but may only be revealed if the individual signal components are fully understood.

4.5 Discussion

This study demonstrated that area hMT+ has a different response pattern to motion coherence when V1 is damaged and can no longer modulate input to this area. The similarity to response patterns in V1 measured in control participants suggests that it may be direct subcortical input that shapes the motion coherence response in patients under these conditions.

It is already recognized that certain aspects of motion processing in hMT+ are retained in the absence of V1. Neurophysiological studies in non-human primates show that a considerable proportion of direction selective neurons retain their responsiveness following striate cortex removal or cooling, even though strength and selectivity of responses is decreased (Rodman et al., 1989; Girard et al., 1992). Thus, V5/MT either has its own intrinsic circuitry sufficient to produce directionally selective responses from non-selective input, or can rely upon direction-selective input from regions other than V1, such as superior colliculus and pulvinar (Rodman et al., 1986; Kato et al., 2011). Whilst the superior colliculus appears important for MT motion responses after striate removal, direction selectivity in the pulvinar is eliminated after striate cortex removal (Bender, 1983), and in the superior colliculus is more attuned to relative rather than absolute direction (Davidson and Bender, 1991). Indeed, the organization of such non-striate pathways remains largely unknown. Whether they can support more complex V5/MT properties such as global motion processing remains to be determined.

4.5.1 The majority of studies suggest a linear relationship between motion coherence and hMT+ response

In macaque V5/MT, many direction-selective neurons show an approximately linear relationship between moving visual stimuli with increasing motion coherence and firing rate (Britten et al., 1993). Of the remaining neurons, roughly equal proportions demonstrate either negatively or positively accelerating nonlinearities, of variable strength. In human studies, Positron emission tomography, magnetoencephalography and fMRI have offered a more indirect and global measure of hMT+ neuronal populations, and have largely concurred that activity increases with coherence (Rees et al., 2000; Braddick et al., 2001; Handel et al., 2007; Becker et al., 2008; Aspell et al., 2005; Nakamura at al., 2003;

Cheng et al., 1995). Given the range of neuronal subtypes and experimental protocols, consistent findings of a linear relationship are perhaps surprising. Indeed, on closer inspection some studies have found a dip in activation at low coherence levels similar to that seen in the current data (Handel et al., 2007; Siegel et al., 2007), which may be missed if fitted to a purely linear model. In this study, it was shown that fMRI activity in hMT+ may reflect an average of different response patterns, one of which may represent a direct linear relationship with coherence.

There are also several studies reporting a negative relationship with coherence in human hMT+ (McKeefry et al., 1997; Harrison et al., 2007; Previc et al., 2000), or no difference between coherence and noise (Smith et al., 2006). Two factors in particular may be important in defining such a relationship: stimulus size and density. A small 4-8^{o} diameter aperture is typically associated with a positive relationship (Rees et al., 2000; Becker et al., 2008) whilst stimuli subtending a wider visual field (greater than 20^{o}) have generated the opposite pattern (McKeefry et al., 1997; Harrison et al., 2007; Previc et al., 2000). This may occur because some direction-selective neurons in V5/MT exhibit surround inhibition (Tanaka et al., 1986; Raiguel et al., 1995). Therefore a wide field containing coherent motion may stimulate directionally-selective inhibitory surrounds, whilst smaller apertures fall solely within the 'classical receptive field', eliciting no suppressive signals (Tanaka et al., 1986). However, this explanation alone can neither account for all negative studies, nor those reporting a positive relationship using large stimuli (Becker et al., 2008; Aspell et al., 2005; Nakamura et al., 2003; Cheng et al., 1995).

Similarly, in the majority of cases, sparse stimuli ≤1dot/^{o2} result in a negative response in hMT+ (McKeefry et al., 1997; Smith et al., 2006; Harrison et al., 2007; Previc et al., 2000). The average density used here was considerably greater, at 8 dots/^{o2}, and associated

with a positive response pattern. A weak switch in direction was also demonstrated in one study comparing fairly sparse (1dot/^{o2}) to dense (6 dot/^{o2}) parameters (Becker et al., 2008). Two exceptions used comparable 60^{o} sparse displays and found greater activity with coherence in regions corresponding to hMT+ (Nakamura et al., 2003; Cheng et al., 1995), restricted in one study to the right hemisphere (Cheng et al., 1995). It is possible that in these two cases, the very large stimuli led to greater activation in MST, known to possess much wider receptive fields (Tanaka et al., 1986) and respond particularly strongly to patterns of global motion such as rotation and expansion (Heur and Britten, 2007).

In the macaque, average receptive field size in V5/MT ranges from 0.6 – 8^{o} diameter at equivalent eccentricities to the stimuli used here (up to 12 degrees; Albright and Desimone, 1987). Therefore if one considers a similar sized sparse display such as Harrison et al. (2007) with dots positioned an average of 5 degrees apart, both V1 neurons and most of those in hMT+ would be stimulated by just one dot per receptive field. It may therefore not be surprising that with such a sparse display, hMT+ responds in the same way as V1 even in the presence of 100% coherence.

4.5.2 Healthy V1 shows a distinct characteristic response to motion coherence

We identified a weak negative trend with coherence in V1 of healthy participants, which was strongly correlated with the pattern of coherence-related activation in hMT+ contralateral to the blind visual field in patients. Whilst V1 has not been investigated as extensively as hMT+ in the past, similar negative responses have been reported in several human imaging studies (Braddick et al., 2001; Harrison et al., 2007; Handel et al., 2007; Costagli et al., 2014). Neurophysiological research has not examined this specifically, but

V1 direction selective cells fire when a preferred direction component is present in the receptive field and do not show significant suppression if opposing motion is also present (Snowden et al., 1991). It has also been suggested that surrounding V1 neurons can show an enhanced response in the presence of opposing motion, due to the presence of increased contrast energy (Heeger et al., 1999). Thus if a single neuron fires similarly with coherent or incoherent motion, it may be inferred that the negative pattern in fMRI reflects a population average, perhaps influenced by the range of directions of motion present within any given voxel and the proportion of directionally selective cells that are activated over time.

In the current experiment non-coherent stimuli had completely random trajectories of motion. Conversely, coherent stimuli moved in eight directions (45^{o} apart), lasting 2 s each. It is possible that over time, and in regions that do not exhibit significant summation and/or subtractive inhibition, a greater proportion of directionally-selective neurons were activated by the greater range of directions during incoherent conditions. This situation would be similar to Braddick et al. (2001) and Handel et al. (2007) which both compared coherent motion in two directions to random noise, and even Harrison et al. (2007) who used two directions in the coherent condition, compared to four in the incoherent condition. An alternative explanation is that top-down signals from higher visual areas cause suppression, perhaps due to prediction error (Harrison et al., 2007; Handel et al., 2007). This could still account for the results in patients if, for example, back-projections arise from the posterior cingulate gyrus where significant activity was seen in the hMT+ model (Table 2), as in Harrison et al. (2007). The current data, however, do not allow these possibilities to be distinguished.

4.5.3 Differences between neural responses to motion in V1 and hMT+

Both neurophysiological and human neuroimaging studies show that motion related responses of hMT+ differ qualitatively from those in V1 in several respects. In particular responses in hMT+ appear to correspond more closely to visual perception than those in V1 (Shadlen and Carney, 1986). One example particularly relevant to the current data is that neurons in the two areas typically respond differently to global and component features of motion. In the rhesus monkey, approximately 30% of neurons in V1 are direction-selective and respond largely to motion of the components within complex patterns rather than the pattern as a whole (Snowden et al., 1991; Movshon and Newsome, 1996; Snowden et al., 1992). This has led to the suggestion that these cells act as 'local motion energy filters' or even a 'gateway' responding to particular bandpass limits for orientation, spatial and temporal frequency, serving to minimize noise from incoherent motion in hMT+ (Handel et al., 2007). In contrast, global motion computation appears to rely on combining of local component measures across space and time (Reppas et al., 1997), and has been suggested to occur after V1, perhaps within MT itself (Movshon and Newsome, 1996; Huk and Heeger, 2002).

How these 'global' receptive fields in hMT+ are informed by V1 signals is described via a motion opponency or linear-nonlinear cascade model in the macaque (Simoncelli and Heeger, 1998; Rust et al., 2006; Tsui and Pack, 2011). However, further work is needed to translate this to the human visual system and the interpretation of fMRI BOLD signal change. Here it was shown that V1 is essential to generate a positive relationship with coherence in contralateral hMT+. Identical stimulus parameters presented in patients and controls elicited very different patterns of activity, whose fundamental difference was the

presence of a positive linear component (Figure 5). Furthermore, the same ipsilesional hMT+ voxels in patients responded in opposing directions dependent upon whether the blind or sighted visual field was stimulated. This implies that a normal response to global motion in hMT+, unlike direction-selectivity, does appear to depend upon contralateral V1 and cannot be derived via direct subcortical pathways. Instead, the relative receptive field size and a hierarchical model of converging inputs can be used to explain the response to global motion in these results and the majority of studies described. This accounts for the positive linear relationship with coherence, however I have also shown that non-global components may contribute to average hMT+ responses. These may reflect direct subcortically driven responses, and/or a proportion of neurons that lack summation of V1 signals.

The simplest explanation of the role of V1 presented here is that it is the loss of V1 input to hMT+ that alters the pattern of activity to motion coherence. However, one cannot exclude the possibility that the critical visual area for the motion coherence response is not V1, but is perhaps modulated by V1. The lack of other extrastriate visual areas that exhibit patterns of response consistent with either V1 or hMT+ (Figures 3 and 2 respectively) makes this interpretation even less likely.

There is an alternate theory that feedback from areas such as hMT+ to V1 is required for processing local details, which cannot be computed by the large receptive fields of extrastriate neurons (Bullier, 2001; Hochstein and Ahissar, 2002). Those models suggest that awareness of global motion features would precede awareness of local detail, computed in V1. Our findings are not entirely consistent with this theory, since in the absence of V1, normal global processing in hMT+ is no longer possible. Rather, the

current data are more consistent with two TMS studies suggesting two critical periods of V1 activity; one preceding and one postdating hMT+ activity (Silvanto et al., 2005a; Silvanto et al., 2005b). In this scenario, V1 may be required for the initial computation of local details, before feeding forward to hMT+ for global motion processing. Subsequent feedback to V1 may then induce a conscious experience. Although it is not possible to uncover the latter point from the current study, reciprocal connections may be important for conscious perception, impaired in patients with V1 damage. Blindsight, by definition, occurs without visual awareness, and may be more akin to the intermediate reports of participants in the TMS study, when V1 was stimulated before V5. In this condition, even though phosphenes remained largely stationary, participants were not always confident that they were not moving (Silvanto et al., 2005a).

4.5.4 Subcortical pathways carry motion information directly to hMT+

hMT+ activation in the presence of (unilateral) V1 damage demands that a mechanism is in place to relay information from corresponding regions of the retina to extrastriate cortex. Numerous non-human primate studies have suggested that direct routes may exist from the lateral geniculate nucleus (Sincich et al., 2004; Schmid et al., 2010) or superior colliculus and pulvinar (Rodman et al., 1986; Kato et al., 2011; Lin et al., 1974; Trojanowski and Jacobson, 1976; Benevento and Rezak, 1976; Maunsell and Van Essen, 1983). Such subcortical pathways could certainly account for the finding of hMT+ activation in patients, in particular given that patterns change to resemble early visual cortex of healthy controls. Very little is known about the organization of non-striate inputs to hMT+. However, subcortical input may follow a similar organization to the geniculate innervation of V1, with a lack of convergence across receptive fields that is likely to be important in the projections between V1 and hMT+. It has been postulated that similar alternate

pathways may account for the phenomenon of blindsight in humans (Weiskrantz et al., 1974; Cowey, 2010), and techniques such as latency analysis of visual evoked potentials, EEG and fMRI signals have been used to infer such connectivity (ffytche et al., 1995; fftyche et al., 1996; Gaglianese et al., 2012) as well as MRI diffusion-based tractography (Bridge et al., 2008; Bridge et al., 2010). All of the patients in this study sustained cortical damage during adulthood, when one may expect that the potential for plasticity is considerably reduced. Furthermore, approximately half of cases underwent testing within one year of lesion-onset. When considered in light of the breadth of evidence for a direct subcortical connection to hMT+, it is suggested this is most likely to represent intact residual pathways in the healthy visual system, rather than a change in connectivity.

4.5.5 Conclusions

This study has shown that in the absence of V1, hMT+ response to global motion coherence resembles patterns in primary visual cortex, perhaps shaped by similar direct subcortical input. It has also confirmed predictions from animal studies that V1 is essential for typical hMT+ global motion responses. It is likely that a direct subcortical pathway to hMT+ does exist in the intact visual system, but may normally be overshadowed by the overwhelming input from V1. By studying patients with V1 damage, it is possible to reveal their influence, which may be useful in developing more accurate models of visual cortex responses.

Chapter 5

The presence or absence of blindsight affects sensitivity of hMT+ to speed of motion

5.1 Abstract

The response of motion area hMT+ to increasing stimulus speed is well-described, and is often depicted as an inverted-U pattern. However, it remains unclear whether this reflects intrinsic properties of hMT+ neurons, or relates to the pathway characteristics underlying these responses. One prevailing theory is that slow motion is mediated via V1, and should therefore not be possible when V1 is damaged. The current study sought to address this controversial theory by measuring behavioural performance and hMT+ responses to increasing speed for the first time in patients with V1 damage. It was found that only blindsight positive patients retained a normal hMT+ response to speed, including slow motion, which was similar to measures of psychophysical performance. Furthermore, blindsight positive patients showed significant activity in the ipsilesional LGN, which was distinct from speed-sensitive responses in healthy controls and highly correlated with hMT+ activity. This suggests that when V1 is damaged, LGN responses become dominated by a distinct neuronal subpopulation. It also shows that speed-sensitivity in hMT+ is independent of V1, but may reflect a direct geniculate input in blindsight positive cases.

5.2 Introduction

The optimal speed associated with visual motion responses tend to vary throughout the visual hierarchy. In the early visual cortex including V1, responses show a stronger preference for motion at the slower end of the spectrum, whilst hMT+ prefers somewhat faster speeds (Rodman and Albright, 1987; Cheng et al., 1994; Van Essen, 1985; Priebe et al., 2006). In neuroimaging and neurophysiology experiments, hMT+ demonstrates a fairly consistent 'classic' response profile of an inverted-U pattern with increasing speed. In particular, this is associated with an optimum response to speeds of 8 – 32°/sec (Chawla et al., 1998). Whilst this pattern is well-described, it remains unclear whether it reflects intrinsic properties of hMT+ neurons, or relates to the characteristics of pathways underlying these responses.

Human MT+ responses to speed in the absence of V1 have never formally been tested using functional neuroimaging. However, early research with patient GY led to the suggestion that blindsight function and hMT+ activity are not possible for slow-moving stimuli after V1 damage (Beckers and Zeki, 1995; fftyche and Zeki 1995). This was argued to be because slow and fast motion possess distinct neural pathways, with slow motion mediated through V1. This theory was adopted by a number of researchers (Kentridge and Heywood, 1999; Chawla et al., 1999), yet is surrounded in controversy. Only two neurophysiology reports have looked at MT responses to speed after striate cortex removal, and both imply that speed tuning may be retained – including responses to slow motion (Rodman et al., 1989; Azzopardi et al. 2003).

Furthermore, even GY has subsequently shown hMT+ responses to slow motion in his blind hemifield (Zeki and fftyche, 1998). Behaviourally, an inverted-U pattern for performance versus speed is also described in the literature (e.g. Azzopardi and Cowey, 1998), reminiscent of the characteristic hMT+ fMRI response (Chawla et al., 1998; 1999). It may therefore be possible for hMT+ to retain a normal physiological response to speed after V1 damage. This could account for a decrease in performance for slow motion, although significant performance at slow (4 °/sec) speeds should not be impossible. This hypothesis is the principal motivation for the current study.

Both psychophysical and fMRI responses to increasing speed of motion were measured in a group of patients with unilateral V1 damage and homonymous visual field loss. Low-luminance stimuli were selected as they are particularly challenging, thus expanding our understanding of the capacity and extent for residual processing after V1 damage. Responses were compared between patients with significant blindsight performance, and those who remained at chance. This included a comparison of subcortical activation, in order to comment on how hMT+ activity may relate to its underlying pattern of innervation. This has particular relevance for potential blindsight pathways, as well as helping to establish conclusively whether slow motion is only mediated via V1 pathways.

5.3 Methods

5.3.1 Participants

Fourteen patients (four female) took part in this study, of which 13 had sustained posterior circulation stroke and one had undergone benign tumour resection (see

Table 1 for details, and Figure 1 for schemata of visual field loss and radiological imaging). Average age at the time of participation was 55.6 years ±15.2 S.D., average time after pathology onset 49 months (range 6-252 months). Eight age-matched, healthy participants (50.1 ±14.6 S.D years of age, four female) served as controls.

Patient	Sex	Age (years)	Pathology	Time since pathology (months)	HVFD
P1	M	76	Left occipital tumour resection	252	RHH
P2	M	66	Left occipital infarct	8	RHH
P3	F	67	Right occipital haemorrhage	6	LUQ
P4	F	46	Left occipital infarct	7	RHH
P5	M	69	Right occipital infarct	16	LUQ
P6	M	55	Left occipital and cerebellar infarct	18	RHH
P7	M	49	Left occipital infarct	84	RHH
P8	M	36	Left occipital infarct	6	RHH
P9	M	70	Left occipital infarct	19	RUQ
P10	M	60	Left occipital infarct	96	RLQ
P11	M	30	Left occipital infarct	156	RHH
P12	M	73	Right occipital haemorrhage	6	LHH
P13	F	42	Left occipital infarct	6	RHH
P14	F	39	Left occipital infarct	7	RHH

Table 1. Clinical details for fourteen patients with unilateral striate cortex damage and homonymous visual field deficits, participating in this study. HVFD = homonymous visual field deficit, LUQ = left upper quadrant, RLQ = right lower quadrant, RHH = right homonymous hemianopia, LHH = left homonymous hemianopia, F = female, M = male.

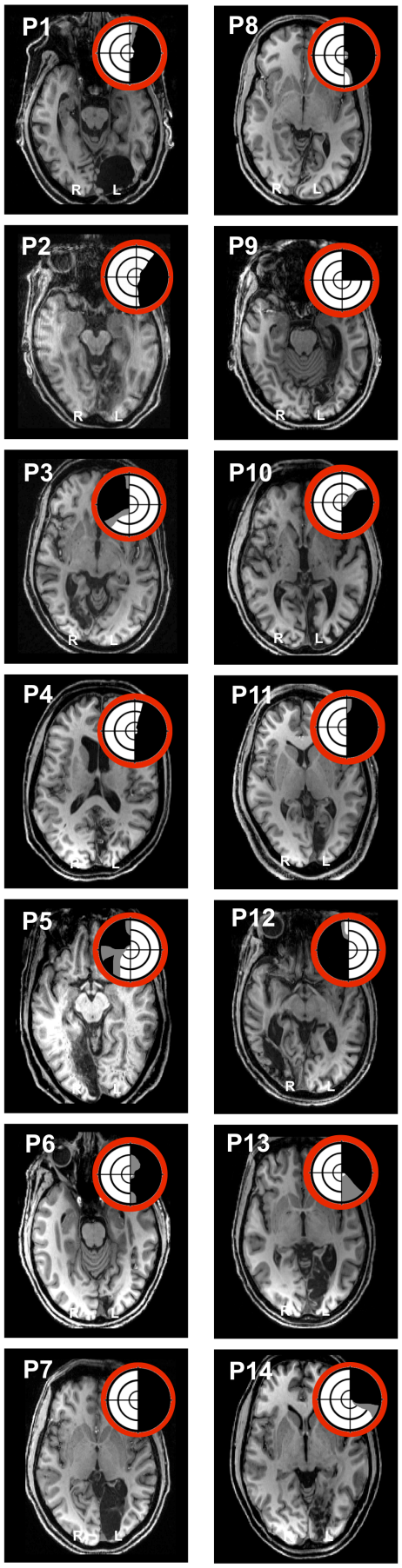

5.3.2 Stimuli

Visual stimuli consisted of an aperture of 5° or 8° diameter, displayed on a uniform grey background. Apertures contained moving or static black dots at an average density of 8 dots/°^{2}. Each dot was 0.075° in diameter, and had an infinite lifetime (Figure 2A and B). Four speed levels were used: 4°/s, 8°/s, 20°/s, and 32°/s, as well as an additional static condition (0°/s).

5.3.3 Psychophysics

Psychophysical testing employed two 2-AFC tasks: (1) 2-AFC temporal detection (2) 2-AFC direction discrimination, see Figure 2 and General Methods (Chapter 2) for details. The presence or absence of blindsight was assessed according to the criteria described in the General Methods. For the purpose

Figure 1. Patient neuroimaging and visual field deficits. Visual field deficits for each patient are represented schematically in red. These are adapted from 30:2 threshold Humphrey visual field perimetry reports, and show dense visual field loss in black (< 0.5%) and partial loss in grey (< 2%). Stimulus location was always restricted to a region of dense visual field loss. Concentric rings represent increments in retinal position of 10 degrees, spanning the central 30 degrees. In addition, example axial slices are taken from T1-weighted structural scans for each patient, to demonstrate the lesion location (radiological convention).

of fMRI analyses, this was determined according to patients' ability to detect stimuli above chance, i.e. Experiment 1.

5.3.3.1 Experiment 1: 2-AFC Detection

A 2-AFC temporal detection paradigm was employed, according to the description in Figure 2A. Stimulus speed was altered parametrically between the five conditions at random, with 20 trials per condition at each session. This included four speed levels, and static controls.

5.3.3.2 Experiment 2: 2-AFC Direction discrimination

Patients carried out an additional task, in which they were asked to indicate whether the direction of motion was horizontal or vertical (Figure 2B). Due to the high difficulty, a number of practice trials were usually required to familiarise patients with its rapid timing and the often complete lack of awareness with these low-luminance stimuli. If required, additional advice was given for patients to wait until the words "End of trial" reappeared on the screen before giving their response (see Figure 2). In that way, patients could be certain that the stimulus had appeared before giving their response. Stimulus speed was altered at random between the four motion conditions, with 20 trials per condition at each session. In this experiment no static trials were carried out.

5.3.4 fMRI procedure

The same four speed levels and a fifth static condition were presented separately to each hemifield during fMRI, representing a 10-condition block design, with

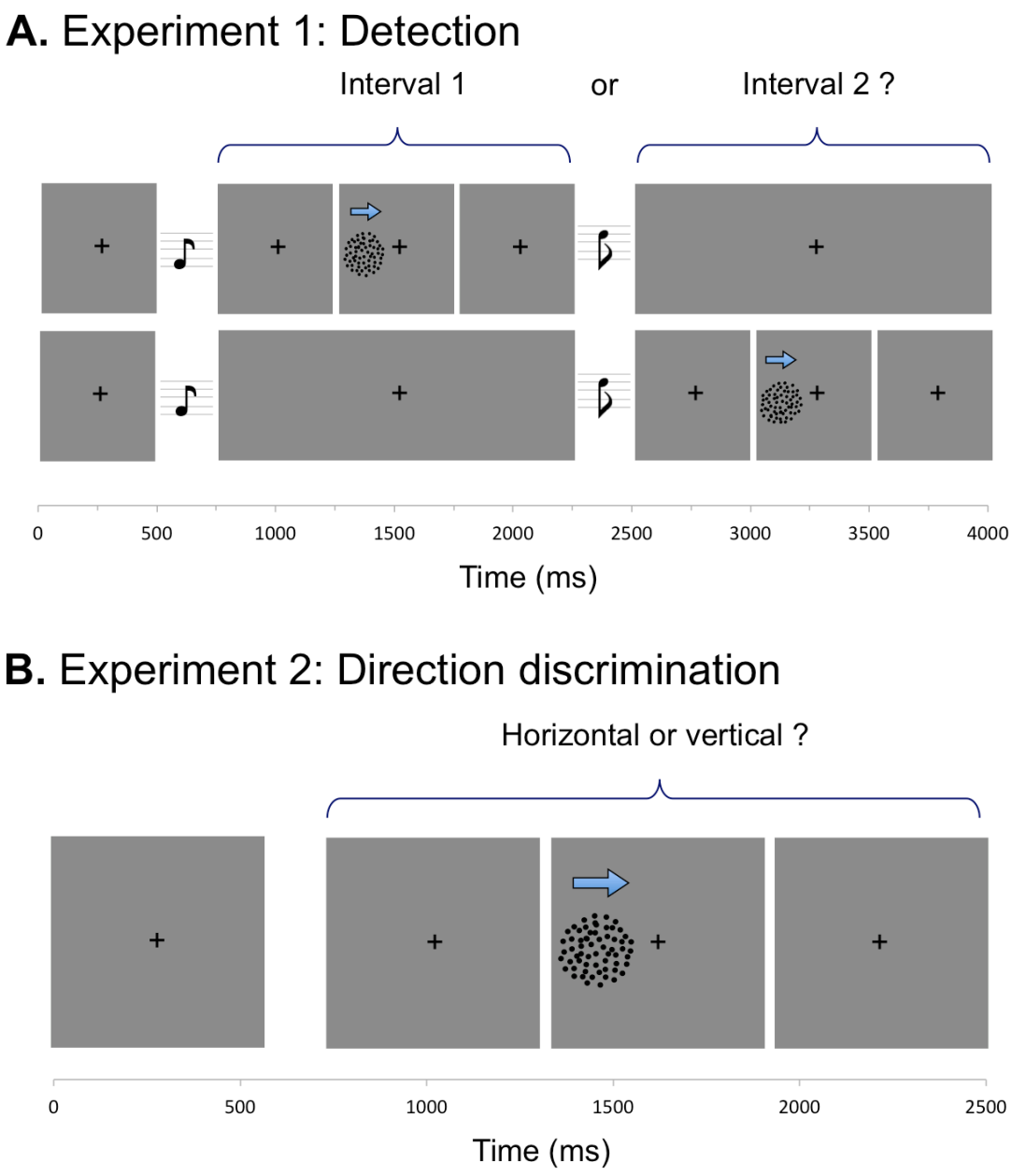

Figure 2. Psychophysics experimental design. (A) Experiment 1. Temporal 2-AFC detection. Participants fixate on a central cross, with the onset of each 1500 ms interval alerted by a low (interval 1) or high pitch (interval 2) tone. The stimulus can appear in either interval, for a period of 500 ms. At the end of the trial, participants are instructed to decide which interval the stimulus appeared. Stimuli consisted of an aperture of 5º or 8º diameter, containing moving or static black dots. Four speed levels were used: 4º/s, 8º/s, 20º/s, and 32º/s, as well as an additional static condition (0º/s). **(B) Experiment 2.** 2-AFC direction discrimination. Throughout each trial of 2500 ms duration, participants are required to fixate on a central black cross. During this time, a stimulus appears for 500 ms with jittered onset. At the end of the trial, patients must indicate which direction the dots were moving, horizontal or vertical. If they saw nothing, they are instructed to guess. Stimuli have identical parameters to Experiment 1, except that static dots are not included. In both experiments, the end of the trial is signified by the appearance of a blank screen containing the text: "End of trial".

equivalent diameter and screen position as used in behavioural testing (see Figure 3A for illustration). For each block, the aperture of moving or stationary black dots appeared for 16 s. Direction coherence was 100%, and dots moved at a constant speed according to the condition being shown. Angle of drift in the motion blocks changed every two seconds (8 directions: 45°, 90°, 135°, 180°, 225°, 270°, 315°, 360°). A 10s rest period followed each block. There were three runs in total, each lasting 260 s.

5.3.5 fMRI acquisition and pre-processing

396 functional volumes were acquired in a single session, duration 13.2 min. For parameter and pre-processing details, please see General Methods (Chapter 2).

5.3.6 fMRI analysis

5.3.6.1 Regions of interest

hMT+ masks were derived according to the procedure in the General Methods. In native space, average hMT+ ROI volume was 94.8 ±35.2 voxels in patients, 100.9 ±42.0 voxels in controls. Average V1 ROI volume was 16.2 ±7.5 voxels in patients (undamaged hemisphere) and 24.4 ±7.1 voxels in controls (averaged across hemispheres), the small volume reflective of the small 5° or 8° diameter stimulus used. For the lateral geniculate nucleus (LGN), binary masks were created by manual inspection and drawing over the anatomical T1-weighted images (Horton et al., 1990), using a radiological brain atlas to aid identification of landmarks (See Figure 3C for examples of all ROI masks in one patient). The average LGN volume in patients

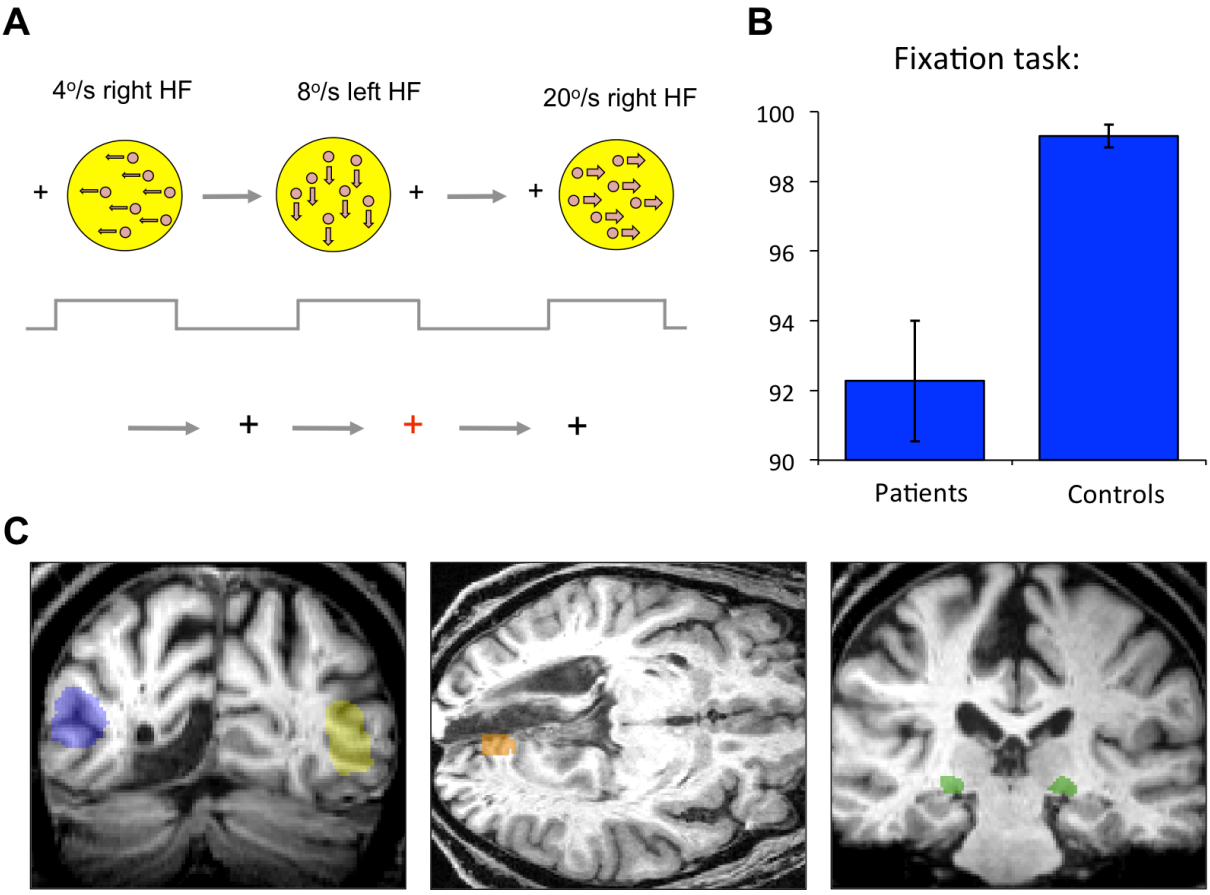

Figure 3. fMRI procedure and regions of interest. **(A)** This simple block design presents an aperture of black dots to the blind portion of visual field, or its equivalent location in the sighted hemifield. Stimuli have identical parameters as in psychophysical testing. Stimulus speed in each block is altered at random across four levels, with a fifth static control. This represents 10 conditions in total, each block lasting 16 s with 10 s rest periods. **(B)** Throughout all condition and rest blocks a fixation task requires participants to press a button every time the central fixation cross changes colour from black to red. Colour changes occur at random lasting 300ms. All participants scored at least 90% on this task, with the mean and standard error of the mean displayed here. **(C)** Example ROI masks overlaid on coronal and axial T1-weighted slices for patient P5. Ipsilesional hMT+ is shown in blue, contralesional in yellow. V1 in the undamaged hemisphere is shown in orange, and bilateral LGN in green.

measured 248 mm^3 in the right, and 246 mm^3 in the left. In controls, average LGN volume was 240 mm^3 in the right and 239 mm^3 in the left.

Each of the 10 fMRI conditions (e.g. left hemifield, 4°/s motion) were entered into the GLM as separate explanatory variables. Please see General Methods (Chapter 2) for details. All subsequent graphs, signal change calculations, and correlation statistics

were calculated for each condition relative to baseline, using data from participants' native space.

5.3.6.2 Whole brain GLM group analysis

Group analyses were also performed to look for differences in activation extent and localization across the whole brain. For this purpose it was necessary to align patient brains to a uniform pathological template, with lesions located in the same 'left' hemisphere, corresponding to a 'right-sided' visual deficit. This required that the structural and functional images of three patients (P3, P5, P12) were flipped in the horizontal plane. All activation coordinates are reported in MNI space, and z statistic images are displayed on mean structural images for the group, which have been transformed to standard space.

This analysis generated eight contrasts of interest. For each contrast, all 10 fMRI conditions had been entered as separate explanatory variables into the GLM. Contrasts 1 and 2 represented all five (static and motion) conditions versus rest blocks for each hemifield (contrast 1 was for the left hemifield, contrast 2 the right hemifield). Contrasts 3 and 4 represented only motion conditions contrasted against baseline fixation. Contrasts 5 and 6 contrasted the static blocks against all motion conditions (static > motion) for each hemifield separately. Contrasts 7 and 8 contrasted motion versus static conditions (motion > static), again for each hemifield separately.

For the whole group, mixed effects analyses were carried out for each hemifield, in patients and controls. A statistical threshold of $p < 0.001$ uncorrected was used to test for significance within V1 and extrastriate cortex, for which there were *a priori* hypotheses. Elsewhere correction for multiple comparisons was made using a cluster threshold of $p < 0.05$ unless otherwise stated. Additional analyses that required separation of the patient group into blindsight positive and blindsight negative cases were carried out using fixed effects, with the same statistical threshold.

5.4 Results

5.4.1 Psychophysics

Eight out of fourteen patients were able to significantly detect the stimulus inside their blind hemifield above chance, of which four could discriminate motion direction (P5, P8, P10, P14).

5.4.1.1 Experiment 1: Temporal 2-AFC detection

Results for Experiment 1 averaged across the whole group show how performance altered as a function of speed (Figure 4A). In particular, this followed an inverted-U relationship with speed, as the optimal performance was for intermediate speeds of 8^o/s and 20^o/s (average detection 61.3% and 60.1% respectively, $p < 0.001$). Although performance for the slower 4^o/s condition was slightly lower, this was also significantly greater than chance (58.2% correct, $p = 0.01$). In contrast, the fastest

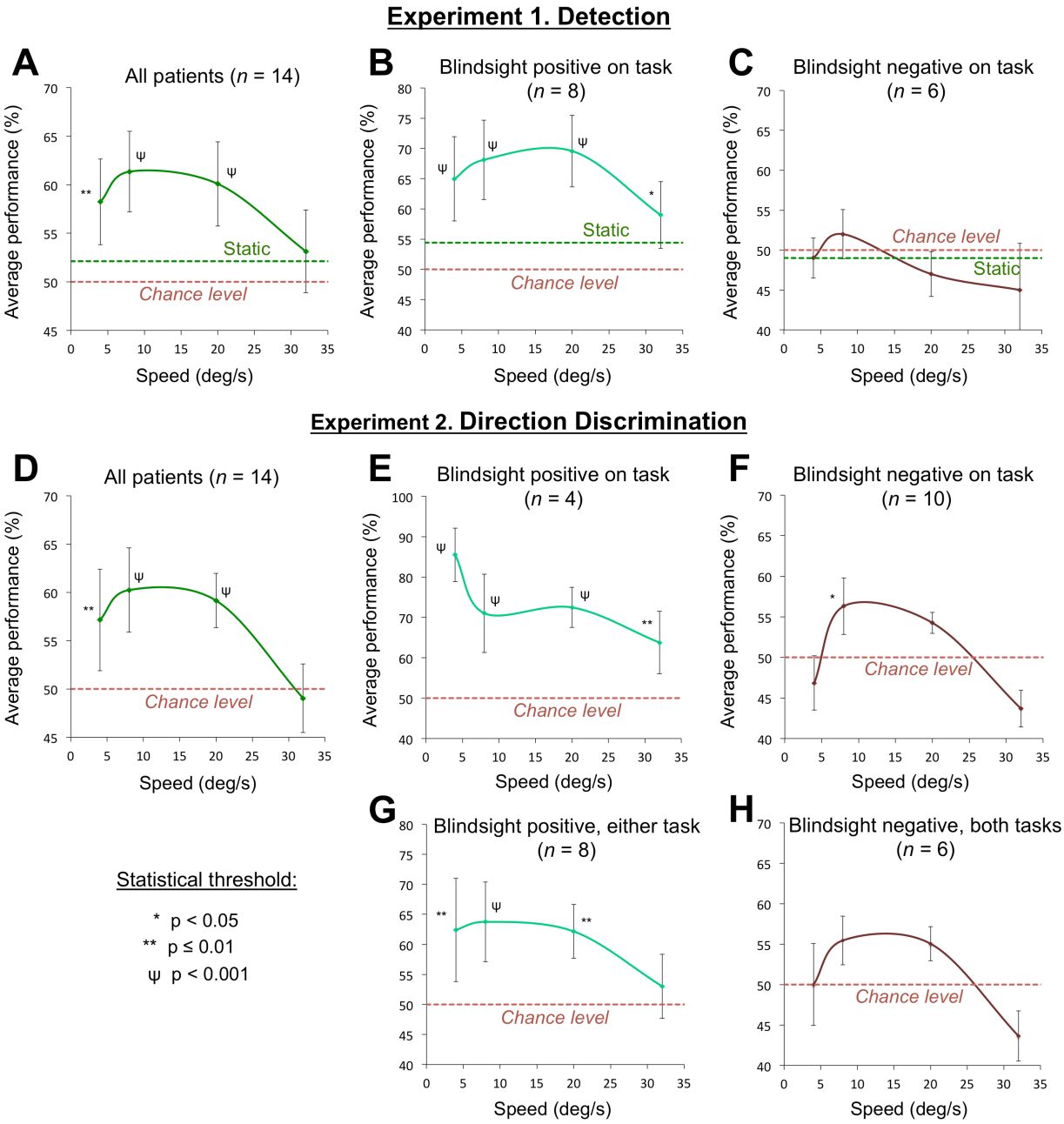

Figure 4. Psychophysical results for all patients, and comparing blindsight positive to blindsight negative groups. (A-C) Experiment 1. (A) Averaged across all 14 patients, performance shows an inverted-U relationship with speed, with peak performance at 8°/s. **(B)** In blindsight positive patients a similar pattern is seen, although more symmetrical in shape. Optimal performance is for 20°/s, but all speeds of 4-20°/s are highly significant. **(C)** In blindsight negative patients, performance remains at chance across all stimulus speeds. **(D-H) Experiment 2. (D)** Averaged across all 14 patients, performance shows a similar pattern as in Experiment 1, with discrimination dropping off at the fastest speed. **(E)** Only four patients were significantly above chance on this task, with similar performance for speeds of 4-20°/s. **(F)** Despite being blindsight negative on this task, patients demonstrate an inverted-U relationship between discrimination performance and speed, with performance significant at 8°/s. **(G)** Patients who were significantly above chance on either task (*n* = 8) again show similar significant performance for 4-20 °/s. **(H)** Patients that were blindsight negative on both tasks (*n* = 6) remained at chance for all speeds, although there is a suggestion that performance may differ slightly with speed.

moving condition (32°/s) and the static condition were not detected significantly above chance.

It is also useful to separate the group according to individual performance, and compare those performing above chance to patients remaining at baseline. This may reveal subtle increases in performance in the 'blindsight negative' group that become significant if accumulated across participants. In the blindsight positive group (n = 8), a similar inverted-U pattern was seen as for the group as a whole, although the curve appeared to be more symmetrical in shape (Figure 4B). The main differences were that performance in the fastest condition (32°/s) was now significantly above chance amongst these patients, whilst the static condition remained at baseline (32°/s: 59.0%, p = 0.02, static: 54.4%, p = 0.17). Also, performance now peaked for the 20°/s condition, with a shallower drop-off for the slow 4°/s condition (65.0%, p = 0.0003).

In the blindsight negative group (n = 6), a very subtle pattern of performance versus speed was visible (Figure 4C), however detection for each condition remained non-significantly different from chance. Peak performance was for stimuli moving at 8°/s, scoring just 52%. The overall effect of speed in the whole group or the two subgroups was not significant, despite notable performance above chance for certain speeds.

5.4.1.2 Experiment 2: 2-AFC direction discrimination

Patients' ability to perform direction discrimination showed a similar pattern to detection performance across the whole group (Figure 4D, n = 14). As for detection, performance was best for the intermediate speeds, but also significantly above chance for the slow 4°/s condition (57.14%, p = 0.001). Performance for the fastest speed condition (32°/s) remained at chance (49.03%, p = 0.65).

In this more difficult task, only four patients were significantly above chance according to their individual performance. Average discrimination performance amongst these patients is plotted in Figure 4E, and interestingly shows that discrimination was most accurate during the slow speed condition, i.e. 4°/s (85.5%, $p < 0.001$). In fact, performance was above chance for all four motion conditions, with a slight drop-off in performance at the fastest speed (32°/s, 63.8%, $p = 0.01$).

When considering performance of the patients who remained at chance on this task, an interesting result is seen (Figure 4F). Despite individually displaying no significant effect of speed on performance, there is a clear group difference in performance across different speeds ($F = 5.03$, $p = 0.005$, $df = 3$, one way ANOVA). Whilst performance scores are generally lower, an inverted-U pattern of performance versus speed is apparent. Optimal performance is again for the intermediate speeds, in particular 8°/s (56.3%, $p = 0.047$).

A relatively large proportion of patients were able to perform Experiment 1 above chance (57.1%), whilst only a small percentage (28.6% overall) were above chance in Experiment 2. Consequently, a number of patients in the 'blindsight negative' group for this task ($n = 10$, Figure 4F) had some blindsight function, even though they were not able to significantly discriminate direction. Because of this, the group was then divided into patients who were blindsight positive on either task ($n = 8$) and those who were at chance on both tasks ($n = 6$). This criteria was also used to subdivide fMRI results, as shall be described. As seen in Figure 4G, performance in blindsight positive patients was now optimal at 8°/s (63.8%, $p = 0.0005$), and remained high for

all conditions except the fastest 32°/s. In the blindsight negative group (Figure 4H), there was still the suggestion of an inverted-U pattern. Across all four conditions, the effect of speed almost reached significance ($F = 2.5$, $p = 0.087$, $df = 3$, one way ANOVA), however none of the conditions were individually discriminated significantly above chance.

5.4.1.3 Awareness and subjective descriptions

In these experiments, only two patients were at, or close to, ceiling in detection performance (Experiment 1, P3 and P10). One further patient (P11) consistently achieved 80 – 85 % for *moving* stimulus conditions. These patients, particularly the first two, possessed some awareness of stimuli within their blind field of vision. The patient at ceiling for all conditions was able to describe a patch of motion in the scotoma reasonably consistently. Indeed, the description of motion awareness was the most robust out of all the patients. However the patient was completely unable to accurately discriminate direction of motion or describe any detail about the stimulus that was shown. The other patient (P10) was confident of the presence of a stimulus, but interestingly was unable to describe what he had seen. He incorrectly guessed that stimuli looked like control images seen previously in his sighted field for a prior experiment. P11 initially stated that he saw nothing, but when forced to guess what the image looked like suggested it may have been a circle. After completing several trials, the patient also became more aware of motion in the stimuli. The remaining patients were mostly unaware of the stimuli in both experiments, and described using techniques of guessing. Occasionally patients would appear more confident, for example P8 on occasions thought he may have seen a moving blur, or P5 that he saw a '*light area'* at times on the screen.

5.4.1.4 Eye-tracker results

7 trials were removed from analysis in Experiment 1, and 2 trials from Experiment 2 due to eye movements towards the stimulus calculated from retrospective eye tracker data analysis. At the time of the Experiment, a further 6 trials were flagged for exclusion in Experiment 1 and 4 in Experiment 2 due to real-time observation of the Experimenter or feedback from the patient. In total, this accounted for 0.93% of trials in Experiment 1, and 0.54% of trials in Experiment 2 that were excluded from analysis due to inappropriate eye position.

5.4.2 Low-luminance motion in the blind hemifield elicits contralateral hMT+ activation

Group-level analyses of the fMRI response to visual stimulation in the blind or sighted hemifield were performed for all patients, and similarly for left and right hemifield stimulation in controls. In patients, this was carried out using a uniform pathological template described in the Methods section, with V1 damage always represented on the left hemisphere, corresponding to a blind right hemifield in all patients. Average activation in response to all experimental conditions (four speeds and static controls contrasted against the baseline fixation task), yielded significant activation of early level visual areas in controls, including contralateral V1, V2, V3, V4 and hMT+ (Figure 5A, Table 2), according to the Juelich histological atlas (Amunts et al., 2000; Rottschy et al., 2007; Malikovic et al., 2007). There was also significant ipsilateral activation restricted to hMT+. For the motion > static contrast, a similar pattern of activity was seen (Table 2, Figure 5B). There was significant activation throughout contralateral

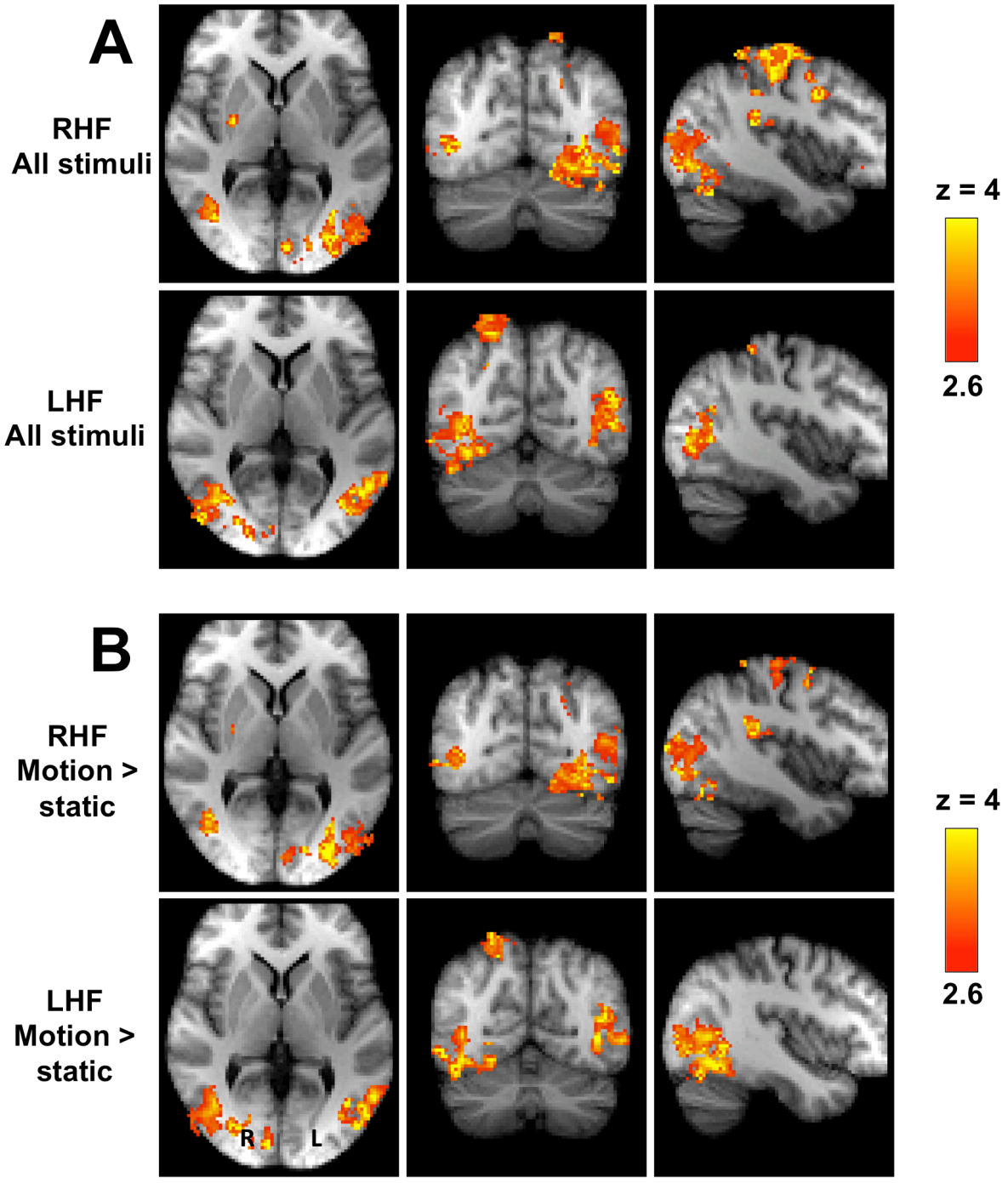

Figure 5. Cortical fMRI responses in healthy controls. (A) Regions demonstrating a significant response to all stimulus conditions versus baseline. Top row is for stimulation of the right hemifield, second row is for the left hemifield. **(B)** Regions demonstrating a significant response to motion versus static stimuli. Top row is for the right hemifield, second row the left hemifield. Mixed effects analysis, $p < 0.001$ uncorrected for *a priori* regions of interest, elsewhere cluster corrected, $p < 0.05$. Results are displayed on the average high resolution structural in MNI space, radiological convention. LHF = left hemifield. RHF = right hemifield.

Controls	**x**	**y**	**z**	**z-stat**		**x**	**y**	**z**	**z-stat**
Right hemifield					Left hemifield				
All conditions vs baseline					*All conditions vs baseline*				
Left V1	-4	-90	2	15.6	Left V5/MT+	-44	-72	2	6.7
Left V4	-16	-72	-10	7.4	Right V5/MT+	38	-66	6	5.3
Left V5/MT+	-50	-70	-2	6.2	Right V2	30	-96	18	5.1
Right V5/MT+	48	-68	4	4.8	Right V1	18	-92	0	4.9
Left V3	-20	-96	-4	4.7	Right V3 // Right V4	28	-80	-16	4.9
Left V2	-4	-92	-8	4.6					
Motion > static					*Motion > static*				
Left V4	-26	-72	-8	10.4	Right V1	8	-92	2	10.2
Right V5/MT+	52	-64	6	7.0	Right V4	44	-82	0	7.0
Left V1	-8	-90	8	5.1	Right V5/MT+	56	-64	-6	5.9
Left V5/MT+	-34	-80	2	4.9	Right V3	20	-74	0	5.3
Left V2 // Left V3	-10	-86	-12	4.9	Left V5/MT+	-46	-74	-6	5.0
					Right V2	8	-72	-6	4.2
Patients	**x**	**y**	**z**	**z-stat**		**x**	**y**	**z**	**z-stat**
Blind right hemifield					Sighted left hemifield				
All conditions vs baseline					*All conditions vs baseline*				
Left inferior temporal gyrus (temporo-occipital)	-52	-66	-12	4.0	Right V1	12	-94	10	8.4
Left V3	-12	-88	-10	3.8	Right V4	26	-76	-8	7.5
Left V1	0	-96	0	3.4	Right V3 // Right V2	14	-76	-10	6.7
Left V5/MT+	-36	-82	-2	3.1	Right V5/MT+	50	-60	6	4.5
Motion > static					*Motion > static*				
Left V5/MT+ // Left V4	-40	-80	-10	4.7	Right V5/MT+	46	-72	4	5.8
Left inferior temporal gyrus (temporo-occipital)	-54	-60	-12	4.3	Right V4	42	-88	0	4.7
Left V2	-10	-54	4	3.7	Right V1	10	-94	-2	4.2
					Right V2	16	-92	-6	3.4

Table 2. Cortical regions demonstrating significant activity in response to all stimulus conditions versus baseline, or to motion versus static stimuli. Only the most significant peak within each region of activation is reported, with its corresponding MNI coordinates and z-statistic. A statistical threshold of $p < 0.001$ uncorrected was used for a priori regions of interest, elsewhere correction for multiple comparisons was made with a cluster threshold of $p < 0.05$, mixed effects analysis. Results are for all patients and controls.

visual cortex, as well as ipsilateral hMT+ for both hemifields. Regions V4 and hMT+ also tended to show greater responses for the motion > static contrast rather than the 'all conditions' contrast, consistent with a preference for moving stimuli.

In the patient group, a similar pattern of activation was seen during stimulation of the sighted left hemifield (see Figure 6 and Table 2, lower half). For 'all' stimulus conditions versus baseline (including the static blocks), greatest activation was seen in contralateral V1, as well as contralateral V4, an area on the boundary of V2 and V3, and hMT+ (figure 6A, second row). These regions also showed activation in response to the motion > static contrast, although the relative weightings were slightly different. In the latter contrast (Figure 6B, bottom row), relatively stronger activation was seen in motion area hMT+, with weaker activation in earlier visual cortex regions V1 and V2.

During stimulation of the blind hemifield, average response to all stimulus conditions elicited greatest activation in a region close, but slightly inferior and anterior to left hMT+. This region is shown in standard space in Figure 6A (upper row), and its MNI coordinates are provided in Table 2. In addition, there was activation in contralateral V3, a small region of V1 at the occipital pole, and in left hMT+. For the motion > static contrast, representing activation specific to low-luminance motion in the blind hemifield, the greatest activity was in a region spanning contralateral hMT+ and V4 (see Figure 6B, upper row and Table 2 for details). There was also weak activation in a region corresponding to left V2, but not V1. These results represent responses for the entire group of patients with V1 damage (n = 14).

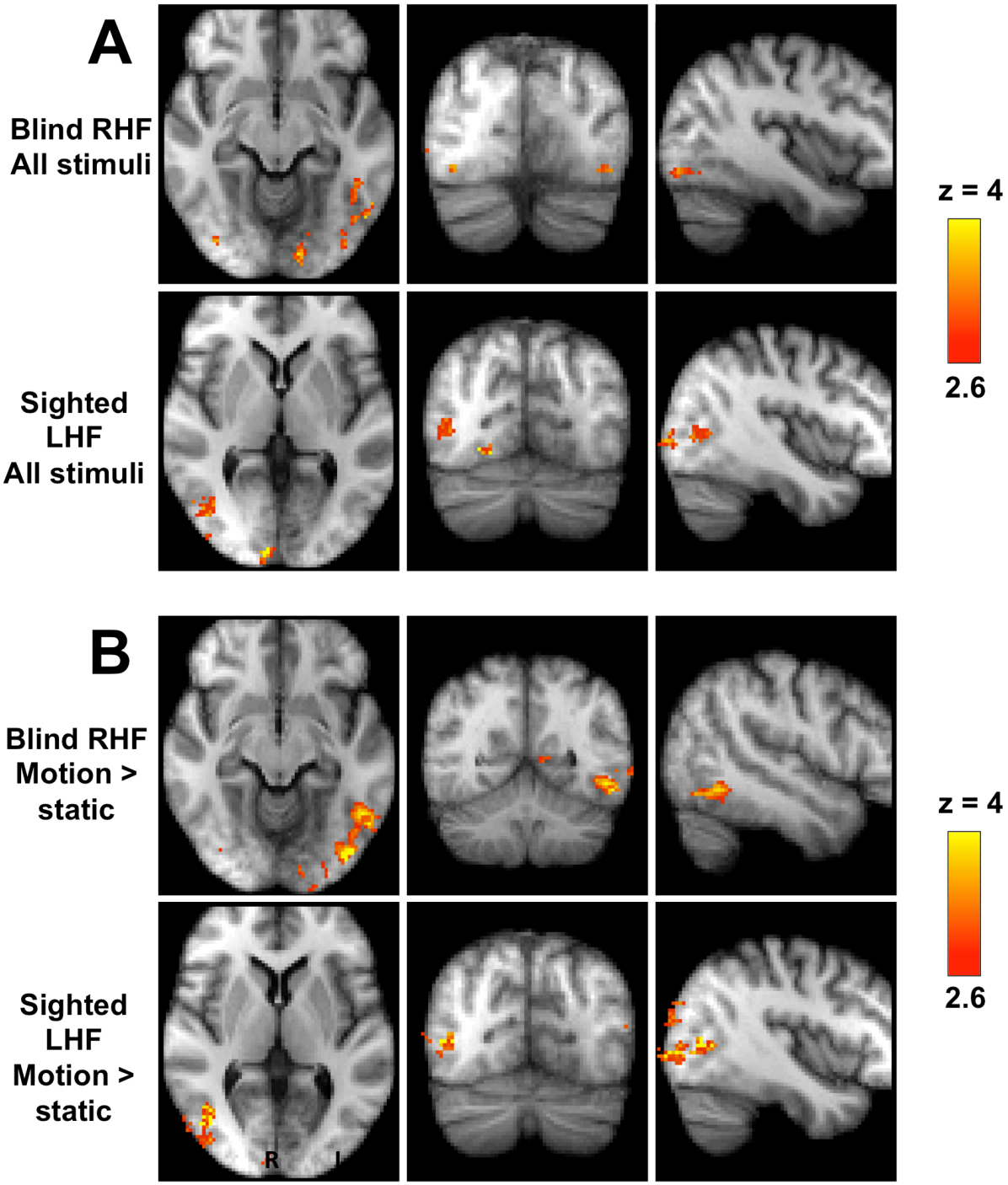

Figure 6. Cortical fMRI responses for all patients (*n* = 14). (A) Regions with a significant response to all stimulus conditions versus baseline. Top row is for stimulation of the blind right hemifield, second row is for the sighted left hemifield. **(B)** Regions demonstrating a significant response to motion versus static stimuli. Top row is for the blind right hemifield, second row the sighted left hemifield. Mixed effects analysis, $p < 0.001$ uncorrected for *a priori* regions of interest, elsewhere cluster corrected, $p < 0.05$. Results are displayed on the average high resolution structural in MNI space, radiological convention.

5.4.3 Blindsight positive and negative patients show slightly different regions of activation during blind field stimulation

Further group analyses were carried out, this time subdividing patients into those who were able to detect stimuli above chance during psychophysical testing (so-called 'blindsight positive', n = 8) and those who remained at chance ('blindsight negative', n = 6). Since the number of patients in each subgroup was considerably reduced, both fixed and mixed effects analyses were carried out. Table 3 shows the mixed effects results, although for display purposes fixed effects statistics maps are shown in Figure 7. For the sighted hemifield, both patient groups had similar patterns of activation in early contralateral visual cortex, as well as hMT+ bilaterally. This is particularly clear in Figure 7A (lower row) and 7B (lower row), but was also found in the mixed effects analysis (see Table 3 for details). For stimulation of the blind hemifield, the blindsight positive group showed activation in a much more classical hMT+ distribution (see Figure 7A versus 7B, top row; Table 3). Peak activation corresponded to hMT+ MNI coordinates: -40, -70, 6 (z = 4.4) in the fixed effects analysis and -42, -70, -2 with mixed effects. Conversely, the blindsight negative group showed activation in a more infero-anterior location in the left inferior temporal gyrus, and the lower boundary between contralateral hMT+ and V4 (MNI: -52, -58, -10), as well as left V3 and the occipital pole (see Table 3 for details).

5.4.4 Normal sighted fMRI response to speed differs in hMT+ and V1

Average signal change from baseline was calculated for each participant in native space, using V1 and hMT+ regions of interest (see General Methods for details). In

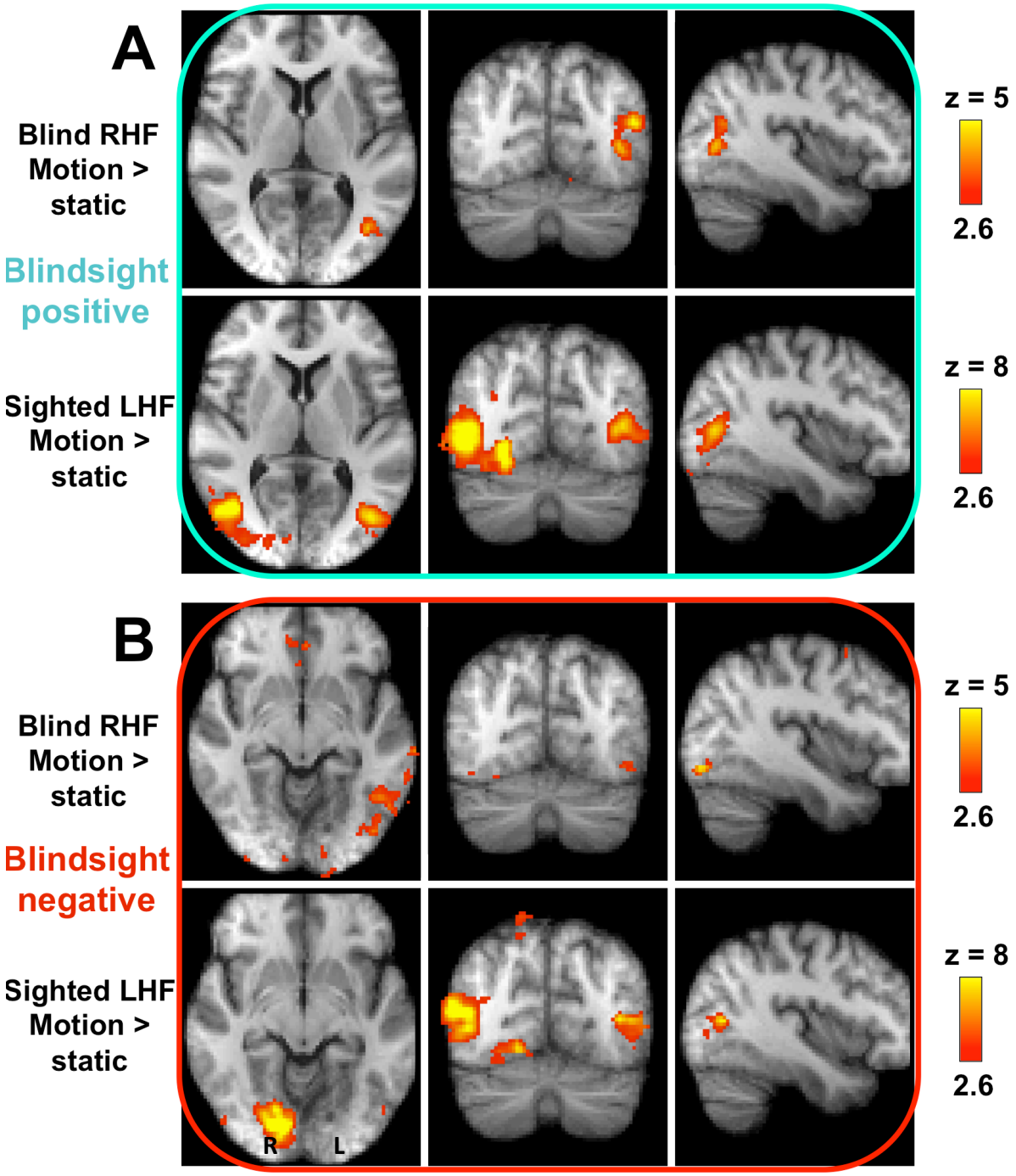

Figure 7. Cortical fMRI responses to motion, comparing blindsight positive and negative patients. (A) Blindsight positive patients (*n* = 8). Regions showing a significant response to motion versus static stimuli. Top row is for stimulation of the blind right hemifield, second row is for the sighted left hemifield. **(B) Blindsight negative patients (*n* = 6).** Regions demonstrating a significant response to motion versus static stimuli. Top row is for the blind right hemifield, second row is for the sighted left hemifield. Fixed effects analysis, $p < 0.001$ uncorrected for *a priori* regions of interest, elsewhere cluster corrected, $p < 0.05$. Results are displayed on the average high resolution structural in MNI space, radiological convention.

control participants, these values were averaged across hemispheres to provide one single measure per ROI. In patients, responses to sighted or blind hemifield stimulation were kept separate. V1 responses were also measured in the undamaged hemisphere of patients, corresponding to sighted hemifield stimulation. This enabled graphs to be plotted for each ROI, representing how signal change altered as a function of stimulus speed.

hMT+ activation in controls and the sighted hemisphere of patients showed a response to static dots that was very close to baseline, around 0.1% signal change (Figure 8A and 8B). In contrast, there was an average response between 0.4 – 0.5%

Blindsight positive (*n* = 8)	**x**	**y**	**z**	**z-stat**		**x**	**y**	**z**	**z-stat**
Blind right hemifield						Sighted left hemifield			
Motion > static						*Motion > static*			
Left V5/MT+	-42	-70	-2	2.9		Right V4 // Right V3	26	-72	-14	4.7
Left V3	-16	-86	-8	2.8		Right V5/MT+	46	-70	-6	4.1
						Left V5/MT+	-40	-74	6	3.7
						Right V2 // Right V1	26	-82	0	3.5
Blindsight negative (*n* = 6)	**x**	**y**	**z**	**z-stat**		**x**	**y**	**z**	**z-stat**
Blind right hemifield						Sighted left hemifield			
Motion > static						*Motion > static*			
Left inferior temporal gyrus (temporo-occipital)	-52	-58	-10	4.2		Right V1	12	-92	4	6.6
Left V4 // Left V5/MT+	-40	-78	-10	4.1		Right V5/MT+	52	-70	2	5.3
Left V3	-14	-88	-12	3.4		Left V5/MT+	-50	-76	6	3.6
Left V1	0	-96	-2	3.4						

Table 3. Cortical regions demonstrating significant activity in response to motion versus static stimuli, comparing blindsight positive and negative patients. Only the most significant peak within each region of activation is reported, with its corresponding MNI coordinates and z-statistic. A statistical threshold of $p < 0.001$ uncorrected was used for a priori regions of interest, elsewhere correction for multiple comparisons was made with a cluster threshold of $p < 0.05$, fixed effects analysis.

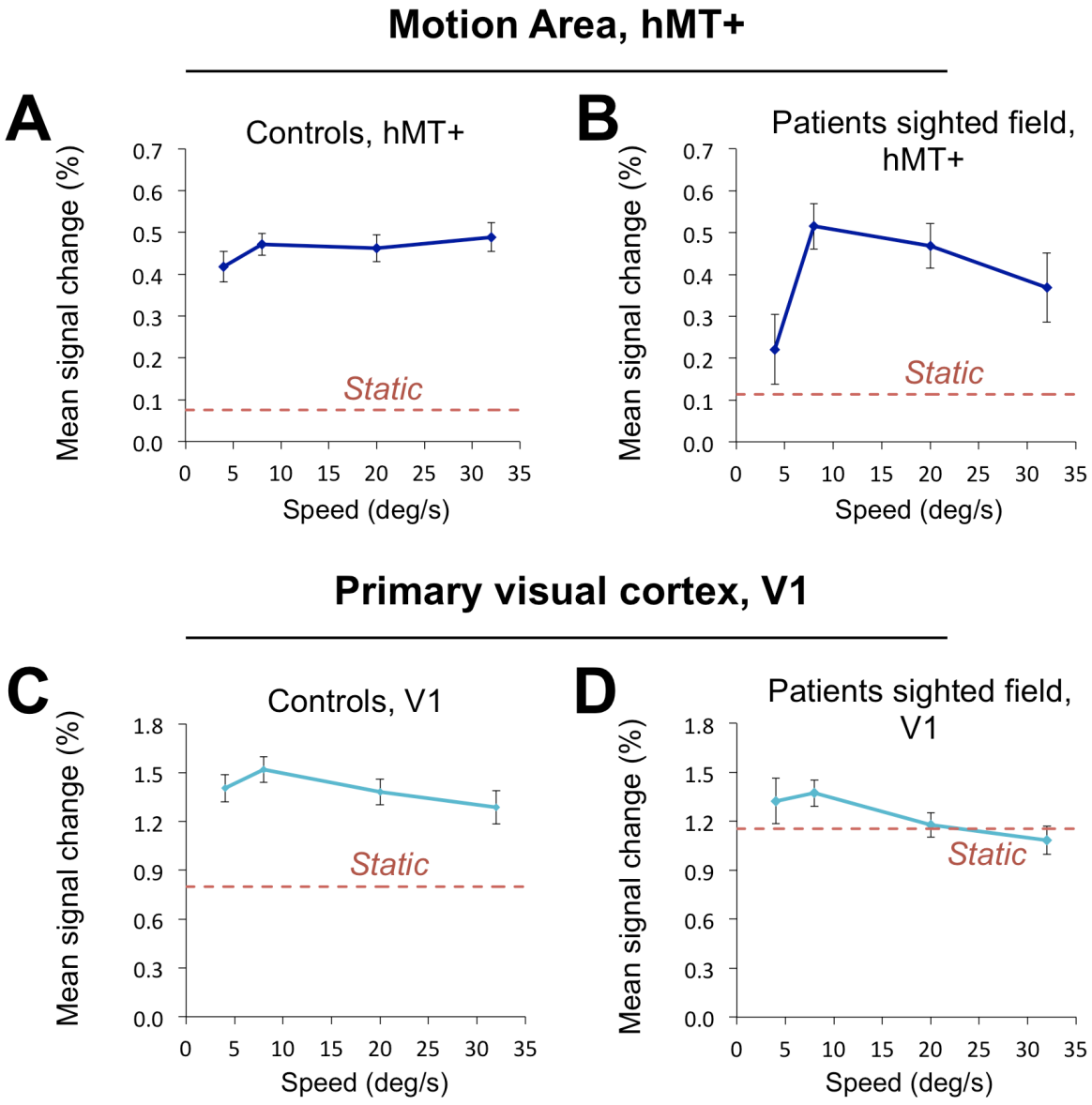

Figure 8. Group plots of mean signal change versus stimulus speed in hMT+ (dark blue) or V1 (light blue) regions of interest. (A) Control group hMT+ shows significant responses for moving stimuli, with the weakest response for the slowest speed. **(B)** hMT+ response in the sighted hemifield of patients shows a more characteristic inverted-U pattern, with signal change also weakest for the slowest stimulus speed. **(C)** In control participants, V1 shows a slight preference for slower speeds, with a peak response for motion at 8°/s and significant activity for static dots. **(D)** Sighted V1 responses in patients undamaged hemisphere are very similar to controls, and also show a preference for slower motion and marked activity for static dots.

signal change with speeds of 4 – 32°/s in controls, and 0.2 - 0.6% in the sighted hemifield of patients. The optimal speed associated with peak hMT+ activity varied between participants in both groups, in some cases with differences between hemispheres even in the same individual. This variability led to a fairly flat response across the group, with the average response curve for controls shown in Figure 8A. For patients sighted hemifield, a similar pattern was seen (see Figure 8B for group average) with preferred speed quite evenly spread amongst the faster 8 – 32°/s conditions.

Response to speed in contralateral V1 showed a similar pattern in controls and the sighted hemifield of patients. Average curves in both groups (Figure 8C and 8D) show a preference for slower speeds in the test range, in particular for 8°/s. Unlike in hMT+, there was a greater drop off in activation for the fastest speed of 32°/s, which showed the lowest mean V1 signal change of all motion conditions. Static dots also elicited a relatively high degree of activity in V1, reaching an average 0.8% signal change in control participants, and 1.1% in patients.

5.4.5 Blindsight positive and negative patients show a different response to speed in contralateral hMT+

During blind field stimulation, hMT+ activity also altered with speed (see Figures 9A and 9B). Averaged across all patients (n = 14), signal change in hMT+ showed a pattern resembling features of both normal V1 and hMT+ activation. However, when the group was subdivided again into patients who were able to detect stimuli above chance ('blindsight positive', n = 8) and those who could not ('blindsight negative', n

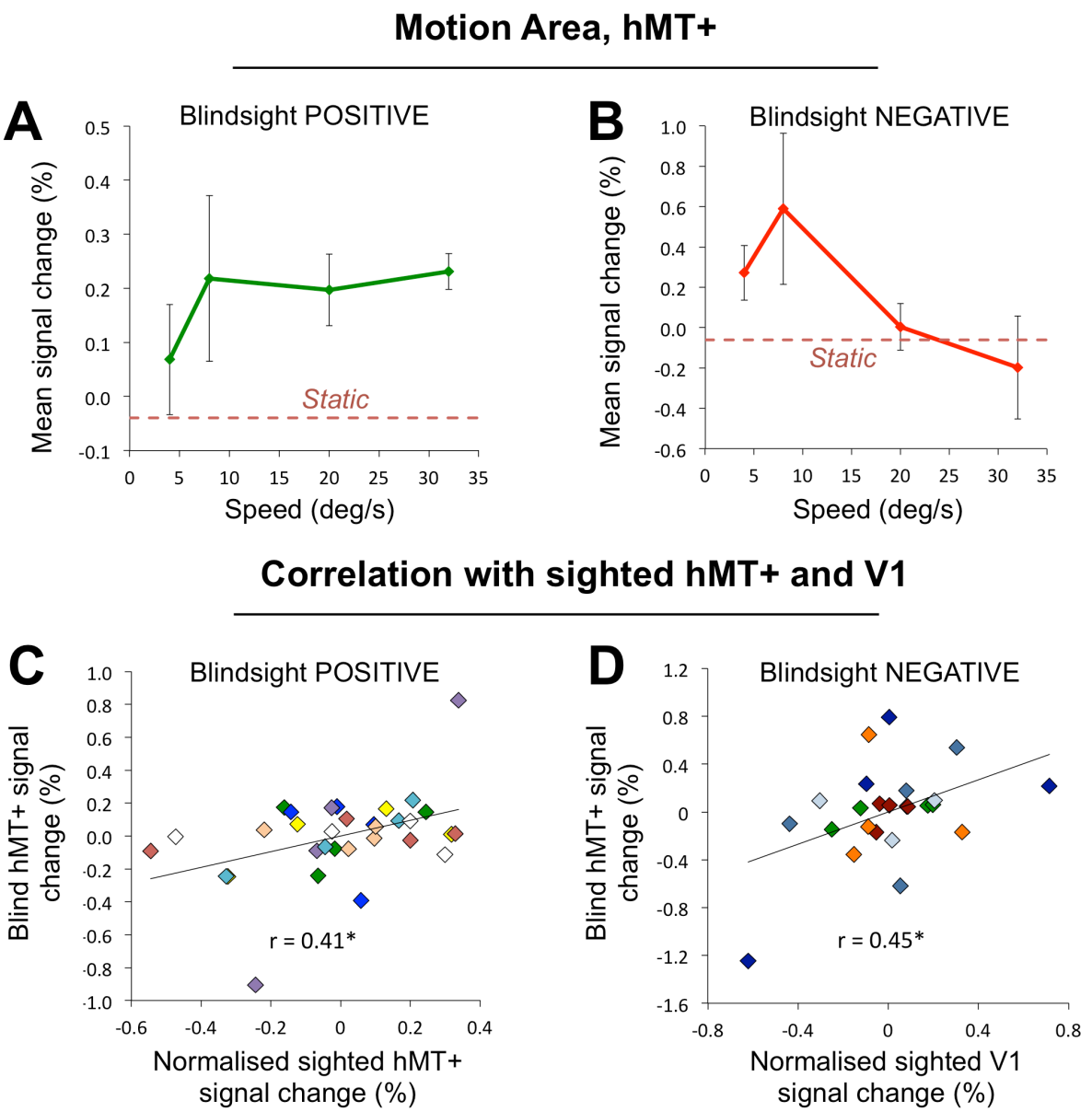

Figure 9. Comparison of hMT+ responses to blind field stimulation in blindsight positive (green) and blindsight negative (red) patients. (A) Plot of mean hMT+ signal change versus stimulus speed in response to blind hemifield stimulation, in blindsight positive patients (*n* = 8). This graph shows a relatively normal hMT+ response to increasing speed. **(B)** Plot of mean hMT+ signal change versus stimulus speed in response to blind hemifield stimulation, in blindsight negative patients (*n* = 6). This graph shows an unusual hMT+ response to speed, more similar to the pattern in healthy V1. **(C)** Blindsight positive patients show a significant correlation between blind and sighted hMT+ responses to speed (*paired Pearson correlation, p = 0.02). **(D)** Blindsight negative patients instead show a significant correlation between blind hMT+ and sighted V1 responses to speed in the undamaged hemisphere (*paired Pearson correlation, p = 0.03). The data in **(C)** and **(D)** was normalized and colour-coded for each participant, allowing the impact of any between-subject differences to be appreciated.

= 6), a different pattern emerged for each group. Average blind field responses are plotted for blindsight positive cases in Figure 9A, and blindsight negative patients in

Figure 9B. As can be seen, both patient groups showed an increase in signal change from baseline during at least some of the motion conditions. Interestingly however, they appear to show quite different responses to changes in stimulus speed. The blindsight positive group showed a response profile that is quite typical of normal hMT+ responses seen in control participants or in the undamaged hemisphere of patients (Figure 8A and 8D). There was relatively low activation elicited by static stimuli (just below baseline), but much higher signal change for the higher speeds of 8 – 32°/s. Conversely, the blindsight negative group only showed signal change above baseline for the slower speed conditions of 4 and 8°/s. Activity dropped off with increasing speed beyond those levels, showing a similar degree of activation to static stimuli (Figure 9B).

In fact, whilst blindsight positive patients showed a pattern fairly typical of normal hMT+, blindsight negative patients showed a response to speed that was more similar to normal V1 patterns. These similarities are highlighted in Figures 9C and 9D, which demonstrate the correlation with patients' sighted hMT+ or V1 responses. Crucially, the data for these analyses were normalized for each participant, thus reducing the impact of any between-subject differences that may have skewed the correlation (Franz and Loftus, 2012). Response to blind hemifield motion stimulation in hMT+ of blindsight positive patients correlated significantly with hMT+ responses to equivalent sighted conditions in the undamaged hemisphere (Figure 9C, $r = 0.41$, $p = 0.02$). These responses did not, however, correlate as well with sighted V1 responses ($r = 0.26$, $p = 0.14$). The same correlation could be demonstrated with control hMT+ responses ($r = 0.98$, $p = 0.02$), but not control V1 responses to speed ($r = -0.1$, $p = 0.9$). Conversely, the blindsight negative patients showed hMT+ activity during blind

hemifield stimulation that correlated significantly with sighted V1 responses in patients (Figure 9D, r = 0.45, p = 0.03). However, responses did not correlate so well with sighted hMT+ (r = 0.29, p = 0.17). Again this was also the case when comparing activity to responses in control participants. There was a significant correlation between blind hMT+ responses in patients to control V1 responses to speed (r = 0.97, p = 0.03), but not control hMT+ responses (r = -0.34, p = 0.66).

5.4.6 Blind field stimulation elicits significant subcortical activation

When considering the origin of cortical responses to motion, subcortical structures such as the LGN normally play an important role as thalamic relay nuclei, transmitting visual signals from the retina to the occipital cortex. Such subcortical structures (including the superior colliculus and pulvinar) are also implicated in transmitting visual signals directly from the blind hemifield of individuals with V1 damage to the extrastriate cortex in cases of blindsight. Although it can be difficult to measure subcortical responses to visual stimulation accurately using fMRI (Chen et al., 1999; Schneider and Kastner, 2005), it would be useful to determine whether such activity can be detected during blind field stimulation, and if so, where this localises to.

One limitation is that subcortical structures possess relatively small anatomical volumes, which may result in their exclusion from cluster-corrected fMRI analyses. It may therefore be necessary to look specifically for activation in subcortical regions using uncorrected statistics and a standard statistical threshold of $p < 0.001$, with a cluster extent threshold > 5 voxels (135 mm^3), corresponding to the average LGN volume reported from human post-mortem investigation (Andrews et al., 1997).

Images displaying significant response to motion in the blind right hemifield of patients are shown in Figure 10, with separate results for blindsight positive (Figure 10A) and blindsight negative individuals (Figure 10B). Control responses to motion in the right hemifield are also shown for comparison (Figure 10C).

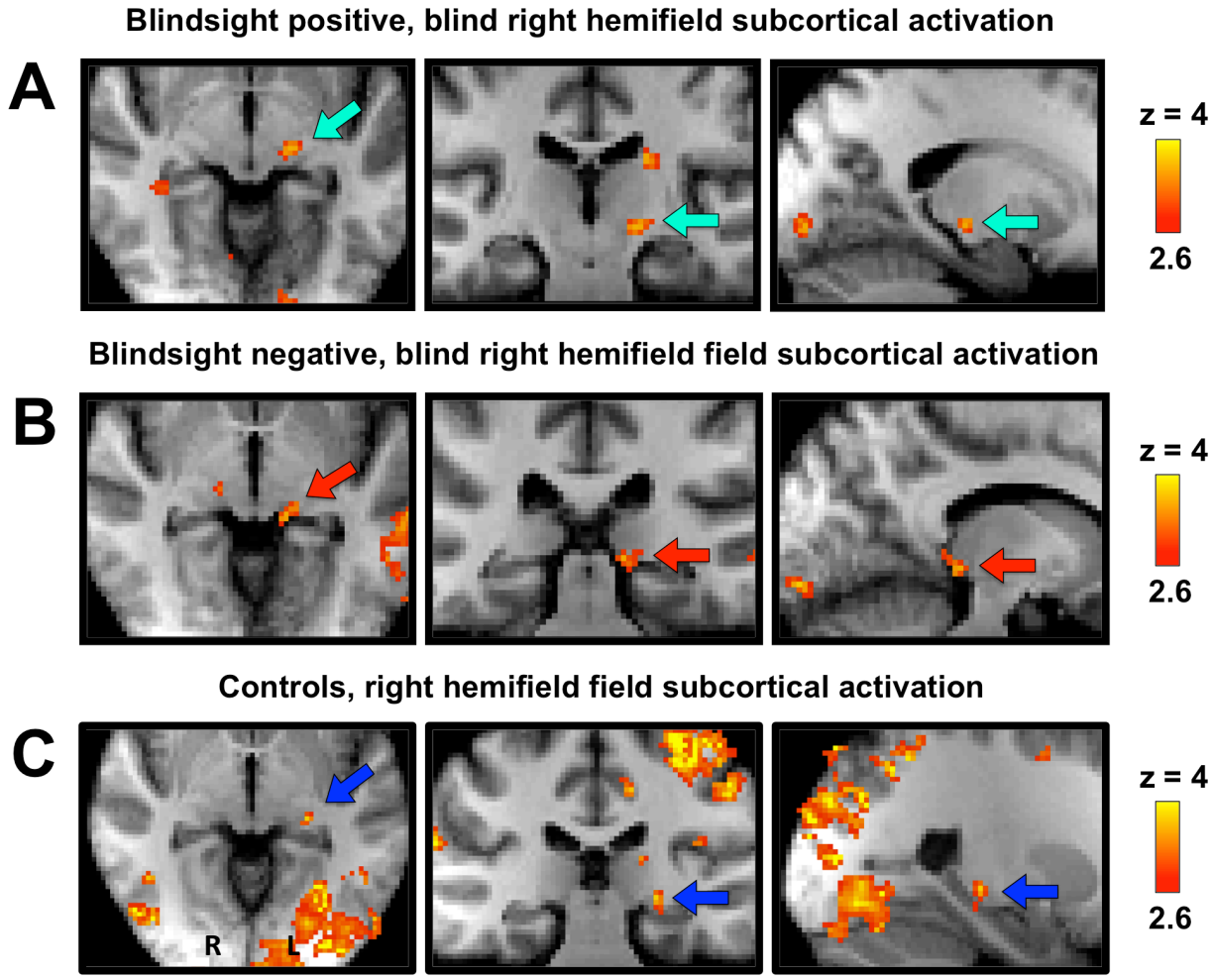

Figure 10. Subcortical fMRI responses to motion versus static stimulation of the right hemifield, comparing blindsight positive and negative patients, and healthy controls. (A) Blindsight positive patients (*n* = 8). The only subcortical region demonstrating a significant response to motion in the blind right hemifield corresponds to the left, ipsilesional LGN (light blue arrow). **(B) Blindsight negative patients (*n* = 6).** Motion in the blind right hemifield is associated with a small region of subcortical activity corresponding to the left, ipsilesional inferior pulvinar (red arrow). **(C) Healthy controls (*n* = 8).** Motion in the right hemifield of controls elicited significant subcortical activity in the left LGN (dark blue arrow). Fixed effects analysis, $p < 0.001$ uncorrected, cluster extent threshold > 5 voxels. Results are displayed on the average high resolution structural in MNI space, radiological convention.

In blindsight positive cases, a small region of activation was seen in what was most likely the left LGN (Figure 10A). This was the only significant region of activity throughout the subcortex, with peak signal change localised to MNI coordinates: -18, -22, -6 (z = 3.5, cluster extent 13 voxels). In blindsight negative cases (Figure 10B) there was also significant subcortical activation, although this was less clearly localisable, with a second, smaller region of activity. The most highly active region in this group was centred on MNI coordinates: -12, -32, -4 (z = 3.5, 13 voxels), which was slightly posterior and medial to that in blindsight positive cases. This corresponds to a part of the left thalamus between the medial and lateral geniculate nuclei, which may in fact represent the inferior border of the left pulvinar nucleus (Talairach and Tournoux, 1988). The smaller second cluster visible in Figure 10B (MNI: 14, -22, -6, z = 3.4) did not reach significance, with a cluster extent of only 4 voxels. For comparison, control participants also showed a significant subcortical response to motion (Figure 10C). Two regions of activity were seen; one cluster was centred on MNI coordinates: -24, -28, -4 (z = 3.7, 6 voxels), corresponding again to the contralateral left LGN. A further region of subcortical activity was located in the right putamen (MNI: 28, -8, 4, z = 4.0, 25 voxels).

5.4.7 The LGN normally shows highly variable responses to speed, more similar to V1

Having established that LGN activation was demonstrable using the current fMRI paradigm, a similar approach to the ROI analysis of areas hMT+ and V1 was applied. This involved extracting the BOLD signal change versus baseline from LGN masks

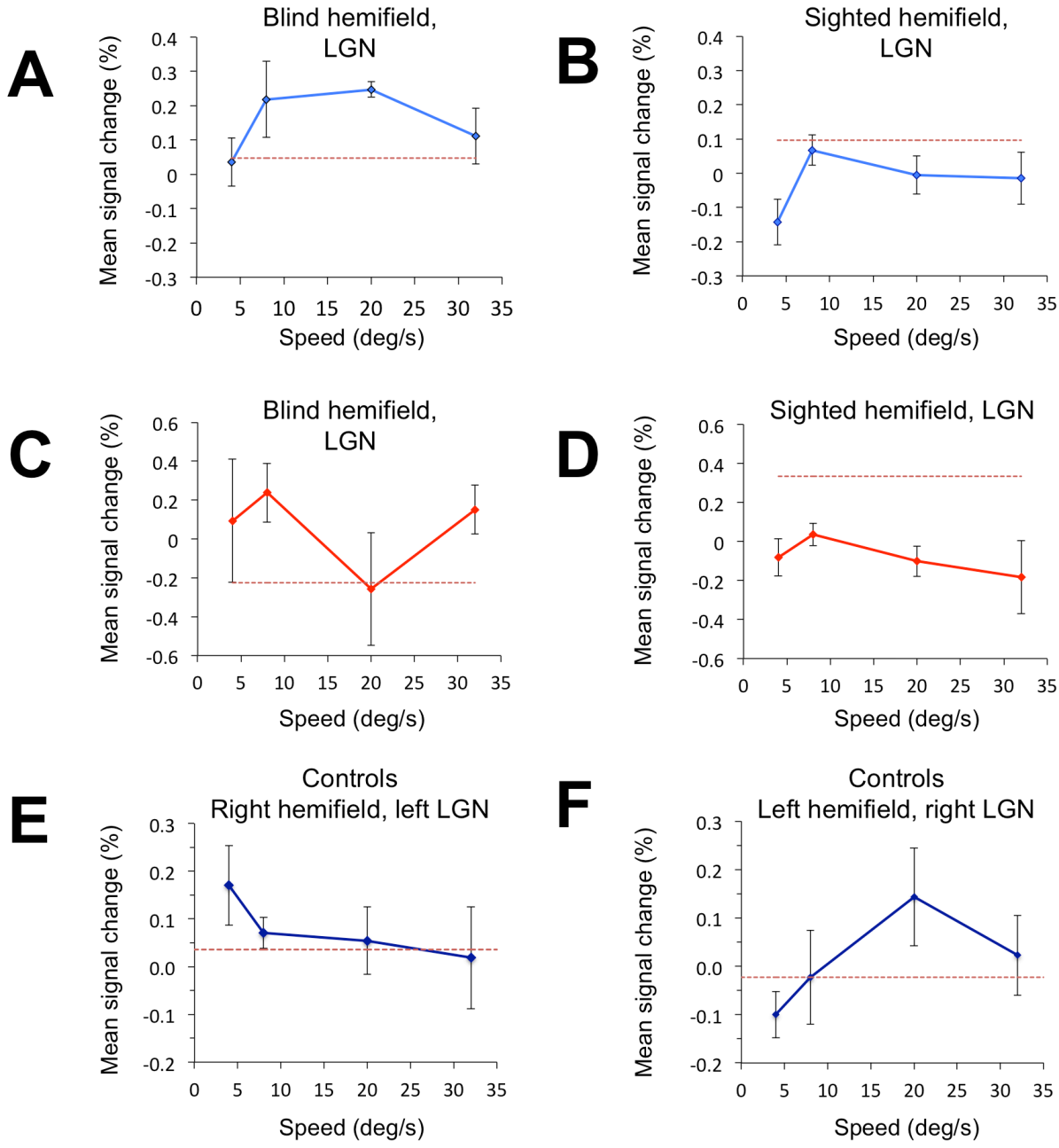

Figure 11. Group plots of mean signal change versus stimulus speed in the contralateral LGN, comparing blindsight positive patients (light blue chart), blindsight negative patients (red chart), and healthy controls (dark blue chart). (A) The pattern of ipsilesional LGN responses to blind field stimulation in blindsight positive patients shows an inverted-U pattern, which is more typical of normal hMT+ speed responses. **(B)** In contrast, LGN responses to the sighted field are more similar to normal V1 patterns. **(C)** In blindsight negative patients, the ipsilesional LGN shows a noisy response to increasing speed in the blind field that does not match either pattern. **(D)** Sighted LGN responses in blindsight negative patients are much more similar to healthy V1. **(E-F)** In controls, stimulation of the right (E) and left hemifield (F) showed slightly inconsistent patterns, however these were in fact highly correlated with control V1 responses, but not hMT+ in a paired correlation analysis.

across different speed conditions, in order to evaluate how LGN response altered as a function of speed. The LGN masks had previously been identified anatomically for each participant according to their T1-weighted structural scan (see Methods for details).

As shown in Figure 11, even controls participants (bottom two graphs) showed highly variable LGN responses between individuals, exhibiting wide error bars, relatively low signal change, and an inconsistent pattern comparing the left (Figure 11E) and right hemispheres (Figure 11F). From the individual data, there was an almost equal preference for optimal speed across all five conditions – including static stimuli. This degree of inconsistency was considerably greater than speed responses in V1 or hMT+, where activity patterns were generally consistent across individuals. In a paired correlation analysis, LGN activity showed a weak correlation with hMT+ responses to speed in the same hemisphere ($r = 0.13$, $p = 0.25$). However, a much stronger correlation was seen with V1 responses in the same hemisphere, particularly on the right ($r = 0.37$, $p = 0.001$ for both hemispheres).

The LGN response to sighted hemifield stimulation in patients (Figures 11B for blindsight positive and 11D for blindsight negative cases) also appeared variable between participants. However when considered across all 14 patients, sighted LGN activity also showed a stronger correlation with sighted V1 responses ($r = 0.43$, $p = 0.0003$), and a weaker correlation with hMT+ in the same hemisphere ($r = 0.31$, $p = 0.01$).

5.4.8 LGN activity in blindsight positive patients correlates highly with hMT+ responses, and shows the greatest similarity to psychophysical performance

During blind hemifield stimulation, blindsight positive cases showed a slightly different pattern of LGN activation (Figure 11A). Instead of responses being similar to V1, LGN activity appeared to respond more like hMT+. Indeed there was a highly significant correlation between blind hemifield LGN responses and hMT+ activity in the same hemisphere ($r = 0.53$, $p = 0.0004$). There was also a significant albeit weaker correlation between blind hemifield LGN and sighted hemifield hMT+ responses in the opposite hemisphere ($r = 0.33$, $p = 0.04$), however there was no correlation with sighted V1 responses ($r = 0.14$, $p = 0.4$).

It is also worth noting that the LGN response to speed in the blind hemifield of blindsight positive patients (Figure 11A), similar to ipsilesional hMT+ (Figure 9A), both shared a resemblance to psychophysical detection performance in blindsight positive patients (Figure 4B). Correlation analysis confirmed that psychophysical performance correlated most strongly with LGN and hMT+ activity during blind field presentation ($r = 0.31$, $r = 0.29$ respectively), although this did not quite reach significance ($p = 0.09$, two participants had to be excluded from analysis due to performance at ceiling). Resemblance to fMRI responses in sighted V1, sighted LGN, and even sighted hMT+ were comparatively weaker ($r = 0.20$, $r = -0.18$, $r = 0.18$ respectively).

Blindsight negative patients did not demonstrate a notable correlation with hMT+ activity. LGN responses to stimulation of the blind field showed a more variable pattern (Figure 11C), in some cases more like hMT+ and other cases V1. Overall the pattern was most similar to blind hemifield hMT+ responses, however this was a very weak correlation that was non-significant ($r = 0.18$, $p = 0.34$).

5.5 Discussion

This study has shown that after V1 damage, fMRI response to low-luminance motion differed according to whether patients could detect the same images in their blind hemifield or not. Patients with significant blindsight function demonstrated more typical motion responses in contralateral hMT+, but which were unusually correlated with LGN activity in the same hemisphere. Normally the LGN response to speed is more similar to that of the early visual cortex. This difference in blindsight positive patients may have important implications for residual visual function and residual pathways following V1 damage.

5.5.1 Patients with V1 damage can detect both slow and fast complex motion

Two of the key findings in this study relate to its behavioural results. Firstly, psychophysical experiments demonstrated that even low-luminance, complex motion elicited significant detection performance in 8/14 patients, and discrimination performance in 4/14 patients with adult-onset V1 damage. The type of complex

stimulus used here is notoriously ineffective at inducing blindsight, (Azzopardi and Cowey, 2001; Barton and Sharpe, 1997) and is generally associated with particularly low levels of awareness.

The reason that this type of stimulus is particularly challenging is likely to relate to the receptive field properties of residual neurons involved in blindsight function. In the current study in particular, many patients had to be guided through the experiment so that they did not give their responses at the wrong times. It was not uncommon for patients to report that they had seen nothing at all. Contrast was likely to be a key factor in both blindsight performance and awareness. As seen in Chapter 3, increases in contrast not only dramatically increase detection performance, but are also associated with an increase in confidence scores and awareness.

With complex motion, movement is also distributed across a number of small components rather than a single, larger object moving through the visual field. It has been shown in Chapter 4 that global motion processing in hMT+ is abnormal after V1 damage. It is likely that normal receptive field properties in hMT+ are heavily influenced by the pattern of inputs from early cortical areas in the visual hierarchy. When these are silenced due to V1 damage, alternative inputs to hMT+ may dominate, which are likely to lack such effective summation of receptive fields to facilitate global motion perception (Ajina et al., 2014). That is not to say that detection would be impossible, indeed Huxlin and colleagues base their rehabilitation therapy around such stimuli (Huxlin, 2008), but that it may be considerably more difficult.

The second important behavioural finding relates to suggestions that blindsight function for slow moving stimuli (under 6°/s) should not be possible after V1 damage. This is because slow and fast motion are postulated to possess distinct neural pathways, with slow motion mediated through V1 (Beckers and Zeki, 1995; fftyche and Zeki 1995). The current study goes against this distinction, as patients have shown significant performance in both experiments for slow-moving dots at 4°/s, whilst identical but static controls could not be detected above chance. This is also supported by previous work showing that V1 lesions in macaques fail to abolish MT responses to slow moving stimuli (Azzopardi et al., 2003).

Patient GY, who has been investigated extensively in the past as a case study for blindsight, exemplified this theory of distinct motion processing streams. In early studies it was found that his blindsight performance was selective for fast moving stimuli (Barbur et al., 1993). It was also shown that EEG activity was absent in response to slow (but not fast) motion (Beckers and Zeki, 1995), and MEG signals arrived more quickly to hMT+ in response to fast motion, but to V1 first with slow motion (fftyche et al., 1995). In fact, these distinct abilities in GY are likely to have improved over time, and the experimenters have since acknowledged that GY can demonstrate neural responses to slow motion in his blind hemifield (Zeki and fftyche, 1998). Whether or not this suggests plasticity, it emphasizes the limitations that arise from single case studies. As shown here and shall be discussed more fully later on, the fMRI response to speed in hMT+ and its 'optimal' speed vary quite considerably between individuals. It would not be surprising therefore if this variability was also reflected in behavioural performance, which may even rely upon activity in this region.

5.5.2 Blindsight positive patients show similar hMT+ responses to speed in the blind and sighted hemifield

fMRI was used alongside psychophysical experiments to try and understand how patients' behavioural responses may have occurred. The results presented here, similar to previous chapters, strongly implicate residual hMT+ in the damaged hemisphere as being critically involved. Blindsight positive cases showed significant activity in what are considered to be classic motion-sensitive regions. The blindsight negative group also showed significant occipital responses to motion, however these tended to be less focal and located more inferior to normal hMT+ coordinates, both anterior and posterior at the border with V4. Blindsight positive patients also showed more typical hMT+ responses to speed within identical, anatomically-defined ROI masks.

While several previous studies have demonstrated hMT+ activity during blind hemifield stimulation (Barbur et al., 1993; Holliday et al., 1997; Zeki and ffytche, 1998; Goebel et al., 2001; Schoenfeld et al., 2002), this is the first to show that fMRI responses to speed remain essentially normal in blindsight patients with V1 damage. Furthermore, there are notable similarities between hMT+ fMRI activity and behavioural performance measures. The inverted-U pattern often described behaviourally (e.g. Azzopardi and Cowey, 1998) and demonstrated here, is reminiscent of the characteristic fMRI response of hMT+ to increasing speed of motion (Chawla et al., 1998; 1999). Whilst a small proportion of the imaging studies listed above comment on the lack of an association between hMT+ activity and

awareness or conscious perception (Goebel et al., 2001; Zeki and fftyche, 1998), the relationship between *performance* and fMRI activity has rarely been addressed. Similarly, the only study to look at speed using fMRI did so in GY because of his distinct awareness for fast and slow motion (Zeki and fftyche, 1998). The investigators noticed that activity was highly significant for fast motion, and weaker although still present during slow motion if less stringent statistical thresholds were applied. Whilst this was interpreted exclusively in the context of awareness, GY's performance at direction discrimination in the two conditions was also different, scoring 100% with fast motion compared to 80% with slow (Sahraie et al., 1997). Therefore it is highly plausible that his behavioural performance was related to the degree of hMT+ activation, similar to the results here demonstrating a correlation between psychophysical performance and LGN/hMT+ activity patterns. This pattern in GY would also be consistent with a normal hMT+ response to speed reported here in blindsight positive patients and healthy controls.

The variability of preferred hMT+ speed between participants (both controls and patients) is consistent with numerous neurophysiology and fMRI reports. Most neurons in MT have an optimal response between 4°/s - 64°/s, although the range can be very wide, spanning 2 – 256°/s (Rodman and Albright, 1987; Cheng et al., 1994). This easily encompasses the range used in the current study (4-32°/s), which may have benefitted from using a wider test range. In comparison, neurons in the striate cortex prefer slightly slower speeds of 1-32°/s, with the vast majority between 2-16°/s (Van Essen, 1985; Priebe et al., 2006). Responses in LGN neurons are less widely described, but show even greater variability. P-cell firing tends to increase up to speeds of 50-80°/s, whilst M-neurons can show a number of different responses,

some responding well to slow speeds, and others responding only to speeds above 20°/s (Lee et al., 1979). Functional MRI represents an indirect measure of neural activation that is likely to reflect an aggregate of neuronal physiology responses, represented by each voxel. fMRI studies suggest a preferred range in hMT+ of 4/7 - 30°/s (Chawla et al., 1998; Chawla et al., 1999), which is also consistent with fMRI results here. As in the current study, they also report a degree of variability between participants and even hemispheres. However, this is understandable given that neuronal measures of optimal speeds in MT are also highly varied, and fMRI cannot resolve responses in individual cells.

To date, there is limited evidence to suggest whether in the absence of V1, hMT+ sensitivity to speed should be affected. On balance, most work supports the notion that hMT+ can respond to speed independently of V1, and is therefore consistent with the results presented here. In the principal study of this kind, Rodman et al. (1989) performed striate cortex removal in the macaque and measured speed tuning responses in MT neurons. They found that cells with receptive fields entirely within the lesion zone could still demonstrate sensitivity for speed of motion (and directional selectivity), with a peak around 32°/s, approximating to the preferred speed in MT (Rodman and Albright, 1987). Azzopardi et al. (2003) also showed that after V1 damage, although generally weaker, ipsilesional MT neurons continue to respond to tested speeds of 4 and 20°/s.

In much later work, Chawla et al. (1998) attempted to uncover whether classical hMT+ speed responses were intrinsic to that region, or dependent on differential sensitivities from parvo or magnocellular pathways. By using targeted chromatic (P)

or luminance-defined (M) stimuli, they showed that there was no difference in speed responses when either channel was isolated, implying that sensitivity to speed was intrinsic or at least insensitive to earlier processing differences specific to the M and P channels (Chawla et al., 1998). In fact this went against their prediction, which had been based upon the theory of distinct fast and slow motion pathways discussed earlier. They replicated the study using optimised methods (e.g. removing absolutely all luminance contrast from the chromatic condition), and suggested that they could now see an interaction between speed and colour/luminance (Chawla et al., 1999). In fact, their new result was in the opposite direction to that expected, and was based upon just one third of their data. Optimal speeds for chromatic contrasts (isolated P channel) were actually *higher* than those using luminance contrast (M-channel). Also, both conditions show quite typical hMT+ responses to speed, which are maintained over 'slow' speeds. This is more in keeping with the conclusions from their earlier study supporting an intrinsic or M/P independent pathway for speed responses in hMT+.

5.5.3 Subcortical pathways underlying motion perception

Critically, the current study also implicates ipsilesional LGN in residual hMT+ responses and blindsight function. Significant LGN activation was elicited during blind hemifield stimulation in blindsight positive patients, and LGN responses correlated well with hMT+ responses in the same hemisphere, and with behavioural measures of blindsight performance. This pattern of LGN activity was unusual, as fMRI responses in controls and the sighted hemifield of patients instead correlate with V1 responses. This suggests that a distinct, hMT+ like component was measured

in blindsight positive patients. One possible explanation is that other components normally contributing to LGN fMRI activity have been diminished, such as P-channel neurons. Another possibility that cannot currently be ruled out, is that reciprocal feedback connections from hMT+ to LGN elicit this response. It may be that assessments of relative fMRI timings would be helpful to comment on this (e.g. Gaglianese et al., 2012).

The LGN can be a challenging region to image because of its small size and deep location (Chen et al., 1999). Nevertheless, fMRI studies have reported heterogeneous response properties in the LGN that are speculated (with sufficient resolution) to correspond to the distinct populations of magno and parvocellular neurons (Schnieder and Kastner, 2004; Schneider and Kastner, 2005). Furthermore, P-cells are believed to outnumber M-cells by at least 8 to 1 in central vision representation in the macaque LGN, (Kaplan, 2012), making it likely that average LGN responses would mostly reflect dominant P-neuron activity. Following V1 damage, transneuronal degeneration is well recognised, and can lead to atrophic changes in the LGN with time (Bridge et al., 2011; Cowey et al., 2011; Millington et al., 2014). Given the critical connection between the parvocellular channel and V1 neurons (e.g. Movshon and Newsome, 1996), those cells appear to be particularly vulnerable after V1 damage. It is therefore possible that the LGN shows an altered response to speed because it is now primarily driven by whatever residual neurons remain. Those residual neurons may also possess direct connections to hMT+ (Sincich et al., 2004). Given this, an interesting follow-up study would be to look for changes in LGN fMRI patterns over time, after V1 damage.

It is also necessary to consider what may be occurring in blindsight negative cases. Six blindsight negative patients showed an abnormal response to speed in hMT+, which was more similar to normal V1 activity. Is it possible that this reflects a difference in their motion-pathway? One possibility is that a different subcortical pathway was driving hMT+ activity, such as via the inferior pulvinar nucleus. In this patient group, a small cluster of activity was seen in a region consistent with reports on the inferior pulvinar (Kastner et al., 2004; Leh et al., 2008). This region has been implicated in studies of indirect and attentional blindsight, where despite a complete absence of awareness, blind field stimulation can indirectly influence sighted-field responses (Leh et al., 2006). The inferior pulvinar is known to receive retinal input from V1 and the superior colliculus, and like the LGN, is suggested to possess a direct reciprocal connection with MT (Benevento and Standage, 1983; Ungerleider et al., 1984; Warner et al., 2010). In the macaque, inferior pulvinar neurons respond to a wide range of velocities, but orientation-sensitive cells (two-thirds of the population) show a preference for motion under 32°/s, similar to V1 (Bender, 1982; Van Essen, 1985). This could account for the different sensitivity to speed seen in this group, although it remains possible that these orientation-sensitive responses are derived solely from striate cortex receptive fields (Bender, 1983).

Regardless, it is important to note that even 'blindsight negative' patients may possess residual visual function. As discussed earlier, the current set of experiments involved particularly challenging blindsight tests. Indeed, in a separate, high-contrast task, three of the six 'negative' cases performed significantly above chance, and were labelled as blindsight positive. Even behavioural performance in the current study hinted at a weak residual sensitivity to speed. It is therefore possible that those six

patients possess the same or similar pathways to the blindsight positive group here, but for some reason elicited insufficient behavioural responses with the current stimuli. Patient GY has also undergone neuroimaging during unaware conditions (Sahraie et al., 1997), and elicited significant activation in the ipsilesional occipital lobe. As was the case in this patient group, his pattern of activity was different to that during aware conditions. However, this does not mean that the two patterns reflected distinct underlying pathways.

5.5.4 Conclusions

In conclusion, this study tested a relatively large group of 14 patients, all of whom sustained unilateral damage to V1 in adulthood. Critically, not all the patients showed the same residual visual function, and fMRI activity could be compared according to the presence or absence of blindsight function. In doing so, it has been possible to uncover the following:

(1) Normal hMT+ response to speed, an important domain of motion processing, is preserved after V1 damage in blindsight positive patients. This suggests that characteristic speed responses may reflect distinct, V1-independent inputs, or are intrinsic to the region and therefore independent of differential sensitivities in all input channels.

(2) Slow motion < 6°/s cannot solely be transmitted to hMT+ by a separate pathway through V1, since both behavioural and hMT+ fMRI responses at 4°/s were preserved after V1 damage.

(3) Ipsilesional LGN is strongly implicated in residual visual function following V1 damage, and shows significant activation during blind field stimulation in blindsight positive patients. Responses to speed show a different sensitivity to normal, which may reflect the activity of residual geniculate neurons that possess direct connections to hMT+.

(4) Psychophysical blindsight performance is likely to reflect the degree of underlying LGN and hMT+ activation, as both these regions showed responses to speed that were similar to performance.

(5) Blindsight negative patients also show significant occipital responses to motion in the blind hemifield, but with a number of different characteristics. It is possible that the presence or absence of blindsight function reflects differences in residual visual pathways, which carry different motion information.

Chapter 6

Category-specific visual processing in the ventral stream following V1 damage

6.1 Abstract

Residual ventral stream processing after V1 damage is a relatively neglected area of study. This is likely to reflect the fact that blindsight performance and neuroimaging responses for ventral stimuli are notoriously difficult to elicit. Despite this, numerous non-striate pathways carry visual information to the ventral visual cortex in non-human primates. This study employed psychophysics and a prolonged fMRI design to explore category-specific processing for faces and places in a large group of patients with V1 damage. As expected, the discrimination of faces and places in the blind hemifield was extremely challenging, but significant performance was demonstrated in certain patients. The majority of patients could also identify the temporal interval of stimuli above chance. Furthermore, those patients showed significant category-specific fMRI responses in ventral regions of cortex associated with normal face and place processing. This implies that category-specific processing is possible in the ventral stream despite V1 damage, and may be more common than first considered.

This supports the presence of intact residual pathways to the ventral stream, bypassing V1.

6.2 Introduction

After V1 damage, examples of ventral stream processing in the blind hemifield are rarely reported in comparison to motion-responses. Similarly, blindsight performance for characteristics associated with this pathway are notoriously difficult to elicit. This is intriguingly similar to unconscious processing in binocular rivalry, where ventral responses in healthy controls are considerably more difficult to detect than dorsal (Lin and He, 2009). However, such processing does occur (Logothetis and Schall, 1989; Sheinberg and Logothetis, 1997; Jiang and He, 2006), and includes category-specific processing for invisible faces and houses when more sensitive multivariate fMRI pattern analyses are employed (Sterzer et al., 2008).

One can speculate a number of reasons why ventral processing is uncommon in patients with V1 damage. Firstly, this region may show a relatively weak signal change compared to activity in the dorsal stream. If extrastriate activity relates to blindsight performance, then one might expect a weaker signal to also account for a relatively poor psychophysical performance. Similarly, ventral activity may be more dispersed than dorsal responses, and may therefore only be detected using more sensitive approaches which consider the spatial pattern of responses, rather than averaging across regions of interest (Haynes and Rees, 2005). A third possibility is that patients with V1 damage simply do not possess residual retinal input to the

ventral visual cortex. Alternatively, retinal input may no longer be possible in patients with large lesions extending to the early ventral visual cortex.

Although rare, ventral responses have been observed following V1 damage (Schmid et al., 2009; Schmid et al. 2013; Goebel et al., 2001; Schoenfeld et al., 2002). There are also examples of significant visual performance for ventral stimulus characteristics (Trevethan et al., 2007; Das et al., 2014). In support of this, non-striate ventral stream pathways are well described in the animal literature. These include direct connections with the LGN, inferior pulvinar and amygdala (Fries 1981; Benevento and Davis, 1977; Turner et al., 1980), as well as interhemispheric cortico-cortical connections (Van Essen et al., 1982). Therefore it appears that ventral processing in the absence of V1 *should* be possible, but is perhaps associated with relatively weak signal change that may be difficult to detect.

The current study was designed to evaluate this; specifically measuring category-specific ventral processing for faces and places in a large group of patients with V1 damage. This included psychophysical tests of detection and discrimination, alongside fMRI. By employing a prolonged fMRI protocol and testing a large number of patients, it was hoped that any presence of residual ventral activity might be detected. Furthermore, this activity could be compared between blindsight positive and negative patients. This would help to establish whether non-striate ventral pathways may exist in patients with chronic V1 damage, and whether such pathways are sufficient to support category-specific processing in the ventral visual stream.

6.3 Methods

6.3.1 Participants

Fourteen patients (three female) took part in the study. Ten cases had damage to the left hemisphere, causing right-sided visual field loss; four cases affected the right hemisphere with left sided hemianopia. Pathology had been caused by posterior circulation stroke in 13 patients, and one patient had undergone benign tumour resection. Average age at the time of participation was 54.9 years ±16.1 S.D., average time after pathology onset 49.6 months (range 6-252 months). Seven age-matched, healthy participants (52.6 ±11.4 S.D years of age, four female) served as controls.

6.3.2 Stimuli

Visual stimuli consisted of two sets of eight unique images, one depicting human faces and another of simple outdoor scenes representing the category of 'places' (Figure 1A). Face stimuli were coloured images of emotionally neutral, expressionless caucasian faces taken from a set of randomly generated images using the Facegen Modeller program (http://facegen.com) version 3.1. The exact procedures including model validation are described in Oosterhof and Todorov (2008). Eight different face identities were chosen, each covering an ellipsoid area subtending either 7.25° or 5° in height. Simple scene images were taken from the revised Snodgrass and Vanderwart's object databank, with colour and texture previously added to the original images for improved recognition (Rossion and Pourtois, 2004). Eight images were selected to represent outdoor places, subtending between 6-7.25° visual angle for large stimuli, or 4.1-5° for the smaller version, for use in patients with

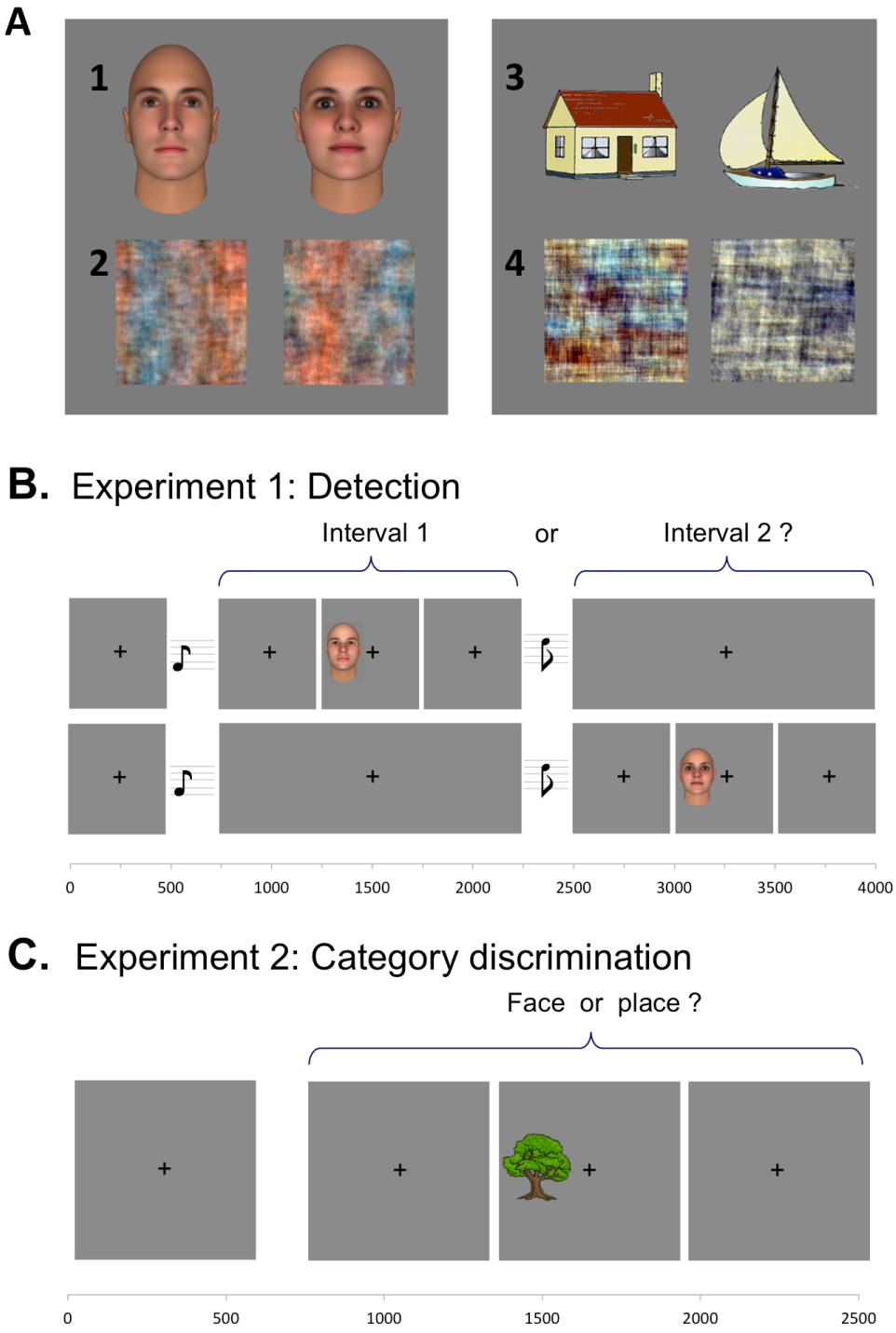

Figure 1. Visual stimuli and psychophysics experiment design. (A) Stimuli consist of a coloured picture of a face, place, or scrambled face or place, subtending 7.25° or 5° in height. (1) Two example face stimuli. (2) The same face stimuli, scrambled. (3) Two example place stimuli. (4) The same place stimuli, scrambled. **(B)** Experiment 1: Temporal 2-AFC detection. Participants fixate on a central cross, with the onset of each 1500 ms interval alerted by a low pitch tone (interval 1) or high pitch tone (interval 2). The stimulus appears in either interval at random, for a period of 500 ms. At the end of the trial, participants must report which interval the stimulus appeared. **(C)** Experiment 2: 2-AFC category discrimination. Throughout each trial of 2500 ms duration, participants are required to fixate on a central black cross. During this time, a stimulus appears for 500 ms with jittered onset. At the end of the trial, patients must indicate whether the stimulus was a face or place. If they saw nothing, they are instructed to guess.

quadrantanopia or those with more peripheral visual field deficits. These images were selected because during piloting with healthy controls, they elicited the strongest category-specific processing in the PPA contrasted against faces. They also shared a relatively simple structure with the computer-generated face images (Figure 1A), which would have been very different to the use of photographs. All images were scrambled for use as controls, by applying a 2D Fourier-transform (Figure 1A). This method changed the position (i.e., the phase) of all affected spatial frequency components whilst maintaining the Fourier 2-D amplitude spectrum across orientations and spatial frequencies. The distribution of energy across the orientations (2-D power spectrum) was thus maintained while their positions (the phase spectrum) were randomized (Honey et al., 2008). Scrambled images subtended 7.25^{o} for large stimuli, and 5^{o} for the smaller set. Scrambled places and faces were kept as separate conditions, assessed separately.

6.3.3 Psychophysics

Psychophysical testing employed two 2-AFC tasks: (1) 2-AFC temporal detection (2) 2-AFC category discrimination (see Figure 1B and 1C for schematic, and General Methods for details). Testing was restricted to the blind hemifield throughout, and patients were not familiarised with the stimuli so that they would not be influenced when describing 'blind-field' images to the experimenter. In addition, confidence ratings were collected wherever possible for each trial, using a scale of 1-10. It was explained that a rating of 10 was to be used if they were absolutely certain, whilst 1 was for a complete guess. 12/14 patients completed both experiments.

The presence or absence of blindsight was assessed according to the criteria

described in the General Methods, for significant performance in either Experiment 1 or 2. One patient (P12) had only completed Experiment 2, but was defined as 'blindsight negative' as he was at chance in Experiment 2 as well as the highly-sensitive contrast detection task in Chapter 3. Another patient (P14) did not complete either experiment, despite undertaking fMRI. He was also at chance during contrast detection and was classified as 'blindsight negative'.

6.3.3.1 Experiment 1: 2-AFC Temporal Detection

Stimuli were selected at random from the two categories of faces or places (see Figure 1B). All 8 images from each were presented once during every block, representing 16 trials per block. After 8-10 blocks of testing, scrambled images were presented as a direct continuation of the experiment. No indication was given to patients that there had been a change in stimulus, and the task remained identical. Due to time limitations, data for scrambled images was collected in 9/12 patients.

6.3.3.2 Experiment 2: 2-AFC Category discrimination

Again face or place stimuli were selected at random, and presented in blocks of 16 unique trials (Figure 1C). Patients were asked to indicate whether the stimulus had been a face or place. There were no scrambled trials. Seven patients completed 10 blocks, and five patients completed 5 – 8 blocks, due to time constraints.

6.3.4 fMRI procedure

Images of faces or places were presented to either hemifield in an fMRI block design, representing 4 different conditions (see Figure 2A for schematic). Conditions were sequenced using a pseudo-random Latin square design, such that each condition

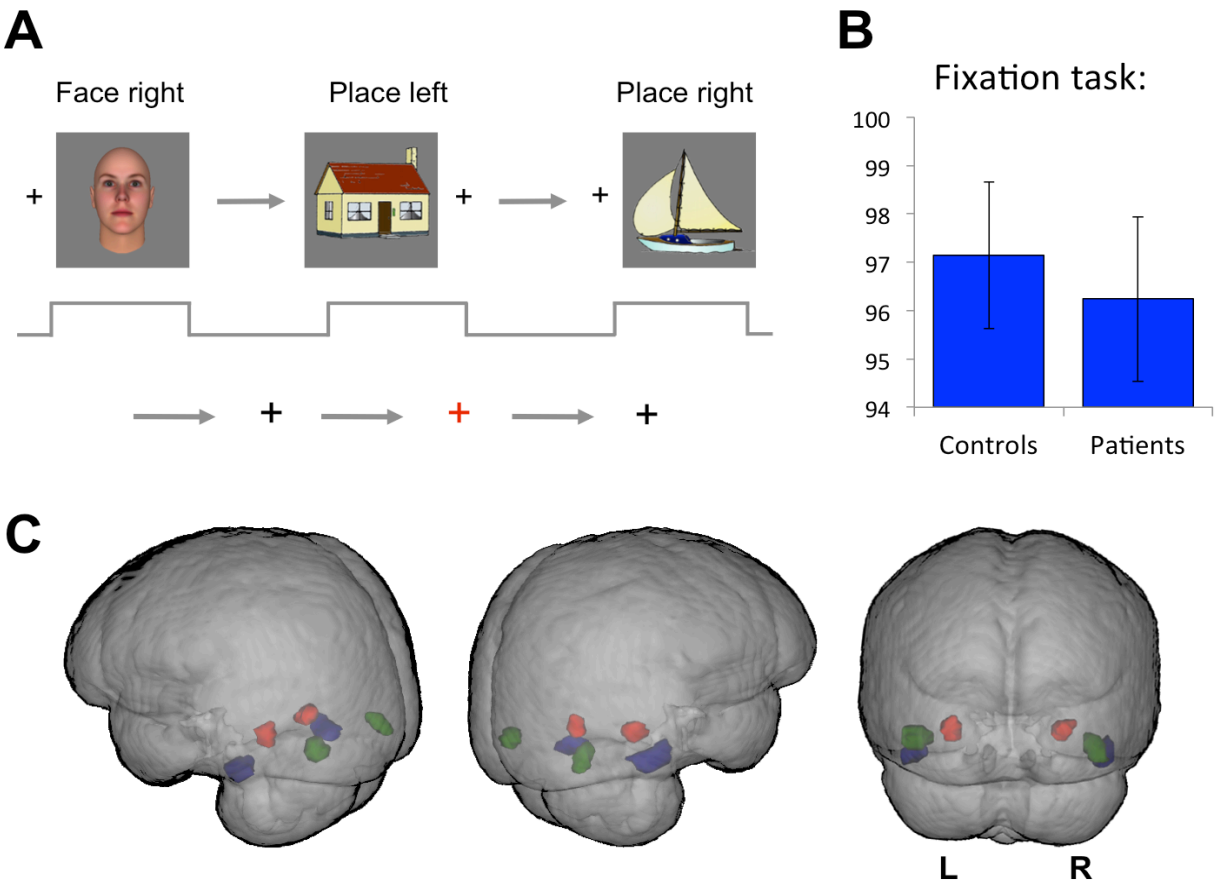

Figure 2. fMRI procedure and regions of interest. **(A)** This simple block design presents each stimulus category (face or place) to the blind portion of visual field or its equivalent location in the sighted hemifield. Each block lasts 16 s with 10 s rest periods. Each condition is repeated twice per run, with six stimulus runs per experiment. The seventh run presents scrambled controls. Stimuli have identical parameters to psychophysical experiments. **(B)** Throughout all condition and rest blocks a fixation task requires participants to press a button every time the central fixation cross changes colour from black to red. Colour changes occur at random lasting 300 ms. All participants scored at least 90% on this task, with the mean and standard error of the mean displayed here. **(C)** Bilateral ROI masks displayed on a 3-D 'glass brain' reconstruction such that both hemispheres are visible. The FFA is shown in blue, PPA in red, and OFA in green.

block was repeated 12 times, and control blocks twice. This was divided into seven runs of equal duration, six showing the test-stimuli and one control run presenting only scrambled images. Eight images from the same category were consecutively presented for 2s each, with an inter-stimulus interval of 500ms. A 10s rest period followed each 16s condition. One block of four conditions lasted 120s, with each run containing two blocks, therefore lasting 240s. Each of the seven runs was carried out with a separate MRI acquisition.

6.3.4.1 fMRI Eye-Tracking

Eye movements in this fMRI experiment were particularly important to consider, since this experiment was designed to simply look for the *presence* of activation during blind field stimulation. Any inadvertent shift of the stimulus into the sighted field of view may result in activation incorrectly labelled as blind-field activity. As a result, a particularly cautious approach was taken for the analysis of blind field fMRI data.

For this experiment, all patients had to have undergone successful eye tracker calibration at the start of scanning, and generated a full set of eye position data for all experimental runs to be included in the analysis. Additionally, a more stringent set of criteria were used to define deviations in eye position during blind hemifield blocks. A significant deviation was defined as an eye position of at least 1.5^{o} away from the central fixation cross towards the stimulus during blind field conditions, lasting for at least 10 ms in duration. All EPI volumes containing any such deviations were excluded from analysis.

Using this criteria, eye tracker data was adequate for blind hemifield analysis in 10 out of 14 patients (7 patients with left V1 damage, and 3 with right V1 damage). Of those ten patients, the average number of volumes excluded from analysis was 5.1 volumes/run (S.D. = 6.9 volumes/run, range = 0 – 24 volumes), with each run containing 126 volumes.

In addition, all participants had to perform over 90% on a concurrent behavioural task, requiring fixation throughout the experiment (Figure 2B).

6.3.5 fMRI acquisition and pre-processing

Each EPI sequence (corresponding to one experimental run) consisted of 126 functional volumes, duration 4 min 12 s. Seven runs were carried out in each scanning session, total duration 29 min 24 s excluding short rest periods between scans. For parameter and pre-processing details, please see General Methods (Chapter 2).

6.3.6 fMRI analysis

6.3.6.1 Regions of interest

Fusiform face area (FFA) and parahippocampal place area (PPA) masks were created from a combination of the control data collected here, and a previous data-set recording fMRI responses to faces and houses in twelve healthy, sighted controls (Bridge et al., 2012). These masks were concordant with published MNI coordinates (e.g. Epstein and Kanwisher, 1998; Park and Chun, 2009). An additional region of interest was created in the occipital face area (OFA), centred around MNI coordinates -40, -80, -8 on the left, and 40, -80, -10 on the right. This region was primarily based upon coordinates obtained from the literature (Haxby et al., 2000; Grill-Spector et al., 2004; Rotshtein et al., 2005; Harris et al., 2012), but was confirmed to be consistent with selective fMRI activity in control participants. 3-D renderings of all masks are shown in Figure 2C.

Masks were defined in $2mm^3$ standard space, where all individual and group-level analyses were carried out. FFA masks had a volume of 122 voxels on the right, centre of gravity: 46, -48, -22, and 137 voxels on the left: -44, -48, -26. OFA masks averaged

at 90 voxels in each hemisphere: MNI coordinates 40, -78, -8 on the right and -40, -80, -6 on the left. PPA masks were 90 voxels on the right (MNI: 28, -44, -12), and 76 voxels on the left (MNI: -26, -48, -12).

For individual fMRI analyses, each run had to first be analysed separately by entering each of the four fMRI conditions (e.g. left hemifield, face) into a general linear model as separate explanatory variables. Two methods of analysis were then performed. The first contrasted each explanatory variable against the baseline fixation task in order to generate contrast of parameter estimates (COPEs) for each condition. The other method contrasted one condition against another, to assess where in the brain neural activity was driven more by one condition than the other, e.g. left hemifield face > place. Each analysis therefore generated eight contrasts, four using the first method, and four using the second. Repeat runs were then averaged using a fixed effects analysis, entering COPEs from each run as separate inputs into a higher level GLM. Two explanatory variables were used; the first represented experimental runs 1 – 6, the second was for the final scrambled control run. Two contrasts were then generated; one simply represented an average of each contrast across the first six runs. The other contrasted face or place responses against their corresponding scrambled condition, e.g. left hemifield face > scrambled face.

Once this second level of analysis was performed, each participant had a measure for every contrast of interest across repeat runs, in standard space. Signal change was then extracted from pre-defined regions of interest for each individual. The percentage signal change was calculated by scaling the COPE by the peak-peak height of the regressor, and dividing by the mean over time. These measures were averaged

across participants to generate group plots for signal change in each contrast, and were used in all subsequent correlation or regression analyses.

6.3.6.2 Whole brain GLM group analysis

Group analyses were also performed to look for differences in activation extent and localisation across the whole brain. For this purpose, patients were subdivided according to which hemisphere had been lesioned. Unlike in the previous three Chapters, it was decided that results should be analysed separately for patients with either left or right hemisphere V1 damage. Previously, a technique had been used to flip certain images in the horizontal plane so that they all conformed to a uniform pathological template. This would be inappropriate here because face/place processing is often considered to be lateralised, irrespective of which hemifield is in receipt of visual stimulation. For example, the right FFA is often cited as being particularly important for face processing (Kanwisher et al. 1997; McCarthy et al. 1997). This is unlike motion processing, where neural activation is consistently greatest in the contralateral motion area hMT+. Such distinctions would be lost if certain patients had their imaging flipped, and would make any inferences on the impact of V1 lesions considerably more difficult to make.

COPEs for each participant were entered into one of three group level analyses. These were carried out separately for (i) the control group, (ii) patients with right hemisphere damage, and (iii) patients with left hemisphere damage. Only the patients with adequate eye tracking data were included in blind hemifield analysis. Therefore in the right V1 damage group, sighted hemifield data was used from four patients, and blind left hemifield data from three. In the left V1 damage group, data for the sighted

field was used from ten patients, and blind right hemifield data from six. Mixed effects analyses were carried out in patients and controls, unless otherwise stated. A statistical threshold of $p < 0.001$ uncorrected was used to test for significance within regions of interest, for which there were *a priori* hypotheses. Elsewhere correction for multiple comparisons was made using a cluster threshold of $p < 0.05$. All activation coordinates are reported in MNI space, and z statistic images are displayed on mean structural images for each group, which have been transformed to standard space.

6.4 Results

6.4.1 Psychophysics

Eight out of twelve patients (66.7%) were able to significantly detect face or place stimuli inside their blind hemifield above chance, but only four patients (33.3%) performed significantly different to chance at discrimination of the stimulus category.

6.4.1.1 Experiment 1: 2-AFC Temporal Detection

Overall 2-AFC detection performance for the patient group was significantly greater than chance for face and place stimuli (Figure 3A), with no apparent difference in performance between the two stimulus categories. However, not all of these patients individually scored above chance. Eight out of the twelve patients tested met the criteria to be labelled as 'blindsight positive' on this task, since they were able to detect stimuli significantly above chance using a minimum statistical threshold of $p <$

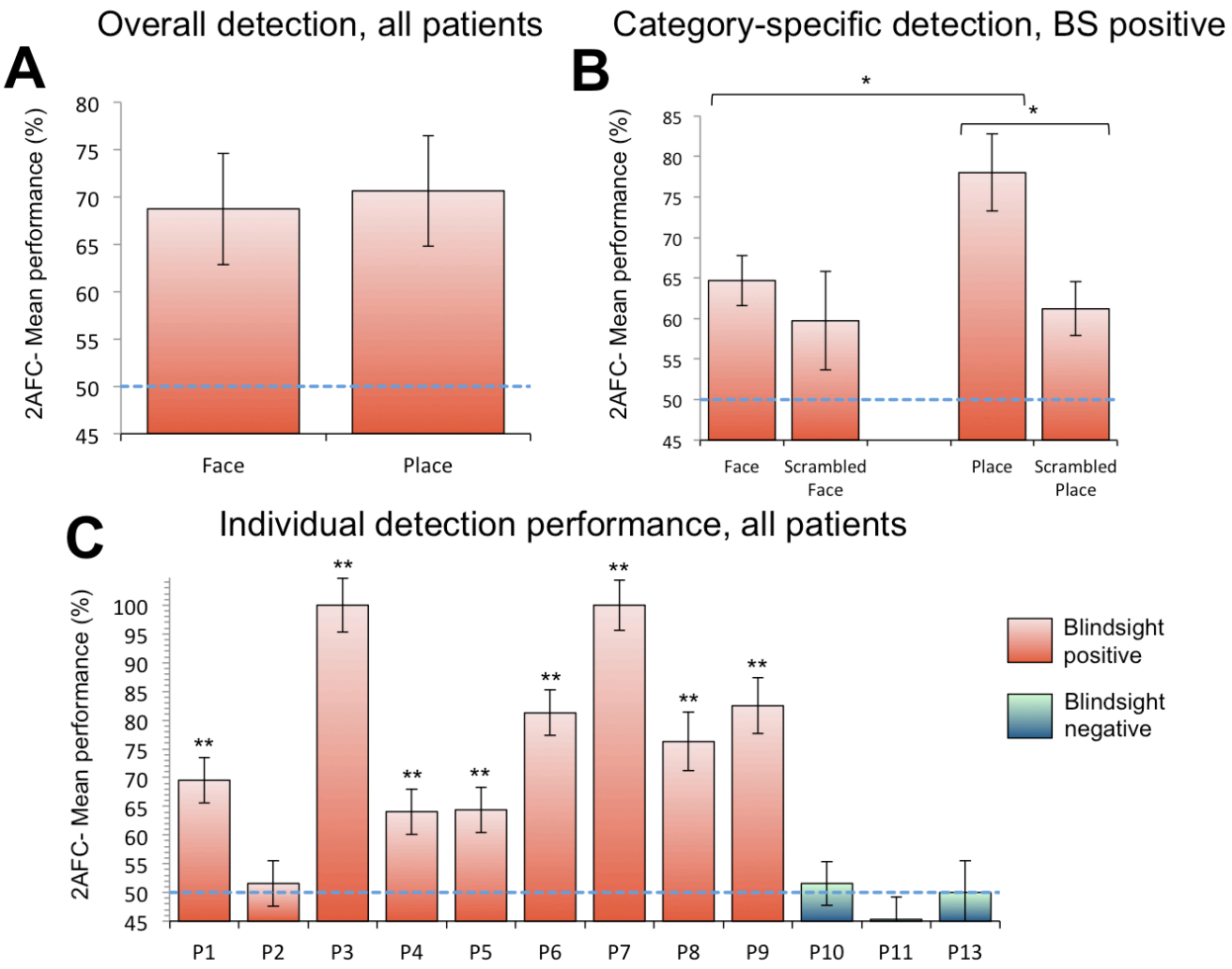

Figure 3. Psychophysics results for Experiment 1. (A) Average detection performance for all patients was significantly above chance for both stimulus categories, with no difference comparing faces to places. **(B)** In blindsight positive patients, the detection of places was significantly greater than faces, and also when compared to scrambled places. **(C)** Individual performance is shown here for each patient. Red bars represent blindsight positive patients, blue bars are blindsight negative. P2 is red as he was above chance in Experiment 2. The dotted blue line in all charts represents chance level (50%). Error bars represent standard error of the mean in group results (A and B), and the standard deviation for individual results (C). * $p < 0.05$, ** $p \leq 0.001$. BS = blindsight.

0.05 (Figure 3C). In fact, all eight patients reached or surpassed a statistical probability threshold of 0.001. Despite this, performance varied quite considerably amongst these individuals, with a range of average scores: 64.1 – 100%. Two patients (P3, P7) were at ceiling, and were able to reliably and confidently detect all stimuli, irrespective of image category. This included detection of scrambled face or place

controls. The remaining six patients who each performed above chance were considerably less accurate, with mean score 71.7%, range: 64.1 – 81.25%.

When performance was analysed solely for the group of blindsight positive patients, a difference in performance between stimulus categories emerged, which was particularly clear when patients at ceiling had been excluded from analysis (Figure 3B). Place stimuli were actually detected at a significantly greater frequency than faces ($p = 0.024$, $t = 3.53$, $df = 4$, paired t-test), and also compared to scrambled controls ($p = 0.026$, $t = 2.8$, $df = 7$, unpaired t test, since not all patients completed the scrambled conditions – see Methods for details).

6.4.1.2 Experiment 2: 2-AFC Category Discrimination

Overall discrimination performance for the group was a lot closer to chance than detection performance (Figure 4A, average performance 51.6%, $n = 12$), highlighting the considerably more difficult nature of this test. Discrimination, either across the whole group or just the blindsight positive group, did not differ for faces or places. In this situation, positive predictive value (PPV) was used to provide a useful surrogate for discrimination performance. This is because it took into account the overall guess rate and any inadvertent bias towards one category, rather than just the presentation frequency. If, for example, a patient almost exclusively reported ‘place’ despite stimuli being presented equally for both category, this would be taken into consideration with the PPV.

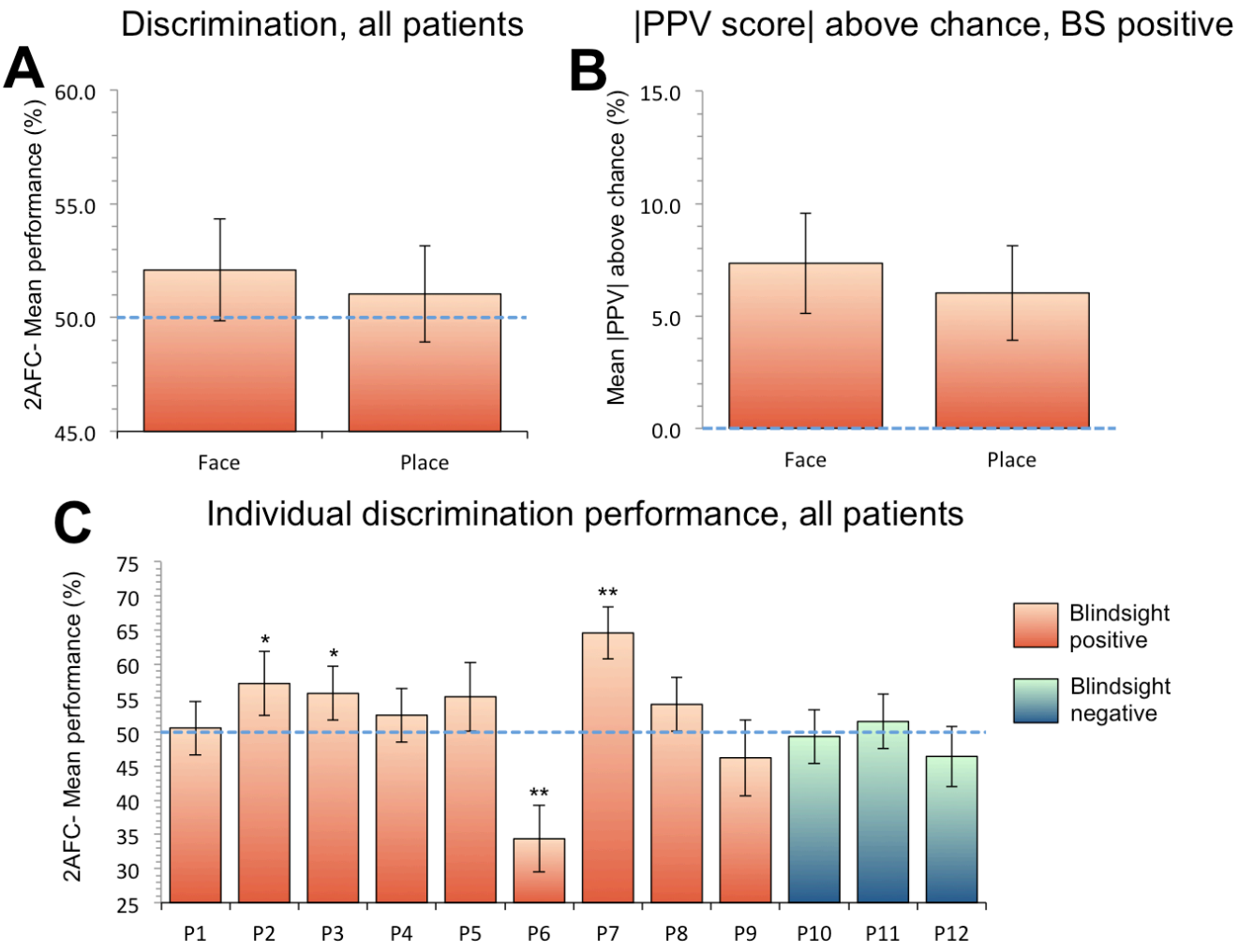

Figure 4. Psychophysics results for Experiment 2. (A) Discrimination performance was calculated for each category separately using the positive predictive value (PPV), which considers each patient's guess rate thus removing response bias. Average discrimination across all patients was much poorer than detection (Experiment 1), and remained at chance. There was also no significant difference between categories. **(B)** This plots the modulus of PPV score minus chance (50%), averaged for only the 'blindsight positive' patients: P1-9. Amongst these nine patients, average discrimination performance was significantly above chance (now represented as 0%), and was very similar for both stimulus categories. **(C)** Individual performance is shown here for each patient, averaged across both stimulus categories. Red bars represent blindsight positive patients, blue bars are blindsight negative. The dotted blue line in all charts represents chance level. Error bars represent standard error of the mean in group results (A and B), and the standard deviation for individual results (C). * $p < 0.05$, ** $p \leq 0.001$. BS = blindsight.

It is also worth noting that discrimination performance could be relevant, even if it was significantly below chance. It may be possible for a patient to correctly discriminate a difference between stimulus categories, yet be unable to label their

category correctly. This would still reflect a preserved capacity for discrimination. Figure 4B plots the modulus of the PPV score minus chance (50%), averaged for only blindsight positive patients, P1-P9. This analysis shows that discrimination performance in the blindsight positive group was significantly greater than chance (now represented as 0%), whilst performance remained similar for both stimulus categories.

Examining the individual data, only four patients scored significantly different to chance according to their individual performance (P2, P3, P6, P7, see Figure 4C), with one patient (P6) significantly below chance. One of these patients (P2) had in fact performed at chance on the detection task in Experiment 1. Two patients showed significant performance for one of the two image categories (P2, P3), both of whom were better at discriminating faces. Aside from these four individuals, two patients were consistently over 50% at discrimination, but did not quite reach significance (P5, P8). The two patients who performed at ceiling in Experiment 1 (P3, P7) were also above chance in Experiment 2, although their performance was dramatically reduced in both cases, averaging at 57.1% and 64.5%. Therefore, although they could accurately detect all images placed within their blind hemifield, they were unable to distinguish whether these were images of faces or places in over a third of trials.

6.4.1.3 Confidence, awareness, and subjective descriptions

As described above, two patients were able to confidently detect 100% of stimuli. However, neither patient was at all confident of their performance in Experiment 2. The first patient, P3, although always aware of an image in the blind hemifield, was never confident about what this portrayed, with a mean confidence ratings of 1.1/10.

P3 also reported to the experimenter that images were only ever '*in black and white*'. The other patient at ceiling in Experiment 1 (P7) was also above chance in Experiment 2. Interestingly, his general impression was that all images were shaped like faces, whilst this was clearly not the case. He also stated that he was not at all confident, and his responses were also almost exclusively guesses.

At least three patients offered descriptions of stimuli that were completely incorrect, and were similar to sighted stimuli used in Chapter 3. For example, P8 thought that the stimuli at times appeared like '*moving ripples, sometimes clearer, like a black and white barrel*'. P6 also described seeing black and white images at times, depicting wavy motion. P11, who was at chance in both tasks, also thought he could see '*thumbprints'* and '*zig-zag lines'* at times.

Of the remaining blindsight positive patients, P4, P5 and P9 gave average confidence ratings of only 2.1 / 3.8 / 3.0 out of 10 respectively for detection. On questioning, P4 guessed that the images looked like '*ringed blobs*', but could not distinguish the image category. P5 described seeing a dark shape at times, like a silhouette, but also felt unable to discriminate different shapes. His confidence rating for discrimination was 1.8/10.

Blindsight negative patients P12 and P13, as well as P2 (who was at chance on Experiment 1, but above chance in Experiment 2) all described their responses as complete guesses.

6.4.1.4 Eye tracker results

12 trials were excluded from analysis in Experiment 1, and 8 trials from Experiment 2 due to eye movements made towards the stimulus. These were identified from retrospective eye tracker data analysis, or flagged for exclusion at the time of the experiment.

6.4.2 Controls show differential fMRI activation for faces and places

Presentation of both stimulus categories elicited marked early visual cortex activity in the contralateral hemisphere, with predominance for each category restricted to well-described regions including the FFA, OFA and PPA. Face stimuli in controls were associated with greater activation in bilateral FFA and contralateral OFA masks compared to place stimuli (Figure 5A and 5B for FFA, 5D and 5E for OFA). This was particularly marked during left hemifield stimulation, which saw significantly greater activation for the face > place contrast (OFA: $t = 3.09$, $p = 0.009$, FFA: $t = 3.32$, $p = 0.006$). When images were presented to the right hemifield, a slightly weaker face > place contrast predominated, which did not quite reach significance (OFA: $t = 1.83$, $p = 0.09$, FFA: $t = 1.21$, $p = 0.24$). Activation in the FFA and OFA was also significantly greater for faces than in response to scrambled faces (Figure 5C and F, FFA: $t = 2.4$, $p = 0.03$, OFA: $t = 4.9$, $p < 0.0001$).

The PPA as expected showed the reverse pattern, with activity markedly greater in response to place stimuli rather than faces in either hemifield (Figure 5G and H, right field $t = 7.9$, $p < 0.0001$, left field $t = 10.4$, $p < 0.0001$). Similarly, activity was greater for places than scrambled controls (Figure 5I, $t = 3.9$, $p = 0.0006$). The place > scrambled contrast also showed greater PPA activation than the face > scrambled

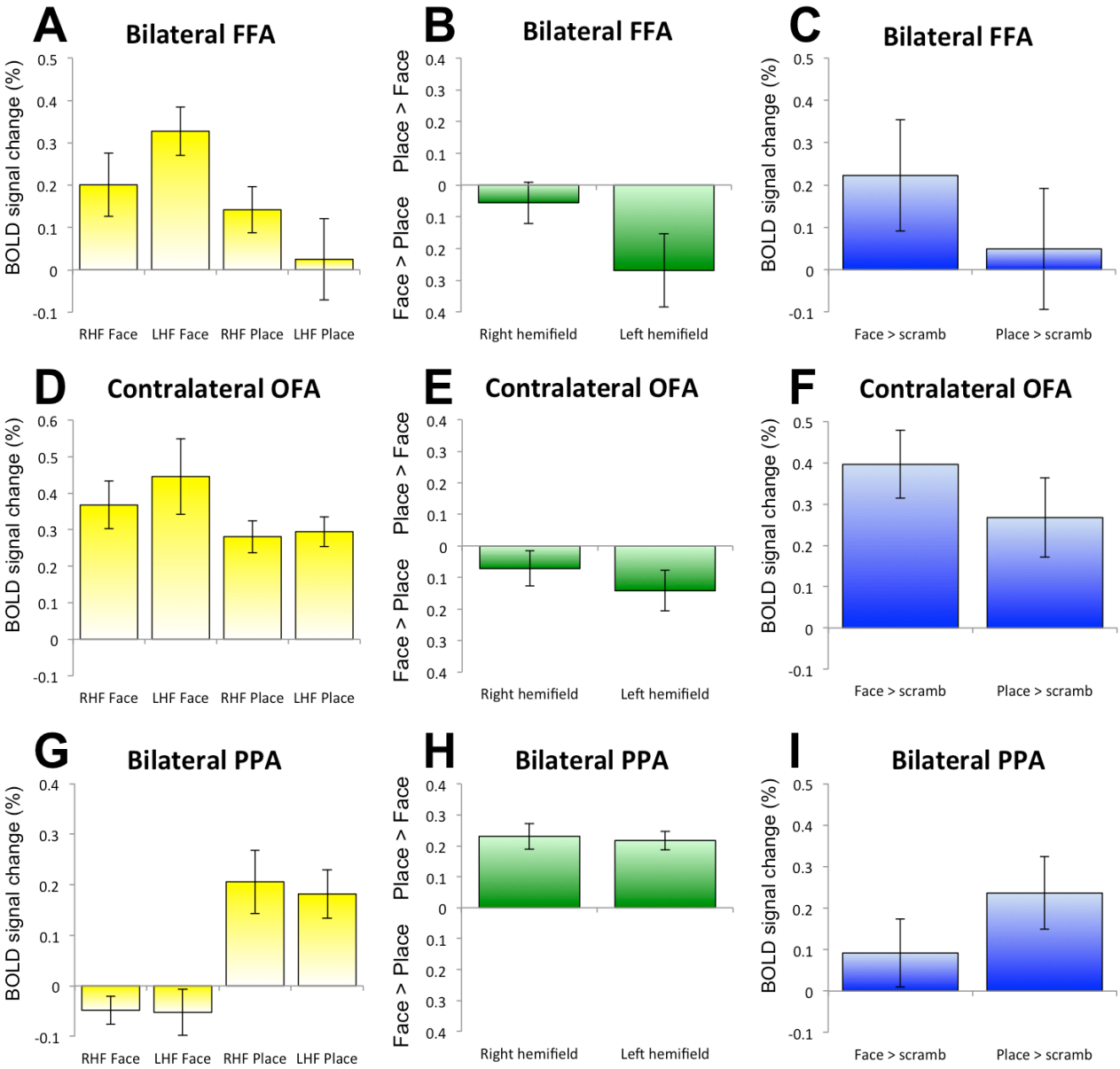

Figure 5. fMRI signal change in control participants. Yellow charts depict signal change in response to faces or places versus baseline. Green charts depict signal change in face > place (lower axis) or place > face (upper axis) contrasts. Blue charts depict responses to faces or places versus scrambled images. **(A-C) Bilateral FFA:** (A) Signal change versus baseline. (B) Positive signal change for face > place stimuli in both hemifields, particularly the left. (C) Signal change for faces and places versus scrambled controls**. (D – F) Contralateral OFA:** (D) Signal change versus baseline. (E) Positive signal change for face > place stimuli in both hemifields. (F) Signal change for faces and places versus scrambled controls. **(G-I) Bilateral PPA:** (G). Signal change versus baseline. (H) Positive signal change for place > face stimuli in both hemifields. (I) Signal change for faces and places versus scrambled controls. All results are derived from low-level subject-specific data, averaged across the group. Error bars represent standard error of the mean. RHF = right hemifield, LHF = left hemifield, scramb = scrambled.

contrast, unlike in the FFA and OFA where the opposite pattern was observed (blue charts, Figure 5).

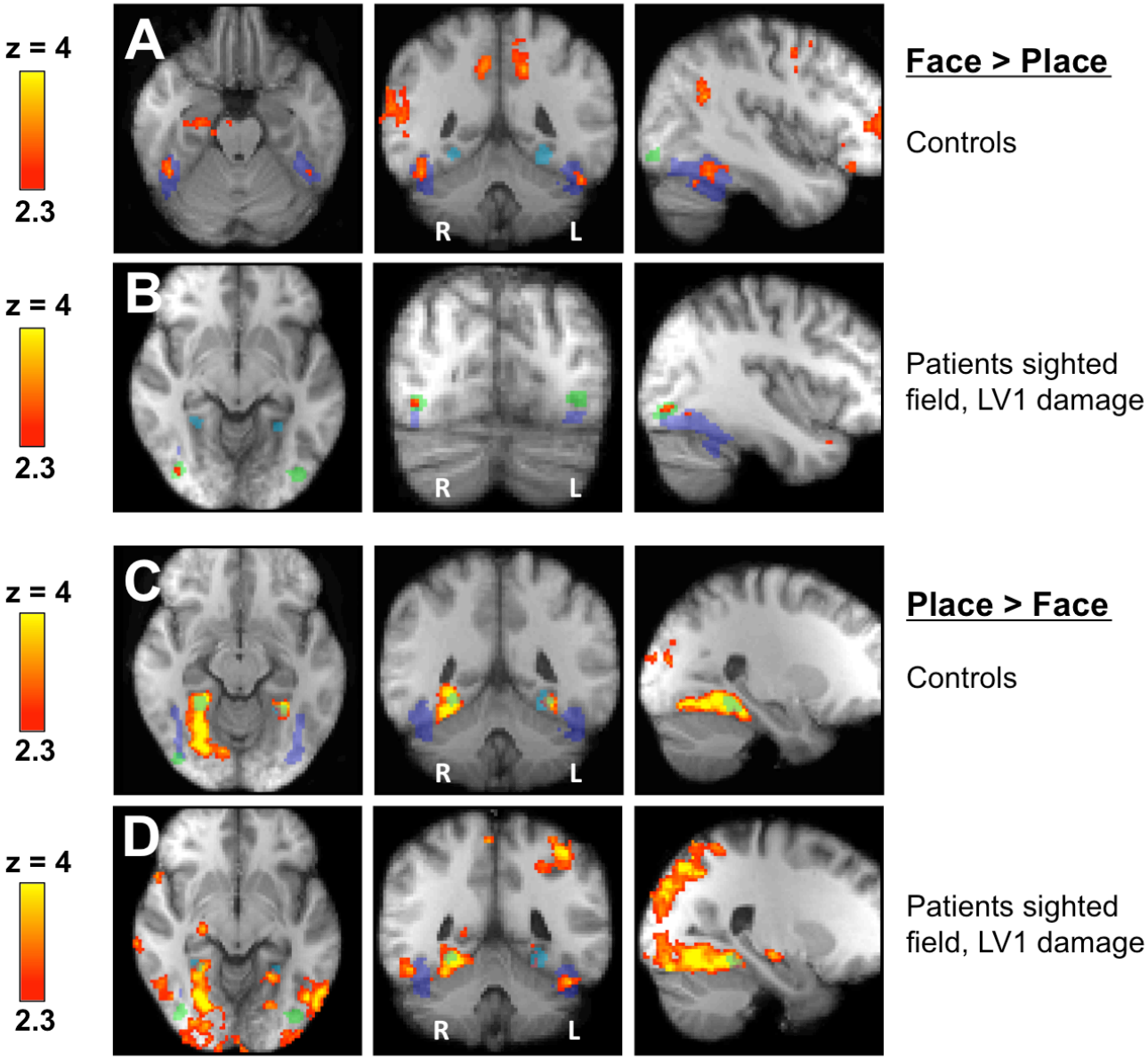

Figure 6. Preferential cortical fMRI responses to faces or places in the sighted left hemifield of controls and patients with left V1 damage. (A-B) Face > place activation. (A) Control participants. (B) Sighted responses in patients. **(C-D) Place > face activation.** (C) Control participants. (D) Sighted responses in patients. Transparent regions of interest are overlaid to aid with visualization, FFA (dark blue), OFA (green) and PPA (light blue). z statistics are displayed on the average high resolution structural in MNI space, radiological convention. Mixed effects analysis for contrasts A, C and D. For contrast B (sighted left hemifield, face > place), there were no significant regions of activation. Therefore for display purposes, results are demonstrated from fixed effects analyses, with the same statistical threshold (see Table 1 for the mixed effect analysis details). Cluster corrected $p < 0.05$ for whole brain analyses, and uncorrected $p < 0.001$ for *a priori* regions of interest.

The location and extent of activity can be appreciated in more detail in Figures 6 and 7, which show the location of significant activation and ROIs (this is also reviewed for patients' sighted hemifield in 6.4.5). As can be seen, the place > face contrasts (Figures 6C and 7C) generated considerably greater and more widespread activation than the face > place contrasts (Figures 6A and 7A), for both left and right hemifield presentations. Despite this, activation remained largely restricted to more lateral ventral regions encompassing the FFA for face > place, and more medial ventral regions including the PPA for place > face.

The difference in activation driving these contrasts in Figures 6 and 7, and in the green charts of Figure 5B, E, and H can be appreciated from the yellow charts in Figure 5. In the OFA and FFA (in response to right hemifield stimulation), place stimuli did in fact elicit fairly robust increases in signal change above baseline, reaching approximately 0.15% in the FFA, and close to 0.3% above baseline in the contralateral OFA. This relatively high level of activation caused by places can go some way to account for the weaker contrast for faces > place in these regions. The PPA, conversely, showed marked activation above baseline in response to places in either hemifield, whilst responses to faces stayed at, or even slightly below baseline, thus facilitating a particularly strong contrast for place > face. In fact, if the ROIs are compared directly, the OFA, which forms part of the lateral occipital cortex (LOC), actually demonstrated a slightly greater increase in signal change for places than the PPA (around 0.3% versus 0.2%). **Consequently, control participant responses to places tended to activate more widespread regions of visual cortex than faces, but to a moderate degree (0.1-0.3%), whilst faces activated predominantly lateral regions, but to a higher degree (0.2-0.4%).**

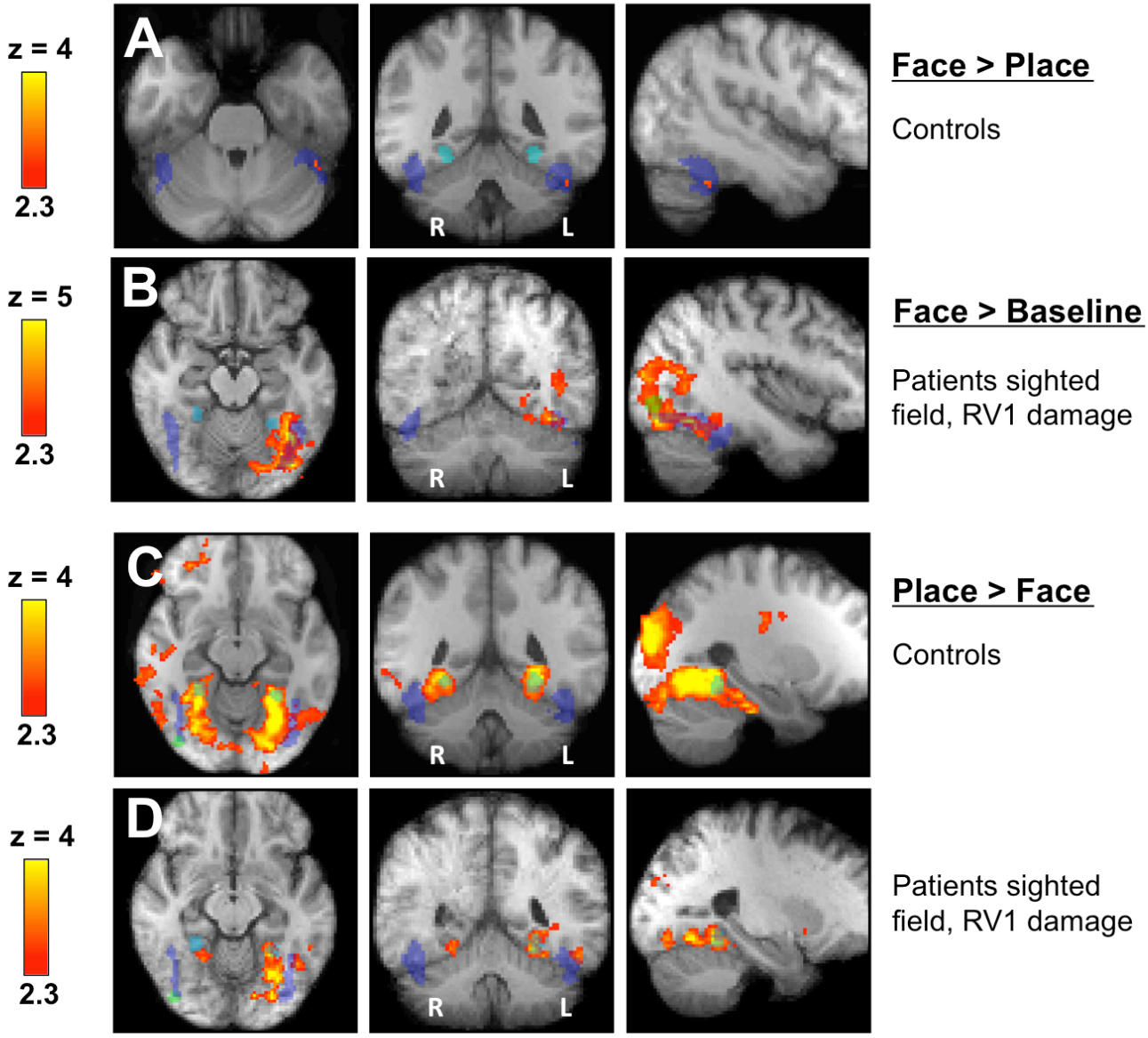

Figure 7. Preferential cortical fMRI responses to faces or places in the sighted right hemifield of controls and patients with right V1 damage. (A) Face > place activation, control participants. **(B)** Face activation versus baseline, sighted right hemifield in patients. **(C)** Place > face activation, control participants. **(D)** Place > face activation, sighted right hemifield in patients. Transparent regions of interest are overlaid to aid with visualization, FFA (dark blue), OFA (green) and PPA (light blue). z statistics are displayed on the average high resolution structural in MNI space, radiological convention. Mixed effects analysis, cluster corrected $p < 0.05$ for whole brain analyses, and uncorrected $p < 0.001$ for *a priori* regions of interest.

With respect to laterality, the prevalence of ipsilateral activation can be appreciated from Figures 6 and 7, and Table 1, which lists the peak z statistic and coordinates for each of the four contrasts and ROIs. The face > place contrast in the right hemifield was largely associated with signal change in the contralateral left FFA (Figure 7A). Left hemifield stimulation, however, showed a more bilateral pattern with significant activity in both left and right FFA (Figure 6A). This is confirmed in Table 1 (top row), where right hemifield activation was centred in the opposite left hemisphere, with some additional weaker activity in the right, ipsilateral FFA. The left hemifield face > place contrast elicited similar activation in the right (z = 3.4) and left FFA (z = 3.3), as well as both OFA ROIs (z = 2.3 in right, 2.0 in left OFA).

For the place > face contrast, although both hemifields elicited a slightly greater contralateral PPA response, there was significant activation bilaterally, which was particularly widespread during right hemifield stimulation (Figure 7C) extending to the ipsilateral right FFA (peak z = 3.0, Table1). Taken together, bilateral PPA and (left) FFA responses in particular tended to show significant activation irrespective of hemifield, implying a degree of lateralisation and cross-hemisphere communication.

6.4.3 Blindsight positive patients with left V1 damage also show category-specific fMRI activation during blind hemifield stimulation

Average fMRI signal change in six blindsight positive patients with left V1 damage and right hemianopia are shown in Figure 8. When considering the presence of activation against baseline (yellow charts), the FFA remained at baseline (Figure 8A), whilst the left OFA showed a slight increase in signal change for faces in the blind

right hemifield (0.1% signal change), despite considerable inter-patient variability contributing to the wide error bar (Figure 8D). The PPA conversely showed a slight increase in signal change in response to places (0.04%), which was fairly consistent across patients (Figure 8G).

With respect to face / place contrasts (Figure 8, green charts), the pattern of activation during blind hemifield stimulation was consistent with that seen in

	Contrast	Peak signal change	Left FFA	Left OFA	Left PPA	Right FFA	Right OFA	Right PPA
Controls	RHF Face > Place	2.9 (Left FFA) -46,-48,-28	2.9 -46, -48, -28	2.2 -40, -80, -6	nil > 0	2.0 46, -40, -24	0.2 38, -76, -4	nil > 0
	LHF Face > Place	3.8 (Right V1) 14, -96, -4	3.3 -48, -50, -28	2.0 -40, -80, -10	nil > 0	3.4 46, -48, -22	2.3 42, -80, -14	nil > 0
	RHF Place > Face	6.5 (Left PPA) -28, -52, -4	3.2 -38, -60, -20	1.3 -32, -78, -8	5.2 -26, -50, -6	3.0 40, -72, -18	1.8 42, -74, -8	4.2 30, -46, -8
	LHF Place > Face	5.3 24, -60, -12	1.5 -36, -42, -24	0.1 -32, -78, -8	4.1 -28, -46, -12	2.5 40, -42, -22	0.5 36, -72, -4	5.2 30, -44, -16
Patients, LV1 damage n = 6 or 10	Blind RHF Face > Place	4.5 (Left OFG) -30, -80, -24	3.1 -36, -84, -12	2.9 -42, -78, 0	0.8 -26, -46, -16	3.3 44, -68, -20	2.0 38, -74, -8	1.3 26, -38, -14
	Sighted LHF Face > Place	3.3 (Ant. RV1) 32, -58, 6	1.8 -38, -50, -12	nil > 0	nil > 0	1.2 42, -40, -80	1.0 72, -78, -8	nil > 0
	Blind RHF Place > Face	2.8 (Right PPA) 26,-44,-12	1.1 -46, -50, -16	nil > 0	1.5 -32, -48, -10	1.3 46, -44, -28	nil > 0	2.8 26,-44,-12
	Sighted LHF Place > Face	5.7 (Right PPA) 26, -46, -12	3.0 -38, -56, -20	2.2 -44, -78, -2	3.3 -22, -52, 0?	4.5 44, -68, -20	1.0 36, -78, -10	5.7 26, -46, -12
Patients, RV1 damage n = 3 or 4	Sighted RHF Face > Place	2.9 (Left FFA) -44, -34, -22	2.9 -44, -34, -22	1.0 -44, -84, -8	nil > 0	1.8 40, -80, -16	2.0 42, -82, -14	0.1 28, -42, -16
	Blind LHF Face > Place	4.1 (Right OFG/ PPA) 26, -74, -12	3.2 -42, -60, -16	1.1 -38, -80, -2	1.3 -28, -52, -12	2.5 42, -58, -24	2.1 38, -70, -6	3.2 26, -46, -12
	Sighted RHF Place > Face	4.7 (Left PPA) -26, -66, -12	3.7 -44, -60, -16	2.1 -38, -74, -8	4.1 -24, -52, -14	2.1 44, -50, -18	1.0 38, -72, -4	2.8 24, -50, -12
	Blind LHF Place > Face	3.2 (Left V3) -16, -92, -14	3.0 -40, -46, -34	1.3 -44, -88, -6	1.4 -30, -44, -12	3.0 52, -54, -26	1.0 38, -78, -4	0.2 28, -42, -8

Table 1. ROI z-statistics for preferential responses to faces or places in controls (top row), patients with left V1 damage (middle row), and patients with right V1 damage (bottom row). All z-statistics represent the peak signal change within each ROI, and their corresponding MNI coordinates. The overall peak in signal change for the occipital lobe is also provided for each contrast of interest (left-most column). All analyses were carried out using mixed effects, higher-level group analyses.

controls. In both the FFA and OFA, activation was significantly greater for face > place versus the place > face contrast (Figure 8B and 8E, FFA: t = 3.4, p = 0.007, OFA: t = 2.9, p = 0.016). Similarly, activation was greater for faces than scrambled faces in these regions (Figure 8C and 8F). Crucially, this pattern of activation was reversed in the PPA (Figure 8H). In the PPA, activity was significantly greater for places > faces in the blind hemifield (Figure 8H, t = 2.4, p = 0.04). When compared to scrambled stimuli (Figure 8I), activity was also greater in response to places (and faces), although more variability was seen, with error bars spanning the baseline.

This pattern of results from ROI analysis is also evident in whole brain analyses, illustrated in Figure 9, and Table 1. During blind right hemifield stimulation, activation for face > place (Figure 9A) was present bilaterally in the FFA, but particularly notable in the ipsilateral, right FFA (peak z = 3.3, see Table 1 for details). Activity was also present in the left FFA, although not quite to the same extent (peak z = 3.1). In the OFA, greater activation was seen in the contralateral left hemisphere (left OFA: peak z = 2.9, right OFA: z = 2.0). For the place > face contrast, the PPA also showed a clearer emphasis towards ipsilateral activation, with greater signal change in the ipsilateral right PPA (Figure 9B), which was also the peak for the whole occipital cortex (z = 2.8, see Table 1 for details). Signal change in the contralateral left PPA was considerably weaker (peak z = 1.5).

One patient with left V1 damage and suitable fMRI data (P12) was not included in this group analysis as he was blindsight negative according to Experiment 2 and a prior detection paradigm assessing high contrast motion. During blind field stimulation, his signal change in the FFA and OFA were either negative or at baseline for both

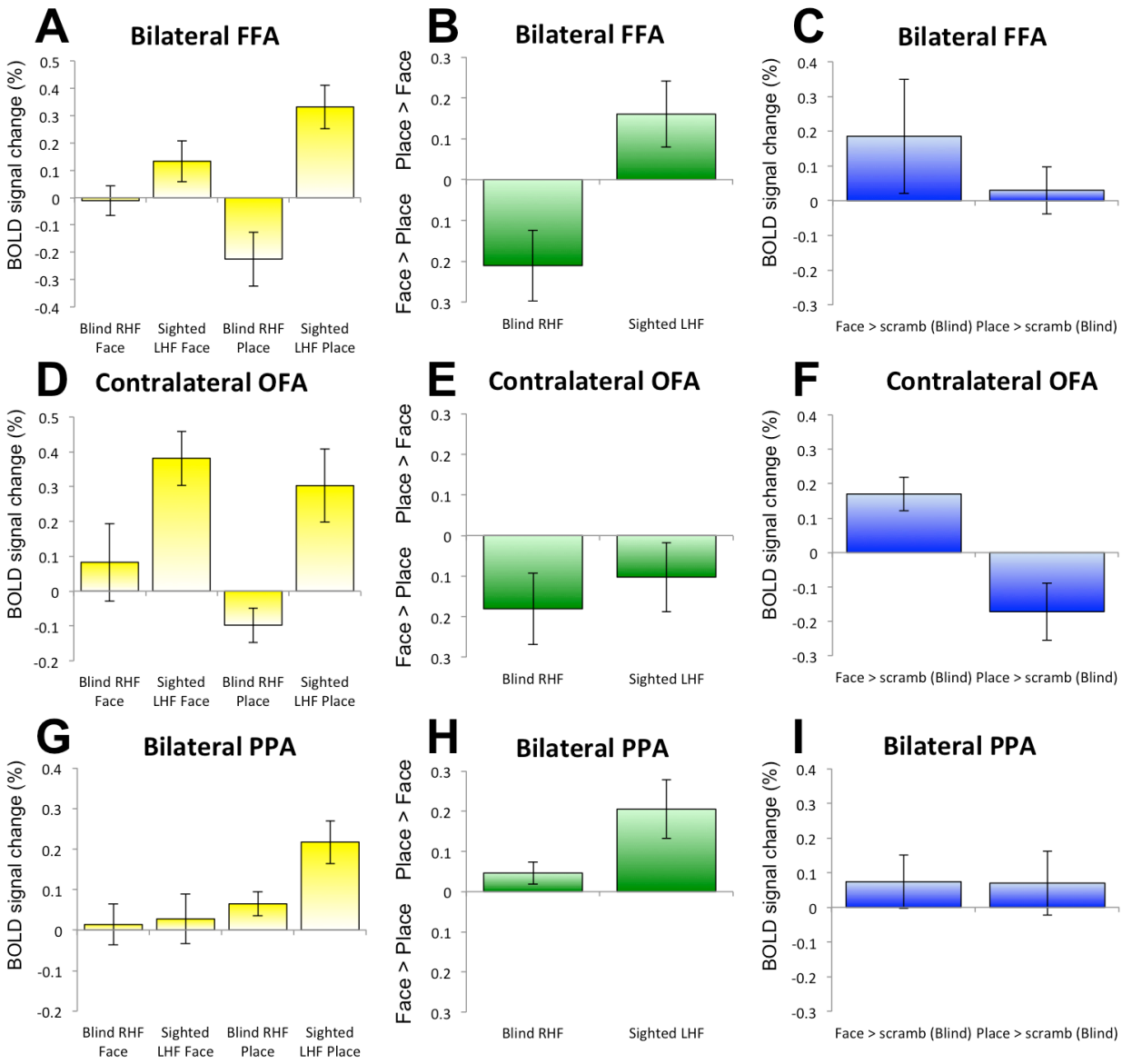

Figure 8. fMRI signal change in 6 or 10 patients with left V1 damage and right homonymous hemianopia. Yellow charts depict signal change in response to faces or places versus baseline. Green charts depict signal change in face > place (lower axis) or place > face (upper axis) contrasts. Blue charts depict responses to faces or places versus scrambled images in the blind hemifield. **(A-C) Bilateral FFA:** (A) Signal change versus baseline, in blind and sighted hemifields. (B) Positive signal change for face > place stimuli in the blind right hemifield. Positive signal change for place > face stimuli in the sighted left hemifield. (C) Signal change for faces and places versus scrambled controls**. (D–F) Contralateral OFA:** (D) Signal change versus baseline, in blind and sighted hemifields. (E) Positive signal change for face > place stimuli in blind and sighted hemifields. (F) Signal change for faces and places versus scrambled controls. **(G-I) Bilateral PPA:** (G) Signal change versus baseline, in blind and sighted hemifields. (H) Positive signal change for place > face stimuli in blind and sighted hemifields. (I) Signal change for faces and places versus scrambled controls. All results are derived from low-level subject-specific data, averaged across the group. Error bars represent standard error of the mean. RHF = right hemifield, LHF = left hemifield, scramb = scrambled.

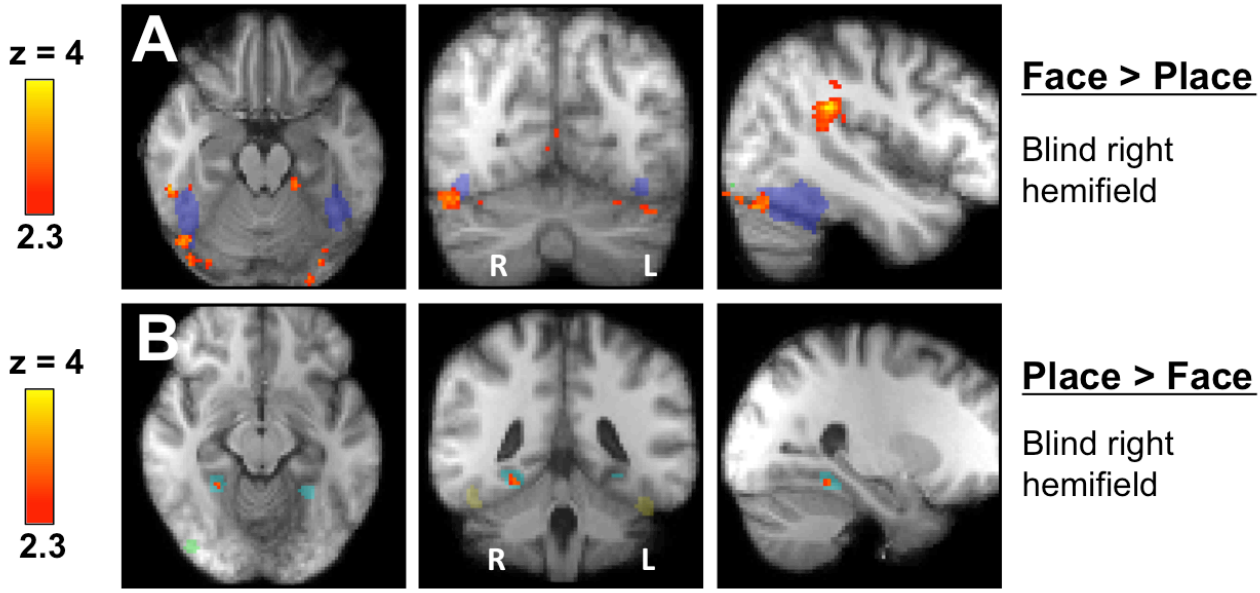

Figure 9. Preferential cortical fMRI responses to faces or places in the blind right hemifield of six patients with left V1 damage. (A) Face > place activation. **(B)** Place > face activation. Transparent regions of interest are overlaid to aid with visualization, FFA (dark blue), OFA (green) and PPA (light blue). z statistics are displayed on the average high resolution structural in MNI space, radiological convention. Mixed effects analysis, cluster corrected $p < 0.05$ for whole brain analyses, and uncorrected $p < 0.001$ for *a priori* regions of interest.

stimulus categories. Therefore the contrasts of two negative BOLD responses are particularly difficult to interpret. In the PPA, activation in the blind hemifield was only just above baseline for faces. Taken together, this patient showed a non-specific pattern of fMRI activity, with a global preference for faces despite negative BOLD responses in some regions.

6.4.4 Right V1 damage patients show an unusual reversal in blind field activation, irrespective of blindsight performance

Only four patients with right hemisphere V1 lesions were included in this study, one of whom did not undergo eye-tracking and therefore was not included in blind field fMRI analyses. As this was a relatively small group and their activation patterns were

largely analogous, their fMRI results were reviewed together, with reference to individual results as necessary. During blind left hemifield stimulation, activation in the FFA showed a negative response to faces when compared to baseline, whilst the response to place stimuli was slightly greater than baseline (-0.08% versus 0.09% respectively, see Figure 10A). This was associated with significantly greater signal change for the place > face contrast ($t = 3.8$, $p = 0.019$, Figure 10B). Furthermore, this predominance of the place > face contrast in the FFA was consistent amongst all three patients.

In comparison to scrambled faces, the face > scrambled contrast was in fact associated with greater FFA activation than the place > scrambled contrast (0.18% versus -0.14% respectively, Figure 10C), although the error bars for both contrasts spanned the baseline. These results were driven by particularly weak activation (below baseline) for scrambled faces, and particularly strong activation for scrambled places. However, scrambled results were particularly noisy as they came from single fMRI runs (compared to six for experimental conditions), in only three patients.

In the OFA a similar group response was seen, with slight predominance for places over faces (Figure 10D and 10E). In this case, however, there was much greater variation between the three patients. One patient (blindsight positive case, P3) showed greater OFA response to faces rather than places (0.07% versus -0.24%), another showed almost identical activation to both (P14: 0.32% versus 0.34%), and the third (P13) showed a greater response to places than faces (0.37% versus -0.19%).

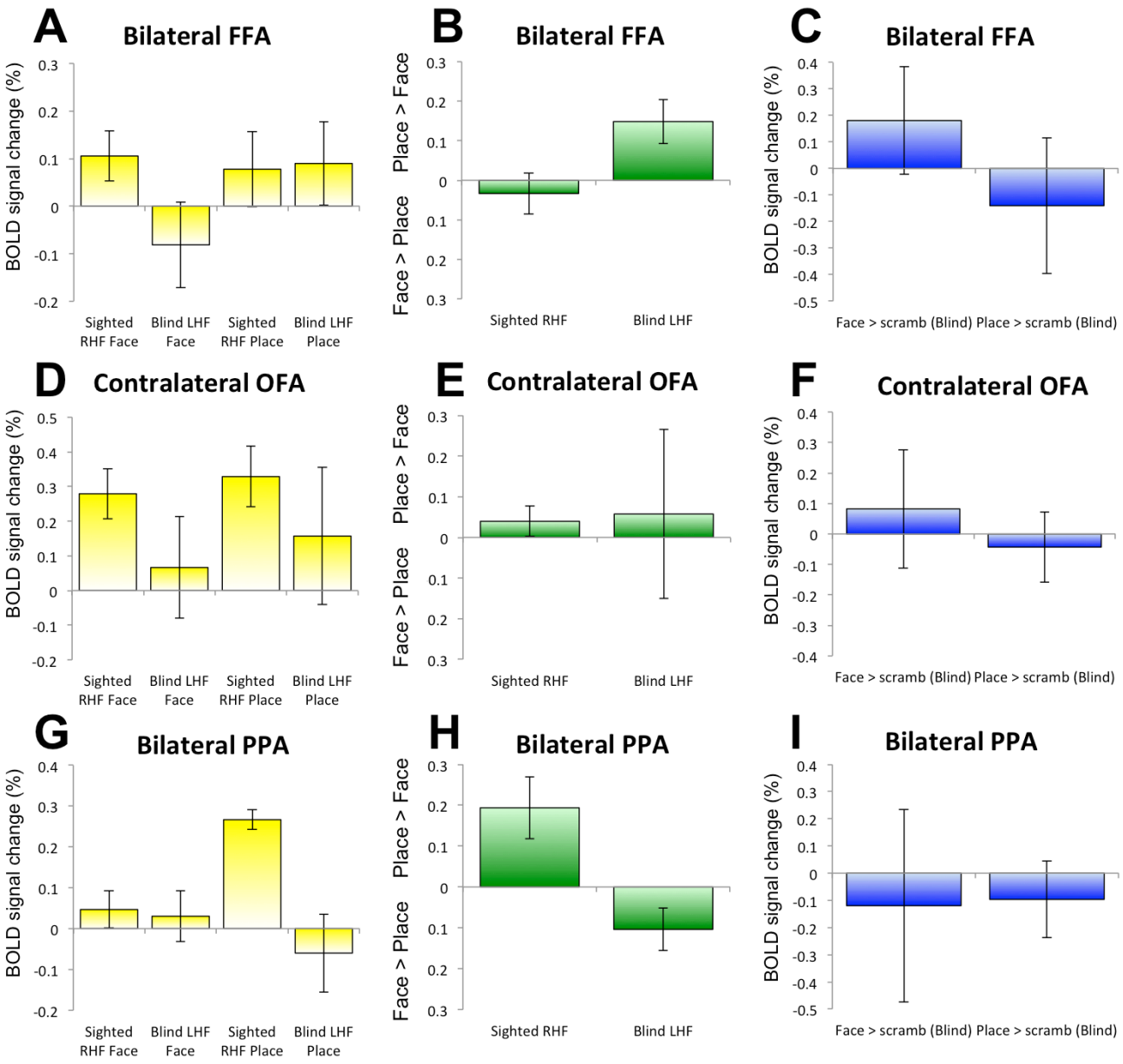

Figure 10. fMRI signal change in 3 or 4 patients with right V1 damage and left homonymous hemianopia. Yellow charts depict signal change in response to faces or places versus baseline. Green charts depict signal change in face > place (lower axis) or place > face (upper axis) contrasts. Blue charts depict responses to faces or places versus scrambled images in the blind hemifield. **(A-C) Bilateral FFA:** (A) Signal change versus baseline, in blind and sighted hemifields. (B) Weakly positive signal change for face > place stimuli in the sighted right hemifield. Positive signal change for place > face stimuli in the blind left hemifield. (C) Signal change for faces and places versus scrambled controls**. (D – F) Contralateral OFA:** (D) Signal change versus baseline, in blind and sighted hemifields. (E) Weakly positive signal change for place > face stimuli in blind and sighted hemifields. (F) Signal change for faces and places versus scrambled controls. **(G-I) Bilateral PPA:** (G) Signal change versus baseline, in blind and sighted hemifields. (H) Positive signal change for place > face stimuli in the sighted right hemifield. Positive signal change for face > place stimuli in the blind left hemifield. (I) Signal change for faces and places versus scrambled controls. All results are derived from low-level subject-specific data, averaged across the group. Error bars represent standard error of the mean. RHF = right hemifield, LHF = left hemifield, scramb = scrambled.

PPA activation showed a consistent, reversed response to that of the FFA. Despite slight variability when compared to baseline (Figure 10G), all three patients showed greater PPA activation for blind face > places ($t = 2.82$, $p = 0.04$, Figure 10H). On average, the PPA showed a greater response to scrambled than unscrambled stimuli in both categories (Figure 10I), although this again showed considerable variation, both between subjects and between ROI voxels in each dataset. The predominance for face > place in the PPA, and place > face in the FFA can also be appreciated in Figure 11A and 11B. Greater responses to faces were unusually located medially, and largely in the contralateral right hemisphere. Small clusters of activity were also present in the left (ipsilateral) FFA and right (contralateral) FFA (see Table 1 for peak statistics and coordinates). Significant responses for places were restricted to lateral regions of

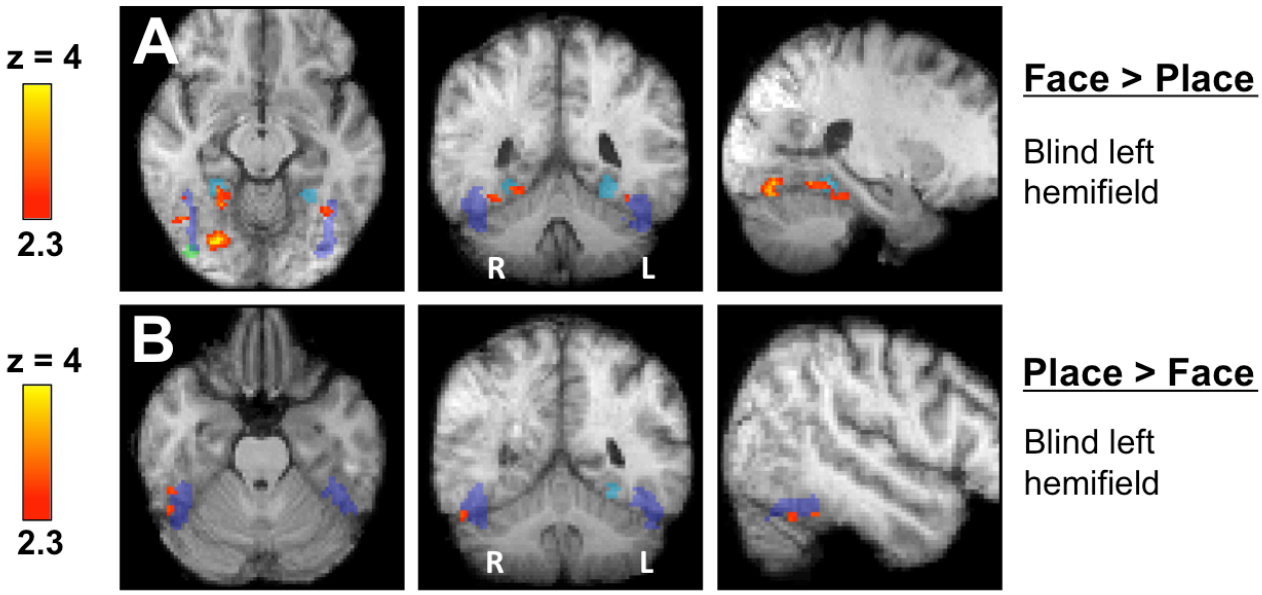

Figure 11. Preferential cortical fMRI responses to faces or places in the blind left hemifield of three patients with right V1 damage. (A) Face > place activation. **(B)** Place > face activation. Transparent regions of interest are overlaid to aid with visualization, FFA (dark blue), OFA (green) and PPA (light blue). z statistics are displayed on the average high resolution structural in MNI space, radiological convention. Mixed effects analysis, cluster corrected $p < 0.05$ for whole brain analyses, and uncorrected $p < 0.001$ for *a priori* regions of interest.

contralateral occipital cortex.

6.4.5 Sighted fMRI responses in patients are not completely normal

Average responses to sighted left hemifield stimulation were determined from data for 10 patients with left V1 damage. This group included three patients who did not have adequate eye-tracking during scanning to enable reliable blind field analysis. It also included the sighted field results for patient P12 (described above), who was blindsight negative. Overall, the pattern of activation within the contralateral OFA and bilateral PPA followed that seen in controls. Faces in the sighted field resulted in marked activity in the right, contralateral OFA (0.38% above baseline, see Figure 8D). There was also significant activation in response to places above baseline in this ROI (0.30%), but the overall contrast was stronger for face > place, although this did not quite reach significance ($t = 1.71$, $p = 0.10$, Figure 8E). The distribution of activation is also demonstrated in Figure 6B, where contralateral OFA activity (ROI shown in green) can be seen, but was only significant using a fixed effects analysis. In the PPA, a more typical response pattern was seen with a large increase in signal change above baseline for sighted places (0.22%), and a much weaker response to faces (0.03%, see Figure 8G). The contrast for place > face was also significantly greater than the converse ($t = 3.97$, $p = 0.0009$, Figure 8H). Extensive activation can be seen in Figure 6D, traversing medial ventral regions of the occipital lobe including the PPA bilaterally, with particular emphasis over the contralateral hemisphere.

In the FFA, a different pattern was seen to controls. As shown in Figure 8A, faces in the sighted hemifield did elicit FFA activation above baseline (0.13%). However,

places also elicited significant activity in this region (0.33%), and the face/ place contrast was significantly stronger for place > face stimuli (0.16%, t = 2.79, p = 0.01). Data from Table 1 can give some indication as to which hemisphere this pattern of FFA activity was driven from, or indeed whether it was bilateral. Response to place > face in the FFA was particularly strong in the contralateral right FFA (peak z = 4.5), although there was also notable signal change in the left (peak = 3.0), therefore it was most likely contribution from both hemisphere FFA masks driving the contrast for places. For the OFA, the ipsilateral left hemisphere (seen in Table 1, but not shown in graphs) also showed particularly strong preference for places > faces. This region showed an opposite pattern in patients when comparing the peak z statistic to the same left hemifield in controls (Patients: face > place z < 0, place > face z = 2.2. Controls: face > place z = 2.0, place > face z = 0.1).

Sighted data was also analysed in four patients with right V1 damage. In the FFA and PPA, a similar response was seen to control participants. Presentation of faces to the sighted right hemifield caused 0.11% single change in the FFA above baseline, which was similar but slightly greater than the mean response to places (0.08%, Figure 10A). FFA activity for the face > place contrast was also greater than the converse, although this difference, like right hemifield responses in controls, was not significant with the standard error straddling the baseline (t = 0.9, p = 0.4, Figure 10B). In the PPA, the group response to sighted places was considerable (0.27%), whilst responses to faces remained close to baseline (0.05%, Figure 10G). This was associated with a significantly greater response to the place > face contrast (t = 3.6, p = 0.01, Figure 10H), similar to that reported in controls (Figure 5H). In the OFA, activation versus baseline was very similar for the two stimulus categories in the

sighted hemifield (0.28% for faces, 0.33% for places, Figure 10D). This was, however associated with a more dominant place > face contrast, although not reaching significance (t = 1.8, p = 0.13, Figure 10E).

In controls, it has already been shown that places elicited more widespread activity than faces, whilst the response to faces was more localised and showed a relatively greater response in lateral regions. To summarise the patient data, patients sighted responses in all ROIs apart from the right OFA, showed a greater activation for places than faces. This must be caused by either weaker than normal responses to faces, or abnormally increased responses to places. According to the yellow charts, both of these differences were seen in patients with right homonymous hemianopia, whilst left hemianopes primarily showed a reduced response to faces. **Taken together, a weaker response to sighted faces was the consistent finding in both patient groups.**

6.4.6 Blindsight performance relates to fMRI activity

To investigate a relationship between fMRI activation and behavioural blindsight performance, data for the six patients with blindsight and left V1 damage was examined. Blindsight negative cases were not included in the analysis as their results may have been driven primarily by noise, potentially skewing any notable trends.

The relationship between signal change in each ROI and detection performance was assessed in turn (Figure 12). Firstly the FFA was examined, and despite all six blindsight positive cases showing greater activation in response to faces than places

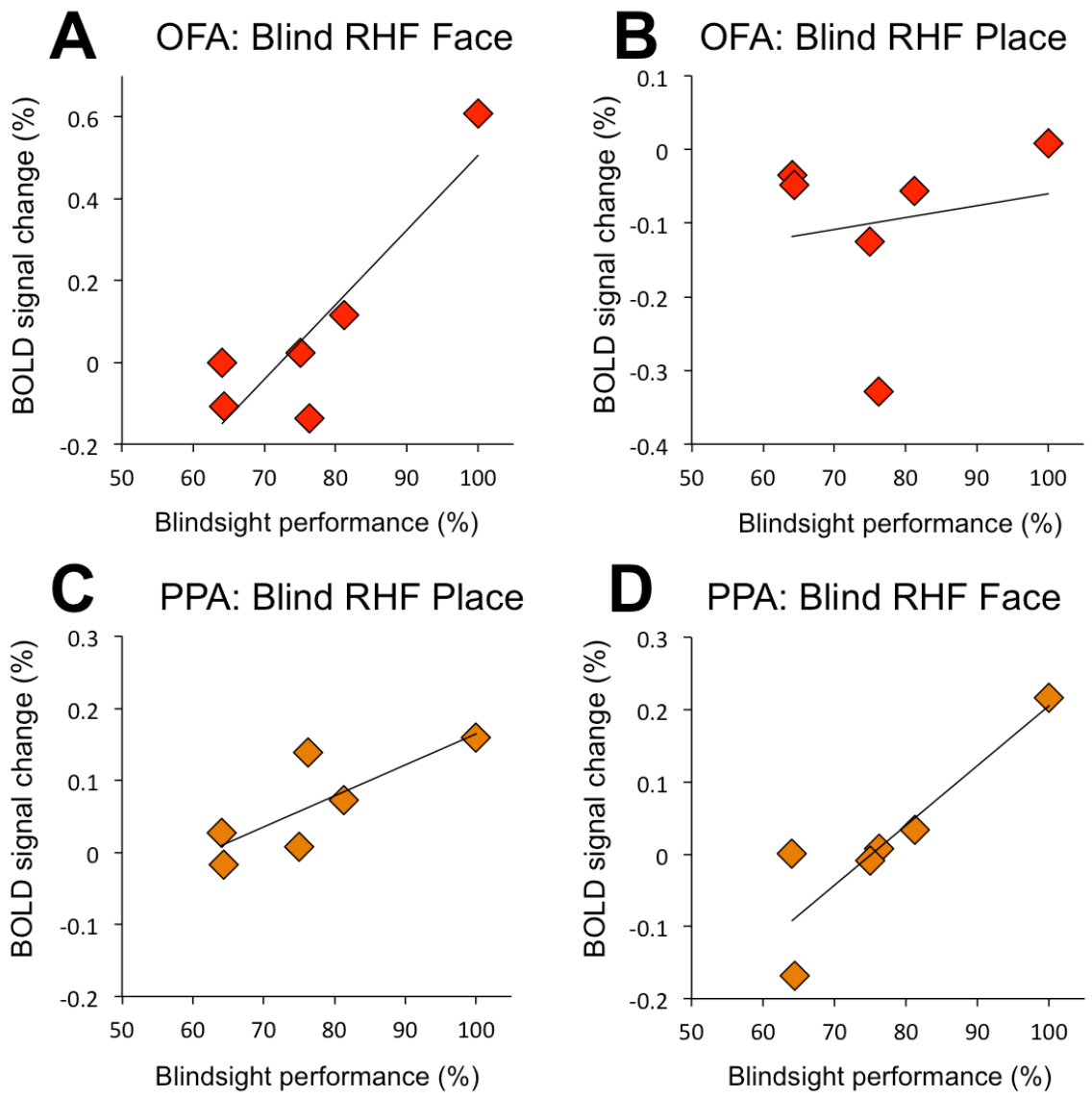

Figure 12. Relationship between fMRI activity for faces or places in the blind hemifield, and psychophysics performance in six blindsight positive patients. (A) The OFA response to faces in the blind hemifield shows a good correlation with blindsight performance (r = 0.88, p = 0.02). **(B)** The correlation between OFA response to places and blindsight performance is considerably weaker (r = 0.18, p = 0.7). **(C)** There is a weak positive correlation between PPA response to places and blindsight performance (r = 0.79, p = 0.06). **(D)** There is a similar positive correlation between PPA response to faces and blindsight performance (r = 0.89, p = 0.02).

in this region, no correlation was found between signal change for either stimulus category and blindsight performance. The OFA response to faces, however, correlated well with blindsight performance (r = 0.88, p = 0.02, Figure 12A). The correlation between OFA response to places and blindsight performance was considerably

weaker (r = 0.18, p = 0.7, Figure 12B). The PPA also showed a positive linear relationship between response to places and blindsight performance (r = 0.79, p = 0.06, Figure 12C), with a similar significant correlation between performance and PPA response to faces (r = 0.89, p = 0.02). These same trends were seen for correlations between fMRI activity and performance in the discrimination task (Experiment 2), although the correlation coefficients were slightly lower in all cases.

This indicates that the degree of activation in the OFA and PPA directly related to blindsight performance. Preference for faces in the FFA, conversely, related more to the presence or absence of blindsight, but not with the degree of performance *per se*. This pattern suggests that the OFA and PPA may both convey the extent of detection ability, whilst selective OFA activation in response to faces (but not places) may also reflect discriminability. Although the PPA showed a greater response to places than faces in 5/6 patients and was thus likely to be important in discrimination, its correlation with blindsight performance was not specific to place stimuli. This may reflect the relatively weak discrimination performance in the group, as individually only 2/6 patients scored significantly different to chance.

6.5 Discussion

This series of experiments was designed to investigate whether residual visual processing may be possible in the ventral visual pathway after V1 damage. Not only could the majority of patients detect the stimuli inside their blind hemifield, but the blindsight positive group also demonstrated significant category-specific fMRI

activity, localised to well-described regions of interest involved in normal face and place processing.

6.5.1 The majority of patients with V1 damage are able to detect static faces and places

8/12 patients were able to detect images of faces and places significantly above chance in their blind hemifield. None of the images possessed any motion component, historically an important factor in blindsight performance, but consisted instead of simple coloured drawings representing each stimulus category. In particular, the detection of places was significantly greater than that for faces amongst blindsight positive individuals. This was not, however, the case for scrambled places, which were associated with much weaker performance. Scrambled places, instead, elicited similar detection scores to scrambled faces, both of which were slightly lower than performance for faces.

Despite the static nature of these stimuli, they clearly possessed a large contrast component relative to the grey background. Luminance contrast, as described in Chapter 3, is associated with increased blindsight performance for stimuli within the blind field (Barbur et al., 1988). It is therefore possible that irrespective of the stimulus category *per se*, better performance with places was attributable to the presence of greater luminance contrast compared to images of faces. Stemming from this, there is also the possibility that place images generated greater light scatter, which can be a legitimate concern in such experiments (Culham and Danckert, 2010). The low-level properties could have been controlled for better if they were matched

for luminance by normalising each stimulus to a specified photometer level. Also the variable chromatic component could be removed with the use of achromatic stimuli, since both colour and luminance contrast are important factors in attention allocation (Itti and Koch, 2000). It is notable, however, that performance for scrambled places dropped to the same level as scrambled faces. This is difficult to reconcile with a sole contribution of contrast or colour, whose mean level for each image would be matched in scrambled images. The application of a 2-D Fourier transform (Figure 1A) also preserves spatial frequency, only disrupting the phase of these components. This makes it a useful control for low-level factors (e.g. Grill-Spector et al., 1998). Differential fMRI activation in response to phase manipulations are restricted to high-level visual areas, leading to the suggestion that it is the phase spectrum of natural images that may be key to high-level visual information, whilst the amplitude spectrum carries lower-level information (VanRullen, 2006). This would be consistent with the results here, as after place images had undergone phase manipulation through scrambling, their high detection performance was lost and became no different to faces or scrambled faces. Having said that, it is still possible for low-level features such as shape, linearity, and even contrast to be important components (together or separately) in explaining why places are recognised as such, and are thus processed in a distinctive way. Although these individual components could be teased out through a number of different 'control stimuli', it is still interesting to evaluate performance for the stimulus as a whole. Beyond acknowledging that the phase spectrum is important, the precise components that convey the category-specificity of places remain unclear (Epstein, 2005).

6.5.2 Category discrimination is possible, but particularly difficult after V1 damage

Despite the fact that two-thirds of patients were above chance at detection, the discrimination ability and stimulus awareness for these stimuli were both relatively low. Only one-third of patients (4/12) performed significantly different to chance at discriminating stimulus category. Even amongst these patients, performance was relativity close to baseline and associated with a very low level of confidence. As a result, it was necessary to employ a large number of trials, simply to detect this subtle difference in performance. An average of 68 trials were carried out per condition (in each patient) to generate the current result. This was considerably more than the previous motion experiments, where even tests of direction discrimination (see Chapter 5) only employed an average of 18 trials per condition. Having said that, this does not mean that discrimination is not possible following V1 damage in adulthood. Instead, the implication is that such performance is possible, but that whatever mechanism may be involved, it is relatively weak and is certainly not associated with residual conscious perception.

Shape discrimination is historically associated with relatively poor blindsight performance, both in human and non-human primate studies (see Cowey 2010 for review). Only a handful of papers have reported significant psychophysical performance, which has come into question at times. The first blindsight case to be tested extensively by Weiskrantz and colleagues, DB, was one such example. In their original paper (Weiskrantz et al., 1974) it was reported that DB could differentiate images of X versus O that were at least 10 degrees in length, and in turn DB could

describe a 'feeling' that the stimulus was jagged or smooth. However, it became apparent that DB's performance remained at chance if discrimination could not be achieved on the basis of orientation cues alone (Weiskrantz, 1987). This latter finding was similar to separate reports, such as Blythe and Kennard (1987) who showed that although a number of patients could respond to transient light within their scotoma, they remained unable to discriminate spatial structure as presented via sequentially flashed spots.

Despite these reports, there are examples of successful shape discrimination in the literature (Pasik et al., 1969; Dineen and Keating, 1981). However, it is often the case that discrimination (similar to the results here) was only present in the minority of cases, or that it required a large number of trials to elicit. One area of blindsight testing that supports shape processing is the work measuring reaching and grasping of unseen objects in the blind field. A number of studies report that patients retain an ability to preform their hand into the specific shapes of objects in their blind field (Marcel, 1998; Perenin and Rossetti 1996). However, it is arguable that such findings lend greater support to components of the dorsal 'action' stream, rather than the ventral 'what' pathway under investigation here (Goodale and Milner, 1992).

Reports of residual processing specific to the ventral stream are perhaps even more sparse. One intriguing example comes from patient DB, mentioned above, who showed a marked improvement in his form discrimination over time. In a recent study, DB could identify low-contrast achromatic outlines of Snodgrass animals and transport images after being told the stimulus category, despite reporting no awareness (Trevethan et al., 2007a). This performance, bizarrely, was significantly

better than the ability in his sighted field or healthy controls. He was also able to freely identify complex images from colour digital photographs. The neurobiological mechanism behind this patient's improvement can only be speculated upon, and suggests that some form of neuroplasticity may have occurred. The authors felt that this was more likely to reflect the passage of time rather than the patient's enrolment in a large number of research studies. Nevertheless, it lends support to preserved processing and the identification of complex stimuli despite V1 damage, which are typically associated with higher-level cognitive functions. This could be consistent with the finding of intact discriminatory performance for faces and places reported here, which similarly occurred in the absence of conscious awareness. It may well be the case that examples of such residual visual capacity are difficult to uncover. The current study highlighted the benefit of both enrolling relatively large patient numbers, and employing a large number of trials. Even here, the number of psychophysical trials per patient could be considered to be rather conservative. If, for example, the borderline cases P5 and P8, tested here with 48 and 80 trials per condition respectively, underwent a longer experimental session, they may have demonstrated significant performance. This would be consistent with their functional MRI results, in which both patients showed category-specific responses to stimuli in their blind field.

6.5.3 Blindsight positive patients demonstrate preserved category-specific processing in the ventral occipital cortex

The key finding in this study was that blindsight positive patients demonstrated fMRI evidence of category-specific processing in response to face and place images within

the blind hemifield. This was preserved in all three regions of interest, such that both the FFA and OFA exhibited a preference for faces, whilst the PPA showed a significant preference for places. This was not the case in blindsight negative cases, although there were fewer patients in this group to compare. The blindsight negative patient with left V1 damage, and the two blindsight negative patients with right V1 damage demonstrated non-specific responses, which were inconsistent between the FFA and OFA, and if anything tended towards an opposite response in right hemisphere patients. Crucially, by insisting that a number of strict criteria were met for eye-tracking during fMRI acquisition, it is possible to be confident that the blind hemifield results are extremely unlikely to be attributable to eye movements.

Very few neuroimaging studies have specifically explored ventral visual processing following V1 damage. In the macaque, visually driven BOLD responses in V2 and V3 have been shown to persist after chronic V1 lesions, despite a reduction in amplitude of approximately 70% (Schmid et al., 2009). In human imaging, Goebel et al., (2001) investigated fMRI responses to coloured images of fruit and vegetables in two patients with unilateral V1 damage. They also found that ventral areas in the lesioned hemisphere (and to a lesser extent the unlesioned ipsilateral hemisphere) responded to images presented in the blind hemifield. Specifically this included significant responses in the lateral occipital cortex (LOC) and the posterior fusiform gyrus (V4/V8). Unfortunately they did not assess blindsight performance, but tested awareness, which occurred in < 10% of trials for one patient. Rossion et al. (2000) measured event-related potentials for achromatic images of faces in the blind field of a well-described patient with blindsight, GY. They found a P1 positive occipital deflection with stimulation of the blind field, which was slightly delayed and reduced

in amplitude compared to normal. Despite this, ERP responses did not show a difference when faces were inverted, or when comparing photographs of cars and faces. Similarly, GY remained at chance in tests of discrimination, suggesting that although extrastriate responses were possible, they were not necessarily category-specific.

One reason for the relative success in the fMRI results presented here may be that neuroimaging time was quite substantial. Six runs of repeats were carried out in all patients, meaning that each stimulus category (face or place) was presented for 192 s, within the blind hemifield. This amounted to a scan time of around 25 minutes per person, excluding scrambled blocks. When averaged across participants, this would contribute even further to a high signal-to-noise ratio. This is an important factor to consider when investigating subtle changes in fMRI signal that are associated with unconscious visual stimulation (Haynes and Rees, 2006). In comparison, Rossion et al. only presented stimuli for a total of 40 s to the blind hemifield. Even Goebel et al., who found significant ventral extrastriate responses, presented stimuli for only 120 s in total.

Away from the blindsight literature, specific models can simulate blindsight amongst healthy participants. One such technique is the use of binocular suppression to render visual stimuli invisible. It is interesting that even binocular rivalry paradigms suggest that non-conscious ventral activity is considerably more difficult to detect than dorsal responses (Lin and He, 2009). However, examples of ventral processing for unconscious visual stimuli have been reported (Jiang and He, 2006; Sterzer et al., 2008). In particular, category-specific activity in the FFA and PPA for invisible faces

and houses, similar to blindsight positive patients here, has been shown using fMRI and multivariate pattern analysis (Sterzer et al., 2008).

Relating to this, an interesting point to consider is that the 'blindsight positive' group of 6 patients was defined by significant performance on the detection paradigm. Only 2/6 of these patients showed significant discrimination performance, with a further 2 patients at borderline. However, all 6 patients showed greater fMRI activation in response to blind faces in the FFA, and 5/6 patients showed greater responses to blind places in the PPA. This has two important implications. Firstly, it suggests that this distinct response pattern on fMRI may not have been sufficient to generate significant discrimination performance in all cases. Perhaps an even greater degree of activity is required to enable some sort of perceptual experience to facilitate discrimination. This would fit with what was found from correlation analyses, i.e. that behavioural performance in both experiments largely correlated with the degree of fMRI activity in both the OFA and PPA. The second important point is that although discriminability was only significant in 2/6 cases, it may be the case that if a patient has the ability to detect these stimuli above chance, they may also possess the capability for discrimination. Perhaps with sufficient trials, or a more sensitive blindsight test, such an ability would be uncovered. This has particularly important implications for rehabilitation, as it suggests that higher-level, ventral processing may be possible and more common than widely considered. If an underlying category-specific mechanism is intact, then it may be possible to improve patients performance or even awareness through targeted training (Sahraie et al., 2006; Huxlin et al., 2009; Sahraie et al., 2013: all targeting the dorsal stream).

6.5.4 Interhemispheric communication and ipsilateral activation may be important for normal and blind field ventral responses

Blindsight positive patients often showed robust activation to stimulation of the blind hemifield in their ipsilateral, undamaged hemisphere. For example in the FFA, although activity was bilateral, the greatest preference for faces was seen in the ipsilateral right hemisphere. This was also the case for places in the PPA, which showed considerably stronger responses to places in the undamaged right side. Healthy controls also show a high degree of ipsilateral activity in the FFA and PPA, resulting in significant bilateral responses. The implication is that intact interhemispheric communication may play an important role in normal higher-level ventral stream responses. In situations where V1 is damaged, this may also provide a potential mechanism for retained category-specific responses.

Bilateral activation is commonly described in category-specific ventral stream processing, including parahippocampal responses to objects or places compared with faces (Epstein and Kanwisher, 1998), and FFA responses to faces or scrambled controls (Farah, 1990; De Renzi, 1997; Kanwisher et al., 1997). Lateralisation of activity, in particular to the right hemisphere when viewing faces, is also not uncommon, although its predominance tends to vary amongst individuals (Kanwisher et al., 1997). In fact, lateralisation is important to consider, as this may explain why patients showed a different response pattern depending upon which hemisphere had been damage. Unfortunately there were probably too few patients with right hemisphere damage in the current study to fully appreciate this, in particular as only one patient demonstrated significant blindsight function.

The underlying mechanism behind residual visual processing in the ventral stream after V1 damage has remained largely unclear. One possibility is for a direct subcortical connection, similar to that proposed in hMT+, which perhaps supplies intact early regions of cortex in the ventral stream, such as V2, V3, and/or the OFA, before in turn innervating higher-level cortical regions such as the FFA and PPA (Bullier and Kennedy, 1983; Adams et al., 2000; Schmid et al., 2009; Schmid et al., 2010). Consistent with this, small clusters of activity were present in ipsilesional V3 and V4, when responses to faces and places in the blind field were compared to baseline. Another possibility is that residual visual processing occurs via intact callosal connections from the undamaged hemisphere (Van Essen et al., 1982; Abel et al., 2000). Given the extent of bilateral activity in ventral category-specific responses in healthy controls and patients, such connections are likely to occur and be important in the ventral stream. Perhaps an interruption to these pathways could even account for the slightly weakened sighted responses to faces found in patients. Unfortunately it is not possible to resolve the underlying pathway from the current data, as both routes could be consistent with the findings reported here. It is possible that alternative imaging techniques such as diffusion MRI tractography applied to the ventral stream, similar to that carried out in Chapter 7 for the dorsal stream, may help to clarify this question.

6.5.5 Conclusions

This study explores the capability for residual processing in the ventral visual stream after chronic V1 damage in adulthood. To date, this has been a relatively neglected areas of study compared to the much more abundant studies of motion. One reason

for this is that ventral processing is notoriously difficult to detect, and that the cognitive functions associated with this pathway such as shape and colour processing, are also relatively poorly performed in blindsight testing. The work presented here has confirmed that the discrimination of faces and places in the blind hemifield is challenging, but nevertheless possible after V1 damage. Furthermore, the majority of patients could detect images above chance, and these blindsight positive individuals demonstrated significant category-specific fMRI activity in well-described ventral regions of cortex involved in normal face and place processing. This confirms that category-specific processing is possible in the ventral stream despite V1 damage, and may be more common than first considered. It also represents a potential target for rehabilitation, in particular since the degree of activation was shown to correlate with blindsight performance. The success of this study was likely to reflect the relatively large number of trials and scan-time, as well as the number of patients enrolled. It highlights the importance of employing methods to maximise signal to noise in detecting subtle differences. These findings support the presence of intact residual pathways to the ventral visual cortex, bypassing V1. Such pathways could serve to support other regions of cortex postulated to be involved in blindsight function.

Chapter 7

Diffusion MRI tractography: Connectivity of the extrastriate cortex underlying blindsight

7.1 Abstract

A number of different pathways have been suggested to underlie visual responses to blind field stimulation when V1 is damaged. These include ipsilateral connections to the LGN or superior colliculus and pulvinar, and interhemispheric connections that appear stronger than healthy controls. This study sought to resolve this fundamental question by employing diffusion MRI tractography in a large group of patients with unilateral V1 damage sustained in adulthood. The strength and integrity of three critical pathways were compared between blindsight positive and blindsight negative patients, and healthy controls. Whilst interhemispheric and collicular pathways were demonstrable in a number of patients, these connections could not account for all blindsight positive cases and were often found to be intact in patients with absent blindsight performance. Instead, all 12 patients with blindsight and none of the blindsight negative patients showed intact ipsilateral geniculo-extrastriate connections. This suggests that when V1 is damaged in adulthood, residual responses to motion may be transmitted via ipsilateral pathways with the ipsilesional LGN.

There was also no evidence for plasticity in blindsight patients, as the number of streamlines and fractional anisotropy in these pathways were comparable to those in healthy age-matched controls.

7.2 Introduction

Diffusion MRI (DTI) offers a practical and non-invasive tool for estimating large-scale white matter tracts and their underlying microstructural properties (Jones, 2013; Johansen-Berg, 2010). This is particularly pertinent to the study of blindsight where several distinct pathways have been implicated, suggestive both of neuroplastic and residual mechanisms (See Cowey 2010 for review).

Over the last ten years, this technique has been used in a small number of studies of patients with V1 damage. However, this work has yielded discrepant results. In some cases, residual ipsilateral connections are implicated in blindsight, such as a connection between the ipsilesional LGN and hMT+ (de Gelder et al., 2008; Bridge et al., 2010). Similar pathways are present in non-human primates, predominantly from the LGN interlaminar zones (Sincich et al., 2006). The LGN is also suggested to be critically involved in residual visual processing after striate cortex lesioning in the macaque (Schmid et al., 2010). Conversely, other DTI studies suggest that blindsight may represent a plasticity phenomenon, evidenced by the strengthening of weak or even absent connections in healthy controls (Leh et al., 2006; Bridge et al., 2008; Tamietto et al., 2012). These include crossing interhemispheric connections with the contralesional superior colliculus, the lateral geniculate nucleus, and/or the extrastriate cortex (Leh et al., 2006; Bridge et al., 2008). A non-striate retinal pathway

to MT from the pulvinar and superior colliculus is also supported by animal research (Warner et al., 2010). And, like the LGN, the superior colliculus is implicated in residual vision after V1 damage - particularly for indirect blindsight and saccadic localization (Mohler and Wurtz, 1977; Kato et al., 2011).

There are several possible reasons for the discrepancy amongst DTI results to-date. Firstly, they represent just a small handful of studies, assessing a very small number of patients. All but one of the reports were based upon single case-studies, and the patient GY was recruited more than once (Bridge et al., 2008; Tamietto et al., 2012). These cases may not represent the majority of patients, in particular when considering the age of brain injury. Three of the five principal DTI studies evaluated patients who sustained their brain damage during childhood, i.e. seven years old and younger, when a greater scope for plasticity may exist (Tinelli et al., 2013). Another criticism is that these studies were primarily ROI based, and were all restricted to predetermined connections of interest. The various pathways implicated in blindsight have therefore not specifically been compared.

This study sought to address these problems by investigating white matter connections in a large group of patients and healthy controls. All of the patients sustained chronic brain damage in adulthood, and were all assessed for the presence or absence of blindsight. The three main pathways implicated by previous imaging studies and the animal literature were compared. These included ipsilateral connections between the LGN and hMT+, superior colliculus and hMT+, and interhemispheric connections between hMT+ bilaterally. As well as evaluating the presence of such tracts, their structural integrity was compared between patient

groups and healthy controls. This will help to uncover which pathways are common to blindsight patients, and whether these are likely to represent residual connections that are similar to healthy controls, or a plasticity phenomenon that is suggested in juvenile-onset cases.

7.3 Methods

7.3.1 Participants

Seventeen patients (five female) took part in this study, of which 15 had sustained posterior circulation stroke and two had undergone benign tumour resection, see Table 1 for details. Average age at the time of participation was 54.9 years ±14.4 S.D., average time after pathology onset 45 months (range 6-252 months). Nine age-matched, healthy participants (54.9 ±11.7 S.D years of age, three female) served as controls.

7.3.2 Psychophysics

Psychophysical testing for this study employed the contrast 2-AFC temporal detection paradigm used in Chapter 3 (Figure 1A and B). Please see Chapter 3 and General Methods for the detailed description of stimulus parameters and experimental procedures.

The presence or absence of blindsight was determined for each patient, as in Chapter 3 and according to the criteria described in the General Methods. This criterion led to the allocation of 12 patients as 'blindsight positive' (PB1-PB12) and five as 'blindsight negative' (PN1-PN5), see Figure 1C and Table 1 for details.

Patient	Sex	Age (years)	Pathology	Time since pathology (months)	VFD
PB1	M	66	Left occipital infarct	8	RHH
PB2	F	67	Right occipital haemorrhage	6	LUQ
PB3	F	46	Left occipital infarct	7	RHH
PB4	F	38	Right occipital tumour resection	36	LHH
PB5	M	55	Left occipital and cerebellar infarct	18	RHH
PB6	M	61	Right occipital infarct	6	LHH
PB7	M	36	Left occipital infarct	6	RHH
PB8	M	70	Left occipital infarct	19	RUQ
PB9	M	60	Left occipital infarct	96	RLQ
PB10	M	30	Left occipital infarct	156	RHH
PB11	F	39	Left occipital infarct	7	RHH
PB12	F	42	Left occipital infarct	6	RHH
PN1	M	76	Left occipital tumour resection	252	RHH
PN2	M	69	Right occipital infarct	16	LUQ
PN3	M	49	Left occipital infarct	84	RHH
PN4	M	73	Right occipital haemorrhage	6	LHH
PN5	M	56	Right occipital infarct	36	LHH

Table 1. Clinical details for 17 patients with unilateral striate cortex damage and homonymous visual field deficits participating in this study. The first 12 patients (PB1 – PB12) were all defined as blindsight positive, and PN1 – PN5 as blindsight negative. This was determined using the contrast 2-AFC detection paradigm described in Chapter 3, according to criteria described in the General Methods. VFD = visual field deficit, LUQ = left upper quadrant, RLQ = right lower quadrant, RHH = right homonymous hemianopia, LHH = left homonymous hemianopia, F = female, M = male.

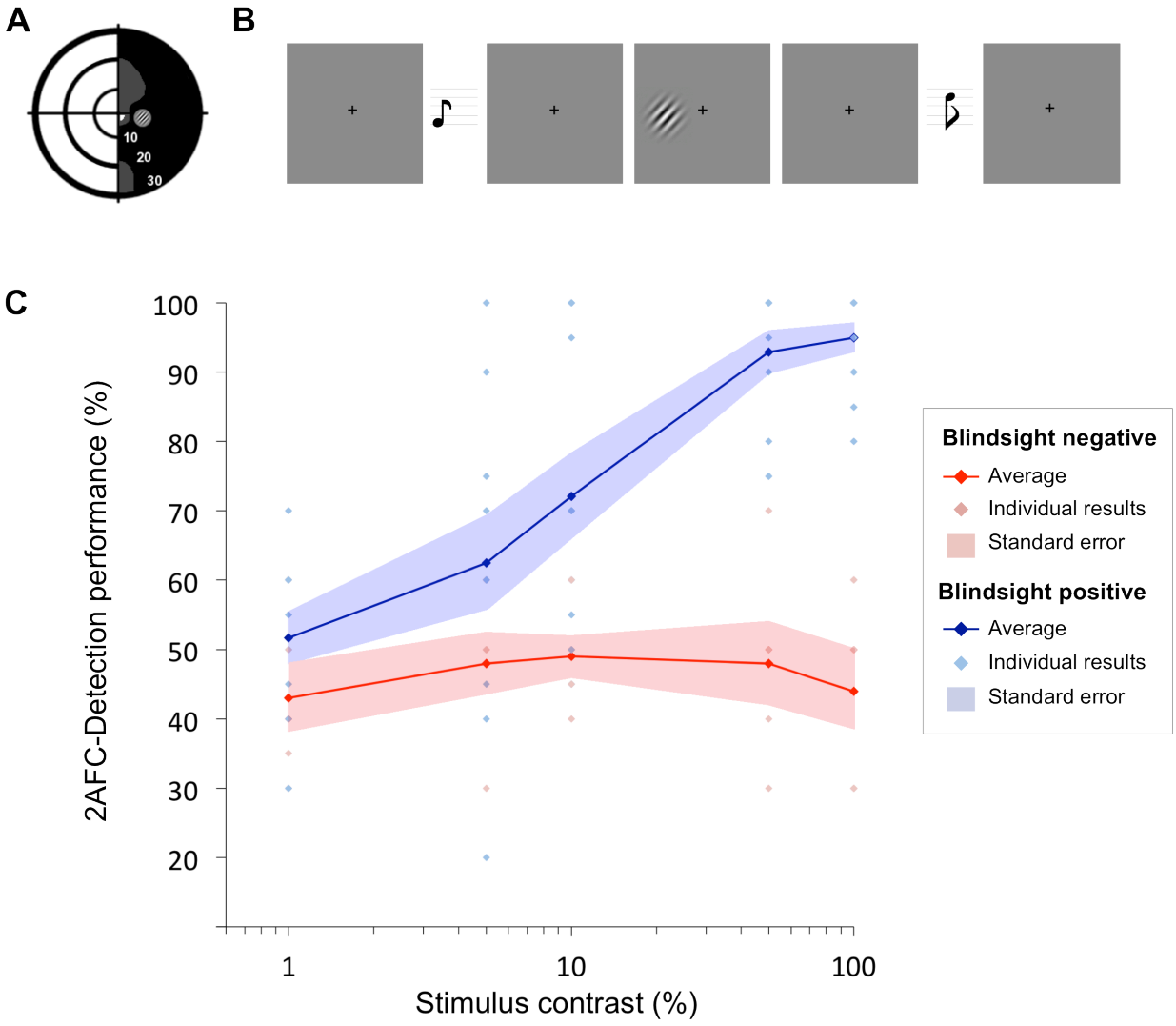

Figure 1. Psychophysics paradigm and results. (A) Example Humphrey visual field deficit drawn schematically, with the location of the target stimulus superimposed. **(B)** Illustration of the 2AFC-temporal detection procedure. Participants fixated on a central cross, with the onset of each 1500ms interval alerted by a low (interval 1) or high pitch (interval 2) tone. The stimulus could appear in either interval, for a period of 500 ms. At the end of the trial, participants were instructed to decide which interval the stimulus appeared. **(C)** Detection performance with increasing stimulus contrast, shown separately for blindsight positive (blue) and blindsight negative (red) patients. Individual results are also plotted for each patient. Chance level is 50%.

7.3.3 MRI Data acquisition and pre-processing

7.3.3.1 Anatomical acquisition

A structural scan was acquired for each participant (see General Methods for details).

7.3.3.2 Diffusion Data

Diffusion-weighted data were acquired using echo planar imaging (EPI; TR = 8900 ms, TE = 91.2 ms, and voxel size of 2 × 2 × 2 mm3). The diffusion weighting was isotropically distributed along the 60 directions (b-value = 1500 s/mm2), and a non-DWI (B0) image was acquired every 16 volumes (total of four B0 volumes per image set). EPI acquisitions are prone to geometric distortions that can lead to errors in tractography. To minimize this, two image sets were acquired with the phase-encoded direction reversed, "blip-up" and "blip-down" (Chang and Fitzpatrick 1992). This results in images with geometric distortions of equal magnitude but in the opposite direction allowing for the calculation of a corrected image (Andersson et al. 2003). Before correcting for geometric distortions, each image set, blip-up and blip-down, was corrected for motion and eddy-current related distortions. These corrections were performed using tools from FSL (FMRIB Centre Software Library, Oxford University; http://www.fmrib.ox.ac.uk/fsl/), with other steps in DTI processing and tractography using the VISTALab (Stanford Vision and Imaging Science and Technology) diffusion MRI software suite. VISTALab image processing software is available as part of the open-source mrDiffusion package available at https://github.com/vistalab/vistasoft/

The corrected 4-D NifTI DTI images from both AP (blip-up) and PA (blip-down) image sets were concatenated in time and aligned to the motion-corrected mean of the non-diffusion weighted (b = 0) images using a rigid body algorithm. DTI images were then aligned to the T1 structural scan, which had been resampled to AC-PC orientation using an automated script.

7.3.4 Diffusion MRI analysis

7.3.4.1 Regions of interest

hMT+ masks were derived according to the procedure in the General Methods. These were non-linearly transformed from MNI to diffusion space for patients and controls to ensure consistency between participant groups (see Figure 2A for an example patient mask, and Figure 2B for the MNI probabilistic mask). Average hMT+ ROI volume was 366 ±60 voxels in patients, 415 ±60 voxels in controls. For the lateral geniculate nucleus (LGN) and superior colliculus (SC), binary masks were created by manual inspection and drawing over the anatomical T1-weighted images (Horton et al., 1990), using a radiological brain atlas to aid identification of landmarks (see Figure 2C and 2E for examples, and MNI templates in 2D and F). The average LGN volume in patients measured 245 mm^3 in the right, and 244 mm^3 in the left (Figure 2C). In controls, average LGN volume was 245 mm^3 in the right and 236 mm^3 in the left. These volumes are similar to previous reports using T1 anatomical and functional MRI scans in living humans (244 mm^3 in the right, 234 mm^3 in the left; Kastner et al., 2004). In post-mortem human tissue, investigation has shown LGN volume ranges from 91 to 157 mm^3 (Andrews et al., 1997). However it has been suggested that this difference may, at least in part, arise due to tissue shrinkage during post-mortem processing (e.g. see Annese et al., 2014). Superior colliculus masks had an average volume of 203 mm^3 in the right and 216 mm^3 in the left of patients (Figure 2E). In controls, SC masks were 214 mm^3 in the right and 218 mm^3 in the left. These are similar in size to previous studies using T1 anatomical and functional MRI scans (Anderson and Rees, 2011). There was no significant difference in hMT+, LGN or SC mask volumes when comparing the blindsight positive, blindsight

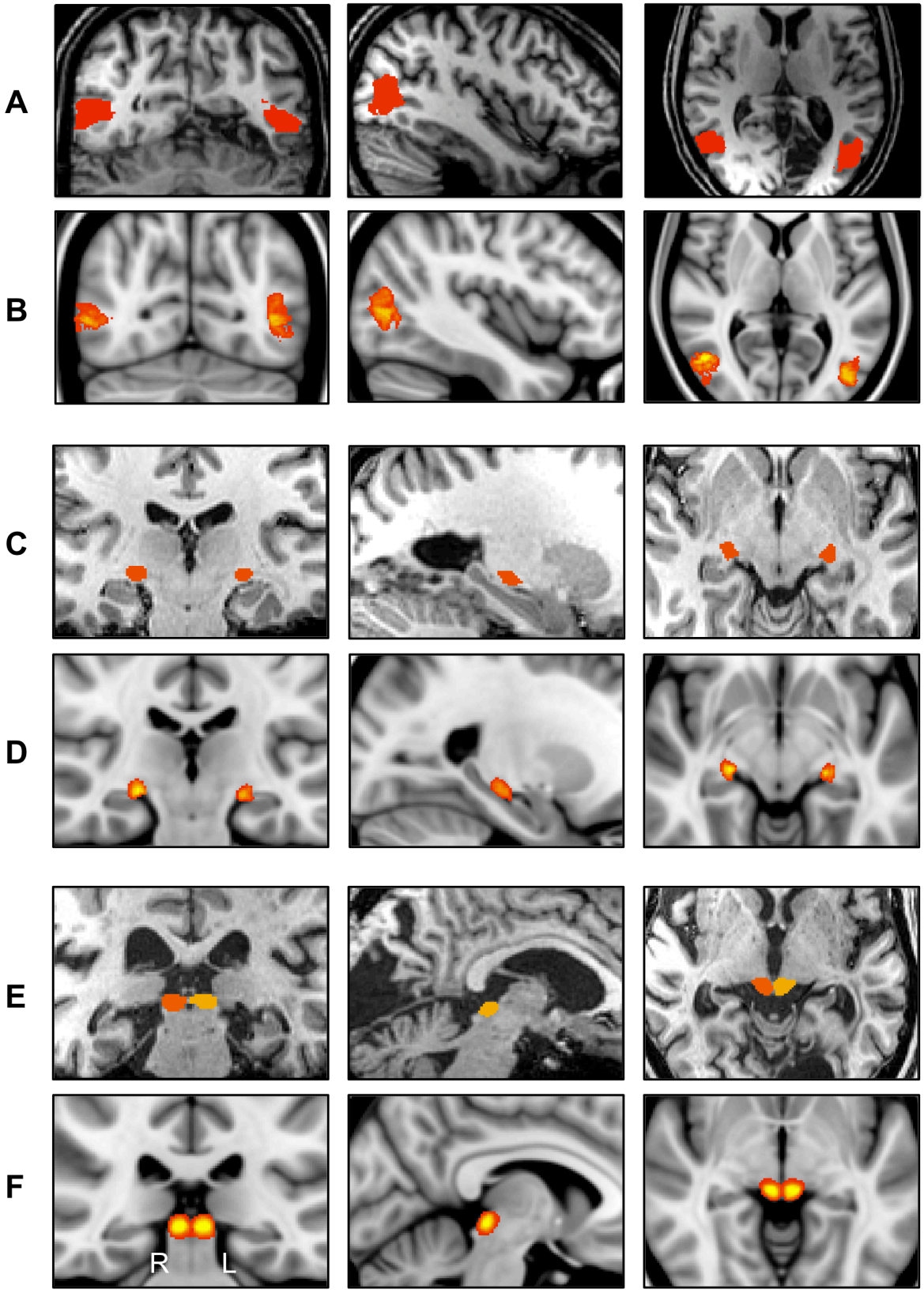

Figure 2. Regions of interest: hMT+, LGN and SC. **(A)** Example hMT+ masks in patient PB3, overlaid on T1-weighted structural images. **(B)** hMT+ masks in standard space, overlaid on an MNI brain. **(C)** Example LGN masks in patient PB11, overlaid on T1-weighted structural. **(D)** LGN location in standard space, overlaid on an MNI brain. **(E)** Example SC masks in patient PN1, overlaid on T1-weighted structural images. **(F)** Summation of all patients' SC masks in standard space, overlaid on an MNI brain. Radiological convention throughout.

negative, and control groups (LGN: F = 0.96, p = 0.4, hMT+: F = 2.0, p = 0.1, SC: F = 0.12, p = 0.9).

7.3.4.2 Fibre tracking

The tracking algorithm was restricted to the white matter, defined as all voxels with a fractional anisotropy (FA) value greater than 0.15. This method of segmentation generated a white matter mask that excluded the ventricles. This was manually inspected and edited for each participant, to ensure optimal segmentation and to remove any satellite voxels.

Streamline tracking was performed with a probabilistic 'region to region' algorithm that uses orientations provided by constrained spherical deconvolution (CSD), a tool inside MRtrix. The methodology has previously been shown to provide superior delineations of a number of known white matter tracts, in a manner that is robust to crossing fibre effects (Tournier et al., 2012; Pestilli et al., 2014). Streamlines were run from 10,000 seeds inside a union mask created by the combination of two ROIs. Tracts had to touch both ROIs and travel only within white matter to be included in the output. A curvature radius threshold of 1mm and step size of 0.2mm was used, the maximum harmonic order (L_{max}) was set to 8. The L_{max} determines the maximum number of deconvolution kernels used to estimate the fibre orientation distribution function in each voxel by the CSD model. The number of parameters for CSD grows with L_{max} as ½ $(n+1)(n+2)$, where n is L_{max}. The L_{max} was set to 8 because this number requires a number of parameters (45) lower than the number of diffusion directions used (60) and because it has been previously demonstrated that CSD-based probabilistic tractography using L_{max} = 8 generates accurate connectomes (Pestilli et

al., 2014). The total number of tracts generated was constrained to a maximum of 1,000,000.

After tracts were created for each pathway of interest, a cleaning process was undertaken to remove outlier streamlines and retain a core fascicle bundle representing the tract. This was performed using an iterative process to remove fibres located more than 2.6 standard deviations away from the core of the tract, and more than 2.8 standard deviations longer than the mean tract length, using a Gaussian distribution to represent the distance and length of tracts. Where this was not possible because of a small number of sparse tracts < 10, this was interpreted as a failure to accurately track between the two regions of interest. All subsequent measures of tract integrity were then carried out using these 'cleaned' fibre bundles. Tracts were processed using MBA (Matlab Brain Anatomy: https://github.com/francopestilli/mba; Pestilli et al., 2014)

Three tracts of interest were identified in this study, all of which pass through hMT+ and have been implicated in blindsight function. These included two ipsilateral pathways between the LGN or superior colliculus and hMT+ in the same hemisphere. The other pathway was a crossing, interhemispheric connection between hMT+ bilaterally.

7.3.4.3 The tensor model

To characterize the properties of the identified tracts, the conventional diffusion tensor model was used. Eigenvalues (λ_1, λ_2, λ_3) from the diffusion tensor were used to compute the mean diffusivity (MD) and fractional anisotropy (FA) within each voxel

(Pierpaoli and Basser, 1996). These are summative measures that describe the mean total diffusion (MD), measured in μm²/ms, and a normalized standard deviation of the three diffusion directions (FA), as described in the equations below.

$$MD = \frac{\lambda_1 + \lambda_2 + \lambda_3}{3}$$

$$FA = \sqrt{\frac{(\lambda_1-\lambda_2)^2+(\lambda_2-\lambda_3)^2+(\lambda_1-\lambda_3)^2}{2(\lambda_1{}^2+\lambda_2{}^2+\lambda_3{}^2)}}$$

FA and MD maps were created, from which the mean and variation along any fascicle bundle could be calculated.

FA provides a measure of the directionality of water molecule movement, which can be used to infer the level of white matter integrity in fibre bundles. Similarly, increases in MD can sometimes indicate a loss of tissue integrity (Werring et al., 2000). Both of these measures are sensitive to a number of tissue properties, such as axonal ordering, axonal density, degree of myelination, etc., although they may not be specifically linked to any one of them. Therefore, a change or difference in FA most probably reflects some change or difference in some aspect of connectivity, although it is not possible to say what precise aspect. Despite shortcomings in its interpretability, diffusion tensor imaging (DTI) has been used extensively to infer about white matter microstructural properties, both in health and disease (e.g. see J-Berg 2010 for review). This includes reports of individual differences in white matter

'integrity' amongst healthy participants, a notion that has become particularly controversial (e.g. Flöel et al., 2009).

In this study, it is acknowledged from the outset that the precise interpretation of MD and FA measures is unknown. Nevertheless, the term 'integrity' is used synonymously with MD or FA. Patients with ischaemic brain damage or tumour resection, by definition, possess damage to their neural tissue. This damage may extend beyond gross lesion boundaries to affect the surrounding tissue, which is of primary interest to this study. In such diseased circumstances, unlike in healthy controls, the use of the term 'integrity' is largely accepted for DTI studies (Jones et al., 2013), although caution in its interpretation remains necessary.

7.3.4.4 Tract-based statistics

In order to compare values across participants, a standardized measure was derived for each tract. The voxel-wise tensor parameters (FA and MD) were combined with the spatial information of the trajectory of tracts within the white matter to compute a tract profile. Tract profiles represented the average FA or MD of the voxels touched by the tract, weighted by the distance from the mean of the tract at each location. This was done by resampling each tract to 100 nodes, distributed equally along the length of the tract (Yeatman et al., 2012). The region between nodes 15 and 85 was then used to represent 'whole tract' profiles, with the proximal and distal 15 nodes ignored to remove potential contamination with grey matter voxels or partial volume effects. This clipped tract profile was used to generate all subsequent measures of mean tract FA and MD. These measures were also used to calculate 'laterality',

representing the relative difference in FA or MD measures for the same tracts in opposite hemispheres.

$$\textbf{Laterality in patients (\%)} = \left| \frac{\textbf{FA/MD}_{\text{(intact)}} - \textbf{FA/MD}_{\text{(ipsilesional)}}}{\textbf{FA/MD}_{\text{(ipsilesional)}}} \right|$$

$$\textbf{Laterality in controls (\%)} = \left| \frac{\textbf{FA/MD}_{\text{(left)}} - \textbf{FA/MD}_{\text{(right)}}}{\textbf{FA/MD}_{\text{(right)}}} \right|$$

This technique of standardization may be preferable to the alternative method of voxel-based analysis, including Tract-Based Spatial Statistics (TBSS, Smith et al., 2006), which computes summary statistics on co-registered voxel skeletons. This is because individual brains show substantial variation in tract location, size, and shape, which may not be sufficiently dealt with by standard techniques that warp FA data onto a template image (Tsang et al., 2010). This can be particularly problematic for more peripheral, long-range tracts such as those being investigated here (Edden and Jones, 2011).

7.3.5 Lesion estimation

I estimated the size of patients' lesions by creating lesion masks from their T1 structural scans. This required a combination of thresholding raw T1 values to isolate damaged tissue (on T1-weighted MRI scans, ischaemic pathology shows low T1

intensity, e.g. exhibiting signal up to 150 UNITS) and manually drawing over unequivocal regions of damage. The 3-D lesion masks were binarized, and the total volume measured in mm^3. I was also interested in estimating the distribution and extent of damage across the brain. Lobar masks were created using the MNI structural atlas in standard space for all four lobes (frontal, parietal, temporal, occipital) in both hemispheres and separately for the subcortex. Masks were transformed into individual structural space using non-linear transformation, similar to the technique to create ROIs. It was then determined whether there was any region of overlap between the lesion and lobe masks, quantified as a percentage of the total lobe volume.

7.4 Results

7.4.1 Blindsight function is present in a subgroup of patients

All patients had profoundly impaired visual function in one hemifield, as revealed by Humphrey perimetry (Appendix A). However, 12 out of 17 patients were able to significantly detect a high contrast, drifting Gabor positioned inside the damaged portion of their visual field. The degree of awareness of the stimulus varied amongst individuals. This ranged from complete guesses and an absence of any awareness in some individuals, to the vague observation that something was moving in the damaged portion of their vision. None of the participants were able to describe in detail the stimuli shown. This question of awareness, and its variability is discussed in more detail in Chapter 3, where results for individual's trial-by-trial confidence ratings are also reported. For the sake of this diffusion MRI study, I was interested in

recording the presence or absence of significant detection of a stimulus in the blind field. If a patient could perform significantly above chance, they were considered to be 'blindsight positive' for all subsequent analyses and discussions. If the patient remained at chance across an average of all trials, and they were specifically unable to detect the highest contrast, most salient stimuli (100%), then they were considered to be 'blindsight negative'.

Results for all patients are plotted in Figure 1C, where the group mean and standard error of the mean in blindsight positive and negative patients are shown. The marked difference in performance between these two groups is evident, as is the association between stimulus strength of contrast and detection performance in the blindsight positive group (discussed in detail in Chapter 3), and is consistent with a wide range of reports in the literature that blindsight function is most robust for high contrast, moving targets. The use of this highly salient stimulus here allowed us to be relatively confident that patients performing at chance did not exhibit blindsight.

7.4.2 LGN > hMT+ pathways are found in the majority of patients

All 12 patients with blindsight, and 9 age-matched controls were found to have ipsilateral, uncrossed tracts between the LGN and hMT+. The number of streamlines was of a similar order of magnitude in both groups, and tracts were present in both hemispheres, including the damaged side containing V1 damage in blindsight positive patients. The numbers of cleaned streamlines for each participant are listed in the first two columns of Table 2 (patients) and Table 3 (controls). The process of cleaning, which removed streamlines more than 2.6 standard deviations away from the core of the fascicle, and more than 2.8 standard deviations longer than the mean

Patient	1. LGN > hMT+		2. Crossing hMT+		3. SC > hMT+	
	ipsi-lesion	intact	left > right	right > left	ipsi-lesion	intact
Blindsight positive patients						
PB1	75	115	*(9)*	*no*	12	12
PB2	19	196	*(6)*	*no*	*no*	18
PB3	50	67	24	24	17	17
PB4	19	315	*no*	*no*	*no*	15
PB5	93	83	7	19	14	14
PB6	12	64	13	15	*no*	17
PB7	397	17	*no*	*no*	16	8
PB8	87	37	12	16	20	17
PB9	635	53	*no*	*no*	16	*no*
PB10	32	29	*no*	*no*	*no*	*no*
PB11	291	47	9	18	12	*no*
PB12	194	17	17	13	15	*no*
Blindsight negative patients						
PN1	157	19	*no*	*no*	15	8
PN2	17	226	13	15	7	21
PN3	351	89	*no*	*no*	19	16
PN4	*no*	101	*no*	*no*	*no*	19
PN5	15	122	*no*	*no*	*no*	13

Table 2. Number of cleaned streamlines for the three pathways of interest in patients: (1) Ipsilateral LGN and hMT+ (2) hMT+ bilaterally via the corpus callosum (3) Ipsilateral SC and hMT+. Results are shown separately for the intact and damaged 'ipsi-lesion' hemispheres. Numbers in brackets represent situations where streamlines were only tracked in one direction, but not in the other; no = zero streamlines survived the cleaning process.

length, removed an average of 75% of all streamlines. This left a core bundle containing only 25% ± 8% of the original streamline numbers. The original numbers are not presented here, but are included in the Appendix C for reference. Even after cleaning, there is considerable variability in streamline numbers, both between participants and, in some cases, comparing hemispheres. This is true for controls (range = 19 - 653) and patients (range = 17 - 635).

Subject	1. LGN > hMT+		2. Crossing hMT+		3. SC > hMT+	
	left	right	left > right	right > left	left	right
C1	308	339	19	14	14	18
C2	619	269	*no*	*no*	39	17
C3	57	59	8	16	18	*no*
C4	176	114	8	6	18	16
C5	84	30	5	8	17	16
C6	57	19	*no*	*no*	15	16
C7	78	46	*no*	*no*	9	*no*
C8	498	182	19	14	35	14
C9	653	62	57	52	31	9

Table 3. Number of cleaned streamlines for the three pathways of interest in controls: (1) Ipsilateral LGN and hMT+ (2) hMT+ bilaterally via the corpus callosum (3) Ipsilateral SC and hMT+. Results are shown separately for the left and right hemispheres; no = zero streamlines survived the cleaning process.

Two example cases in each participant group are illustrated in Figure 3, where the 3-dimensional trajectory of bilateral LGN > hMT+ pathways is shown. Although these

white matter pathways share broad similarities between participants, anatomical variations are evident including in controls (Figure 3C and F), and can be appreciated using visualisations such as these.

Unlike in controls and blindsight positive patients, it was not possible to track any pathways between the LGN and hMT+ in the damaged hemisphere of one patient without blindsight (PN4). Ipsilesional LGN > hMT+ tracts were successfully tracked in the other blindsight negative patients, with a similar number to blindsight positive patients (Figure 3B and E, Table 2 columns 1-2). However all of these patients

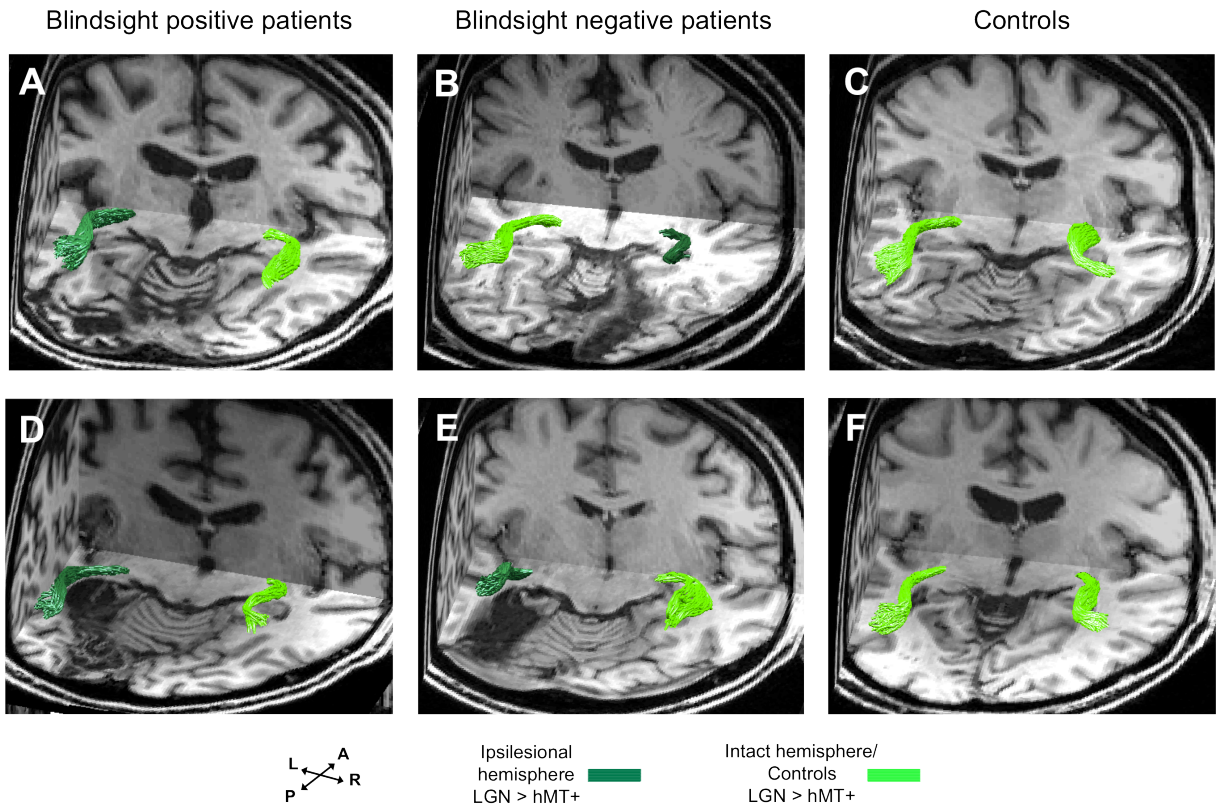

Figure 3. 3-D representations of ipsilateral streamlines between the LGN and hMT+. (A) Blindsight positive patient, PB9. **(B)** Blindsight negative patient, PN2. **(C)** Control participant, C8. **(D)** Blindsight positive patient, PB8. **(E)** Blindsight negative patient, PN3. **(F)** Control participant, C4. Dark green streamlines are in the ipsilesional damaged hemisphere, light green streamlines are in the intact hemisphere and controls. Streamlines are overlaid on a 3-D representation of participant's structural T1-weighted images.

showed a relatively marked difference in MD and FA measures in these tracts compared to their intact hemisphere.

7.4.3 FA and MD in the LGN > hMT+ pathway differs in blindsight positive and negative patients

As shall be discussed in 7.5.4, it is important not to put too much emphasis on streamline numbers without also considering measures of tissue microstructure. Mean FA and MD measures were calculated for each tract, and averaged across participants to generate separate measures for the ipsilesional and intact hemispheres. Mean FA, calculated across all blindsight positive patients and collapsed along the whole LGN > hMT+ pathway, was 0.43 ±0.05 S.D. in the damaged hemisphere and 0.49 ±0.05 S.D. in the intact hemisphere, corresponding to a laterality of 13.7%. This is illustrated in detail in Figure 4A, which plots the mean and standard error of FA along the length of the entire tract. As seen in Figure 4A, there was slightly greater laterality over the early-mid portions of the pathway. In blindsight negative patients (Figure 4B), the integrity of ipsilesional tracts was also reduced. Mean FA across the whole pathway was 0.35 ±0.1 S.D. on the ipsilesional side, versus 0.47 ±0.03 S.D. in the intact hemisphere (laterality = 34.7%). In comparison, control participants (Figure 4C) show a left-right laterality of 3.3% for FA, and 1.6% for MD (mean FA = 0.51 ±0.03 S.D. left, 0.49 ± 0.03 S.D. right hemisphere; mean MD = 0.73 ± 0.03 S.D. left, 0.72 ± 0.03 S.D. right hemisphere).

Tract MD in patients was also consistent with the findings for FA. In blindsight positive cases, mean MD was 0.81 ±0.07 S.D. in the damaged hemisphere, and 0.73 ±0.05 S.D. in the intact hemisphere (laterality = 9.6%). Conversely, blindsight

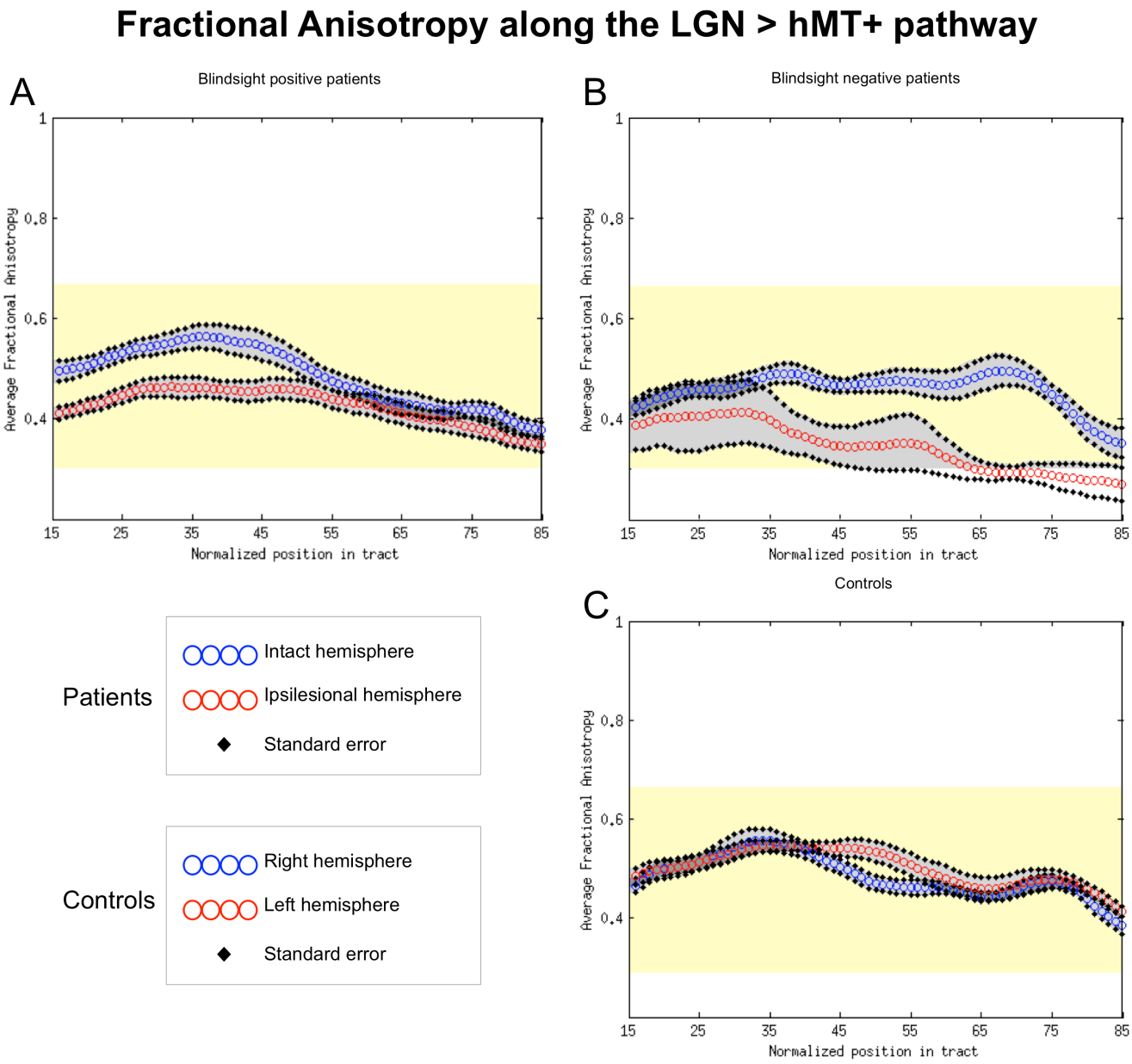

Figure 4. Average fractional anisotropy along the ipsilateral LGN > hMT+ pathways of blindsight positive patients, blindsight negative patients, and controls. **(A)** Blindsight positive patients show a slight reduction in anisotropy over the proximal half of the ipsilesional pathway, although the distal half shows no notable difference to the intact hemisphere. **(B)** Blindsight negative patients show a marked reduction in FA in the damaged hemisphere beyond the 35th node, continuing to the end of the tract. **(C)** Control participants show similar results for both hemispheres, with FA close to 0.5 throughout. The control range for this pathway is displayed in yellow on all charts.

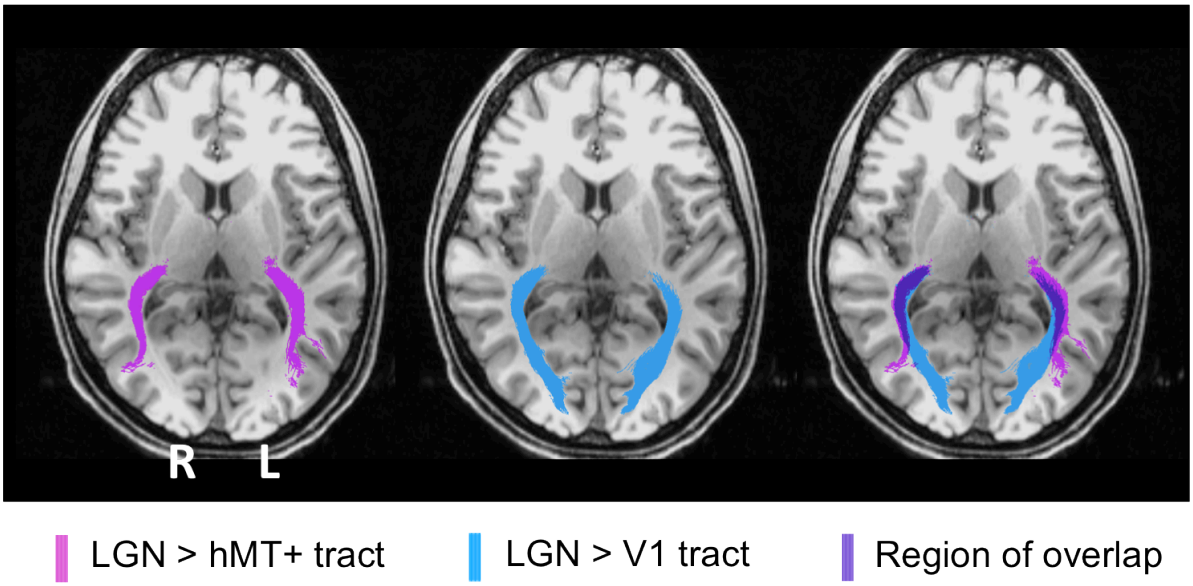

Figure 5. Normal ipsilateral streamlines between the LGN and hMT+, and the LGN and V1 demonstrate a proximal region of overlap. Streamlines are demonstrated in a control participant, C2, comparing ipsilateral connections between the LGN and hMT+ (pink) and the LGN and V1 (blue). When these pathways are superimposed, there is a significant region of overlap in the proximal portion of these pathways. In cases of V1 damage where there is retrograde degeneration, this overlapping region of the LGN > hMT+ pathway may become contaminated by degenerated tracts in the V1 path. It may therefore be more reliable to evaluate just the distal section of the hMT+ tract, which has separated away from this common bundle.

negative patients had a mean MD of 1.05 ±0.22 S.D. in the damaged hemisphere, compared to 0.77 ± 0.05 S.D. on the intact side, representing a laterality of 27.0%.

It is possible that the slight laterality in patients may, at least in part, be driven by an overlap with degenerated geniculate tracts supplying damaged V1. Figure 5 shows how this overlap can occur in the early-mid portions of the LGN > hMT+ pathway. In the central nervous system, neuronal degeneration can be either anterograde (Wallerian) in which injury to the cell body or proximal axon leads to distal degeneration, or retrograde when death of the cell body follows axonal injury. Consequently, the integrity of fibres innervating damaged V1 would gradually decline throughout their course. Where an overlap with such fibres occurs, DTI methods are

unable to distinguish between separate axonal bundles due to a limitation in spatial resolution (restricted here to $2mm^3$ voxel size). Thus measures of the LGN > hMT+ tract could become contaminated with overlapping degenerated radiation fibres. It may therefore be useful just to measure the FA spanning the distal portion of the LGN > hMT+ tract, which has branched away from large geniculate-radiation bundle. This may represent a purer measure of the LGN > hMT+ pathway, removing artefacts due to overlapping tracts. If the pathway to hMT+ were indeed damaged, one would still expect this measure to reflect the damage.

When examining just the distal nodes in the LGN > hMT+ pathway (between nodes 60-85), mean FA in blindsight positive patients was 0.39 ±0.06 S.D. in the damaged hemisphere and 0.42 ±0.04 S.D. in the intact hemisphere, corresponding to a laterality of 7.7% (mean MD = 0.79 ±0.06 S.D. versus 0.73 ±0.06 S.D., laterality = 7.6%). Individual data also confirmed that the standard deviation of the FA or MD for the two tracts in each blindsight positive patient was always overlapping. Overall, this implies a less pronounced impairment in integrity than was first suggested for the tract as a whole.

In blindsight negative patients, mean FA in the distal portion of this tract was 0.29 ±0.07 S.D., compared to 0.44 ±0.05 S.D. in the intact hemisphere (laterality = 51.7%), mean MD = 1.04 ±0.23 S.D. versus 0.74 ± 0.07, (laterality = 28.8%). Therefore unlike the blindsight positive group, blindsight negative patients still showed a relatively marked and significant drop in integrity throughout this purer LGN > hMT+ measure when compared to the intact hemisphere. (Mean FA: $F = 14.6$, $p < 0.001$ for blindsight negative patients, $F = 2.0$, $p = 0.15$ blindsight positive patients. Mean MD: $F = 12.8$, p

< 0.001 blindsight negative patients, F= 3.1, p = 0.06 blindsight positive patients). This is shown in Figure 6, which compares the FA and MD in this distal portion of the LGN > hMT+ tract for each hemisphere, in blindsight positive and negative patients. Furthermore, if the integrity range is used from age-matched controls as a guide for the normal range in this pathway (FA range: 0.30 – 0.66, MD range: 0.56 – 0.91), the ipsilesional pathway in the blindsight positive group falls within this control range, whilst it does not for the blindsight negative group (see Figures 4 and 6).

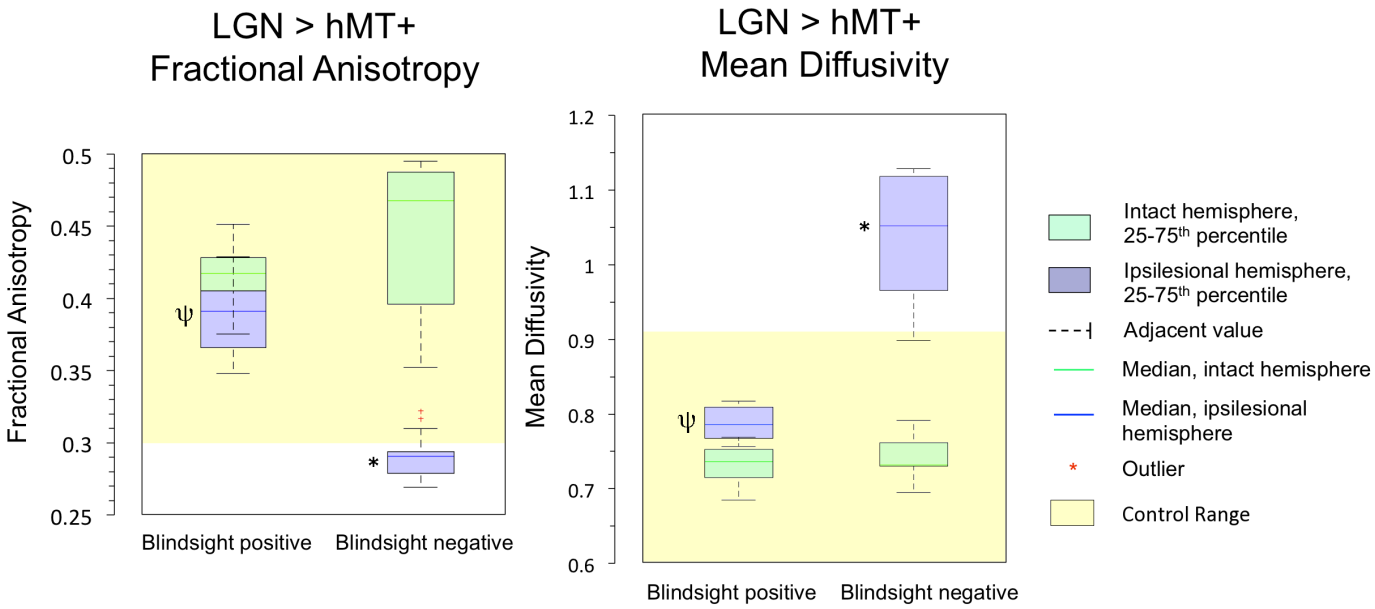

Figure 6. Box plots comparing FA and MD in the ipsilateral pathway between the LGN and hMT+, in blindsight positive and negative patients. Blindsight positive patients show significant overlap in the FA of this pathway in the damaged and sighted hemispheres. There is a slight increase in MD on the damaged hemisphere, however this is not marked and both measures fall within the control range. In comparison, blindsight negative patients show a marked difference in FA and MD for this pathway in the damaged and sighted hemispheres. The ipsilesional measures extend beyond the control range, implying that they are pathological and significantly impaired. Adjacent values are defined as the lowest and highest observations that are still inside the region defined by the following limits: Lower Limit = Q1 – 1.5 x IQR, Upper Limit = Q3 + 1.5 × IQR. The control FA and MD range for this pathway are displayed in yellow. ∗ $p < 0.001$, Ψ non-significant at 5%, F-test comparing tract integrity in ipsilesional versus intact hemispheres.

Interestingly, it is also possible to appreciate this difference visually by inspecting the tracts in the white matter, and their corresponding FA and MD maps. Figure 7 shows two examples of blindsight positive and two blindsight negative patients who have bilateral tracts between LGN and hMT+. In the damaged hemisphere of the blindsight positive patients (rows A and B), the region directly underlying tracts corresponds to relatively intact MD and FA measures that are not notably different from the opposite, intact hemisphere. In contrast, both blindsight negative patients (C and D) have tracts in the damaged hemisphere that appear to traverse a region of white matter displaying very abnormal FA and MD levels. The implication is that although tracts successfully propagated through this region, they were passing through regions of profoundly abnormal, damaged tissue.

7.4.4 Alternative pathways cannot account for the presence of blindsight

In addition to a direct geniculate connection to hMT+, which has been implicated in a number of previous studies (Schmid et al., 2010; Bridge et al., 2010) and in work presented here (Chapters 3 and 5), two alternative pathways were considered that are also believed to play an important role in blindsight function. Both involve connections to the same region of hMT+, one with the superior colliculus (Leh et al., 2006; Leh et al., 2010) and the other connects to hMT+ in the intact contralateral hemisphere (Bridge et al., 2008; Silvanto et al., 2007 and 2009). A number of blindsight positive patients were found not to possess a connection between hMT+ and the superior colliculus, or contralateral hMT+, or both, and intact connections between these regions can exist in blindsight negative cases.

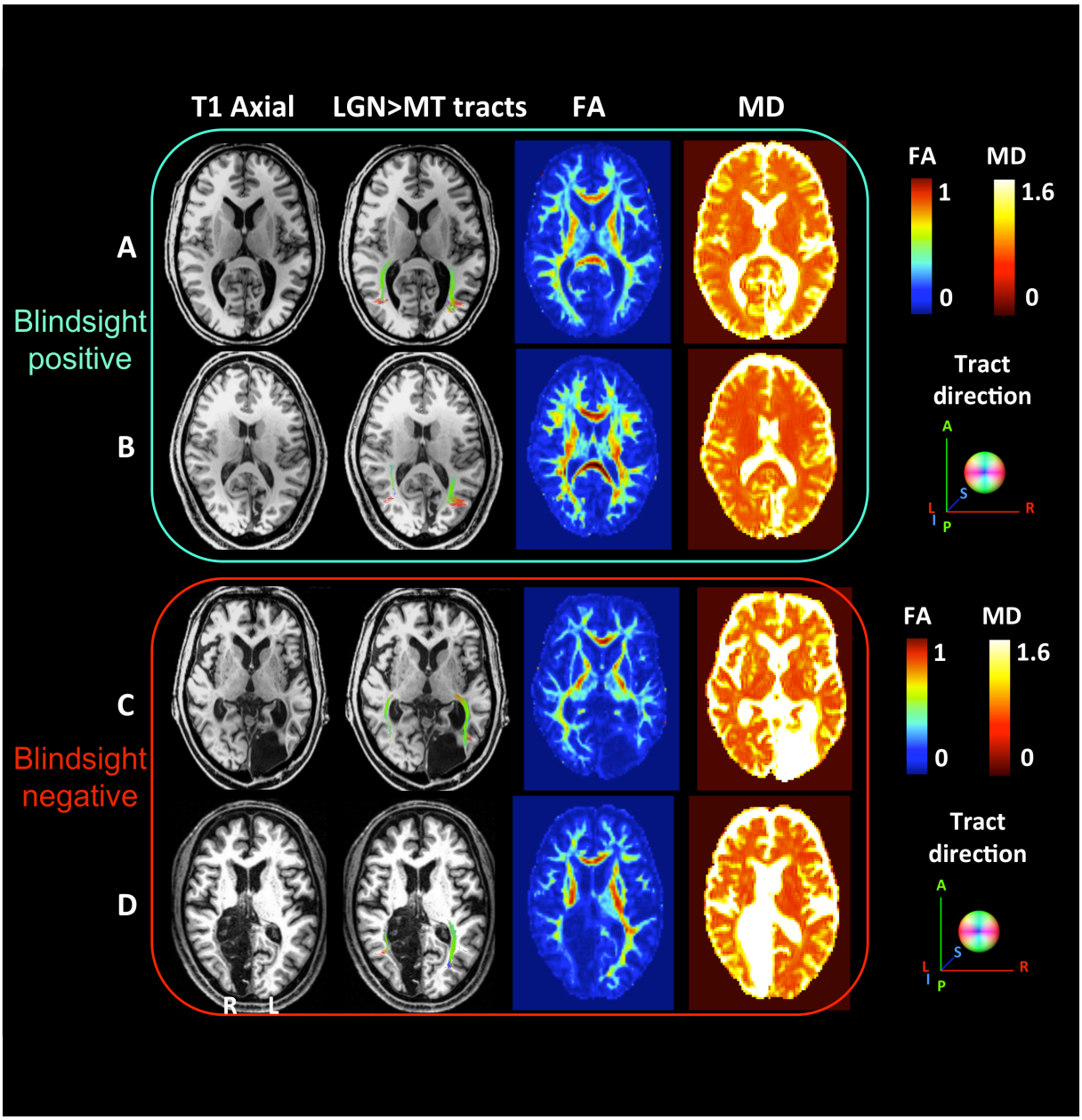

Figure 7. FA and MD maps in blindsight positive and negative patients, demonstrating the spatial relationship to LGN > hMT+ pathways. (A–B) Blindsight positive patients. Individual results for two patients (A) PB5, and (B) PB10. **(C–D) Blindsight negative patients**, (C) PN1, and (D) = PN5. All four patients generated bilateral ipsilateral streamlines between the LGN and hMT+, including the damaged hemisphere (column two). However, streamlines in the damaged hemisphere of patients in C and D traverse a region of tissue with notably impaired integrity, demonstrating low FA and high MD values (columns three and four). This impaired integrity is also apparent on the T1-weighted axial scan in case C, shown in the first column.

Overall it was clear that both pathways generated lower streamline numbers than the LGN > hMT+ pathway, with an approximately ten-fold difference (mean 18.9/18.7 versus 202.8 in controls, and mean 15.6/15.0 versus 122.7 in blindsight positive patients). The SC > hMT+ tracts also tended to appear more erratic and less compact in their course (see Figure 8D, E, and F for 3-D visualizations of cleaned fibres).

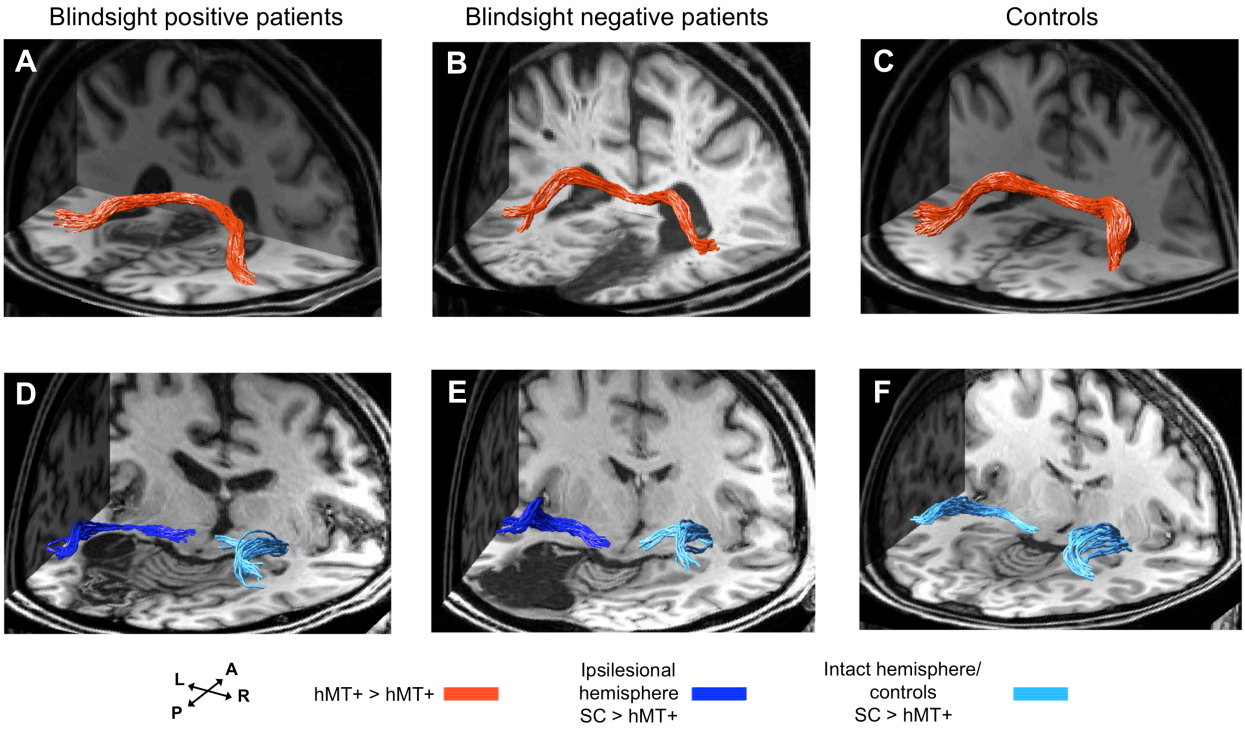

Figure 8. 3-D representations of (i) Interhemispheric connections between hMT+ bilaterally, (ii) Ipsilateral connections between SC and hMT+. (A) hMT+ > hMT+ streamlines in blindsight positive patient, PB3. **(B)** hMT+ > hMT+ streamlines in blindsight negative patient, PN2. **(C)** hMT+ > hMT+ streamlines in control participant, C9. **(D)** Ipsilateral SC > hMT+ streamlines in blindsight positive patient, PB8. **(E)** Ipsilateral SC > hMT+ streamlines in blindsight negative patient, PN3. **(F)** Ipsilateral SC > hMT+ streamlines in control participant, C2. Red streamlines represent crossing, interhemispheric connections between hMT+ bilaterally. Dark blue streamlines are connections between SC and hMT+ in the ipsilesional damaged hemisphere, light blue streamlines show the same SC > hMT+ pathway in the intact hemisphere, and in controls. Streamlines are overlaid on a 3-D representation of participant's structural T1-weighted images.

(i) Intact hMT+ > hMT+ tracts can be found in blindsight positive and negative cases

Crossing tracts between hMT+ bilaterally were identified in only six patients with blindsight, i.e. 50% of blindsight positive cases (Table 2, columns 3-4). Similarly, crossing hMT+ > hMT+ pathways were reliably identified in six out of nine controls (66.7%, Table 3). As expected, pathways always crossed to the opposite hemisphere via the corpus callosum (see Figure 8A-C). Where present, tracts also appeared to largely be intact. In blindsight positive cases, mean FA was 0.64 ±0.07 S.D. and mean MD 0.70 ±0.03 S.D., averaged along the entire tract for both directions (left to right, and right to left), and across participants (see Figure 9A for plots along the pathway). These values were similar to the control group (mean FA = 0.64 ±0.07 S.D., mean MD = 0.67 ±0.05 S.D., see Figure 9C). Indeed, the FA range in controls, which may serve as an estimate of the normal range for this pathway, was 0.28 – 0.91 for this pathway.

In blindsight negative patients, it was not possible to track interhemispheric connections between hMT+ in the majority of cases, with the exception of one patient (PN2; Table 2, columns 3-4, Figure 8B for 3-D visualisation). Furthermore this tract appeared to be largely intact, staying within the control FA range (0.28 – 0.91), with mean FA = 0.59 and MD = 0.73 (see Figure 9B for FA plots along this path).

(ii). Superior colliculus tracts are similar in blindsight positive and negative patients

A similar result was found for the superior colliculus > hMT+ pathway, which was impossible to track in certain cases of blindsight, but could be tracked in some blindsight negative individuals. These pathways were tracked in eight out of twelve

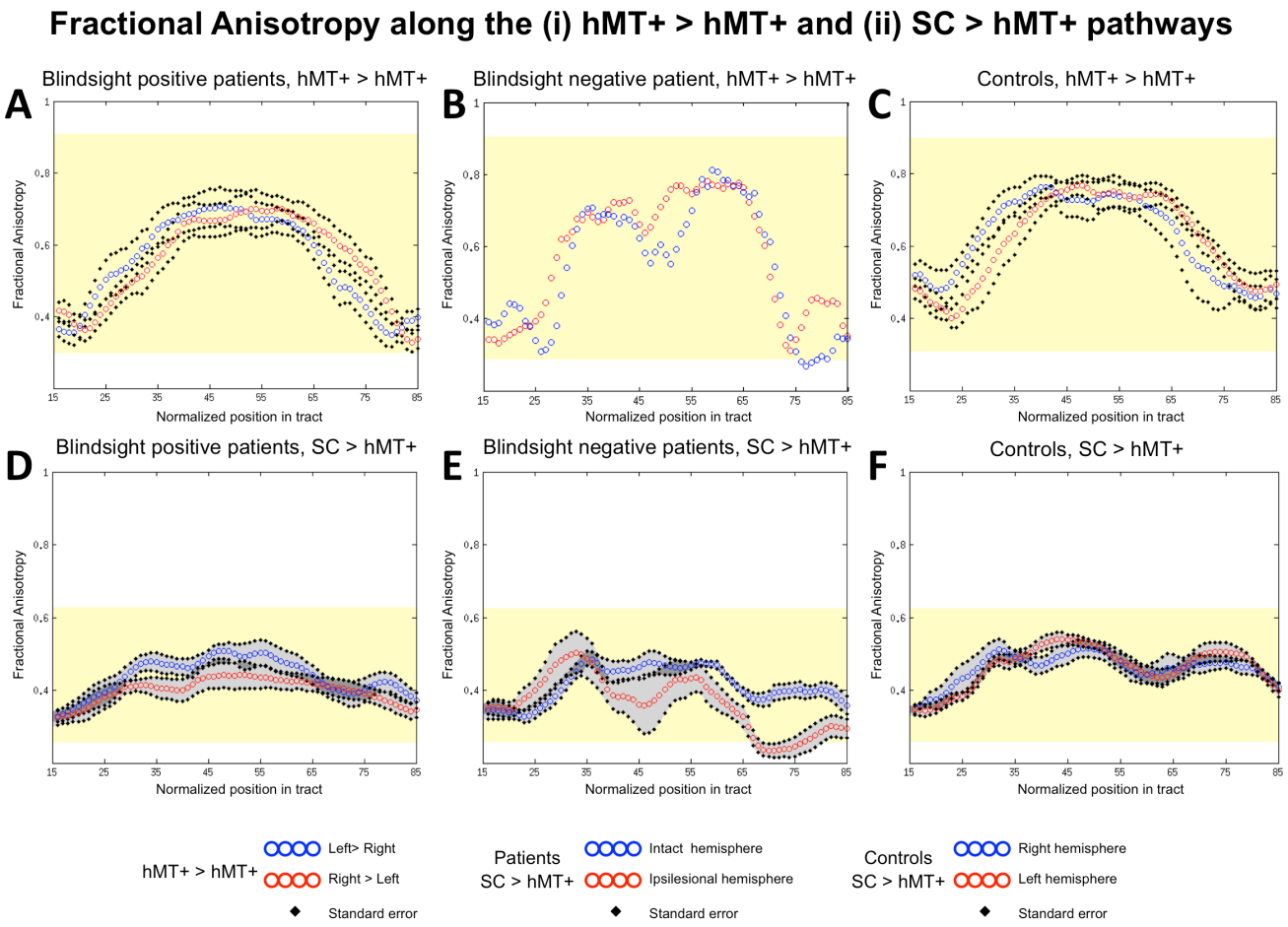

Figure 9. Average fractional anisotropy along the (i) Interhemispheric hMT+ pathway, (ii) Ipsilateral pathway between SC and hMT+. (A) Blindsight positive patients show a similar FA to controls along the length of interhemispheric hMT+ connections. **(B)** Blindsight negative patient, PN2, also shows a similar FA to controls along the length of this pathway. **(C)** Control participants show a normal peak in FA at the centre of the hMT+ > hMT+ connection, representing the high degree of anisotropy at the corpus callosum. **(D)** Blindsight positive patients show a similar FA in the ipsilesional SC > hMT+ pathway as the intact hemisphere and controls. **(E)** Blindsight negative patients show a slight drop in mean FA in the distal third of the ipsilesional SC > hMT+ pathway. **(F)** Control participants show a fairly constant FA along the length of the SC > hMT+ pathway, around 0.4. The control range for each pathway is displayed in yellow.

blindsight positive patients in the damaged hemisphere (66.7%, see Figure 8D for a 3-D visualisation). The same proportion of patients had tracts identified in their intact hemisphere, although this was not necessarily in the same cases (Table 2, columns 5-6). In comparison, a pathway between the superior colliculus and ipsilesional hMT+ was present in 3 out of 5 (60%) blindsight negative patients (Figure 8E). Control

participants showed these pathways in all nine cases (100%) on the left, and seven (77.8%) on the right (Figure 8F).

Of the patients demonstrating this pathway, mean FA was 0.40 ±0.05 S.D. in the damaged hemisphere of blindsight positive cases, versus 0.46 ±0.03 S.D. on the intact side, with some regions of overlap along their trajectory (laterality of 13.9%, see Figure 9D for FA plots). Mean MD was 0.78 ±0.08 S.D. versus 0.69 ±0.04 S.D. (laterality = 10.8%). In blindsight negative patients (Figure 9E), a more irregular pattern in FA was apparent. This pattern was different to other tract profiles seen in Figures 4 and 9, which showed smoother transitions along their trajectories. Collapsed along the pathway, mean FA was 0.37 ±0.05 S.D. versus 0.42 ±0.03 S.D. on the intact side (laterality = 14.0%), and MD was 0.83 ±0.13 S.D. versus 0.77 ±0.07 S.D. (laterality = 7.5%). In fact, this laterality and drop in FA towards the end of the SC > hMT+ pathway is strongly influenced by data from one patient (PN1). The other two blindsight negative patients (PN2 and PN3) show similar integrities in both hemispheres. This is true when considering the whole SC > hMT+ pathway ($t = 0.43$, $p = 0.7$, mean FA = 0.40 vs 0.41), or just the distal portion of the tracts ($t = 1.7$, $p = 0.2$, mean FA = 0.32 vs 0.37), despite being impaired in the LGN > hMT+ pathway ($t = 12.2$, $p = 0.007$, mean FA = 0.34 vs 0.48). This is important as it implies that intact tracts from the SC can occur in blindsight negative patients. However, it is worth noting that the FA in one of these two patients (PN2) does drop below the control range, reaching an FA of 0.22 between nodes 69-79 (control range = 0.26 – 0.62). Controls (Figure 9F) have a mean FA of 0.48 ±0.03 S.D. on the left versus 0.47 ±0.05 S.D. on the right (laterality = 1.1%), mean MD 0.72 ±0.04 S.D. on the left, 0.70 ± 0.07 S.D. on the right (laterality = 1.7%).

7.4.5 Lesion size and location

In addition to performing tractography between pre-defined regions of interest, a useful and unbiased approach to understand why certain patients have blindsight and others do not, is to analyse their lesion extent and location. This is particularly valuable in larger patient cohorts, moving away from the single case study approach. Figure 10 shows the total lesion volume and distribution of damage across all patients. Average lesion volume in the blindsight positive group was 13,461mm^3 ±7101 mm^3 S.D., compared to 36,923mm^3 ±23,035 S.D. in the blindsight negative group. On average, blindsight negative patients had lesions approximately 2.5 times larger than the blindsight positive group, although Figure 10B shows the overlap of occipital lobe damage between patients. There was a significant association between the extent of occipital lobe damage and integrity of ipsilesional LGN > hMT+ pathways across all patients (FA: r = -0.59, p = 0.015; MD: r = 0.63, p = 0.009). This reinforces the likelihood that impaired tract integrity in blindsight negative individuals reflects an involvement of surrounding white matter pathways in occipital lesions.

There was no clear association between blindsight function and the presence of additional, non-occipital damage. As seen in Figure 10 B-D, situations did occur where damage extended to other regions, including the temporal lobe (PB8, PN3, and PN5) or parietal lobe (PN4 and PN5). However the presence or absence of such damage was not consistent between the two groups. Furthermore, only one participant showed evidence of significant subcortical pathology (PN5), seen to extend to a region including the ipsilesional LGN and pulvinar, whilst the superior colliculi appeared intact.

A Lesion size

Patient	Total Lesion Volume
Blindsight positive	
PB1	20,224 mm³
PB2	7080 mm³
PB3	8752 mm³
PB4	28,736 mm³
PB5	16,432 mm³
PB6	4320 mm³
PB7	8408 mm³
PB8	8744 mm³
PB9	15,220 mm³
PB10	14,984 mm³
PB11	8584 mm³
PB12	20,048 mm³
Blindsight negative	
PN1	30,066 mm³
PN2	15,000 mm³
PN3	42,384 mm³
PN4	20,897 mm³
PN5	73,121 mm³

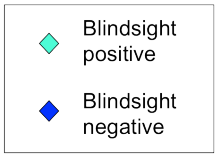

B Lesion location

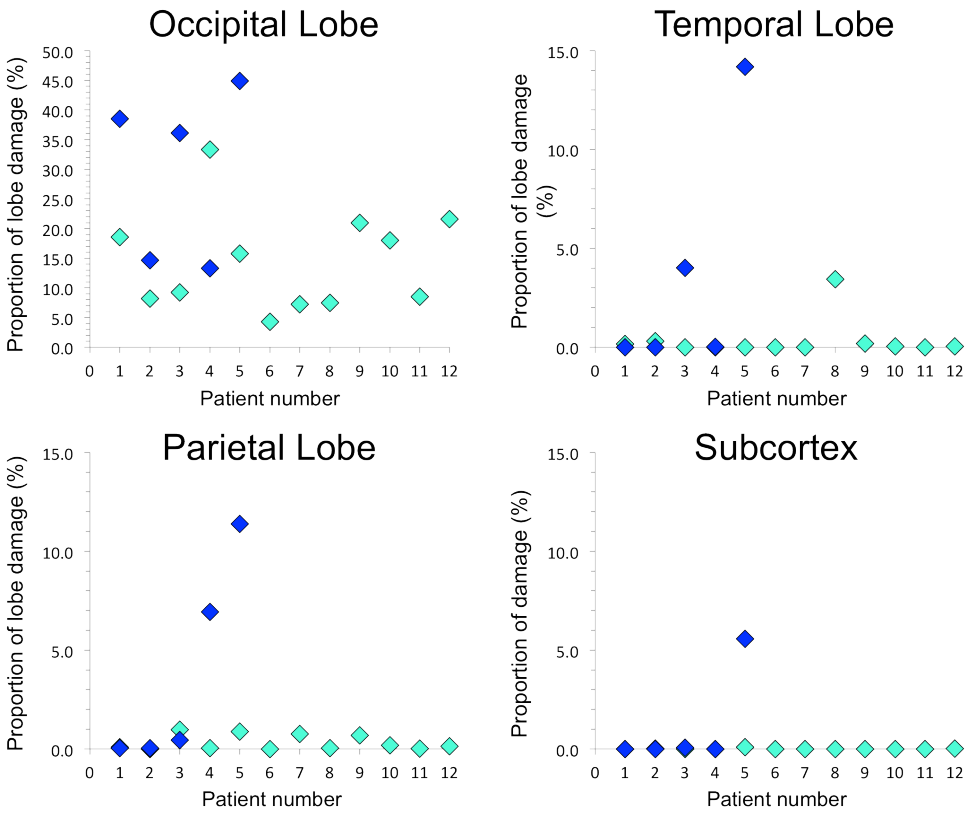

Figure 10. Comparison of lesion size and location in blindsight positive and negative patients. (A) Lesion size is demonstrated for each patient, and demonstrates a wide range of volumes in both patient groups. **(B)** Lesion location shows the proportion of lobe damage in each patient, within the occipital, temporal, and parietal lobes, as well as the subcortex. Subcortex incorporates the thalamus (including lateral geniculate nucleus and pulvinar), striatum, and superior colliculi, with an approximate unilateral volume of 50,000mm^3. Only one patient, PN5, demonstrated some involvement of this region, including the ipsilesional LGN and pulvinar, but not the superior colliculi.

At least three patients with blindsight showed complete destruction of calcarine cortex or its underlying white matter (PB1, PB4, PB10). Similarly there were blindsight negative cases with small regions of V1 apparently intact (PN2, PN4). The majority of cases with lesions affecting less than 20% of the occipital lobe had some small area of V1 sparing. This usually corresponded to the occipital pole, or a region of cortex far anteriorly. These regions would in turn be associated with visual field preservation at the very centre of vision, so called 'macular sparing', or in the far periphery. All patients had psychophysical tests performed in portions of their visual

field that would not be supported by regions of V1 sparing (see Appendix A for all perimetry reports).

7.5 Discussion

This is the first study to perform MRI diffusion tractography and a comparison of the microstructural tissue properties of visual pathways in a large group of patients with adult-onset V1 damage, who have been categorized according to blindsight function. All of the patients were labelled as blindsight positive or negative according to their ability to detect a highly salient stimulus in their blind hemifield. This was the most sensitive blindsight assessment used in the current thesis, and has been described elsewhere to detect blindsight function in the majority of patients with isolated V1 damage (Sahraie et al., 2008). By combining the results from these psychophysical and MRI techniques, it has been possible to directly relate residual visual function to the underlying properties of neural connectivity in the visual system. Furthermore, by testing such a large group of patients it has been possible to address some of the well-known limitations that arise in DTI, relating to consistency.

7.5.1 Direct geniculate connections are required for blindsight function

The principal finding here was that all patients with blindsight function showed intact, undamaged connectivity between the LGN and hMT+ in the same hemisphere as V1 damage was located. This was not the case in blindsight negative patients, where such geniculo-extrastriate connections were either not found, or demonstrated

a significant impairment in tract integrity as determined by a marked increase in mean diffusivity, and a decrease in fractional anisotropy when compared to the intact hemisphere or age-matched controls. This has led to two important inferences supporting geniculate connections in blindsight function. (1) Intact connections between the LGN and hMT+ are *necessary* for blindsight function, since there were no patients with blindsight function who demonstrated an absence or impairment in these pathways. (2) Intact connections between the LGN and hMT+ are *sufficient* for blindsight function. This was supported by the results in blindsight negative patients, as none of the patients without blindsight function possessed normal, intact connections in this pathway. These findings also lend no support to the suggestion of plasticity in cases of blindsight whose brain injury occurred in adulthood. Equivalent intact ipsilateral pathways were also present in all control participants, and there was no suggestion of a difference in connection 'strength' when compared to the blindsight positive patient group.

7.5.2 Intact collicular or interhemispheric pathways may not be necessary or sufficient for blindsight

Unlike direct geniculate connections, there were examples of patients with blindsight function who had absent or impaired collicular and interhemispheric pathways. Similarly, there were blindsight negative cases who seemed to possess undamaged connections to these regions. These results suggest that neither of these other putative blindsight pathways were necessary or sufficient for blindsight function, but support the argument that in blindsight positive cases, some other pathway must have facilitated visual performance. This does not mean that these, or other alternate

pathways categorically do not play a role in blindsight. As shall be discussed, it is possible that in certain individuals, or perhaps in different aspects of blindsight function, such alternative routes become more important. It is also possible for separate pathways or structures to work together to support residual vision in patients with V1 damage.

7.5.3 Important differences with existing DTI studies

A small number of studies have already measured DTI in patients with V1 damage and blindsight function. In fact, these studies have elicited a number of different results. One of the first studies of this kind assessed four patients following partial hemispherectomy for severe intractable epilepsy, two of whom had attentional blindsight according to a spatial summation paradigm (Leh et al., 2006). They demonstrated that only patients with blindsight showed crossing tracts between the superior colliculus in the damaged hemisphere and regions of the intact hemisphere, and strong ipsilateral connections with the damaged hemisphere. These crossing tracts were also seen in some control participants, although were arguably less prominent.

Two independent studies in patient GY related either to residual visual motion (Bridge et al., 2008), or to emotional processing, so-called affective blindsight (Tamietto et al., 2012). GY shows evidence of blindsight function using both stimulus types, although different pathways are considered to be involved – supported by these two studies. In the work relating to motion, he was found to possess a direct ipsilateral connection between LGN and hMT+ in the damaged hemisphere, similar to

the results for blindsight positive patients presented here. However, it was also suggested that he showed unusual patterns of connectivity that may be suggestive of plasticity. These included a cortico-cortical callosal connection between hMT+ bilaterally (tested here, but found to be absent in 6/12 blindsight positive patients) and a crossing pathway between LGN in the undamaged hemisphere and ipsilesional hMT+. In both cases these unusual pathways were mostly demonstrable in controls, however GY showed a considerably greater number of samples (Bridge et al., 2008).

Finally, there are two case reports of bilateral striate cortex damage that suggest that interhemispheric callosal connections are not important for blindsight function, thus again lending support to the results presented here (de Gelder et al., 2008; Bridge et al., 2010). One study demonstrated intact ipsilateral pathways between the LGN and hMT+, displaying the same integrity as healthy controls (Bridge et al., 2010). The other remained unclear about where blindsight function may have arisen, but demonstrated a severe reduction in posterior callosal connections (de Gelder et al., 2008).

From this small handful of DTI studies, a number of different findings are apparent. Some implicate the intact hemisphere and crossing interhemispheric connections from the superior colliculus, or LGN. Others suggest that there are direct, ipsilateral subcortical pathways. Aside from the obvious limitation of single case studies, there are a number of differences that could account for these discrepancies. One concern is that these studies, including the current work, are ROI-based and thus restricted to predetermined regions or connections of interest. An important subcortical structure that was not explicitly tested here, but is implicated in blindsight function is the

pulvinar nucleus (Warner et al., 2010). In theory this region would be incorporated into SC > hMT+ pathways, which are believed to pass through the pulvinar along route to the visual cortex (Benevento and Standage, 1983; Lyon et al., 2010). However a more conclusive (albeit time-consuming) option may have been to take an unbiased approach and compare connectivity between hMT+ and every other voxel in the brain, thus removing the constraint of pre-determined ROIs.

Another important factor to consider is the age at which V1 damage has occurred. GY sustained left hemisphere damage in childhood (aged 7 years) as a result of a traumatic brain injury. The four patients enrolled in Ptito's research also sustained severe structural brain damage either at birth or in early childhood, despite undergoing resective surgery later in life. Researchers in both cases noted increased interhemispheric connectivity in blindsight positive cases. However it is certainly possible that there is greater scope for plasticity when damage is sustained early in life. In particular this may account for these stronger interhemispheric connections, as it has been shown that the cross-sectional area of the corpus callosum continues to grow at least until early adulthood (Keshavan et al., 2002). In contrast, both of the bilateral patients sustained their damage in adulthood, and their results were more in keeping with intact ipsilateral pathways similar to the current study. All seventeen patients enrolled in this study sustained brain damage during adulthood. In fact, this was an important inclusion criterion, since the question of age and plasticity has remained under dispute. The results presented here suggest that plasticity may not be necessary for the presence of blindsight, and simply that the presence of intact residual connections may be critical.

The other important factor to consider is how blindsight function is assessed, and the *type* of blindsight present. It has been argued in the past that different forms of blindsight may be mediated by distinct anatomical pathways (Danckert et al., 2005). For example, collicular processing may be involved in 'action' or 'attention' blindsight, whilst the LGN is implicated in perceptual characteristics, described as 'agnosopsia' by Zeki and colleagues (Zeki and Ffytche, 1998).

Even in the two bilateral cases, blindsight function differed considerably. Only one patient was above chance using 2-AFC tests similar to those used here (and Saharie et al. 2008). The other patient was only able to perform certain navigational and 'action' tests, and interestingly showed fairly extensive cortical loss throughout both occipital lobes. The blindsight positive cases in Leh et al. (2006) had also been tested for indirect or 'attentional' blindsight. Neither blindsight positive patient possessed any degree of awareness for the stimulus or any direct response to blind field stimulation at all. Although this was only tested at 30% contrast, a similar result was also reported using an LED target of 40cd/m2 on a background < 1cd/m2 (Tomaiuolo et al., 1997). The implication is that if these patients had been tested with the same direct 2-AFC method of blindsight assessment as used here, they may have remained at chance. In other words, indirect blindsight assessments may be more sensitive than the 2-AFC tests used here, and may even rely on different structures. It is interesting that since Ptito's patients had been hemispherectomised, by definition it was not possible for ipsilesional occipital structures to underlie the residual function. Instead, the authors consider that the intact hemisphere must be important, or perhaps even that subcortical activation alone is sufficient to elicit this type of blindsight. The only way to tackle this would be to improve consistency amongst

experiments, and perhaps to include multiple methods of assessing blindsight in future work.

7.5.4 Limitations of streamline number as a useful measure in clinical populations

A significant concern that arose from the current study was that it was possible to track robust fascicles of tracts in patients that traversed regions of extremely impaired tissue integrity. Indeed, it may even be the case that streamlines were biased towards narrow regions of white matter that run alongside a lesion boundary. Patient PN1, for example, showed almost ten times more streamlines in the LGN > hMT+ pathway of his damaged hemisphere compared to the intact side, even though tracts quite clearly passed through a region of abnormal (damaged) tissue. This is apparent from the MD and FA maps, as well as close inspection of his T1 anatomical images (see Figure 7C, and Table 2.1 for relative streamline numbers). These tracts are unlikely to be functional, as implicated by the negative psychophysical performance.

This finding highlights the danger of putting too much emphasis on streamline numbers, without also considering measures of tissue microstructure. In fact there are many reasons why streamline numbers provide unreliable measures of true axonal projections and function (Jones et al., 2013). Even if the 'true' fibre count is uniform within a bundle, the number of reconstructed streamlines may be different purely because of the length, curvature, and degree of branching present (Jones et al., 2010). This is also true for the number of streamlines passing through a given voxel.

Such variability was apparent from tractography results here. Even in control participants, there were marked discrepancies in streamline laterality and between individuals. If these figures had been reported alone as the principle measure of connectivity, they would have generated very misleading results. Whilst this was not the case here, a number of key early papers focused on this measure. Both Leh et al. (2006) and Bridge et al. (2008) used sample numbers as their sole estimate of connectivity, without considering white matter integrity. In Leh et al., the magnitude of tissue damage was extremely widespread and clearly extended to subcortical structures. Thus it would have been particular important to consider whether streamlines from the ipsilesional superior colliculus were indeed viable and had normal integrity. The other study interpreted a difference in sample numbers as suggestive of plasticity (Bridge et al., 2008). Whilst this may be correct, any tractography algorithm with a bias for peri-lesional pathways could have contributed to these findings. An interesting way to address this in the future may be to consider methods that actually assess the accuracy of an estimated connectome and tract, such as Linear Iterative Fascicle Evaluation (LiFE, Pestilli et al., 2014).

7.5.5 Absent streamlines do not necessarily mean an absent pathway

Perhaps one of the more controversial uses of MRI diffusion tractography is to comment on the existence or absence of a specific pathway (e.g. see Sherbondy et al., 2009). False positive (and to a lesser extent, false negative) connections have clearly been described in comparisons of DTI tractography to more reliable histological measures (Gao et al., 2013), using probabilistic or deterministic techniques. This is

not surprising if one considers that the success or failure of streamline propagation in tractography algorithms, similar to the number of streamlines, is essentially arbitrary and is influenced by a number of factors including data quality, tractography algorithm, number of seeds, curvature radius threshold etc., as well as features of the pathway already mentioned such as geometry and FA.

An additional source of variation is the process of 'cleaning' tractography results to try to isolate tracts that are robust and consistent, and to minimise the over-interpretation of noise. In the current study this process involved removing outliers that lay more than a specified standard deviation away from the mean in terms of length and distance to the bundle core. Also in this process of 'cleaning', if the number of generated streamlines (from a seed of 10,000) was less than 10 before outlier removal, this was interpreted as a failure to adequately track that pathway. This cut-off resulted in 3/9 control participants being classified as showing no interhemispheric pathway between hMT+ bilaterally, when in fact all of these individuals showed at least four streamlines that touched the target ROI. This finding is somewhat troublesome, as one might expect all healthy controls to demonstrate a crossing pathway between hMT+. But is it likely that the presence of four, slightly erratic streamlines is reflective of a true fascicle bundle? The answer is probably no, although it is acknowledged that this cut-off is somewhat subjective. If a less stringent cut-off had been used, then these pathways would have been demonstrable in 100% of control cases. Conversely, if other studies applied a more conservative threshold, they may have demonstrated similar results to those reported here (i.e. absent crossing hMT+ pathways in 3/7 controls, Bridge et al., 2010).

In the patient data, the use of this cut-off would not have altered the finding that two patients with blindsight showed no crossing hMT+ tracts, or that one patient who was blindsight negative had no connection between LGN and hMT+ in their damaged hemisphere. However, at least one streamline was present in the raw data of ipsilesional collicular pathways of all blindsight positive patients (four patients had ≤ 5 streamlines). While a less stringent cut-off could have suggested these tracts to be present, when visualized it was clear that these pathways were largely implausible. Therefore if anything, this result reinforces the usefulness of a cleaning process to improve data reliability.

7.5.6 Is laterality or raw integrity a more useful marker of impaired tissue structure?

In measures of white matter integrity, both laterality and control ranges can provide useful comparisons for patient data. Laterality compares a pathway's integrity to its corresponding measure in the opposite hemisphere of the same individual. In contrast, control measures can indicate the normal range for a similar group of individuals. Both measures have been used throughout this chapter, however it might normally be argued that laterality is more useful - particularly since the participants here spanned a wide age-range. White matter integrity is known to change quite markedly with age and the presence of comorbidities, such as small-vessel disease (Salat et al., 2005; Jones et al., 1999). One problem, however, is that laterality assumes that white matter in the intact hemisphere is associated with *functional* pathways. The current study is interested in relatively weak 'alternative' pathways, which may not actually have an important role in the intact, healthy visual system.

This is emphasized by the fact that collicular and interhemispheric tracts have not been demonstrable in all control participants.

One blindsight negative patient (PN2) showed absent laterality in his SC > hMT+ path, but marked laterality in the LGN > hMT+ path, despite the raw integrity in both ipsilesional pathways being similar. This difference was being driven by a relatively low integrity in the SC > hMT+ pathway of his undamaged hemisphere, which might even be considered to be pathological. Even though no laterality was present, his ipsilesional collicular tract may still have been damaged. In such cases an integrity range may be particularly helpful, i.e. when assessing tracts of unclear functional significance whose integrity may be 'silently' impaired without clinical signs or symptoms (Auriel et al., 2014).

If laterality cannot exclusively be relied on, is there an acceptable range for microstructural measures? In diffusion imaging, the extent to which the movement of water molecules is impeded in any one direction will depend on a number of factors such as fibre diameter, density, membrane permeability, and myelination (Johansen-Berg, 2010), and FA is naturally low in areas of white matter where fibres cross. So far it is not possible to determine which specific factor(s) may be altered, particularly where the anisotropy is reduced. However in cases of pathology, a considerable increase in diffusion is usually taken to indicate the presence of structural damage, such as in chronic stroke (Jones et al., 1999, LeBihan and Johansen-Berg, 2012). Unfortunately, there is no official 'cut-off' for diffusion values that implies a tract is damaged beyond functionality. For example, one might suggest from the literature and from data in this study that an MD > 1.0 x 10^{-3} mm^2 s^{-1} is likely to be pathological.

However this threshold is essentially arbitrary. Indeed, such a universal measure would prove problematic given that anisotropy varies considerably throughout the white matter, for example showing most restricted diffusion around the splenium of the corpus callosum (Brander et al., 2010). That does not mean that such a guide would not be possible to create, and research appears to be moving towards that direction (e.g. Yeatman et al., 2012). It would, however, require a great deal of normative, age-matched DTI and behavioural data, and would need to provide specific ranges for each region of white matter.

7.5.7 Conclusions

In summary this work provides strong evidence to support direct geniculate connections to extrastriate cortex as being essential for blindsight function in adult-onset V1 damage. Although alternate interhemispheric and collicular pathways were also demonstrable in a number of patients, these connections were unable to account for all blindsight cases and were often found to be intact in patients with absent blindsight performance. Despite the limitations in tractography and diffusion tensor models, this technology has continued to advance and can provide important measures of tissue structure and connectivity that are not possible from structural imaging alone. In future work it will be interesting to relate the results obtained here to alternative, 'indirect' measures of attentional or action blindsight. These tests are arguably more sensitive measures of residual vision, and may even be possible in the absence of visual cortex innervation.

Chapter 8

Visual field rehabilitation with motion stimuli transfers learning to the ventral stream

8.1 Abstract

Homonymous visual field loss is extremely difficult to treat, and is a common and debilitating consequence of stroke. However, residual visual processing in the blind field despite V1 damage offers an exciting potential for rehabilitation. Strategies targeting this have been criticised for several reasons, including a failure to adequately control eye movements, the non-transferability across stimulus properties, and the fact that blindsight is, by definition, an unconscious phenomenon. However, these criticisms may no longer be valid. This study assessed the effect of three months of blindsight training using a motion stimulus in four patients with chronic V1 damage. A number of improvements were demonstrated deep within the scotoma, including a transfer of learning to static images classically associated with the ventral visual stream. This goes against an exclusive role for motion-sensitive pathways in training-effects. Residual early visual cortex may also be involved, and may facilitate a transfer across modalities. Future work will explore the mechanisms underlying this, and may benefit from training multiple visual streams and parameters.

8.2 Introduction

Homonymous visual field loss is a common consequence of stroke and traumatic brain injury. It is associated with an adverse functional prognosis and has implications on day-to-day activities such as driving, reading, and safe navigation. Early recovery is expected in around half of cases, and may be associated with a return in V1 activity. However, in stable disease recovery is unlikely beyond three and certainly six months (Zhang et al., 2006b).

Rehabilitative approaches generally target three main areas, encompassing a range of techniques with variable success and popularity: (1) Visual aids aim to expand or relocate the affected visual field; (2) Eye movement training builds upon compensatory strategies to improve explorative saccades; (3) Visual field restitution (VRT) aims to improve visual processing within the damaged field itself. All these approaches seem to offer modest improvements with repeated practice, with promising findings in recent VRT studies suggesting that it may be an important strategy to focus on.

8.2.1 Optical aids

A number of optical devices can be used to improve perception of the visual scene by expanding or relocating the visual field. This is most commonly achieved through use of prisms, which are fitted onto spectacles on the side of the field loss, and reflect images onto the functional side of the retina. Although this is a relatively simple and

inexpensive technique, it relies on patients wearing glasses to gain the benefit. It is also frequently associated with central diplopia, which can be very disorientating to the patient (Peli, 2000; Bowers et al., 2008).

8.2.2 Eye movement training

Explorative eye movements can be trained to improve visual perception and obstacle avoidance, and have been available to patients for a number of years. The general principle is based upon the observation that some patients with visual field loss perform visual search in an unsystematic and time-consuming way, reducing their ability to appreciate the visual scene as a whole (Zihl 1995).

Training methods include encouraging large saccadic eye movements to targets in the blind field (Zihl 1995), or performing repeated visual search tasks (Pambakian et al., 2004; Roth et al., 2009). These are associated with improved stimulus detection and reduced search times, but only minor differences in activities of daily living or self-reported real-word performance, and no improvement in reading speeds (Jacquin-Courtois et al., 2012; Lane 2010). Also, many patients already show compensation strategies with adequate exploration of their blind field, and may not therefore benefit from further training (Martin et al., 2007; Hardiess, 2010).

Another approach for right-sided field loss is to target reading by improving step-wise eye scanning (Zihl 1995, see Schuett 2008 for review). Hemianopic alexia is a debilitating consequence of hemianopia, and reading speeds can be improved by

training with rolling text (Spitznya et al. 2008). Although the benefits are very specific, they are readily available via internet 'apps' (Ong et al., 2012).

8.2.3 Visual Field Restitution (VRT)

8.2.3.1 Border-field VRT

Visual field restitution (VRT) is the general term given to improving visual processing within the damaged field itself. It is an area that has proved controversial at times, but still continues to receive much support. In reality VRT encompasses a number of different approaches to visual field recovery, although VRT as a term is generally synonymous with the work of Sabel, Kasten and colleagues (NovaVision), to be referred to here as 'border-field VRT'.

Initial work on VRT came from Zihl and von Cramon in the 1980s, which sought to replicate work on non-human primates (Zihl and von Cramon, 1982 and 1985). Later, Sabel and Kasten elicited visual field expansion in patients using a computer-based therapy targeting the 'transition zone', an area representing the border region between intact and damaged visual-fields (Kasten and Sabel, 1995; Kasten et al., 1997). They proposed that these zones were functional representations of partially spared neuronal structures in areas of the brain that were only partially injured (Kasten et al., 1998). A significant criticism of this work was that saccadic eye movements were not fully controlled for, nor appropriately taken into account. This concern was upheld in a follow-up study using a scanning laser ophthalmoscope (Reinhard et al., 2005) in which no improvements in field size were found using microperimetry or Tuëbingen automated perimetry (Schreiber et al., 2006).

8.2.3.2 Blindsight VRT and perceptual learning

Although not often considered a unique subgroup in visual rehabilitation, there is a growing literature on perceptual learning in homonymous visual field loss. Perceptual learning refers to the improvement in psychophysical performance with practice, and anyone undergoing repeated visual field testing might expect to see a degree of improvement in sensitivity. In one respect, this may be a confounding factor when assessing VRT (Horton 2005). However, it is also argued that repetitive training can help the damaged visual system relearn how to process visual information (Das and Huxlin, 2010).

A large component of this work comes from so-called 'blindsight VRT' led by Sahraie and Huxlin's research groups, and both employing more rigorous controls of fixation. There are also a number of studies employing blindsight-stimulating techniques without necessarily labelling them as such (e.g. Raninen et al., 2006, Henriksson et al., 2007). The principal is for repetitive presentation of salient stimuli, custom-designed to undergo blindsight via particular spatial and temporal properties. By using this technique, patients with chronic V1 damage have demonstrated improvements in sensitivity, detection and awareness deep within visual field defects, accelerated with positive feedback (Sahraie et al., 2006; 2010).

A criticism of this work is that, similar to blindsight, improvements may be tuned to stimuli of specific spatial and temporal properties that may not translate to different stimulus types. Also, the very nature of blindsight is that it occurs without conscious perception. However, there are recent examples of training that transfers to different

stimulus properties, and can be associated with improvements in awareness (Das and Huxlin, 2010; Sahraie et al., 2013). Therefore the approach is promising, and represents one of the first techniques to generate improvement deep within the scotoma. It will be important to try to uncover the mechanisms behind these findings, and the extent to which recovery may be possible.

8.3 Methods

8.3.1 Participants

Four patients (two female) took part in this study, all of whom had sustained posterior circulation stroke at least 6 months before enrolling (Figure 1). Average age at the time of participation was 57.9 years ± 11.2 S.D., average time after pathology onset 16.8 months (range 7-23 months).

8.3.2 Training protocol

8.3.2.1 Training apparatus

The training procedure was conducted at patients' homes on an IBM compatible personal computer, mounted on a frame (see Figure 2 for illustration of experimental setup). Gamma corrections had been conducted on all monitors using an LMT luminance meter (LS100; Konica Minolta, Inc., Tokyo, Japan) at 256 equi-stepped logical colours. Participants sat with a chin rest at a distance of 40 cm from the monitor, adjusted to ensure their line of site was approximately equal to the fixation point. Viewing was binocular throughout the experiment.

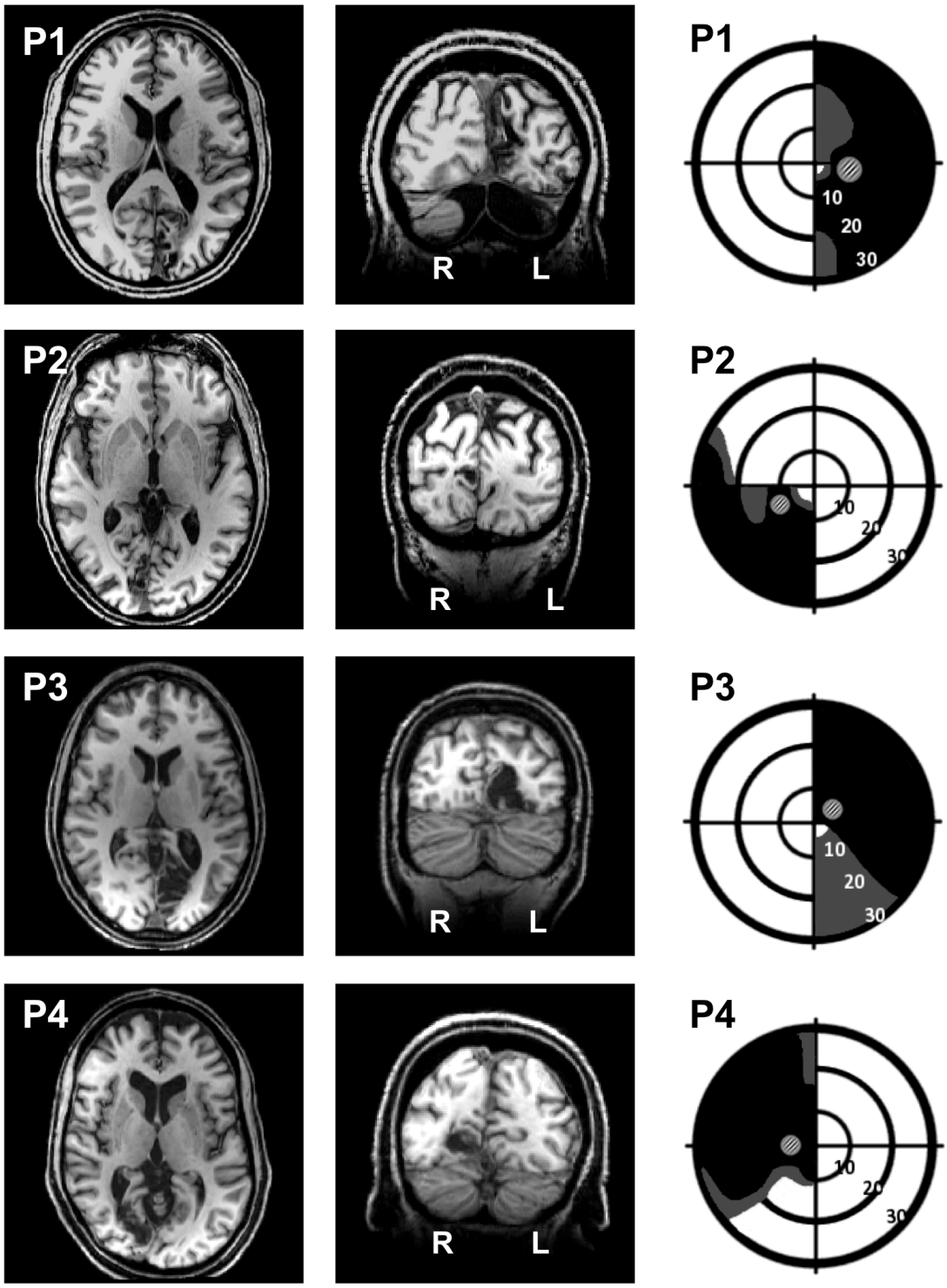

Figure 1. Patients' structural scans and visual field training/testing targets. T1 structural images of axial and coronal slices demonstrating lesion locations. Visual field deficits (right column) are adapted from 30:2 threshold Humphrey visual field perimetry reports, and show dense visual field loss in black (< 0.5%) and partial loss in grey (< 2%). Stimulus location (demonstrated by the superimposed Gabor) for training and testing was different for each patient, and was restricted to a region of dense visual field loss. Concentric rings represent increments in retinal position of 10 degrees, spanning the central 30 degrees.

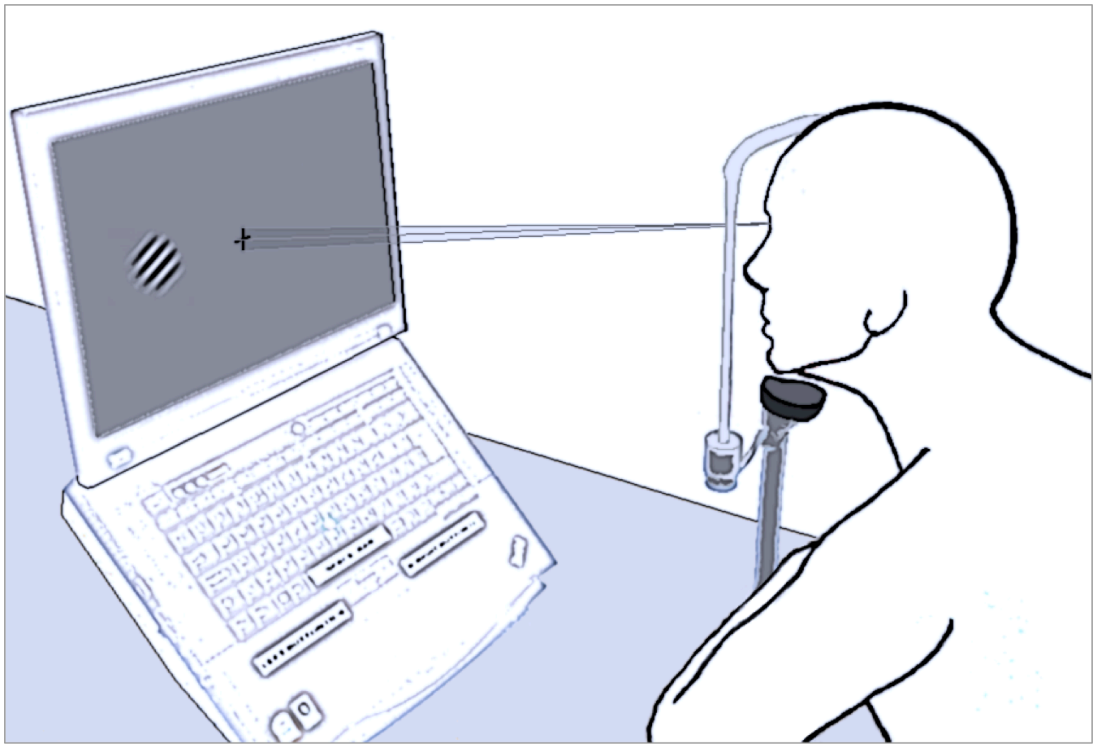

Figure 2. Diagram of the training apparatus. Participants sit with a chin rest at a distance of 40 cm from the monitor, mounted on a frame. The training task consists of a 2-AFC temporal detection task, presenting a spatially and temporally modulated Gabor patch in one of two intervals whilst the patient maintains fixation centrally. The target contrast is algorithmically controlled to maintain difficulty. Participants provide their response by pressing the left or right response buttons, and positive auditory feedback is provided if they were correct. Each training session lasts approximately 25 minutes, with a 3-min rest imposed half way through.

8.3.2.2 Training stimuli

Training stimuli consisted of achromatic Gabor patches of vertically-oriented gratings, with spatial smoothing of the boundaries. The spatial frequency was 1 c/^{o}, temporal frequency 10 Hz, and size was 6^{o} diameter. Stimuli were separately presented at three predetermined retinal eccentricities in a randomly interleaved order. One of these three locations corresponded to the deepest part of the field defect that could be targeted with the current apparatus, away from the border of the scotoma. The exact location was tailored to each individual patient's deficit (see Figure 1, right-hand column). This region would be comparatively less likely to be targeted by occasional small eye movements than more central regions, and

represented the primary target of the current rehabilitation study. This region was used as the location for all psychophysical assessments, carried out before and after the training interval. The other two regions underwent training, but were not tested.

8.3.2.3 Training procedure

The training task consisted of detection of a temporally modulated spatial grating patch using a temporal two-alternative forced-choice (2-AFC) task. Patients were required to report whether a target stimulus was presented during the first or second of two intervals. Intervals were separated by auditory cues of "one" or "two", announcing the start of each. The stimulus itself appeared on screen for 2 s. This was associated with a pre- and post-stimulus interval of 500 ms. The alternative blank interval also lasted 2 s in duration, therefore each trial lasted 6 s in total. Once both intervals had completed, the patient would hear another cue indicating "press". This informed participants that they must now provide their response by pressing either the left or right button on a response box corresponding to the first or second interval, respectively. Positive auditory feedback was provided if they were correct, via a response of "correct".

Each training session lasted approximately 25 minutes, and consisted of 50 trials at each of the three eccentricities (total 150 trials). To manipulate task difficulty, the target contrast was algorithmically modulated such that if the detection performance at any given location was at or above 84% for three consecutive sessions, the stimulus contrast was reduced by 10%. Reduction in performance to 64% and below resulted in an increase of 5% in contrast in the next training session. Therefore, the algorithm for determining the subsequent target contrasts was biased to provide a

conservative estimate of contrast detection. In the absence of improvements in detection performance, and when the detection ability is noisy, it is more likely for contrast levels to remain high than for them to be reduced. Contrasts ranged from 5 – 90% throughout the training period. Presentation of trials was self-paced. A 3-min rest was imposed after 75 trials to ensure patients did not become fatigued. It was emphasized that whilst conducting therapy sessions, patients must keep their eyes firmly on the black fixation cross. A few practice trials were conducted with the stimulus in the sighted field to ensure that patients understood the procedure.

8.3.2.4 Number of training sessions per patient

Over a three-month period, P1 completed 85 training sessions, P2 41 sessions, P3 59 sessions, and P4 36 sessions. Figure 3 provides the details of the training protocols for each participant, and their performance over time.

8.3.3 Pre- and post-training psychophysics

8.3.3.1 Stimuli

Four sets of visual stimuli were used, corresponding to the four functional imaging Chapters (3-6). These images precisely matched the stimulus parameters used in earlier Chapters, and therefore will not be described in detail here. These included: **(1) Contrast:** Drifting achromatic Gabor patches of variable luminance contrast, Chapter 3. **(2) Motion Coherence:** Apertures containing moving black dots of variable motion coherence, Chapter 4. **(3) Speed:** Apertures containing moving black dots of variable speed, Chapter 5. **(4) Face/Place:** Coloured images of human faces or outdoor scenes representing the category of 'places', Chapter 6. All stimuli were displayed on a uniform grey background.

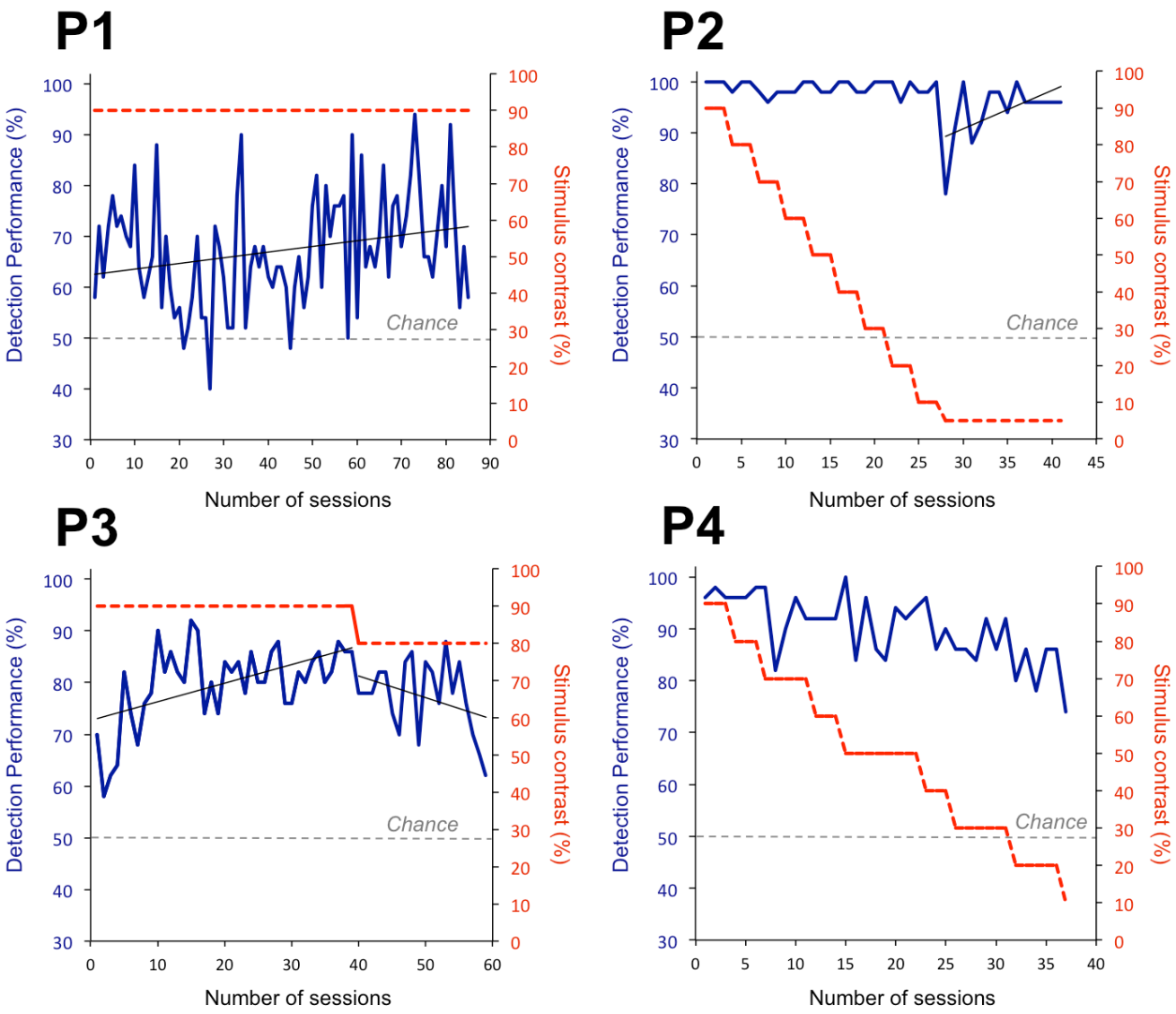

Figure 3. Adaptation of individual training parameters with performance, over the training period. Blue lines represent performance on the 2-AFC detection task throughout training (left y-axis) for each of the four patients (P1–P4). The dotted red line corresponds to stimulus contrast (right y-axis), which is reduced when performance is consistently ≥ 84%, and ranges between 95% and 5%. Superimposed on the performance curves are lines of best fit (thin black lines), calculated for any period lasting more than 10 sessions duration in which the contrast level remained constant. Chance level is at 50%, shown in grey.

8.3.3.2 Procedure

(i) 2-AFC Temporal Detection

This procedure required patients to indicate whether a stimulus appeared in the first or second time-interval. The same stimulus conditions were used for each experiment as described in Chapters 3-6. The general procedure is described in detail in the

General Methods. For Experiment 2 (Motion Coherence) each coherence level was tested once per block so that there were six trials per block. Global motion direction was horizontal. One patient did not perform Experiment 2 (P3), and another did not perform Experiment 4 (P2) due to time limitation.

(ii) 2-AFC Discrimination

For these experiments, patients had to discriminate a specific aspect of the stimulus within their blind hemifield from a choice of two. Again, identical stimulus conditions were used as in earlier Chapters (3-6), and in the General Methods. For Experiment 2 (Motion Coherence), each coherence level was tested once per block so that there were six trials per block. Global motion direction was randomly assigned as horizontal or vertical. Patients were asked to discriminate this direction at the end of each trial. After completing this, 10 additional blocks tested the equivalent sighted hemifield. One patient did not perform Experiment 4 due to time limitation (P2).

8.4 Results

Figure 3 depicts how the training parameters altered over the training period. This includes average detection scores (solid blue line) and the stimulus contrast (dotted red line) for each patient. P1 remained on the same level of contrast (90%) throughout the entire training period. Over this time, his performance varied quite considerably from session to session (see Chapter 9.2.2 for a discussion on the effect of attention on blindsight), but demonstrated a positive trend overall. P2 started around ceiling, and continued to perform well as contrast levels were reduced. Once contrast dropped to the lowest level (5%), his performance saw a steep decline, before gradually improving to approximately 95% detection over the

	P1	P2	P3	P4
1. Contrast detection	✓	✗	✓	✗
2i. Motion coherence, detection	✓	✓	n/p	ceiling
2ii. Motion coherence, discrimination	✓	✓	✗	n/p
3i. Speed, detection	✓	✓	✗	ceiling
3ii. Speed, discrimination	✗	✓	✗Ψ	✗
4i. Face/Place detection	✓	n/p	✓*	ceiling
4ii. Face/Place discrimination	✓	n/p	✓	✓

Table 1. Summary of results. Which experiments show a significant improvement after training. A tick denotes a significant improvement in that patient's performance following training, and a cross denotes no significant improvement. Ψ After training, P3 achieved an average of 65% at 20°/s, which was close to significance ($p = 0.13$). * In face/place detection, P3 showed no improvement in the detection of places ($t = 0.5$, $p = 0.6$), but did show a small but significant improvement for the detection faces after training ($t = 4.0$, $p < 0.001$). n/p = experiment not performed; ceiling = patient could perform the task at or close to 100% at baseline, before training had been started.

subsequent twelve training sessions. P3 trained at 90% contrast for almost 40 sessions before seeing a consistent improvement, enabling the contrast to be lowered to 80%. At this lower level, her 2-AFC performance remained between 62-88%, but if anything saw a slight decline before training completed at 59 sessions. P4 started close to ceiling at 90% contrast, and generally continued to perform well as the target contrast was decreased over time. She remained above 90% for at least two consecutive sessions until session 17, when the target decreased to 50% contrast. From this point onwards, performance tended to show a slight decline as difficulty continued to increase. Once the contrast reached 20%, performance remained under 90%, with an average of 81.7% over this period (sessions 31-36).

8.4.1 Psychophysical performance

A summary of performance, and the presence or absence of significant improvement for each experiment is provided in Table 1. Although not an explicit aim, P3 underwent an additional 'control' period of training that targeted a distinct region of the blind visual field. Her performance before and after training was recorded in the same (non-trained) region of visual field as described in Figure 1, therefore it was possible to consider the retino-specificity of training effects in this individual. In future studies, it would be useful to carry out similar control experiments in all patients, and to assess for a global effect of training in non-trained regions of the visual field that may indicate an effect of attention.

8.4.1.1 P1

Contrast: Performance at contrast detection at baseline was already significantly above chance for the strongest, 100% contrast stimulus. However after training P1 showed a significant improvement in detection at intermediate contrasts, so that his performance was now significantly above chance. Detection improved from 80% ± 8.0% to 96.7% ±3.9% at 50% contrast ($t = 9.4$, $p < 0.001$), and from 60% ±9.8% to 90% ±6.0% at 10% contrast ($t = 13.1$, $p < 0.001$).

Motion Coherence: Detection of moving dots in the motion coherence task was no different to chance when assessed at baseline (Figure 5, blue line). However, after training there was significant improvement across all coherence levels (pre-training detection = 49.2%, post-training = 77.5%; $t = 4.9$, $p = 0.0007$). There was, however, still no suggestion of a correlation between coherence and performance ($r = -0.01$).

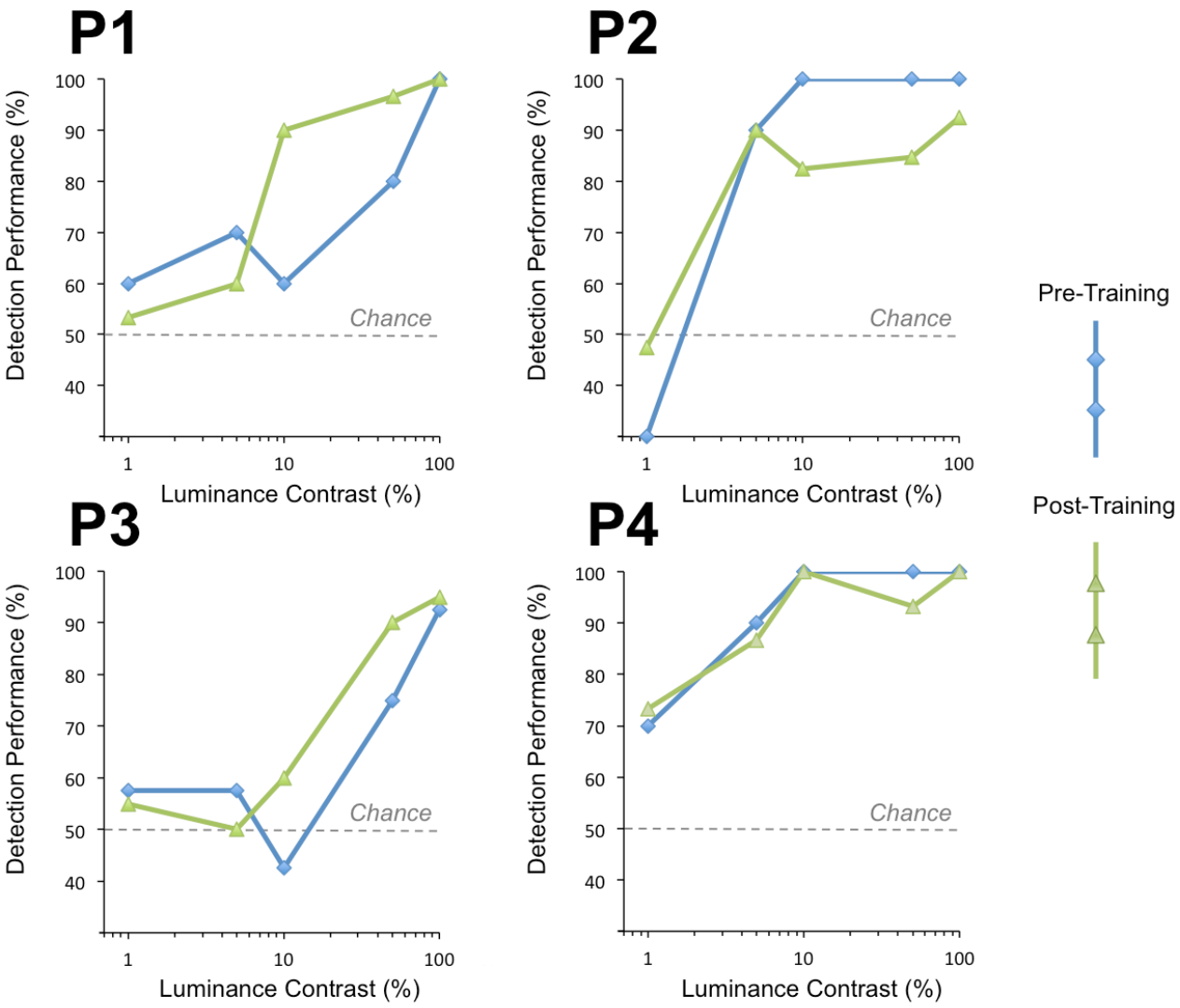

Figure 4. Pre- and post-training performance on 2-AFC contrast detection. Blue lines represent performance prior to training, and green lines show post-training measures, for each patient separately. At baseline, all four patients could detect the highest 100% contrast stimulus significantly above chance. Following training, only P1 and P3 showed significant improvments in performance, extending to 50% and to a lesser extent, 10% contrast.

Direction discrimination was also assessed (Figure 6) and also was not greater than chance at baseline. If anything, P1 appeared to show performance below chance for stimuli at 100% coherence (30% ±10.2%, p = 0.06), implying that he was able to distinguish a difference between the two conditions, but could not label them correctly. After training, his performance at 100% coherence increased to the same extent *above* chance (70% ± 10.2%, p = 0.06). Performance at all other coherence

levels remained at baseline, however his average performance across all coherence levels significantly improved in the second session (pre-training discrimination = 41.7%, post-training = 53.3%; $t = 2.3$, $p = 0.04$).

Speed: Before training, P1 was unable to detect any of the motion stimuli above chance, irrespective of speed. After training, he showed marked improvement and was now able to detect all four motion conditions significantly above chance (Figure 7, green line), but not static dots. Performance at direction discrimination, however, remained at chance both pre- and post-training (Figure 8).

Face/Place: P1 showed significant improvement in both face/place experiments. Detection increased for both stimulus categories (Figure 9, left column), pre-training places = 68.8% ±5.8% post-training places = 89.1% ±5.2% ($t = 16.7$, $p < 0.001$); pre-training faces = 59.4% ±6.2%, post-training faces = 80.0% ±7.7% ($t = 14.1$, $p < 0.001$). Discrimination also showed an improvement, as performance at baseline was no different than chance (160 trials). After training, P1 scored 56.8% across 176 trials, which was significantly greater than chance ($p = 0.04$, Figure 9, right column).

8.4.1.2 P2

Contrast: At baseline, P2 was able to significantly detect stimuli of 5% contrast and above, and this remained similar following training (Figure 4). Performance at 1% contrast was also unchanged, and remained at chance.

Motion Coherence: Detection in this paradigm showed a global improvement following training, across all coherence levels (pre-training detection = 65.0%, post-

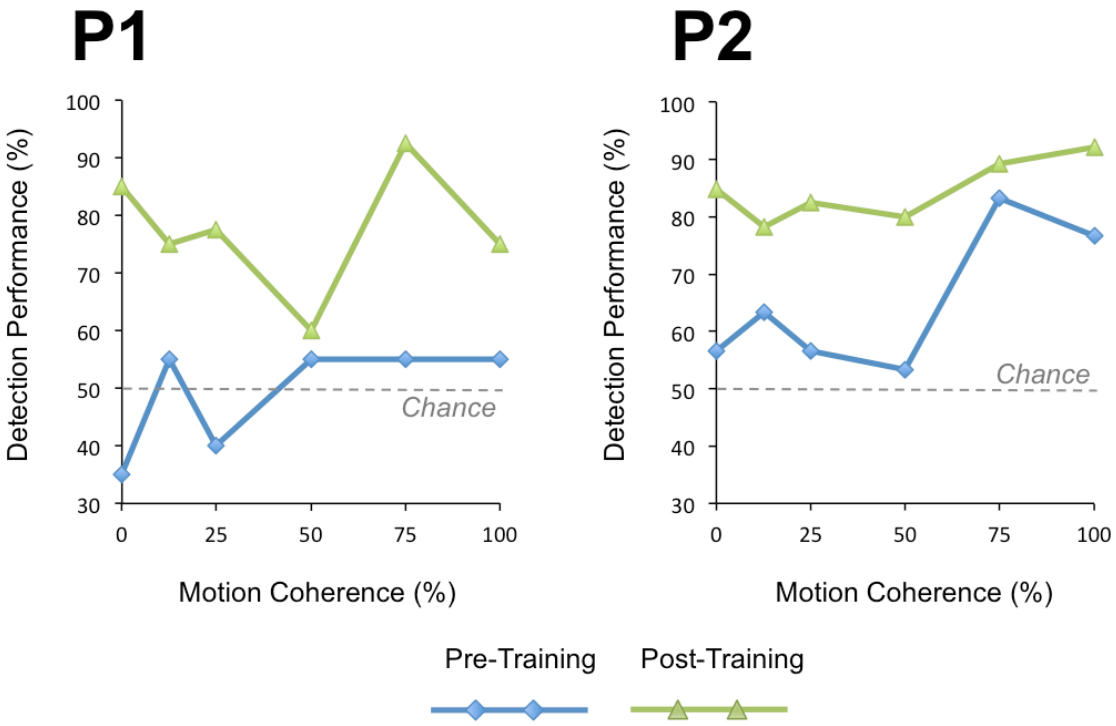

Figure 5. Pre- and post-training performance on 2-AFC detection with increasing motion coherence. Blue lines represent performance prior to training, and green lines show post-training measures, for each patient separately. After training, both P1 and P2 showed significant improvment in detection performance, averaged across all stimulus conditions. There was no significant association between detection performance and the proportion of motion coherence, although this showed a weakly positive trend in P2 ($r = 0.7$, $p = 0.09$). P3 did not complete the task, and P4 was at ceiling at baseline, therefore were not included here.

training = 84.5%; $t = 3.6$, $p = 0.005$, Figure 5). This was particularly notable for lower coherence conditions, which P2 had been unable to detect significantly above chance prior to training. Both pre- and post-training, P2 showed a similar, weak correlation between detection performance and coherence ($r = 0.7$, $p = 0.09$). In direction discrimination, performance at baseline was only significantly greater than chance at 100% coherence (70%, $p = 0.02$). However, in the session after training P2 was able to discriminate the direction of motion at the top three coherence levels (50%, 75% and 100%) significantly above chance. For the low coherence conditions (0-25%), performance was similar pre and post-training. In the sighted hemifield, direction

discrimination increased above chance at 12.5% (70%), and continued to increase at 25% (90%) before reaching ceiling at 75% coherence and above.

Speed: Before and after training, P2 showed an inverted-U pattern of detection with increasing speed, with optimal motion detection at 20°/s (Figure 7). Despite retaining this relationship after training, performance globally increased across all speeds ($t = 2.8$, $p = 0.02$). Furthermore, although this was only significant at 20°/s pre-training, post-training all conditions were detected above chance according to a statistical threshold of $p < 0.05$, including static controls. Direction discrimination showed a marked improvement after training (Figure 8). At baseline, P2 was unable to discriminate direction at any of the four speeds. Following training, performance increased significantly to over 75% at 4°/s, 8°/s and 20°/s ($p < 0.001$), whilst remaining at chance at the fastest 32°/s speed.

8.4.1.3 P3

Contrast: P3 showed a slight, but consistent improvement at contrast detection post-training at the highest three contrast levels (i.e. 10-100% contrast, see Figure 4). In particular, detection improved significantly from 75% ± 6.8% to 90.0% ±6.7% at 50% contrast ($t = 8.1$, $p < 0.001$).

Motion Coherence: P3 only performed the direction discrimination task of this experiment. On balance, there was no significant difference in performance pre and post-training (average pre-training = 50.0%, post-training = 51.7%; $t = 0.3$, $p = 0.7$, Figure 6). In both sessions, P3 was unable to discriminate the direction of motion of the moving dots above chance, at any coherence level.

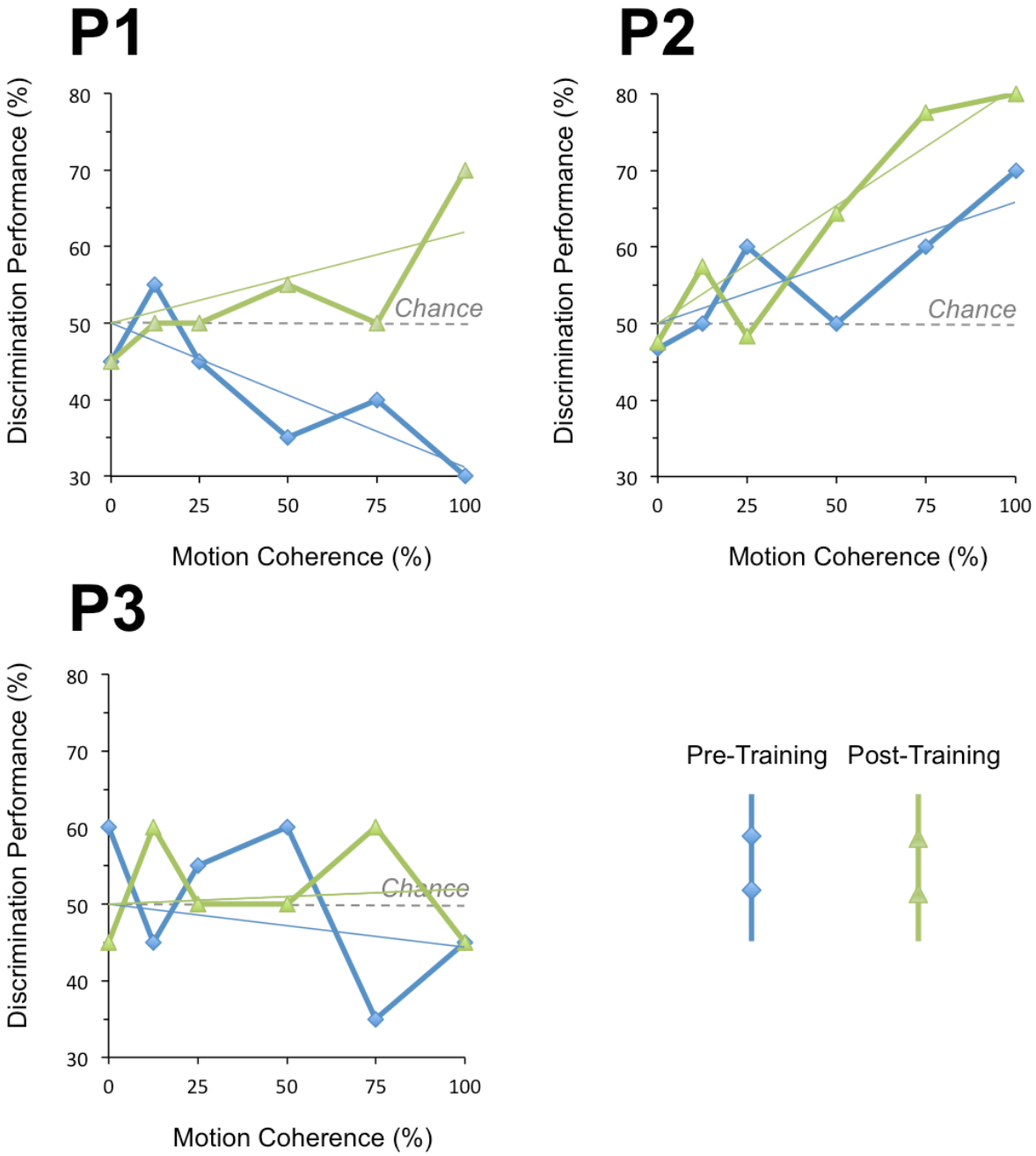

Figure 6. Pre- and post-training performance on 2-AFC direction discrimination with increasing motion coherence. Blue lines represent performance prior to training, and green lines show post-training measures, for each patient separately. After training, P1 and P2 showed significant improvement in discrimination performance at 100% coherence, and for P2 also at 50% and 75% coherence. Both of these patient showed a positive increase in the relationship between performance and coherence after training. P3 remained at chance before and after training. P4 did not complete the task, therefore was not included here.

Speed: Detection of dots in this experiment also remained at chance in both sessions, and showed no significant effect of training (average pre-training = 55.0%, post-training = 49.0%; t = 1.4, p = 0.2, Figure 7). Both performance curves demonstrated a

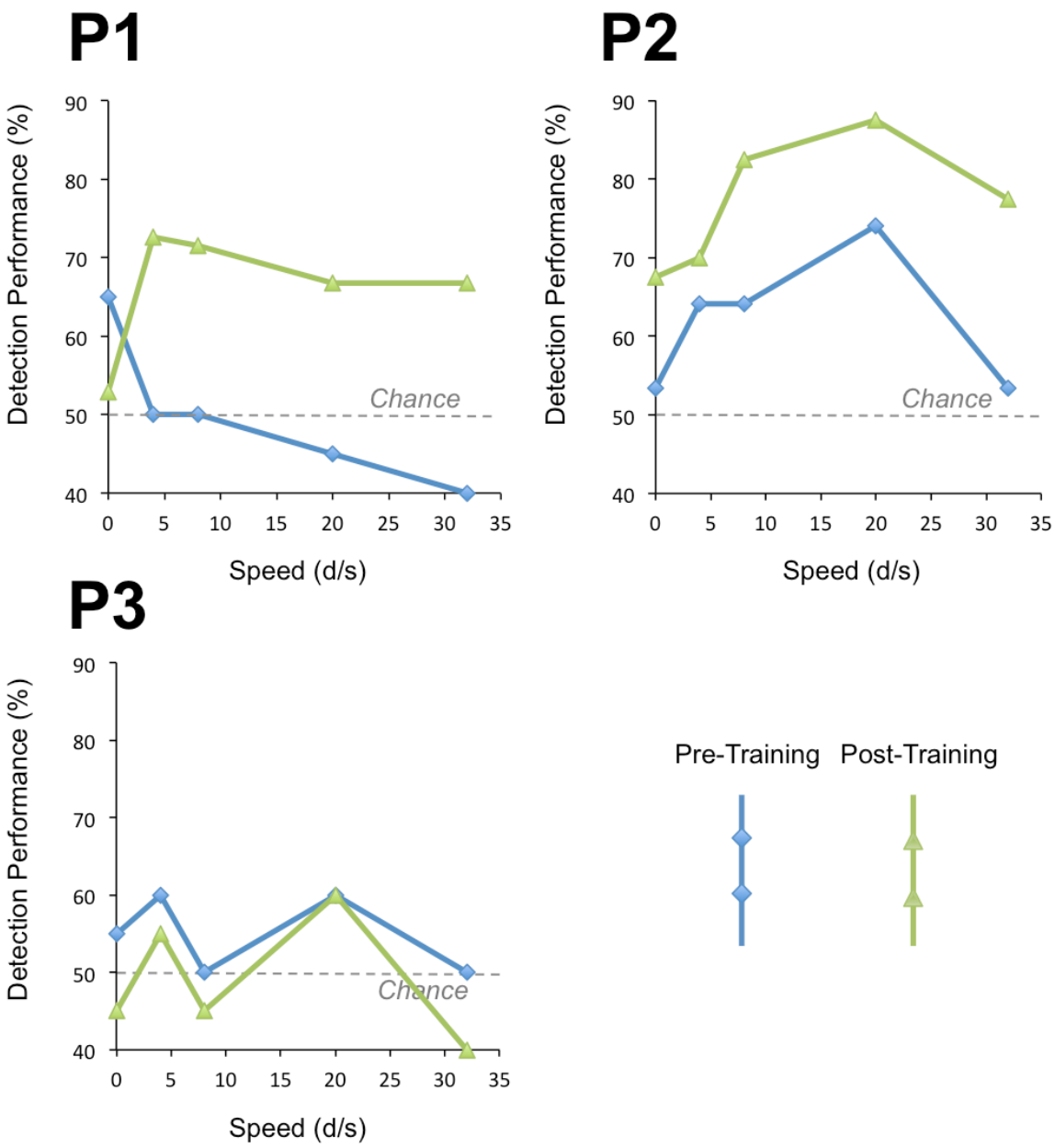

Figure 7. Pre- and post-training performance on 2-AFC detection with increasing stimulus speed. Blue lines represent performance prior to training, and green lines show post-training measures, for each patient separately. After training, P1 and P2 showed significant improvement in detection performance. For P1, this was notable for moving stimuli at all speeds (4 – 32°/s). In both cases, the pattern of performance across the different speed conditions remained similar following training. P3 remained at chance before and after training. P4 was at ceiling at baseline, therefore were not included here.

similar pattern with speed, with optimal performance at 20°/s. However none of the speeds elicited detection significantly above chance level. For direction discrimination, there was also no overall difference pre and post-training (Figure 8).

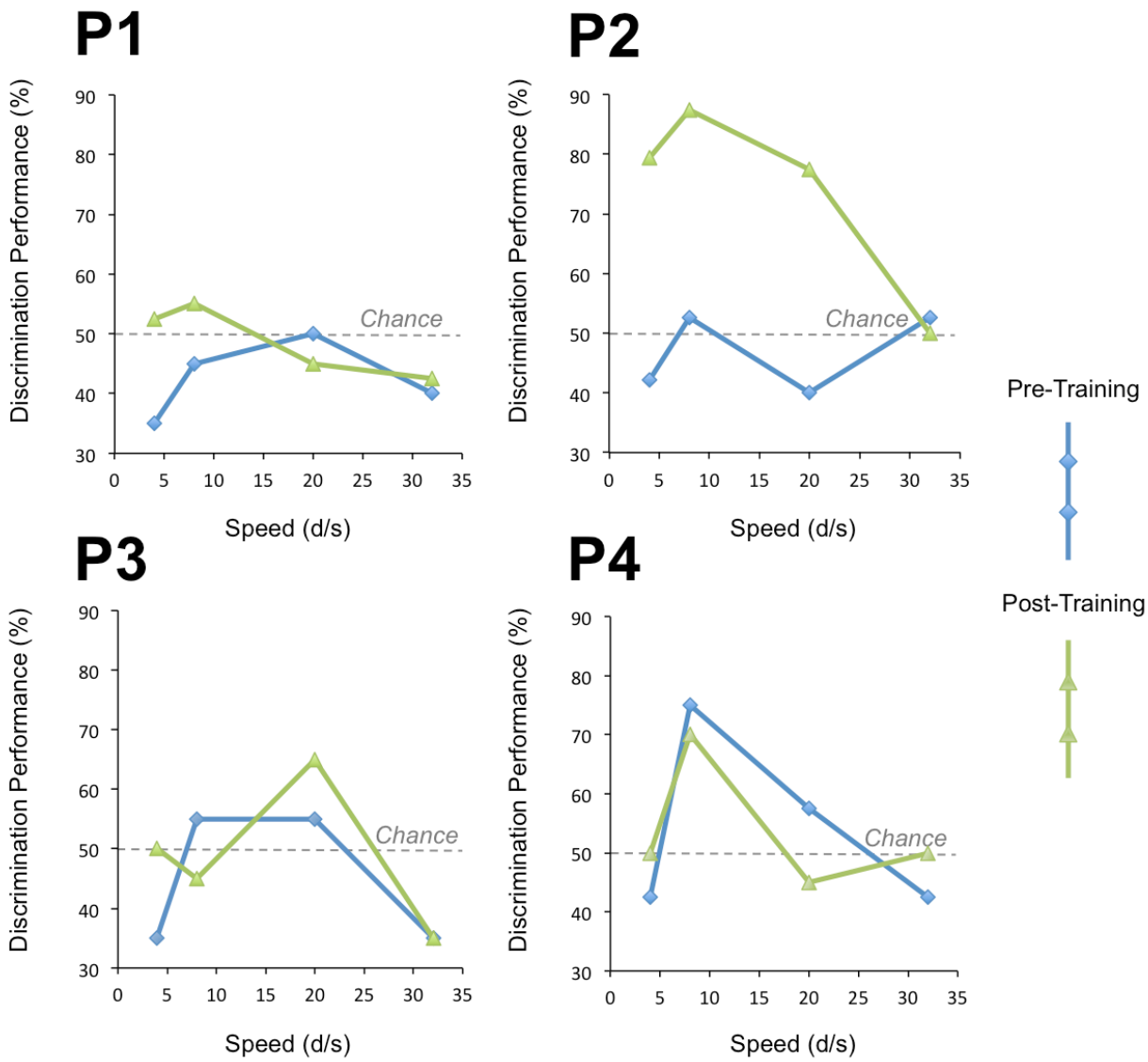

Figure 8. Pre- and post-training performance on 2-AFC direction discrimination with increasing stimulus speed. Blue lines represent performance prior to training, and green lines show post-training measures, for each patient separately. After training, only P2 demonstrated a significant improvement in discrimination performance. This was marked for motion of 4-20°/s speeds, but not with the fastest 32°/s condition. P3 showed a weak improvement for discrimination at 20°/s, although this was not quite significant. P4 showed significant direction discrimination at 8°/s both before and after training, which remained unchanged. P1 was at chance before and after training.

However at 20°/s, P3 achieved an average score of 65%, which was close to significance ($p = 0.13$).

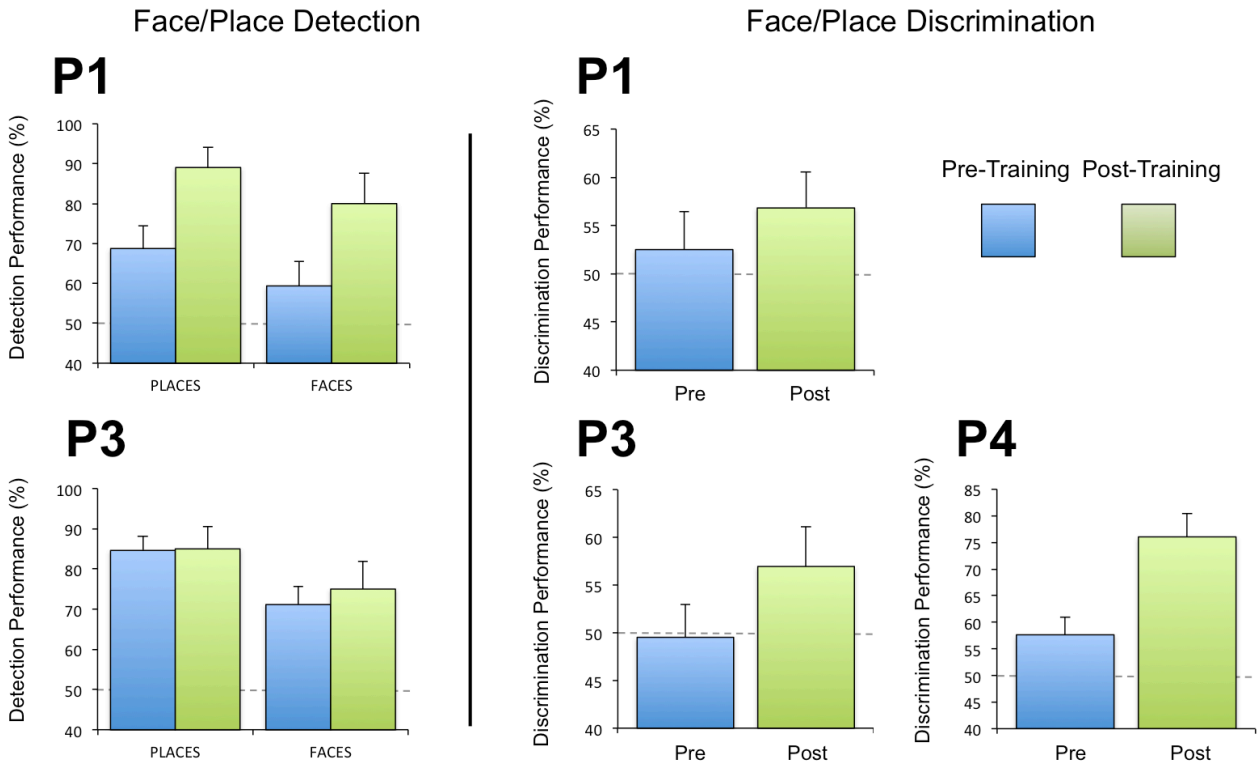

Figure 9. Pre- and post-training performance on 2-AFC detection (left) and 2-AFC category discrimination of faces and places. Blue bars represent performance prior to training, and green bars show post-training measures, shown for each patient separately. Error bars represent the standard deviation for each patient's performance. **(A) Face/Place 2-AFC detection.** After training, both P1 and P3 showed significant improvement in the detection of faces and places. This was particular robust in P1, whilst P3 only showed a significant improvement for the detection of faces. P2 did not complete the task, and P4 was at ceiling at baseline, therefore were not included. **(B) Face/Place 2-AFC discrimination.** Interestingly, all three patients showed a significant improvement in the discrimination of faces and places after training. For P1 and P3, performance had been at (or very close to chance) at baseline, but both participants could perform the task significantly above chance after rehabilitation. P2 did not complete the task, therefore was not included.

Face/Place: At baseline, P3 was able to significantly detect both stimulus categories above chance, with slightly stronger performance for places. Following training, P3 showed no difference in the detection of places ($t = 0.5$, $p = 0.6$), but demonstrated a small but significant improvement for faces ($t = 4.0$, $p < 0.001$, see Figure 9, left column). A significant improvement was also seen in the discrimination of stimulus category, for which P3 was at chance before training (49.5% ±3.5%, $p = 0.6$). After training, P3 scored an average of 56.9%, which was now significantly greater than

chance (p = 0.05), and was significantly greater than performance at baseline (t = 16.6, p < 0.001).

8.4.1.4 P4

Contrast: This patient, similar to P2, already showed very strong performance for stimuli of 5% contrast and above, which remained similar following training (Figure 4). At 1% contrast, although performance tended towards significance in both sessions, this was not quite the case across the 10 and 15 trials carried out (pre-training 70%, p = 0.17; post-training 73.3%, p = 0.06).

Speed: This patient was at ceiling for detection of both static and moving dots pre-training, therefore the task was excluded from rehabilitation assessments. Direction discrimination, however, proved considerably more difficult. At baseline, P4 was only able to discriminate the direction of motion at a speed of 8^{o}/s (Figure 8, 75% p = 0.001). After training, this pattern was maintained with optimal performance at 8^{o}/s (70%, p = 0. 04), however no improvement was seen after training (t = 0.1, p = 0.95 across all conditions).

Face/Place: P4 was also at ceiling for baseline detection in this experiment. Mean discrimination at baseline was 57.6% ±3.3%, which was significantly greater than chance (p = 0.01, 229 trials). After rehabilitation, discrimination showed a notable improvement to 76% ± 4.4% overall (t = 41.3, p < 0.001, see Figure 9).

8.5 Discussion

All four patients demonstrated an improvement in at least one measure of psychophysical performance following rehabilitation. In particular, improvements were not restricted to motion detection, which had been the target of the training paradigm. These results suggest that a period of training targeting the damaged hemifield can improve certain aspects of residual vision. Furthermore, the effects may be transferable across stimulus domains that were not specifically targeted during training. Although these improvements were not dramatic and none of the patients completely recovered their vision, this study highlights the potential in targeting blindsight, or residual vision in the rehabilitation of this condition. This work also provides a strong basis for future neuroimaging studies to investigate the mechanisms underlying these changes.

8.5.1 Training effects are transferable across stimulus domains

Two very different motion stimuli were used in psychophysics assessments, only one of which was similar to the target stimulus used in training. Throughout rehabilitation, patients were trained with a 6-degree vertically-oriented drifting Gabor (1 c/^{o}, 10 Hz). This was very similar to the stimulus in contrast experiments, which was 5 or 8^{o} in diameter, 1.3 c/^{o} and 10Hz, drifting at either 45^{o} or 135^{o} relative to the vertical meridian. 2-AFC assessments of contrast detection showed a significant improvement in contrast sensitivity in 2/4 patients. This is similar to previous studies, which have also demonstrated improvements in contrast detection following training with Gabor targets (Sahraie et al., 2006; 2010; 2013). However, the question

of whether these effects are transferable to other stimulus features remains a subject of much interest and debate.

Improvements with perceptual learning in healthy participants are often specific to the features of the stimuli used for training, such as orientation, or spatial frequency (Fiorentini and Berardi, 1980). This has led to speculation that early retinotopic visual cortical areas must be crucially involved in their mediation (Gilbert et al., 2001). Nevertheless, transfer to untrained stimulus features has been reported, and has been shown to vary according to test conditions such as task difficulty (Ahissar and Hochstein, 1997; Liu, 1999). Furthermore, it is possible to train non-human primates to discriminate novel visual stimuli, associated with selective responses in higher-level infero-temporal cortex neurons (DiCarlo and Maunsell, 2000; Jagadeesh et al., 2001). Similarly, higher cortical areas are suggested to show a greater transfer of learning effects, associated with their underlying receptive field properties (Hochstein and Ahissar, 2002). It is possible that extends to perceptual learning in the absence of V1.

In the current study, 2/3 patients (P1, P2) improved in the detection of complex motion in the motion coherence and speed paradigms. Of these patients, one was completely at chance pre-training, thus regaining an ability that he did not demonstrate previously. Essentially these two experiments used the same visual stimulus, an aperture containing multiple low luminance, moving dots. The two patients also improved in direction discrimination of the same stimuli. This was restricted to the coherence experiment in P1, however this may simply have reflected the optimal speed used in that paradigm (5^{o}/s). Consequently, at least two patients

demonstrated significant improvement with motion stimuli and parameters (direction sensitivity) that had not been targeted by training.

Huxlin et al. (2009) have also looked into the transfer of learning across motion stimuli and task conditions, and have reported the reverse of the findings presented here, i.e. they showed that training of global direction discrimination with random dot kinetograms could transfer to contrast sensitivity with drifting gratings. They used perceptual learning to train patients to discriminate global direction of moving dots via a staircase learning procedure. After several thousand trials, patients improved direction discrimination thresholds. Additionally, whilst not specifically trained for, patients also showed an improvement in contrast thresholds, measured using drifting sine-wave gratings. Therefore both studies support the transfer of training from one motion stimulus (in their case complex motion) to another. One possible explanation, which would be consistent with the above literature, is that higher-level visual areas may underlie these learning effects and neuroimaging studies may help to determine this.

Outside the motion domain, some surprising results emerged using stimuli typically associated with the ventral visual stream. Both the detection and discrimination of faces and places in the blind field showed significant improvement in all patients tested following training (3/3). In fact, this was arguably the most consistent of all psychophysical results reported. Perhaps, at least in part, this reflects the large number of trials employed in these experiments. Nevertheless, it puts into question what regions may be involved in training-effects, and has important implications on the extent of recovery that may be possible after V1 damage. These findings also

appear to be consistent with another recent, surprising result. Das et al. (2014) reported that patients were able to learn orientation discrimination of non-flickering, non-moving Gabors with slow (250 ms) onsets and offsets in their blind fields. The absence of any significant motion component in their training paradigm suggests that motion-sensitive pathways were not primarily recruited. Instead, the authors suggest that learning may have relied on direct inputs from the dorsal LGN to V2, V3, and/or V4 (Cowey et al., 1989; Hendry and Reid, 2000; Schmid et al., 2010), cortical areas that are rich in orientation-selective units. Perhaps such regions could also be recruited in motion training paradigms, thus conveying the improvement on face/place processing reported here.

To date, the focus on visual field restitution has been on visual motion pathways. However, face and place images are an enormous component of everyday visual experience, and are emotionally highly salient. If ventral or non-motion visual pathways could be targeted by rehabilitation (Chapter 6), this may prove to be a very useful addition to current training regimes. This leads to another important point to consider, which is the perception that patients have of training effects, and whether results such as these confer any real-world difference. Researchers have started to look into this, employing questionnaires to assess quality of life or independence (e.g. Nelles et al., 2001; Raninen et al., 2007). Sahraie et al., (2006, 2013) have also looked into how awareness changes after training, and suggest that a continuum between detection and awareness may exist for stimuli in the blind field. Of the four patients recruited here, none reported any marked subjective improvement in their vision after training was complete. P1 did, however, think that he could now perceive moving cars in his damaged visual field, which he could not prior to training. P2 also

reported that whilst he did not feel his vision had improved and was still unable to drive, he had gained enormously from engaging with the therapy. Unfortunately the research into visual field rehabilitation is still in its early stages, as the extent and mechanism for recovery continue to remain unclear. It is likely that both subjective and objective measures will be helpful in guiding the research forward. Ultimately the goal is for patients to see an improvement in their conscious vision, even if the quality remains somewhat degraded compared to normal.

8.5.2 Retinotopic-specificity of training may not transfer to other regions of the visual field

One criticism of perceptual learning, particularly relevant to visual field restitution after V1 damage, is that training effects appear to be specific to the targeted region of visual field. Both Huxlin and Sahraie have suggested that psychophysical improvements appear to be retinotopically restricted to trained field locations (Huxlin and Pasternak, 2004; Sahraie et al., 2013). In the current study, although not specifically examined, this finding was corroborated through the results of one patient who underwent an additional period of training targeting a separate portion of the visual field. P3 initially underwent training in the lower visual field for 61 sessions, whilst psychophysical testing pre-and post-training was restricted to the right upper quadrant. Following this training period she showed no improvement in any of the tested domains, even though (as presented here) the subsequent period of training to her upper visual field (59 sessions) elicited a number of improvements to that region. The initial negative result, as shall be discussed, suggests that the training effect was not attentional. This case, however, adds to the literature suggesting that

retino-specificity is a feature of this type of rehabilitation. A related point is that blindsight function itself may be isolated to discrete, albeit large portions of the damaged visual field (Kentridge et al., 1997). Taken together, this implies that an element of retinotopic hard-wiring may underlie residual vision and its pathways. Perhaps where damage is not in V1, but restricted to the optic radiations, a change to the retinotopic organisation of residual pathways may be possible over time (Dilks et al., 2007). However this kind of reorganisation is yet to be established when V1 is damaged. A more pragmatic approach may therefore be to engage in a training paradigm that sweeps through the visual field.

8.5.3 Attention is unlikely to explain the results

Selective attention is an important factor in blindsight performance, which tends to decline if stimulus onset is uncertain, and improves with appropriate spatial or temporal cues (Cowey and Stoerig 2004; Kentridge et al. 1999a; Kentridge et al. 1999b). In rehabilitation, repetitive training of the blind field may increase the likelihood that a patient will attend to that region of their damaged field (Chokron et al., 2008). This is widely recognized to be important, but has rarely been assessed specifically in rehabilitation studies. One example of such a comparison is Lane et al., (2010) who compared an exploratory training paradigm to attentional training in assessments of eye movement rehabilitation, an alternate approach to visual field restoration (VRT) in hemianopia. Although their findings remained inconclusive, the work reinforces that a 'placebo-controlled' approach can help to address and quantify the contribution of attention on training effects. As well as attention, it has been suggested that simple improvements in test strategies, such as the cue a patient uses

to give their response, may evolve with training completely independent of an improvement in their underlying vision.

In fact, there are a number of features in the current data that suggest that attention or strategy-training cannot solely account for the improvements here. For instance if this were the case, one might expect to have seen global improvements in psychophysical performance across experiments, as a generic effect of attention. Similarly, one might expect improvements to be restricted to detection paradigms, if for example patients had adopted a strategy that even the slightest flicker in their blind field must indicate a stimulus. This was not the case in both regards, as performance did not alter globally but remained unchanged in certain domains. Patients also showed improvements in discrimination, such as discriminating faces from places, which improved in all three patients tested. Another important point is that one patient in the study (P3) effectively acted as their own control by undergoing a separate period of rehabilitation to another, nearby part of the visual field. This initial 'control' training period conferred no improvement in psychophysical tests, whilst the subsequent test period did, suggesting that the results could not be attributed to a global improvement in attention to the blind field. Consequently, although attention is likely to be important and has even been suggested to facilitate recovery (Sahraie et al., 2010), it is unlikely to account for all the results here.

8.5.4 Focussed training paradigms (on low-contrast targets) could benefit certain patients

Patients P1 and P3 showed significant improvement in contrast sensitivity after

training. Of note, neither patient had been at, or close to ceiling in their baseline performance. Nevertheless, both patients could detect a drifting Gabor at 100% contrast in their blind hemifield, thus demonstrating at least some residual visual capacity prior to training. In comparison, P2 and P4 both showed relatively high contrast sensitivity at baseline, and yet neither patient saw any significant improvement in this measure after training. One possible explanation for this lack of effect in P2 and P4 comes from the training paradigm. There are two fundamental criticisms of the current approach that have been highlighted from this study: (1) The training protocol takes an extremely long time to adapt to patients with high baseline sensitivity. (2) The minimum level of contrast used in training is 5%. As seen in Figure 3, it took P2 and P4 over 25 sessions to reach a target level of contrast close to their threshold. This is because patients must achieve at least 84% in three consecutive sessions, before the contrast is reduced by 10% in the following session. Furthermore, P2 in particular was never trained below 5% contrast, even though he was already able to detect this stimulus at 80-90% at baseline. Although not quite at ceiling, his performance was very close to it, and he would not have been particularly challenged using stimuli at this contrast level.

The training procedure in the current study was therefore, arguably, quite generic, as it followed a specific protocol in relation to contrast and performance targets. Employing this kind of paradigm has both positive and negative features. In support, it offers simplicity and comparability across individuals, and lends itself to scaling-up the therapy to considerably larger, multi-centre translational studies. Conversely, a 'one-size-fits-all' approach potentially wastes valuable training sessions with non-challenging stimuli, and may never reach a useful level of training in certain

individuals. That is not to say that P2 did not benefit from the current training paradigm, as he demonstrated a number of improvements reported here. However, there could have been a more dramatic effect had the training been tailored to his deficit and residual visual function.

8.5.5 What are the neuroplastic mechanisms that may underlie training-related changes?

In the early years of blindsight research, individuals such as GY were recruited to take part in a vast number of studies. The early onset of his brain damage (7 years) led many researchers to question whether his residual vision and apparent neuroplasticity was translatable to patients with damage later in life. It is certainly possible that cases such as GY exhibit unique features relating to their relatively young age of onset (Bridge et al., 2008), and may show more extensive reorganization following damage (Payne et al., 1996). Nevertheless, a considerable body of work now comes from patients who have suffered their lesion in adulthood (Sahraie et al., 2003; 2006; 2008; 2013, Huxlin et al., 2009; Nelles et al., 2002; Morland et al., 2004; deGelder et al., 2008; Bridge et al., 2010; Henriksson et al., 2007; Raemakers et al., 2011). This data strongly supports a capacity not only for residual visual processing, but also for perceptual learning that is still preserved during adulthood, and can be targeted in cortical blindness acquired late in life.

Very few neuroimaging studies have investigated the neural changes associated with visual rehabilitation. Stoerig described one patient with striate cortex damage at 58 years, who developed ipsilesional ventral visual cortex fMRI activity in response to

coloured images simply after taking part in numerous research studies over a 9-month period (see Stoerig, 2008). In contrast, Henriksson et al. (2007) implicated the contralesional hemisphere in the effects of training. They employed fMRI and MEG following training with a challenging detection task of flickering discs and recognition of flickering letters twice a week over 2 years in an adult-onset stroke patient with V1 damage. They found that after training, stimulation of the blind hemifield with a large reversing checkerboard activated contralesional (ipsilateral) regions of visual cortex, including hMT+, V3a, and to a lesser extent V3, dorsal V2, and a border region between V1 and V2d. Although fMRI had not been measured pre-training, MEG had shown no initial response. This implicates interhemispheric connections in training, and suggests that ipsilateral neurons either gained a second receptive field, or perhaps a subpopulation of neurons in a voxel shifted their receptive field to the ipsilateral hemifield. In fact, this result was inconsistent with a later study (Raemakers et al., 2011), performing fMRI retinotopy pre- and post-VRT in patients with post-chiasmal damage. They found no evidence for a second representation in the intact hemisphere after training. Instead, they could only find small changes in early visual cortex receptive fields, primarily in the damaged hemisphere, which could not account for the larger visual field improvements seen in some of their patients. The mechanism behind those larger-field changes remained unanswered.

Overall the evidence so far is therefore mixed, nevertheless there is growing support for some sort of plasticity-driven process employing either ipsi- or intact contralateral visual cortex. Currently, we must look to chronic fMRI and DTI imaging studies to suggest where such neuroplasticity may arise (e.g. Goebel et al., 2001; Bridge et al., 2008). Further well-controlled training studies using neuroimaging will

be necessary to try to understand the underlying mechanisms further, and perhaps help to refine and improve current treatment strategies.

8.5.6 Conclusions

This work has shown that patients with adult-onset visual field loss and V1 damage can show a number of improvements in their residual vision following a period of targeted training. In particular, these effects of training transferred not only to other motion parameters, but to the discrimination and detection of static images classically associated with the ventral visual stream. There is still considerable progress to make before patients can be offered anything close to a full recovery. At the centre of this, we still do not understand the mechanisms underlying neuroplasticity, nor the potential for recovery. Intriguingly, however, the findings here go against an exclusive role for motion-sensitive pathways in training-effects. Instead, residual early visual cortex may also play an important part in training, and may facilitate the transfer of learning across modalities. Research will be needed to build on this by measuring the neural changes associated with such training paradigms. Future work points to rehabilitation strategies that target multiple visual streams and parameters, as well as tailoring the rehabilitation to patients' residual visual capacity.

Chapter 9

General Discussion

9.1 The visual pathways underlying blindsight

9.1.1 Motion response in hMT+

All of the functional imaging experiments investigating motion processing in the blind hemifield demonstrated significant contralateral hMT+ activity. This occurred in response to a high contrast drifting Gabor (Chapter 3), as well as to low-luminance complex motion using a random dot kinetogram (Chapters 4 and 5). In each experiment, ipsilesional hMT+ activity tended to be isolated, with no additional region of extrastriate or occipital cortex activity, in either hemisphere. Furthermore, this cluster of activity was slightly weaker and showed a reduced spatial extent in comparison to hMT+ responses for the sighted hemifield, or in healthy controls.

This altered pattern of activity is consistent with neurophysiological recordings of MT neuronal responses after striate cortex removal or cooling in non-human primates. Direction-selective responses are maintained in approximately 75% of neurons (Rodman et al., 1989; Girard et al., 1992), which includes long-standing cases of unilateral V1 ablation sustained in adulthood (Azzopardi et al., 2003). The proportion

alone could account for the reduction in spatial extent, and perhaps also the weaker z-statistic in hMT+ fMRI responses found here in patients. However, in addition to this, the strength and selectivity of neuronal responses are also frequently decreased. In Rodman et al., only 5% of neurons gave responses classified as 'strong', compared to over 90% in normal controls. In Girard et al. (1992) this was slightly greater. It would therefore be expected that any measure reflecting an average of neuronal responses would show a reduction in activity compared to normal.

In human neuroimaging experiments, this is certainly not the first time to see significant contralateral hMT+ activity after V1 damage. A range of neuroimaging modalities have been used, in particular with patient GY, to demonstrate similar ipsilesional hMT+ responses during presentation of motion in the blind hemifield (Barbur et al., 1993; Holliday et al., 1997; Zeki and ffytche, 1998; Goebel et al., 2001; Schoenfeld et al., 2002) or activation isolated to the lateral portion of the occipital cortex (Morland et al., 2004). The current work, however, found no significant ipsilateral hMT+ responses in the undamaged hemisphere. It is not uncommon to see additional ipsilateral hMT+ activity in healthy controls, perhaps equating to MST, although this tends to be weaker than contralateral hMT+ activity (Tootell et al., 1988). This difference in patients may reflect the relatively weak activation during blind field responses. If ipsilateral hMT+ is weaker still (as in controls), this may not be sufficient to reach significance.

The relative importance of the ipsilesional hemisphere is also emphasised from two patients with blindsight and bilateral V1 damage, one of whom also demonstrates significant hMT+ activity (Bridge et al., 2010; de Gelder et al., 2008). This suggests

that responses from the undamaged hemisphere cannot underlie all residual function in this area. Furthermore, ipsilateral geniculo-extrastriate tracts are demonstrable using DTI and show normal measures of white matter integrity, whilst the corpus callosum is degenerated.

Isolated hMT+ activation in the undamaged hemisphere has been reported in the past, and interpreted as a possible indication of plasticity despite being considerably less common. One such study assessed a group of stroke patients with hemianopia, and reported bilateral extrastriate activity, stronger on the ipsilateral (contralesional) side (Nelles et al., 2002, 2007). However these results are somewhat questionable given the absence of fixation or eye position monitoring during scanning. Furthermore, the ipsilateral activity reported as 'extrastriate' cortex in fact appears to correspond to V1, thus is strongly suggestive of eye movements rather than anything else (MNI: 12, -90, 0, *Fig.3. page 37*, Nelles et al., 2007). More consistent is the suggestion of increased interhemispheric connectivity in certain patients with early onset V1 damage (Leh et al., 2006; Bridge et al., 2008). However, this structural change is not necessarily associated with the presence or predominance of functional activity in the intact hemisphere (Leh et al., 2010; Barbur et al., 1993; Holliday et al., 1997; Baseler et al., 1999).

9.1.2 Physiological properties of non-striate input to hMT+

This work has confirmed the involvement of contralateral hMT+ in residual visual responses of patients with V1 damage. The experiments employed here, however, went beyond simply the presence or absence of fMRI activity. Instead, a parametric

approach was employed to understand the neurophysiological properties underlying voxel responses. Each experiment contributed a different aspect to this, and the results are consistent with the diffusion tractography measures.

In Chapters 3 and 4, hMT+ responses to contrast and motion coherence were very different to normal. This strongly implies that both of these 'classical' responses are critically dependent on V1. The pattern of residual responses also provides clues about the nature of non-striate pathways underlying this activity. For contrast, an unusual linear relationship with signal change in hMT+ of patients makes it extremely unlikely that residual vision is mediated via the magnocellular channel, which shows very high contrast sensitivity and a saturation at low contrast levels. With motion coherence, it can be inferred that the non-striate input to hMT+ possesses relatively sparse receptive field summation, since hMT+ responses in patients were similar to healthy V1. Non-striate input to the extrastriate cortex is historically ignored in neuronal models of visual cortex connectivity. However, the results in Chapter 4 suggest that such input is likely to occur and perhaps even contribute to normal hMT+ responses.

Chapter 5, conversely, suggests that normal hMT+ responses to speed can still be possible in the absence of V1. The origins of characteristic hMT+ speed preferences are even less clear, and have been the source of much investigation (Zeki and fftyche, 1998; Chawla et al., 1998; 1999; Priebe et al., 2006). Work here suggests that either way, normal speed responses are not dependent on V1 input. Instead, responses are either intrinsic, or mediated via non-striate input such as connections with the LGN, or pulvinar and superior colliculus. A difference in responses between blindsight

positive and negative patients strongly suggests that the subcortical input may be critical.

9.1.3 Subcortical anatomical connections with hMT+

9.1.3.1 Direct geniculate connections

The fMRI and psychophysics results from Chapters 3 and 5 both implicate ipsilesional LGN in responses to blind hemifield stimulation in patients with blindsight. Furthermore, the results from Chapter 4 suggest that non-striate inputs to hMT+ are present and contribute to normal hMT+ responses in healthy controls. The DTI investigation of 17 patients with V1 damage (Chapter 7), 12 of whom demonstrate significant blindsight performance supports each of these findings. Of the three critical pathways under investigation, only the direct ipsilateral connection between the LGN and hMT+ was consistent and intact in all blindsight positive patients. Similarly, no blindsight negative patients showed intact connections or normal integrity in this pathway. Finally, this tract was identified in both hemispheres of all control participants, supporting its existence in the normal visual system.

Neuroanatomical studies have lent increasing support for the presence of a direct connection between the LGN and extrastriate cortex (Benevento and Yoshida, 1981; Cowey and Stoerig, 1989), which is suggested to be critical for blindsight function (Schmid et al., 2010). Connections include specific projections to MT (Fries, 1981), with half of labelled LGN neurons located in, or close to, the interlaminar layers. Immunostaining for CaMK2 identifies a strong K presence in such MT projections, leading to the suggestion that it is the K-channel that may be important in blindsight

(Sincich, 2004; Rodman, 2001). The K-channel carries chromatic short-wavelength signals to V1, however there is increasing evidence that it has a more heterogeneous role in vision, perhaps associated with distinct neural pathways to V1 and MT (Shostak et al., 2002; Szmajda et al., 2008; Warner et al., 2010). For example, around 70,000 intercalated K-neurons do not project to MT (Sincich, 2004), but could include recipients of S-cone signals projecting to V1 (Jayakumar et al., 2013). Contrast responses in the K-channel also appear to be heterogeneous, with a range of contrast sensitivities, more comparable to the P-channel (C_{50} 10-60%), while spatial and temporal frequency preferences are similar to M-cells (Xu et al., 2001), particularly in koniocellular populations that are not driven by blue-on signals.

Unfortunately, it is not yet possible to differentiate between the three geniculate channels using diffusion weighted imaging and tractography. Such distinctions can only be inferred from behavioural and fMRI experiments. Beyond discounting the M-channel, a clear distinction between the parvo or koniocellular channels is more difficult to make. This is particularly challenging given the paucity of physiological data on normal neuronal responses. Anatomical studies in non-human primates implicate the K-channel in geniculo-extrastriate connections, supported by reports that parvocellular LGN neurons undergo preferential retrograde degeneration following V1 damage (Rodman et al., 2001; Cowey and Stoerig, 1989). The current behavioural, fMRI and DTI data would be consistent with this route in blindsight positive patients.

9.1.3.2 Alternate pathways to hMT+

The pulvinar and superior colliculus are also implicated in blindsight and non-striate

pathways to hMT+. The inferior pulvinar in particular receives retinal input from both V1 and the superficial layers of the superior colliculus and, like the LGN, is suggested to possess a direct reciprocal connection with MT (Benevento and Standage, 1983; Ungerleider et al., 1984; Adams et al., 2000; Lyon et al., 2010; Warner et al., 2010). The pulvinar normally plays a role in controlling eye movements, and the modulation of attention suggesting it may act as a gateway for incoming information to the cortex (Ungerleider and Christensen, 1977, 1979; Robinson and Petersen, 1992; Snow et al., 2009).

Neurophysiological responses in the inferior pulvinar typically show little or no modulation with stimulus contrast (Bender, 1982), and pulvinar lesions spare normal contrast sensitivity. This would not be consistent with the results in Chapter 3. Superior colliculus neurons are also weakly modulated by contrast with high sensitivity to low contrast levels (Schneider and Kastner, 2005), which is also inconsistent with these results.

Inferior pulvinar neurons possess a range of speed-sensitivities, mostly preferring slower motion under 32°/s (Bender, 1982; Van Essen, 1985). This is not dissimilar to V1 responses, and could be consistent with the slower, V1-like preference found in hMT+ of blindsight negative patients. However, it is suggested that those responses may arise from striate cortex inputs and thus could not account for results after V1 damage (Bender, 1983). Most pulvinar neurons do not possess direction-selectivity, although this is clearly demonstrable in a proportion of cells – perhaps driven by V1 input (Bender, 1982; Rodman et al., 1989). In the superior colliculus, which provides alternate retinal input to the pulvinar, speed preferences are massively varied,

extending to several hundred°/s (Marrocco and Li, 1977; Sterling 1969). This makes it extremely difficult to infer whether a collicular-pulvinar pathway could account for the pattern of fMRI responses in patients.

After striate cortex removal, pulvinar and superior colliculus neurons can retain their response to visual stimulation, although this is considerably weaker and is present in just 15% of pulvinar neurons (Burman et al., 1982, Bender 1983; Schiller et al., 1974; Mohler and Wurtz, 1977). Directionally-selective responses in MT also stop if the superior colliculus is additionally destroyed (Rodman et al., 1989; Rodman et al., 1990). However there is no effect if the superior colliculus alone is removed. Similarly, monkeys retain saccadic eye movements towards a target in their blind field after a V1 lesion, but that this ability and the potential for recovery is lost if the ipsilesional colliculus is also inactivated (Mohler and Wurtz, 1977; Kato et al., 2011).

In human neuroimaging, a small number of studies have also implicated the superior colliculus in non-aware blindsight (Leh et al., 2006; Sahraie et al., 1997; Tamietto et al., 2010). However, all the patients in these studies sustained brain damage at birth or in early childhood. In Chapter 7, a consistent ipsilesional collicular pathway was not identified in blindsight positive patients, implying that it may not be so relevant in adult-onset pathology. This is similar to interhemispheric connections, which appear to be most relevant in juvenile-onset cases (Bridge et al., 2008).

Interestingly, no human or animal research has demonstrated direct involvement of the pulvinar in blindsight. This is despite extensive anatomical evidence for a direct pathway between the pulvinar and hMT+. This has led some scientists to suggest that

the 'critical' role of the superior colliculus may instead be through connections with the lateral geniculate nucleus, and that the pulvinar is either not involved at all, or provides a supplementary pathway to this collicular-geniculate-extrastriate connection, which becomes important when V1 lesions are complete (Schmid et al., 2010; Kato et al., 2011). This is particularly appealing given the strength of support for both the colliculus and LGN throughout the literature, as well as the emphasis of K-channel projections in residual vision. The suggestion of two complementary pathways by Kato et al., (2011), one SC > LGN > hMT+, and the other SC > pulvinar > hMT+ would also be consistent with the distinct hMT+ response pattern and subcortical activity observed in blindsight positive and negative patients in Chapter 5. In the LGN, K-neurons, unlike M and P cells, receive direct input from the superficial layers of the superior colliculus (Lachica and Casagrande, 1993; Harting et al., 1991). This offers an important opportunity for interaction in generating non-striate MT responses, either in a direct or modulatory capacity.

It remains a subject of on-going debate whether LGN projections to the extrastriate cortex receive direct input from retinal ganglion cells or indirectly from midbrain structures (Benevento and Yoshida, 1981; Warner et al., 2010). For example, retinal afferents have been shown to synapse with direct MT relay neurons in the LGN, however these synapses tend to be on proximal dendrites rather than cell bodies, which may imply a more modulatory role (Warner et al., 2010). In the current work, although the DTI findings in Chapter 7 appear to support a direct retino-geniculate-hMT+ pathway in blindsight, the retinal input to the LGN has not been assessed. It is also unclear whether tractography can sufficiently handle disynaptic pathways (e.g. Tamietto et al., 2012). If the superior colliculus connects to hMT+ *via* the LGN, such a

pathway could be underestimated with an inadequate tracking algorithm. This may be particularly problematic where connections are not truly disynaptic, but involve interneurons within the relay nucleus, or if incoming synapses to the dendrite are at a notable distance from the axonal output. It is therefore only possible to state from the work here that there was no support for a *direct* collicular-hMT+ connection in blindsight patients. It was not possible to confidently state that an indirect pathway between the superior colliculus or even pulvinar and hMT+ could account for blindsight responses.

In future work it will be interesting to address this question of retinal input by comparing optic tract to collicular-geniculate connections in blindsight positive and negative patients. The optic tract undergoes considerable transneuronal retrograde degeneration after V1 damage, whilst retino-collicular connections appear relatively spared (Cowey et al., 1989; Cowey et al., 2011). One hypothesis is that the extent of damage in these pathways will correlate with residual blindsight performance. An additional study could also be to compare blindsight performance in patients with V1 and additional subcortical damage. Of the 17 patients recruited to the DTI study here, only one had significant subcortical pathology involving ipsilesional LGN and pulvinar, but not the superior colliculus. This was a deliberate decision to recruit a homogenous group of patients. However, a comparison between patients with selective subcortical damage could help to establish whether just the LGN, or multiple subcortical structures are critical for blindsight.

9.1.4 Ventral stream pathways and processing

The ventral visual stream is a relatively neglected area of study in blindsight research and non-striate visual pathways. One reason for this may relate to relatively poor blindsight performance in classic tests of shape discrimination (Cowey, 2010). Similarly, neural activity associated with unconscious dorsal stream stimulation tends to be more marked than equivalent stimulation of the ventral stream (Baseler et al., 1999; Lin and He, 2009).

If the P-channel is degenerated following V1 damage (Cowey et al., 1989), the processing of high spatial frequencies associated with fine detail and discrimination is likely to become severely impaired, if not completely absent. This, however, does not mean that low-grade processing cannot be supported within the ventral cortex. There are examples of intact ventral processing in the absence of V1 in the literature. In the macaque, visually driven electrophysiological and fMRI responses in V2, V3, and V4 occur after V1 lesions, despite a reduction in amplitude (Schmid et al., 2009; Schmid et al. 2013; Schmid et al., 2010). In patients, fMRI activity is also seen in V2/V3, the lateral occipital cortex, and posterior fusiform gyrus (V4/V8) in response to complex images of objects in the blind visual field (Goebel et al., 2001; Schoenfeld et al., 2002).

Ventral regions such as V2-V4 are also implicated in perceptual learning of static orientation-specific features, and the transfer of learning effects after V1 damage (Das and Huxlin, 2014). This is particularly relevant to Chapter 8, where blindsight performance showed robust and consistent improvements in face and place

discrimination after training with motion. A functioning ventral pathway in the absence of V1 is therefore likely to possess interconnections with the dorsal stream.

There are a number of direct subcortical projections to the ventral visual cortex, independent of V1. These include direct connections between the LGN and extrastriate cortex areas V2, V3, and V4 (Bullier and Kennedy, 1983; Fries 1981; Cowey et al., 1989), which may involve the K-channel as they are mostly confined to the interlaminar zones (Bullier and Kennedy, 1983). Such geniculo-extrastriate connections to V4 are particularly implicated in blindsight processing (Schmid et al., 2010).

The infero-lateral pulvinar also connects to several ventral visual areas including V2-V4 (Benevento and Davis, 1977; Adams et al., 2000). However it remains to be seen whether such pulvinar inputs might activate ventral cortex in the absence of V1. Abundant connections are also present between the amygdala and infero-temporal cortex (Amaral and Price, 1984). However, the amygdala appears to play a specific role in emotion and threat (Adolphs et al., 1994). Although it may underlie emotionally salient responses when V1 is damaged (Morris et al., 2001; Pegna et al., 2005; Burra et al., 2013), this is not so relevant to the processing of neutral expressions (Chapter 6). FFA activity is demonstrable for unconscious neutral faces, but is independent of amygdala activation – unlike for emotional faces (Jiang and He, 2006). This implies activity may arise from a distinct path, separate to the amygdala.

Lastly, it is possible for signals to reach the ventral stream via interhemispheric callosal connections (Van Essen et al., 1982). Significant ipsilateral activation was

observed in patients in Chapter 6, dissimilar to the predominant contralateral response to motion (Chapters 3-5). Bilateral activity is common in the ventral stream (Epstein and Kanwisher, 1998; De Renzi, 1997), and could support activity when V1 is damaged.

Unfortunately the current findings do not enable a confident distinction to be made between these pathways. Different connections are likely to co-exist, and may work together to facilitate residual visual processing. Diffusion MRI, as used in Chapter 7 for the dorsal stream, may help to clarify this in future work. The current results highlight that ventral stream processing is possible after V1 damage, and is likely to share communication with dorsal 'motion' pathways.

9.1.5 The evidence against residual V1

An early but persistent criticism of blindsight research is that residual visual processing is mediated via intact 'islands' of spared V1 (Campion et al., 1983; Fendrich et al. 1992; Morland et al., 2004). Many studies have responded to such criticisms by stating that significant extrastriate activity, or blindsight performance was seen in the absence of retinotopically corresponding V1 input (e.g. Schmid et al., 2009; ffytche and Zeki, 2011). This is also the predominant stance of the work presented here. In group studies such as these, it is possible for a number of patients to possess spared regions of calcarine cortex. However, these predominantly correspond to intact areas of vision at the centre of the visual field ('macular sparing'), or in the far periphery.

As explained in the introduction, neurons in V1 and the early visual cortex demonstrate rigid retinotopic organization of their receptive fields (Van Essen et al., 1984). Because of this, it is generally accepted that a specific region of V1 damage can be confidently equated to the corresponding field loss if supported by (i) visual field perimetry (ii) structural MRI images (ffytche and Zeki, 2011). Throughout the experiments in this thesis, visual images were presented to the most dense region of visual loss in the blind hemifield, as measured by perimetry. Therefore any fMRI activity or behavioural performance should not be mediated by spared V1. Furthermore, none of the experiments here demonstrated significant V1 activity during stimulation of the blind hemifield.

Another argument against residual V1 is that many of the results here showed an abnormal pattern of fMRI activity. If V1 had been involved e.g. in Chapter 3, residual activity would reflect an intact magnocellular channel and would thus respond normally. Furthermore, one would expect stimulation to elicit perceptual awareness of some sort. However, in tasks employing low contrast images, the majority of patients showed no conscious experience at all, despite significant performance above chance (Chapter 5).

Lastly, at least three patients exhibited blindsight despite complete destruction of the calcarine cortex or its underlying white matter (Chapter 7). There also were blindsight negative cases with small regions of V1 apparently intact. This makes it very unlikely that it was the presence of spared V1 that provided the critical feature for blindsight, and would account for the results presented here.

9.2 Awareness and perception

9.2.1 A continuum of consciousness

9.2.1.1 The complete dissociation between awareness and performance

The initial definition of blindsight, the ability to respond to a visual stimulus in the absence of conscious awareness, was centred around the critical issue that there should be no conscious representation of any stimulus attributes (Weiskrantz et al., 1974). This was one of the key features to distinguish blindsight from another well-described form of residual vision after brain damage, the 'Riddoch Phenomenon'. In this syndrome, patients with striate cortex damage were unable to discriminate or detect stationary stimuli but could reliably detect moving stimuli, and this residual ability was always accompanied by a conscious experience of motion (Riddoch, 1917).

In fact, it later became apparent that in patients such as GY, the use of certain stimuli could elicit some sort of awareness in the blind hemifield (Weiskrantz et al., 1995). Apparently GY denied ''seeing'' the stimuli that he detected and discriminated, despite acknowledging at times that he had been aware of them. This led Weiskrantz to suggest that blindsight shows a distinction into Type 1 and 2 (1998). Type I is the original form of blindsight which is observed in the absence of any acknowledged awareness, whereas Type 2 reflects the fact that patients can be aware that a stimulus has occurred without experiencing a visual percept. In other words, Type 2 blindsight allows for ''nonvisual'' awareness of visual stimuli, which is an abstract rather than a phenomenal awareness associated with normal veridical vision.

Whilst many methods exist to test for blindsight, arguably the most common approach is to offer patients a binary choice for a stimulus inside their blind hemifield, 2-alternate forced choice questioning (2-AFC), which was the technique employed here. This could include deciding when or where a stimulus had been presented, or which of two possible stimuli had been shown. Performance on such tests can be very impressive despite a complete absence of acknowledged awareness. This dissociation seems to be particularly true for salient non-preferred images. GY, for example, could score around 80% at direction discrimination for slow-moving stimuli and denied any awareness at all, thus representing Type 1 blindsight. When the stimulus speed was increased slightly, he improved his performance to almost 100%, but this also transformed his experience to one of acknowledged awareness (Weiskrantz et al. 1995). This is very similar to the results here for intermediate contrast stimuli. Unlike 100% contrast, which tends to be associated with a much greater increase in confidence, intermediate contrast levels were associated with significant performance despite a confidence score of around 3/10 (Chapter 3).

Throughout the experiments here, low-contrast complex motion in Chapter 5 elicited the most consistent and classical type-1 blindsight responses, involving the majority of patients. The discrimination task in particular, which did not include auditory cues, gave patients the most trouble in timing their responses. 6/8 blindsight positive patients showed significant performance despite mostly denying seeing anything at all. This, however, does not mean that these patients could not become aware of stimuli within their blind field. If the stimulus was changed to a high contrast drifting Gabor, almost all of the same patients became aware of something. Thus the presence

of Type 1 or 2 blindsight is not fixed for an individual, but can be influenced by the stimulus characteristics.

Less direct methods of blindsight testing may elicit different sensitivities, and can perhaps even probe distinct underlying mechanisms. Indirect processing may be inferred if it influences responses to targets in the normal hemifield. For example, a patient may respond faster to a seen target in the normal hemifield if simultaneously shown an additional stimulus in the blind field (e.g. Marzi et al., 1986; Tomaiuolo et al., 1997). Using such paradigms, Marzi suggests there is a distinction between sub-cortical processing that cannot give rise to conscious experience and cortical processing which may give rise to such experience, and argues that indirect blindsight may reflect activation of subcortical structures alone. If cortical connections are unnecessary for this type of processing, this could account for an increased sensitivity using indirect tests, as some patients may still have intact subcortical structures, whilst the connections to the extrastriate cortex are damaged. Although not employed here, it would be interesting to compare indirect tests to the current results.

Another potential omission in blindsight testing here was that vision in the blind hemifield was not compared to equivalent detection or discrimination thresholds in the *sighted* hemifield, which would also require a measure of awareness for every trial undertaken. The reason that this is highlighted as important stems from early criticism and debate surrounding the importance of consciousness in blindsight. It was claimed by certain critics that the unconscious aspect of blindsight was "essentially trivial" because normally sighted observers behave in the same way at

and around psychophysically determined thresholds (Campion et al., 1983). This troubled researchers such as Cowey and Weiskrantz, who felt that they had identified a unique situation in which there was a complete dissociation between performance and awareness, i.e. that blindsight performance was completely unconscious, and was distinct from normal, degraded vision. They counter-argued that visual stimuli in the blind field can sometimes be discriminated almost faultlessly in the absence of awareness (as described for GY above, and in certain circumstances in the current work), whereas in the seeing field, stimuli even just above threshold are invariably accompanied by conscious visual awareness. Their opinion was that it is this absence of visual qualia despite an ability to discriminate as if present that makes blindsight so interesting (Cowey, 2010). However the question still remains whether this really does matter? Even if a perfect dissociation does not exist between performance and awareness, the mechanism behind visual performance in the absence of V1 is still extremely interesting. There are clearly frequent occasions when performance and consciousness are dissociated, however this does not appear to be true all of the time. What is perhaps more interesting is how processing transcends from the unconscious to the semi-conscious non-visual experience, and perhaps even further to elicit some kind of crude *visual* percept, and whether this can be manipulated.

9.2.1.2 Subjective patient descriptions are rarely accurate

As described above, it is clear that a number of blindsight patients can report some sort of conscious experience during presentation of visual stimuli in their blind field. This is also associated with some controversy, and has led certain researchers to question whether blindsight is simply explainable in terms of the Riddoch Phenomenon. Their concern arises from the finding, demonstrated very clearly in the

contrast experiments here (Chapter 3), that patients can show an association between performance and awareness with stimuli of increasing salience, and this is more likely to represent the Riddoch Phenomenon than blindsight (Kentridge and Heywood, 1999). In response, it is possible to become overshadowed by definitions and again lose sight of what is interesting and important. Namely whether or not conscious vision is possible in the absence of V1, and what the limitations and extent of such visual function are. The original definition of Type 2 blindsight is that patients experience a non-visual percept, despite being able to describe where in the visual field this has occurred (Cowey, 2010). Possible mechanisms include activity in the frontal eye fields, where TMS does not evoke visual qualia. Alternatively it has been speculated that this may represent an autonomic phenomenon that can elicit a 'gut feeling', but cannot explain abilities like orientation discrimination. In fact, this definition rapidly becomes very complicated, as even back in the 1980's, GY demonstrated a number of examples suggestive of 'visual' rather than abstract awareness. Barbur et al. (1980) stated that GY reports seeing ''dark shadows'' in response to flashed targets, and together with Zeki and colleagues, claim that when blindsight patients are aware of detecting visual stimuli, this is a phenomenal visual experience rather than a 'feeling of knowing' (Zeki and fftyche, 1998; fftyche and Zeki, 2011).

In this study, I included reports of patient's descriptions for the images they were shown. Patients were frequently unable to describe any visual image at all, and if offered a pen to draw the stimulus would return it back with resignation. In the speed experiments, arguably the least salient of the three stimulus categories (moving black dots), most patients reported seeing nothing at all. However one patient thought he

might have seen a "*moving blur*" on occasions. Another suggested seeing a "*light area*" at times on the screen, although this was by no means consistent, occurring perhaps ten times out of a couple of hundred trials. Of the two patients at ceiling for detection, one described "*a patch of motion*" in the blind field, but could not describe any detail about it. The other incorrectly guessed that the image looked like a previous sighted stimulus. In the face/place experiments, at least three patients provided similar mistaken descriptions of "*wavy motion*" or "*moving ripples*" that were again similar to the seen stimuli of a previous task. Other suggestions included "*ringed blobs*", and "dark shapes at times", however no-one could describe the correct shape, let alone the stimulus features. In the most salient contrast task, descriptions again varied. However there were more consistent reports for higher contrast stimuli in a number of patients, eliciting descriptions of "*movement*", "*something fuzzy/murky*", "an *after-image*", and "*grey clouds*".

Therefore on balance, the subjective descriptions of patients who felt able to provide them were mostly highly inaccurate and showed little in common with the stimuli actually presented. However, in the minority of cases for the most salient images, there were a few relatively consistent descriptions of a dark or even light shadow, after-image, or silhouette, which could be pointed to in space, may have been moving, and was not dissimilar to the reported description provided by GY. This suggests that certain patients, akin to GY and the descriptions of patients collated by Zeki and fftyche (1998) had experienced a level of awareness that may have included a visual component. This was, however, clearly very different to phenomenological vision. So what are the implications for the definition of blindsight? The exploration of GY's visual capacity, in fact, went even further and showed that he can accurately match

stimuli in his blind field to a selection of images or speeds in his sighted field with a remarkably high degree of precision (Stoerig and Barth, 2001; Morland 1999). This suggests that his supposedly abstract experience of awareness might in fact contain a significant amount of visual information. It also leads to a number of unanswered questions surrounding this issue; namely does matching *per se* require conscious experience? Can awareness be visual in the absence of V1? When does awareness stop being blindsight? Is it when the patient can accurately describe what they are seeing?

Another criticism of blindsight research particularly relevant to Type 2 cases, relates to the nature of 2-AFC versus clinical visual testing (Campion et al., 1983). Clinical perimetry is characterized by yes/no questioning, to which a participant's judgment depends not only on their sensitivity to the target, but also on any tendency to select one or another response independently of their sensitivity, i.e. response bias. If the participant is particularly cautious, then 'no' responses are likely to predominate. Conversely, 2-AFC methods are less prone to response bias and can lead to lower detection thresholds. In other words, someone can be declared officially blind on what are considered to be gold-standard perimetry reports, yet exhibit significant performance on 2-AFC testing that is based purely upon their extreme response bias. This bias can also inadvertently be influenced according to how participants are instructed at the start of the test. In Humphrey perimetry, patients are often instructed to press the button only when they are certain that they have seen a light, and they are encouraged not to keep pressing too frequently or to guess, because this might invalidate the test. The logic behind this is to reduce the number of 'false positives', and thus in theory to improve the test reliability. This is important for a

clinician in clinic, who needs to decide whether or not someone is safe to drive. It may, however, result in an overestimation of the patient's true deficit. This kind of instruction, if adhered to, is likely to push a participant towards a response bias that is very different from the approach in 2-AFC, where patients are encouraged to try to guess the correct answer and go with a gut feeling. It is difficult to know whether this discrepancy means that researchers should move away from using clinical reports such as these with the potential for response bias (Azzopardi and Cowey, 1997), or whether this dissociation between clinical and psychophysical results provides a useful distinction for research purposes.

9.2.1.3 Visual perception in the absence of V1

Another enduring problem in blindsight research is why V1 alone should be indispensible for phenomenal vision, given the degree of evidence highlighting other factors that should be intact after V1 damage (Cowey, 2010). However, as alluded to above, there are several examples here and in the literature, which suggest that visual experience is possible despite V1 damage. Patients' retained ability for perceptual matching (Stoerig and Barth, 2001; Morland 1999), their descriptions of highly salient images (Chapters 3 and 6, Barbur et al., 1980; ffytche and Zeki, 2011), the retention of phenomenal visual imagery despite bilateral V1 damage (Bridge et al., 2010), and the ability for patients (or indeed macaques) to improve performance and awareness (Chapter 8; Humphrey, 1974; Sahraie et al., 2011) all suggest that the brain retains the capacity to support some kind of visual perception even when V1 is destroyed. This is further emphasised by an exciting recent study in which two patients with adult-onset V1 damage perceived phosphenes in their blind field during TMS of the ipsilesional hemisphere alone (Mazzi et al., 2014). Thus a range of

evidence appears to support some sort of visual capacity after V1 damage. Whether this reflects 'conscious' vision remains a matter of debate, as the experience reported by patients is still very different to normal conscious perception.

A major criticism of blindsight VRT (Chapter 8) is that there is little point in improving performance if it can only ever remain unconscious. However, even in the absence of conscious awareness, patients can respond to visual stimuli in order to avoid situations of danger (Streimer et al., 2009). Furthermore, there are recent reports suggesting that patients with V1 damage can improve their performance from Type 1, to Type 2, to being able to report visual experiences (Sahraie et al., 2013). This supports the suggestion that conscious awareness may reflect a continuous spectrum, and that targeted training can even lead to an improvement in phenomenological vision. The work in this thesis also hints at such a spectrum, illustrated by the difference in patients' reports of awareness and their descriptions of stimuli as salience is increased. Rather than going against the literature, this could be consistent with a large proportion of it if one moves away from restrictive classifications, which have already needed adapting for new observations (Weiskrantz, 1998).

A possible explanation underlying this theory could be that visual awareness relates to the level of activation in the extrastriate cortex. A sufficient amount of appropriate activity may be required to generate some sort of basic visual experience (see Chapter 3 discussion; also suggested by Stoerig, 2006). In Chapters 3, 5, and 6, a relationship was found between performance and fMRI activity. This level of activity may not normally be reached by non-striate retinal pathways to the visual cortex, but

may be achievable with particularly salient images that are known to elicit stronger levels of activation (e.g. Chapter 3). In such a scenario, it should be possible to manipulate this level of activity and its associated visual experience, whether through training (Sahraie et al., 2013; Humphrey, 1974) or over time as with patient DB (Trevethan et al., 2007a; Trevethan et al., 2007b; Schoenfeld et al., 2002). This could be mediated by subcortical connections that are normally present in the adult visual system (Chapter 7), or through supplementary 'novel' connections that further boost extrastriate activity, and thus push perception into consciousness (Bridge et al., 2008; Silvanto et al., 2009). Indeed GY, who demonstrates such additional connections and may have experienced greater plasticity due to his young age at brain injury, appears to demonstrate particularly strong levels of ipsilesional fMRI activity (Goebel et al 2001).

9.2.2 Behavioural consistency and attention

An interesting observation reported by several patients was that their visual loss appeared to alter in severity according to how fatigued they felt, and their level of concentration. Furthermore, on at least one or two occasions such reports anecdotally corresponded to psychophysical performance. Patients normally attended two experimental sessions, separated by one or two weeks. On one occasion, a patient reported that he had been suffering from an illness with abdominal pain and loss of sleep over the days leading up to his second assessment – although this had fully recovered by the time he was seen. This was only relayed to the experimenter after it had been noticed that his performance was somewhat less consistent to previously.

Attention is likely to play an important role in blindsight and psychophysical performance, and may contribute to apparent fluctuations in visual loss with alertness, noticed by patients. Visual attention can be directed to a particular region of space to enhance the neural processing of attended stimuli, whilst suppressing those that are deemed irrelevant (Tong, 2003). In both early and higher-level visual cortex, top-down attention can strongly bias responses and cause an overall enhancement of signal change (Kamitani and Tong, 2005; Chawla et al., 1999). This is necessary although not sufficient for awareness, as indicated by numerous examples where differences in awareness can occur despite sustained attention, similar to blindsight (He et al., 1996). Where attention is absent, such as in a patient with hemianopia and additional visual neglect, one might expect blindsight performance to be lost.

Apart from a global effect on blindsight, it is suggested that attention can fluctuate on a trial-by-trial basis that can impact psychophysical performance over time (Zeki and ffytche, 1998). Whilst this is likely to be averaged out across an experiment, it provides a strong case for the use of online psychophysical measures during fMRI scanning. In all the experiments here, patients undertook separate psychophysical testing outside the MRI scanner. This was always carried out on the same day as fMRI scanning, specifically within one to three hours of scanning. On balance this was felt to be justifiable, given that the primary motivation behind fMRI was to measure bottom-up visual processing and uncover the characteristics of residual responses in the absence of V1. Although of interest, the main intention was not to record the 'neural correlates of awareness' in blindsight. This is a very different question, which

may benefit from a slightly different approach more similar to Sahraie et al. (1997). There were also a number of practical reasons for choosing offline behavioural measures. This included the possibility for interaction with patients, particularly during low-salience tasks, which could have been disregarded as pointless exercises by patients experiencing nothing at all. Whilst specific performance feedback was never provided, it was sometimes helpful to offer encouragement to patients and reiterate task instructions to maintain engagement with the task. Another benefit was the decreased scan-time, which would have been excessive with an event-related design.

Another example of the importance of attention in blindsight is the provision of cues for oncoming targets (Kentridge and Heywood, 1999). In the methods here, auditory cues were provided to signify the onset of the first and second intervals during temporal 2-AFC testing. However, similar cues were not given during discrimination 2-AFC. In retrospect, this would have been a useful addition to the paradigm. A number of instances occurred when patients became confused about the correct timing of their response, and required the experimenter to intervene. An auditory cue would have been considerably more noticeable than text on a screen, and thus may have helped to minimise this. Considerable evidence suggests that psychophysical performance improves with appropriate spatial and temporal cues (Kentridge et al., 1999a; Kentridge et al., 1999b), whilst performance declines when the moment of stimulus onset becomes uncertain (Cowey and Stoerig 2004).

9.3 Group studies and patient heterogeneity

Eighteen patients in total took part in this work, all of whom had sustained unilateral damage to the primary visual cortex at least 6 months previously, and beyond 18 years of age. This in itself was a challenging task, and involved six UK NHS or research centres to identify potential candidates. Additional criteria were also applied to try to exclude patients with extensive damage to the extrastriate cortex or involving subcortical nuclei. Similarly, any patient with possible right parietal cortex involvement was screened for visual neglect (see Appendix D). The intention behind this was to provide a reasonably consistent and homogeneous group of patients, from whom it would be easier to carry out group analyses.

Whilst this was largely successful, it was interesting that the patients within this group still showed quite marked differences in their performance and subjective experience of stimuli in the blind visual field. One can speculate that these differences were largely related to the variability in size and extent of pathology (Pasik et al., 1969; Cowey et al., 1999). Such differences probably include the presence of damage in striate cortex, optic radiations, V2, V3, and V4. As noted in Chapter 7, one patient was also noted to have sustained damage to the LGN and pulvinar that was probably highly relevant to his psychophysical performance. The age of lesion onset is also likely to impact visually-guided behaviours, but only when considering juvenile-onset cases (Tinelli et al., 2013). When the damage has occurred in adulthood this is unlikely to influence performance, and did not appear to be important in these patients; nor did the duration following lesion onset, or age at investigation. Similarly,

these factors did not appear to be important for an effect of rehabilitation (Chapter 8, see also Stoerig, 2006).

The variability amongst naturally occurring human V1 lesions has been highlighted as a limitation of human research amongst researchers focusing on non-human primates (Schmid et al., 2009). Indeed, it certainly highlights the limitations in carrying out individual case studies, which have unfortunately predominated in the blindsight literature over the last several decades. However, the heterogeneity in the precise location of structural damage has in fact proven to be extremely useful, and has undoubtedly permitted the group of patients to be subdivided according to their distinct residual visual performance. By determining which connections and characteristic fMRI responses are consistent amongst blindsight positive and negative patients, it is possible to identify which underlying structures and pathways may be involved (Chapters 3,5,7).

9.4 The limitations of BOLD functional MRI

The use of neuroimaging continues to grow in research and clinical settings, driven by its non-invasive approach to recording both structure and function in the living human brain. Both techniques employed here, BOLD fMRI and diffusion MRI have been in use for over two decades (Kwong 1992; Le Bihan and Bretton, 1985), however their indirect approach and certain technological limitations can restrict what might be inferred from their results. For diffusion MRI, this is discussed in

section 7.5 of Chapter 7. However, it is useful to discuss some common issues for functional MRI here, as they are relevant to Chapters 3-6.

9.4.1 Optimising the signal to noise ratio

Blood oxygenation level dependent (BOLD) activity provides a surrogate for functional activation in the brain by measuring tissue perfusion and changes in the concentration of oxygen in the blood. Specifically, it utilises the oxygen delivery system in the blood, haemoglobin, to infer neuronal activity. When neurons are active there is an increased oxygen demand, and the local response is to increase the blood flow to those activated regions. In turn, this neuronal activity causes a change in the concentration of oxygen in the blood. Initially there is a very brief decrease in oxygenation, known as the initial dip in the haemodynamic response (Figure 2A). This is followed by a period where the blood flow increases to such a level that it supplies a surplus of oxygen beyond the demand, so the concentration of oxygen increases. The increase in blood flow normally peaks after around 6 seconds, before falling back to baseline.

fMRI signal change reflects a difference between the signal during a particular event or stimulus, and that recorded at baseline. Over the course of an experiment, this is averaged across all the times that the condition occurred. Classically this can follow a block-design, as carried out here, where conditions are grouped into blocks of 10-30 second duration, interspersed by rest blocks. Alternatively the conditions can be altered on a trial-by-trial basis using an event-related design. In either case, the quality of data is enhanced as the signal increases, and the amount of noise is

minimised. Aside from the important scanning parameters described in the General Methods section, which were selected to optimise this signal to noise ratio (SNR), a number of steps in the experimental design can be taken to try to enhance this. One basic principle is to maximise the length of time a signal is acquired as much as is possible, without increasing the experiment to an unacceptable level. This is a relatively simple task in experiments measuring just one or two conditions compared to baseline. However, the motivation behind the fMRI experiments in Chapters 3-5 was to go beyond the presence or absence of activity. Instead, a novel fMRI design was required, which would incorporate a number of critical factors limiting this SNR:

(1) A parametric design was used to compare signal change as the stimulus sequentially underwent alterations in either contrast, speed or coherence level. Therefore there were at least five or six condition 'levels', depending upon the experiment. This approach would enable an enquiry into the physiological characteristics of fMRI responses, beyond simply the presence or absence of activity.

(2) Stimuli had to be presented separately to the blind hemifield, and to the equivalent location in the sighted hemifield, in order to serve as a comparison. If a central stimulus traversing both visual fields was used instead, as during standard localiser paradigms, it would have been impossible to determine whether activity had been driven by stimulation of the blind or sighted hemifield.

(3) In blindsight studies specifically, as illustrated by the results here, it appears that the most highly salient images are associated with higher levels of signal change. Previous fMRI studies in hemianopia always presented the most salient high-contrast

moving stimuli, such as gratings, checkerboards, and spirals (e.g. Goebel et al., 2001; Nelles et al., 2002; Morland et al., 2004; Bridge et al., 2010). However the nature of the current experiments meant that the most salient condition, such as 100% contrast Gabor in the blind hemifield, was only presented for 1/10th of the total stimulus duration. Any contrasts that average across conditions such as motion versus baseline, or motion versus static, would therefore reflect an average of salient and non-salient conditions. This would be expected to have a much lower signal than if the maximum salience stimulus had been presented alone for the entire experiment duration.

In summary, these fMRI paradigms were considerably more complicated than previous imaging studies of blindsight, and have only ever been approached in non-human primates in the past (Schmid et al., 2010). Each condition in the blind hemifield was presented for a very limited duration in total, ranging from 48 - 64 seconds depending on the experiment. Meanwhile the total fMRI duration was between 15.2 – 21 minutes for each experiment. This would account for a relatively low SNR in individual patient data. However, by averaging the signal change across participants, this SNR would have improved dramatically. An alternative option may have been to invite fewer patients to take part in a greater number of repeat scans. However, these experimental regimes were extremely demanding and would have been a considerable demand to ask of patients. Furthermore, it is interesting to obtain data from a number of patients as this enables a better appreciation of the consistency of findings amongst patients with V1 damage. This is particularly relevant given the criticism that the majority of inferences in blindsight have come

from single case studies, and that blindsight may only represent unique and extremely rare cases.

9.4.2 Negative BOLD fMRI responses

In the fMRI results reported here, there were a number of observations of negative BOLD signal change during stimulation of the blind hemifield. This was particularly common in motion tasks involving lower salience images. In Chapter 3, for example, which assessed the effect of luminance contrast on fMRI activity, only conditions of 50% and 100% contrast elicited activity in hMT+ above baseline. This was also true for certain conditions in the motion coherence paradigm (Chapter 4) and in LGN activity amongst both patients and controls in assessments of speed (Chapter 5). It is important to note, however, that in each of these examples, the pattern of fMRI activity was still preserved. In the contrast and motion coherence experiments, signal change was shown to be highly correlated with the normal pattern of activation in V1. Similarly, in the LGN data in Chapter 5, highly significant correlations were observed between LGN and V1 or hMT+ responses. Thus the relationship between signal intensity and each of the three parametric manipulations had been maintained, despite the fact that certain data points now dropped below zero.

This is not the first observation of negative BOLD signal changes, which are frequently reported in the literature. For instance, in the study of speed-dependent motion in hMT+, Chawla et al., presented a number of examples where individual participants showed average BOLD responses below zero for non-preferred speeds (Chawla et al., 1998; Chawla et al., 1999). Similarly, Schmid et al. showed that non-human primates demonstrate blind hemifield responses to low luminance contrast in

V4 that are below baseline – very similar to the results reported in Chapter 3 (Schmid et al., 2010, supplementary information).

Despite these observations, it is important to consider why this has occurred, and whether it is likely to have any important significance. The possibility for a visual stimulus to cause widespread suppression or inhibition is unexpected, and would be hard to uncover a mechanism for. A simpler explanation may be found from our understanding of the 'baseline' level, and whether this always reflects an accurate measure of neural activity during rest. In a basic 'stimulus versus rest' paradigm as was used here, the baseline level of fMRI signal within any region of the brain should very simply reflect that region's activity during rest blocks. Although no stimulus is being presented, there would naturally be a great deal of activity reflecting any number of different conscious and unconscious processes (Binder et al., 1999). This is particularly true if there is an on-going task, as was the case with the simple fixation task during experiments here. This continuous global neural activity underlines the reason for measuring baseline levels, so that an estimate can then be derived for stimulus-specific responses.

Practically speaking, it is actually more common to calculate the percentage signal change using a baseline from the mean time series for a voxel (Mazaika, 2009), rather than the level at rest. This technique is employed as standard in analysis software packages such as SPM and FSL, and was also used here (www.fsl.fmrib.ox.ac.uk). Bearing this in mind, it would not be so surprising for activation to fall below this 'baseline' level during certain weaker stimulus conditions. Instead, the baseline would be directly influenced by the presence of peaks and troughs in signal intensity

over time. During the experiments here, each condition was repeated three or four times in a random sequence. Therefore every voxel will experience stimuli presented to either the sighted or blind hemifield at some point, and with varying saliency. During blind hemifield stimulation, it is known that signal change is significantly weaker than normal fMRI responses to stimulation of the sighted hemifield (Chapters 3-6, Schmid et al., 2009; 2010; Bridge et al., 2010). Consequently, peaks in signal intensity would probably be associated with high salience, sighted blocks. This would contribute to an overall increase in mean signal intensity, and would thus increase the baseline level. In turn, it would increase the likelihood for signal intensity during blind condition blocks to fall below baseline. An example time series illustrating raw data and the partial and full general linear models for one patient are depicted in Figure 1. This was obtained for data in one voxel, representing a single condition during the Contrast Experiment in Chapter 3. As can be seen, the baseline (easiest to appreciate from the green line) was derived from an average of the raw data (red line, Figure 1C). Of the two models generated, the partial model (Figure 1A) only considers blocks belonging to the condition of interest (in this case left hemifield stimulation, 5% contrast). However the full model considers all 30 condition blocks over the course of the experiment (Figure 1B), with greatest emphasis on the three blocks belonging to this condition. If the average signal intensity were to fall below baseline during those conditions of interest, this would elicit a negative parameter estimate and therefore a negative signal change (Mumford, 2007).

The second factor to consider is the contribution of drops in signal intensity, primarily driven by rest periods. In order to evaluate this, it is first necessary to consider the haemodynamic response function (HRF), which is crucial to the

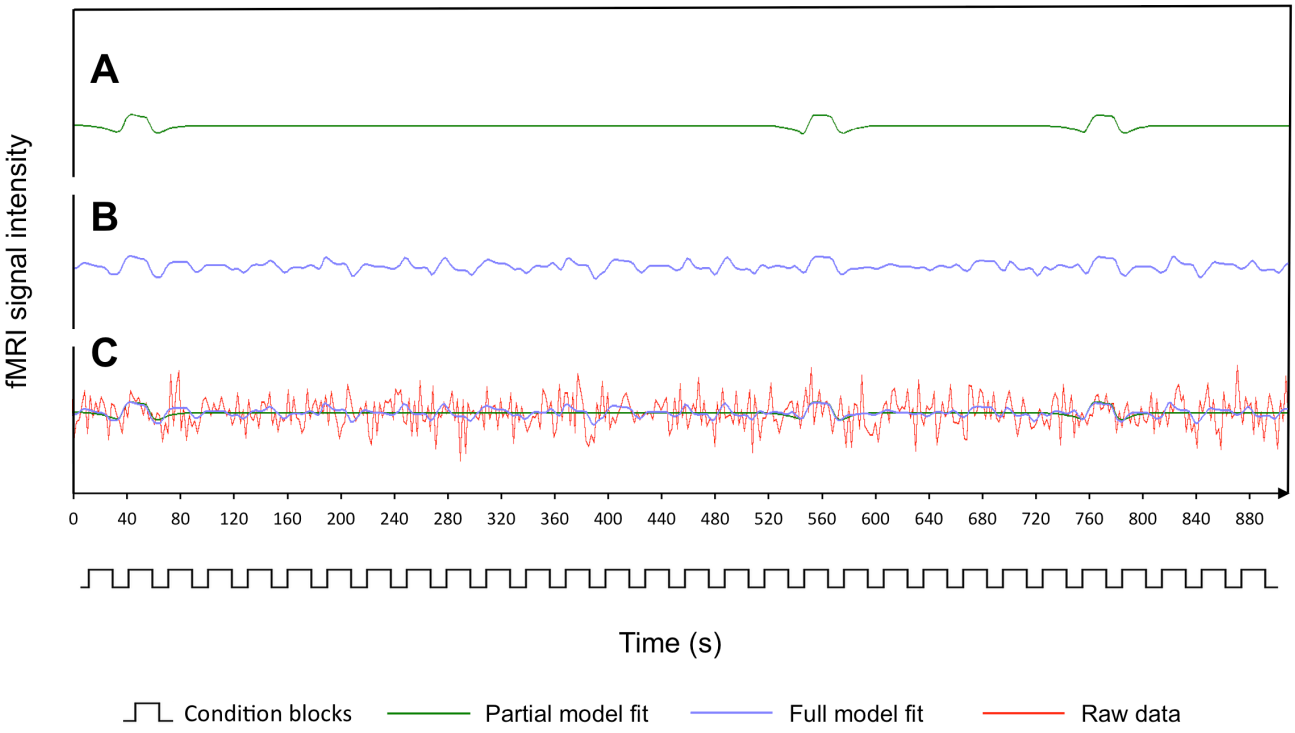

Figure 1. Raw fMRI data and the general linear model representing a single voxel in one patient during the contrast fMRI paradigm, Chapter 3. This is an example time series illustrating the raw fMRI signal data (red line), partial model fit (green line) and full general linear model fit (blue line) for a patient undertaking the contrast fMRI paradigm in Chapter 3. There are 10 conditions in total, with 3 repeats i.e. 30 blocks over the entire time course. Each block lasts 16 s with 10 s rest periods in-between. The data is for a single voxel, and the model represents a single contrast – in this case, left hemifield stimulation, 5% luminance contrast versus baseline. **(A)** The partial model fit shows the three blocks clearly, in which this condition of interest appears. **(B)** The full model fit puts particular emphasis on this particular contrast, but also considers the nine other contrasts within this paradigm. **(C)** When superimposed with the raw data, it can be seen that the baseline corresponds to the mean of these time series. For the current contrast of interest, this is relative to activity during other conditions and rest periods.

interpretation and understanding of fMRI activity. The HRF describes the haemodynamic response that occurs in reaction to a stimulus, and is typically delayed by 5–8 sec and dispersed by 3–4 sec (Friston et al., 1994; Sorensen et al., 1996). The purpose of modelling this response function is to achieve greater specificity in the detection of functional activation in the presence of noise (Kruggel and von Cramon, 1999). Most neuroimaging analysis software packages convolve fMRI data to a predicted HRF as standard. The double-Gamma HRF used in analysis here was a

preset function within FSL, which is a mixture of two Gamma functions: a standard positive function at normal lag, and a small, delayed, inverted Gamma, which attempts to model the late undershoot. An example of this function is shown in Figure 2A, with the specific HRF model representing the block design in Chapter 3 shown in Figure 2B. As can be seen, it takes several seconds for the signal intensity to return to the true baseline after a stimulus has been presented and subsequently removed. It is this delay that may be critical in influencing the accuracy of measures during rest. In Chapter 3, the fMRI block design consisted of 20 s condition blocks, interspersed by 10 second rest periods. In Chapters 4 and 5, a similar design was used with 16 s long condition blocks, followed by 10 second rest periods. If these rest periods were too short in duration, there may not have been sufficient time for the signal intensity to fully settle. This may result in the signal being more heavily influenced by lagged responses to stimuli presented just before and just after that rest period.

A simulation of two scenarios is illustrated in Figure 2B-E. The left column represents the actual design employed in Chapter 3. This is compared, in the right column, to a hypothetical scenario in which rest blocks were extended to 20 s. The HRF model was generated by FSL according to these parameters and, as seen in Figure 2B, did not fully settle at baseline during rest periods (signified by the black columns). Instead it showed a rapid decline and increase, before the next condition appeared. A similar paucity of troughs during rest can be appreciated from the full model fit in Figure 1B. It is possible to estimate from these models the signal intensity associated solely with rest periods (Figure 2D). This was calculated to be 28% higher than the true baseline level – represented by an intensity of 1 in this simulation (due to an undershoot in the classical HRF, Figure 2A). If, in contrast, the scenario involved the longer rest

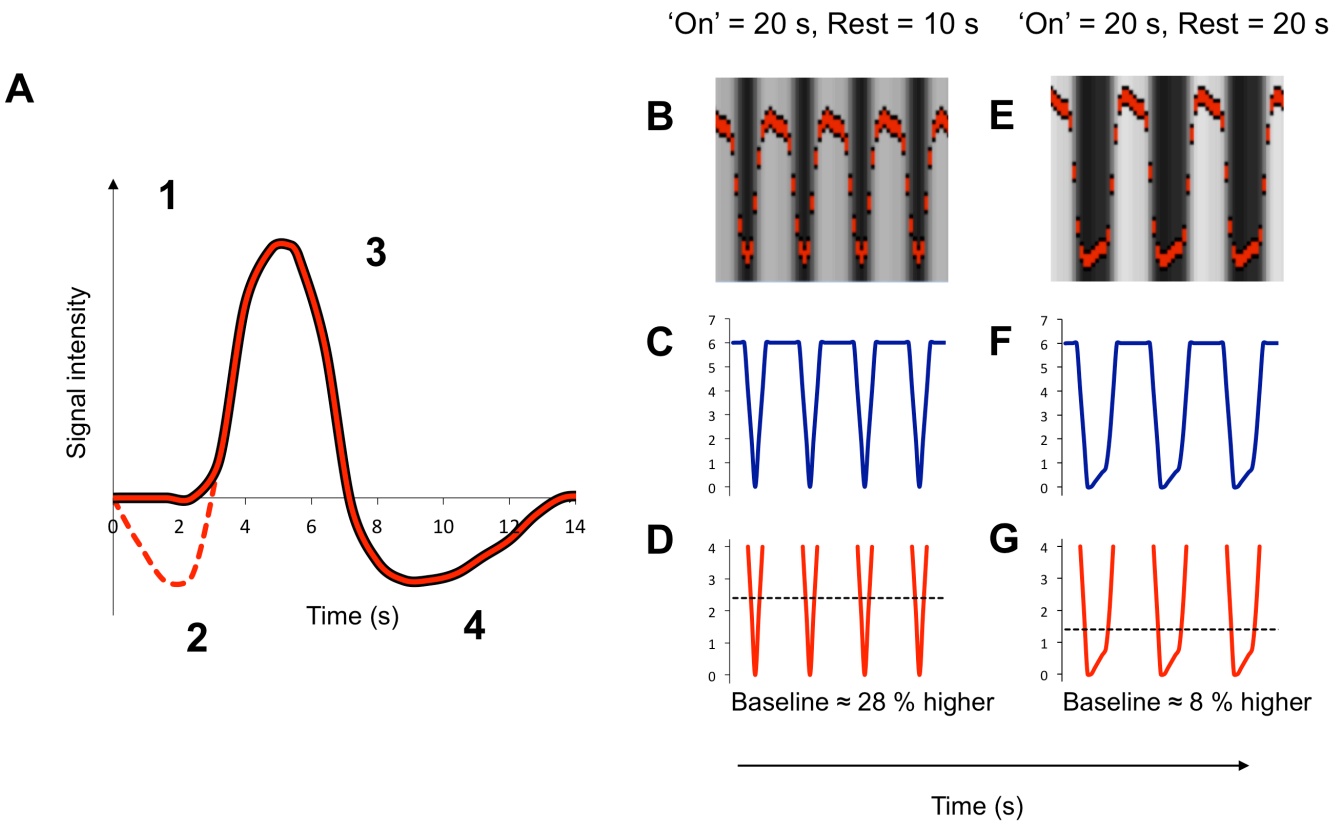

Figure 2. The haemodynamic response function, comparing two fMRI block-designs with different rest durations. (A) The normal haemodynamic response function (HRF) (1) generates an impulse response to a brief stimulus, (2) with a brief initial 'dip' due to a local change in blood flow. (3) This is followed by a more sustained positive BOLD response, representing larger scale blood flow changes and an excess of oxygenated haemoglobin. (4) Signal then drops, with a post-stimulus undershoot at around 8 seconds post-stimulus onset. The blood flow returns to normal, but it takes several more seconds for the cerebral blood volume to fully normalise. **(B-E) The impact of rest duration on signal baseline.** The left column represents the HRF with a block duration of 20 s, and a rest period of 10 s. The right column models the same block duration (20 s), but has a longer rest period of 20 s. (B) This illustrates the HRF model according to the parameters used in Chapter 3. As can be seen, the short rest periods do not provide sufficient time for the signal to fully normalise between blocks. (C) This is represented graphically, so that an estimate of the baseline can be calculated. (D) Compared to a 'true' baseline of 1, this design generates a baseline signal change approximately 28% higher than it should be. (E-F) A longer rest-period design allows the fMRI signal enough time to normalise before the subsequent block. (G) When the baseline is now calculated, it is estimated to be only 8% higher than if the signal had completely returned to rest.

duration of 20 s, as in Figure 2E-F, then the baseline measure would be much closer to reality. Now the mean signal intensity is only 8% above the theoretical baseline, which would represent a much more accurate recording than the first scenario engaged here.

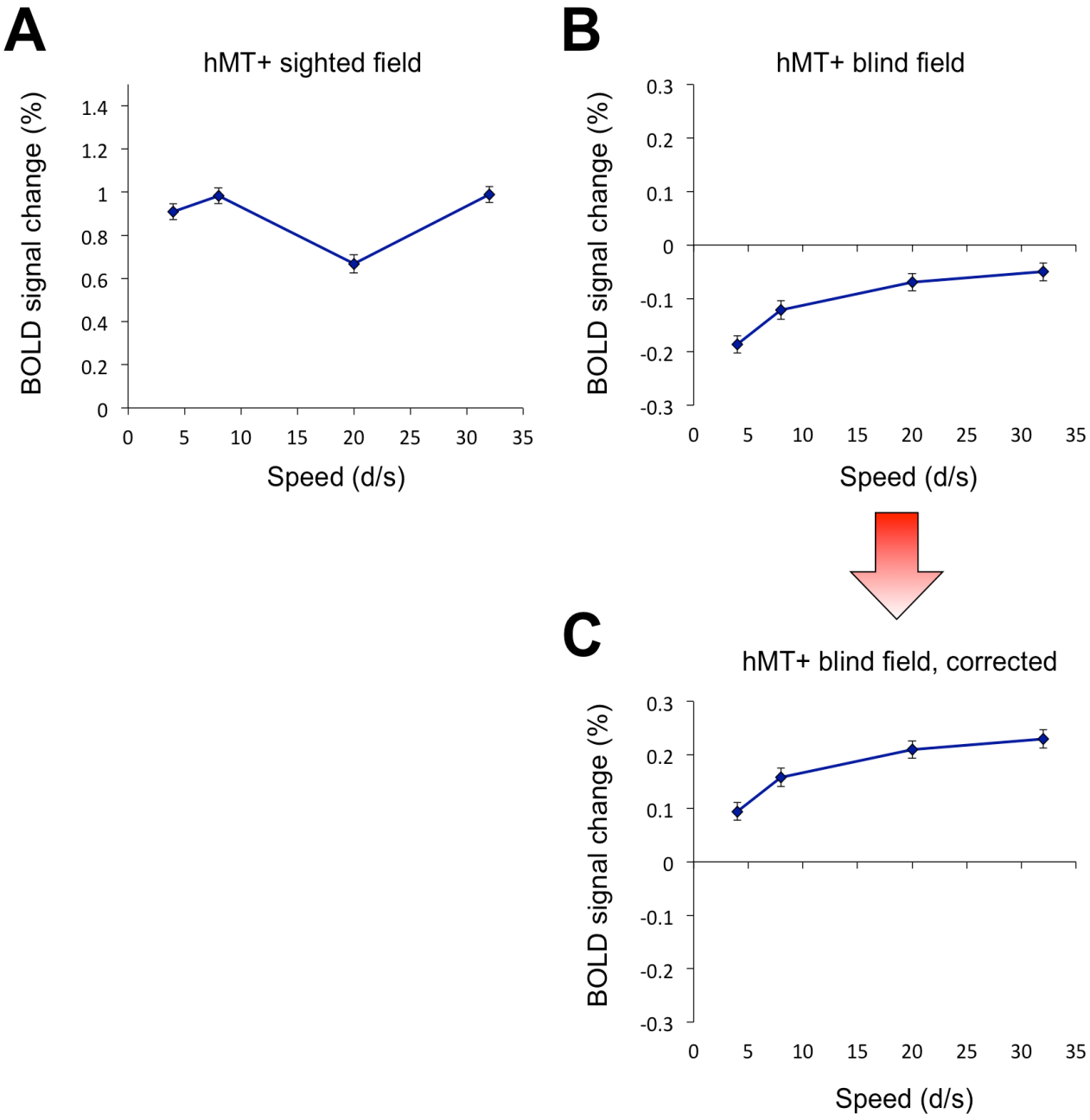

Figure 3. The effect of rest duration on signal change in one patient undertaking the speed fMRI paradigm, Chapter 5. (A) For comparison, data for the sighted hemifield demonstrates a highly positive signal change in contralateral hMT+ for all speed conditions compared to baseline. **(B)** In the blind field, there is also a clear relationship between signal change and speed, however all the data points show a negative signal change. **(C)** If the estimate of baseline error derived in Figure 2 is taken into consideration, the corrected results now show a positive signal change in the blind hemifield. The pattern/relationship between signal change and speed remains unchanged. Error bars represent variance across ROI voxels.

The contamination of rest-period recordings from stimulus blocks therefore provides another explanation for why relatively weak signal intensities during blind conditions may end up below baseline, i.e. a negative BOLD signal change. The impact of this can be appreciated from Figure 3, which illustrates example data for a patient in the Speed Experiment, taken from Chapter 5. If the estimate from Figure 2D was accurate, then the baseline should be 28% lower than was actually recorded. In most cases this would translate to a positive signal change for responses in the blind hemifield. As can be seen, signal change in hMT+ during sighted conditions reached a peak around 1% above baseline (Figure 3A). In the blind hemifield however, responses all fell below this baseline level (Figure 3B). With a new corrected baseline there would be a pattern of signal change depicted in Figure 3C. This now represents a positive change in signal for all stimulus speeds, although the response pattern itself is of course unchanged. This is a potential limitation of the current fMRI methodology, which could be improved in future studies by increasing the duration of rest periods to at least 20 seconds (Figure 2G). In any case, it explains why certain study designs and common analysis techniques elicit negative BOLD responses. It highlights the fact that such measurements do not necessarily reflect underlying differences in neurophysiological responses, but that the important feature of data here was the pattern of signal change between conditions.

9.4.3 Imaging clinical populations

A final point of discussion is the use of BOLD imaging in clinical populations, particularly relevant here since the majority of patients suffered ischaemic stroke. This implies, by definition, that patients possess an abnormality in their cerebral

vasculature that may be different to a healthy population. This could be accounted for by recruiting age-matched controls, which is also important since BOLD changes occur with age (D'Esposito et al., 2003). Nevertheless, there was still the potential for patients to show a difference that was confounded by the presence of neurovascular differences (Gazzaley and D'Esposito, 2005). Although important to consider, this should not directly impact the design and purpose of investigation here. Of primary interest was the comparison of activity patterns with changes in stimulus parameters, rather than a global change in response magnitude comparing patients to controls. Also, the healthy hemisphere of patients could serve as a type of control, and provided a useful point of comparison to responses in the damaged hemisphere and healthy controls. On balance, there are clearly many limitations in BOLD fMRI. However, so long as such limitations are considered, it arguably still provides the best available tool for understanding neural function of patients after V1 damage.

9.5 Final Conclusions

Residual vision, or blindsight, following V1 damage has been recognised for almost a century. Yet the mechanism and pathways, and the extent of visual function remain unclear. This work has gone some way to try to address these questions, and specifically in visual field loss acquired in adulthood. Results here have reinforced the recent controversial suggestion that blindsight is more common than was first thought, and can extend across a number of characteristics involving both the dorsal and ventral streams. It also suggests that visual function need not be completely unconscious, but that certain salient stimuli can elicit both non-visual and crude visual experiences. Novel neuroimaging paradigms have revealed a number of

physiological properties of non-striate input to the extrastriate cortex, which were previously unknown. Together with tractography, these results point to the ipsilateral lateral geniculate nucleus as being involved in residual function, perhaps through direct connections with the extrastriate cortex. Future work can evaluate how visual information reaches this structure, whether through direct retinal input or via the superior colliculus and pulvinar. We can also start to probe the mechanism and extent of training effects when these pathways are targeted by rehabilitation.

Bibliography

Abel PL, O'Brien BJ, Olavarria JF. Organization of callosal linkages in visual area V2 of macaque monkey. J Comp Neurol. 2000; 428(2):278-93.

Adams MM, Hof PR, Gattass R, Webster MJ, Ungerleider LG. Visual cortical projections and chemoarchitecture of macaque monkey pulvinar. J Comp Neurol. 2000; 419(3):377-93.

Adolphs R, Tranel D, Damasio H, Damasio A. Impaired recognition of emotion in facial expressions following bilateral damage to the human amygdala. Nature. 1994; 372: 669–672.

Ahissar M, Hochstein S. Task difficulty and the specificity of perceptual learning. Nature, 1997; 387, 401–406.

Ajina S, Kennard C, Rees G, Bridge H. Motion area V5/MT+ response to global motion in the absence of V1 resembles early visual cortex. Brain. 2014, DOI: http://dx.doi.org/10.1093/brain/awu328

Albright TD, Desimone R. Local precision of visuotopic organization in the middle temporal area (MT) of the macaque. Exp. Brain Res 1987; 65(3): 582-92.

Amano K, Wandell BA, Dumoulin SO. Visual field maps population receptive field sizes and visual field coverage in the human MT+ complex. J Neurophysiol 2009; 102(5):2704-18.

Amaral DG, Price JL. Amygdalo-cortical projections in the monkey (Macaca fascicularis). J Comp Neurol. 1984; 230(4): 465-96.

Amunts K, Malikovic A, Mohlberg H, Schormann T, Zilles K. Brodmann's areas 17

and 18 brought into stereotaxic space-where and how variable? Neuroimage. 2000; 11(1):66-84.

Anderson EJ, Rees G. Neural correlates of spatial orienting in the human superior colliculus. J Neurophysiol. 2011;106(5):2273-84.

Andersson JL, Skare S, Ashburner J. How to correct susceptibility distortions in spin-echo echo-planar images: application to diffusion tensor imaging. Neuroimage. 2003; 20(2): 870-88.

Andersson JL, Jenkinson M, Smith SM. Non-linear optimisation. FMRIB technical report 2007; TR07JA1.

Andrews TJ, Halpern SD, Purves D. Correlated size variations in human visual cortex, lateral geniculate nucleus, and optic tract. J Neurosci. 1997; 17: 2859–68.

Annese J, Schenker-Ahmed NM, Bartsch H, Maechler P, Sheh C, Thomas N, Kayano J, Ghatan A, Bresler N, Frosch MP, Klaming R, Corkin S. Postmortem examination of patient H.M.'s brain based on histological sectioning and digital 3D reconstruction. Nat Commun. 2014; 5:3122.

Aspell JE, Tanskanen T, Hurlbert AC. Neuromagnetic correlates of visual motion coherence. Eur. J Neurosci 2005; 22(11): 2937-45.

Auriel E, Edlow BL, Reijmer YD, Fotiadis P, Ramirez-Martinez S, Ni J, Reed AK, Vashkevich A, Schwab K, Rosand J, Viswanathan A, Wu O, Gurol ME, Greenberg SM. Microinfarct disruption of white matter structure: a longitudinal diffusion tensor analysis. Neurology. 2014; 83(2): 182-8.

Azzopardi P, Cowey A. Blindsight and visual awareness. Conscious Cogn. 1998; 7(3):292-311.

Azzopardi P, Cowey A. Is blindsight like normal, near-threshold vision? Proc Natl Acad Sci U S A. 1997; 94(25): 14190-4.

Azzopardi P, Cowey A. Motion discrimination in cortically blind patients. Brain. 2001;124(1):30-46.

Azzopardi P, Fallah M, Gross CG, Rodman HR. Response latencies of neurons in visual areas MT and MST of monkeys with striate cortex lesions. Neuropsychologia. 2003; 41(13):1738-56.

Barbur J, Forsyth PM, Findlay JM. Human saccadic eye movements in the absence of the geniculocalcarine projection. Brain. 1988; 111: 63-82.

Barbur JL, Ruddock KH, Waterfield VA. Human visual responses in the absence of the geniculo-calcarine projection. Brain. 1980; 103(4): 905-28.

Barbur JL, Watson JDG, Frackowiak RSJ, Zeki S. Conscious visual perception without V1. Brain. 1993; 116:1293–302.

Barton, JJ and Sharpe, JA. Motion direction discrimination in blind hemifields. Ann. Neurol. 1997; 41: 255–264.

Baseler HA, Morland AB, Wandell BA. Topographic organization of human visual areas in the absence of input from primary cortex. J Neurosci. 1999; 19(7): 2619-27.

Becker HG, Erb M, Haarmeier T. Differential dependency on motion coherence in subregions of the human MT+ complex. Eur J Neurosci 2008; 28(8): 1674-85.

Beckers G, Zeki S. The consequences of inactivating areas V1 and V5 on visual motion perception. Brain. 1995;118 (1):49-60.

Bender DB. Receptive-field properties of neurons in the macaque inferior pulvinar. J Neurophysiol. 1982; 48(1):1-17

Bender DB. Visual activation of neurons in the primate pulvinar depends on cortex but not colliculus. Brain Res. 1983; 279(1-2):258-61.

Benevento LA, Standage GP. The organization of projections of the retinorecipient

and nonretinorecipient nuclei of the pretectal complex and layers of the superior colliculus to the lateral pulvinar and medial pulvinar in the macaque monkey. J. Comp. Neurol. 1983; 217: 307–336.

Benevento LA, Davis B. Topographical projections of the prestriate cortex to the pulvinar nuclei in the macaque monkey: an autoradiographic study. Exp Brain Res. 1977; 30(2-3): 405-24.

Benevento LA, Rezak M. The cortical projections of the inferior pulvinar and adjacent lateral pulvinar in the rhesus monkey (Macaca mulatta): An autoradiographic study. Brain Res 1976; 108: 1-24.

Benevento LA, Yoshida K. The afferent and efferent organization of the lateral geniculo-prestriate pathways in the macaque monkey. J Comp Neurol. 1981; 203(3): 455-74.

Binder JR, Frost JA, Hammeke TA, Bellgowan PS, Rao SM, Cox RW. Conceptual processing during the conscious resting state. A functional MRI study. J Cogn Neurosci. 1999; 11(1): 80-95.

Blythe IM, Kennard C, Ruddock KH. Residual vision in patients with retrogeniculate lesions of the visual pathways. Brain. 1987; 110 (4):887-905.

Bola M, Gall C, Sabel BA. The second face of blindness: processing speed deficits in the intact visual field after pre- and post-chiasmatic lesions. PLoS One. 2013; 8(5):e63700.

Bowers AR, Keeney K, Peli E. Community-Based Trial of Peripheral Prism Visual Field Expansion Device for Hemianopia, Arch Ophthalmol. 2008; 126: 657–664.

Braddick OJ, O'Brien JM, Wattam-Bell J, Atkinson J, Hartley T, Turner R. Brain areas sensitive to coherent visual motion. Perception 2001; 30(1): 61-72.

Brainard DH. The Psychophysics Toolbox. Spatial Vision 1997; 10, 433-436.

Brander A, Kataja A, Saastamoinen A, Ryymin P, Huhtala H, Ohman J, Soimakallio S, Dastidar P. Diffusion tensor imaging of the brain in a healthy adult population: Normative values and measurement reproducibility at 3 T and 1.5 T. Acta Radiol. 2010; 51(7): 800-7.

Bridge H, Harrold S, Holmes EA, Stokes M, Kennard C. Vivid visual mental imagery in the absence of the primary visual cortex. J Neurol. 2012; 259(6): 1062-70.

Bridge H, Hicks SL, Xie J, Okell TW, Mannan S, Alexander I, Cowey A, Kennard C. Visual activation of extra-striate cortex in the absence of V1 activation. Neuropsychologia 2010, 48:4148-4154.

Bridge H, Jindahra P, Barbur J, Plant GT. Imaging reveals optic tract degeneration in hemianopia. Invest Ophthalmol Vis Sci. 2011; 52(1):382-8

Bridge H, Thomas O, Jbabdi S, Cowey A. Changes in connectivity after visual cortical brain damage underlie altered visual function. Brain. 2008; 131: 1433-1444.

Britten KH, Shadlen MN, Newsome WT, Movshon JA. Responses of neurons in macaque MT to stochastic motion signals. Vis Neurosci 1993; 10(6): 1157-69.

Bullier J, Kennedy H. Projection of the lateral geniculate nucleus onto cortical area V2 in the macaque monkey. Exp Brain Res. 1983; 53(1): 168-72.

Bullier J. Integrated model of visual processing. Brain Res Rev 2001; 36: 96-107.

Burman, D., G. Felsten, and L. Benevento; Visual properties of neurons in the lateral pulvinar of normal and occipital lobectomized macaques. Assoc. Res. Vis. Ophthalmol. 1982; Suppl. 22: 237.

Burra N, Hervais-Adelman A, Kerzel D, Tamietto M, de Gelder B, Pegna AJ: Amygdala Activation for Eye Contact Despite Complete Cortical Blindness. J Neurosci 2013, 33:10483-10489.

Campion J, Latto R, Smith YM. Is blindsight an effect of scattered light, spared cortex and near-threshold vision? Behav. Brain Sci. 1983; 6: 423–428.

Celebisoy M, Celebisoy N, Bayam E, Kose T. Recovery of visual-field defects after occipital lobe infarction: a perimetric study. J Neurol Neurosurg Psychiatry. 2011; 82: 695-702.

Chawla D, Buechel C, Edwards R, Howseman A, Josephs O, Ashburner J, Friston KJ. Speed-dependent responses in V5: A replication study. Neuroimage. 1999; 9(5):508-15.

Chawla D, Phillips J, Buechel C, Edwards R, Friston KJ. Speed-dependent motion-sensitive responses in V5: an fMRI study. Neuroimage. 1998; 7(2):86-96.

Chen W, Zhu XH, Thulborn KR, Ugurbil K. Retinotopic mapping of lateral geniculate nucleus in humans using functional magnetic resonance imaging. Proc Natl Acad Sci U S A. 1999; 96(5):2430-4.

Cheng K, Fujita H, Kanno I, Miura S, Tanaka K. Human cortical regions activated by wide-field visual motion: an H2(15)O PET study. J Neurophysiol 1995; 74(1): 413-27.

Cheng K, Hasegawa T, Saleem KS, Tanaka K. Comparison of neuronal selectivity for stimulus speed, length, and contrast in the prestriate visual cortical areas V4 and MT of the macaque monkey. J Neurophysiol. 1994; 71(6):2269-80.

Chokron S, Perez C, Obadia M, Gaudry I, Laloum L, Gout O. From blindsight to sight: cognitive rehabilitation of visual field defects. Restor Neurol. Neurosci. 2008; 26(4-5):305-20.

Costagli M Ueno K, Sun P, Gardner JL, Wan X, Ricciardi E et al. Functional Signalers of Changes in Visual Stimuli Cortical Responses to Increments and Decrements in Motion Coherence. Cereb Cortex 2014; 24(1): 110-118.

Cowey A, Alexander I, Stoerig P. Transneuronal retrograde degeneration of retinal ganglion cells and optic tract in hemianopic monkeys and humans. Brain. 2011;134(7):2149-57.

Cowey A, Stoerig P, Perry VH. Transneuronal retrograde degeneration of retinal ganglion cells after damage to striate cortex in macaque monkeys: selective loss of P beta cells. Neuroscience. 1989; 29(1): 65-80.

Cowey A, Stoerig P, Williams C. Variance in transneuronal retrograde ganglion cell degeneration in monkeys after removal of striate cortex: effects of size of the cortical lesion. Vision Res. 1999; 39(21): 3642-52.

Cowey A, Stoerig P. Projection patterns of surviving neurons in the dorsal lateral geniculate nucleus following discrete lesions of striate cortex: implications for residual vision. Exp Brain Res. 1989; 75(3): 631-8.

Cowey A, Stoerig P. Stimulus cueing in blindsight. Prog Brain Res. 2004;144: 261-77.

Cowey A. The blindsight saga. Exp. Brain Res 2010; 200(1): 3-24.

D'Esposito M, Deouell LY, Gazzaley A. Alterations in the BOLD fMRI signal with ageing and disease: a challenge for neuroimaging. Nat Rev Neurosci. 2003; 4(11): 863-72.

Danckert J, Culham JC. Reflections on blindsight: neuroimaging and behavioural explorations clarify a case of reversed localisation in the blind field of a patient with hemianopia. Can J Exp Psychol. 2010; 64(2): 86-101.

Danckert J, Rossetti Y. Blindsight in action: what can the different sub-types of blindsight tell us about the control of visually guided actions? Neurosci Biobehav Rev. 2005; 29(7): 1035-46.

Das A, Huxlin KR. New Approaches to Visual Rehabilitation for Cortical Blindness: Outcomes and Putative Mechanisms. Neuroscientist. 2010; 6: 374–387.

Das A, Tadin D, Huxlin K. Beyond blindsight: properties of visual relearning in cortically blind fields. J Neurosci. 2014; 34(35): 11652-64.

Davidson RM, Bender DB. Selectivity for relative motion in the monkey superior colliculus. J Neurophysiol. 1991; 65(5): 1115-33.

de Gelder B, Tamietto M, van Boxtel G, Goebel R, Sahraie A, van den Stock J, Stienen BM, Weiskrantz L, Pegna A. Intact navigation skills after bilateral loss of striate cortex. Curr Biol. 2008; 18(24): R1128-9.

de Gelder B, Vroomen J, Pourtois G, Weiskrantz L: Non-conscious recognition of affect in the absence of striate cortex. Neuroreport 1999, 10:3759-3763.

De Renzi E. Prosopagnosia. In: Behavioral neurology and neuropsychology (Feinberg TE, Farah MJ, eds). 1997; New York: McGraw-Hill; pp 245–255.

Derrington AM, Lennie P. Spatial and temporal contrast sensitivities of neurones in lateral geniculate nucleus of macaque. J Physiol. 1984; 357:219-40.

DiCarlo, JJ, Maunsell, JH. Form representation in monkey inferotemporal cortex is virtually unaltered by free viewing. Nature Neurosci. 2000; 3(8): 814–821.

Dilks DD, Serences JT, Rosenau BJ, Yantis S, McCloskey M. Human Adult Cortical Reorganization and Consequent Visual Distortion. J of Neurosci. 2007; 27: 9585–9594.

Dineen J, Keating EG. The primate visual system after bilateral removal of striate cortex. Survival of complex pattern vision. Exp Brain Res. 1981; 41: 338–345.

Dougherty RF, Koch VM, Brewer AA, Fischer B, Modersitzki J, Wandell BA. Visual field representations and locations of visual areas V1/2/3 in human visual cortex. J Vis. 2003; 3(10):586-98.

Dumoulin SO, Wandell BA. Population receptive field estimates in human visual cortex. Neuroimage 2008; 39: 647–660.

Edden RA, Jones DK. Spatial and orientational heterogeneity in the statistical sensitivity of skeleton-based analyses of diffusion tensor MR imaging data. J Neurosci Methods. 2011; 201: 213–219.

Epstein RA, Kanwisher N. A cortical representation of the local visual environment. Nature. 1998; 392(6676): 598-601.

Epstein RA. The cortical basis of visual scene processing. Visual Cognition. 2005; 12(6): 954 – 978.

Farah, MJ. Visual Agnosias. 1990; MIT Press, Cambridge, MA.

Feinberg TE, Pasik T, Pasik P. Extrageniculostriate vision in the monkey. VI. Visually guided accurate reaching behavior. Brain Res. 1978; 152: 422–428.

Fendrich R, Wessinger CM, Gazzaniga MS. Residual vision in a scotoma: implications for blindsight. Science. 1992; 258: 1489-91.

ffytche DH, Guy CN, Zeki S. Motion specific responses from a blind hemifield. Brain 1996; 119 (6): 1971-82.

ffytche DH, Guy CN, Zeki S. The parallel visual motion inputs into areas V1 and V5 of human cerebral cortex. Brain. 1995; 118 (6):1375-94.

Ffytche DH, Zeki S. The primary visual cortex, and feedback to it, are not necessary for conscious vision. Brain. 2011; 134(1): 247-57

Fiorentini A, Berardi N. Perceptual learning specific for orientation and spatial frequency. Nature. 1980; 287(5777): 43-4.

Fitzpatrick D, Itoh K, Diamond IT. The laminar organization of the lateral geniculate body and the striate cortex in the squirrel monkey (Saimiri sciureus). J Neurosci. 1983; 3(4):673-702.

Flöel A, de Vries MH, Scholz J, Breitenstein C, Johansen-Berg H. White matter integrity in the vicinity of Broca's area predicts grammar learning success. NeuroImage. 2009; 47: 1974–1981.

Foster KH, Gaska JP, Nagler M, Pollen, DA. Spatial and temporal frequency selectivity of neurones in visual cortical areas V1 and V2 of the macaque monkey. Journal of Physiology. 1985; 365: 331–363.

Franz VH, Loftus GR. Standard errors and confidence intervals in within-subjects designs: Generalizing Loftus and Masson (1994) and avoiding the biases of alternative accounts. Psychon Bull Rev. 2012; 19:395–404.

Fries W. The projection from the lateral geniculate nucleus to the prestriate cortex of the macaque monkey. Proc R Soc Lond B Biol Sci. 1981; 213(1190): 73-86.

Friston KJ, Jezzard P, Turner R. Analysis of functional MRI time-series. Human Brain Mapping. 1994; 1(2): 153–171.

Fujino T, Kigazawa K, Yamada R. Homonymous hemianopia: A retrospective study of 140 cases. Neuro-ophthalmology. 1986; 6: 17-21.

Gaglianese A, Costagli M, Bernardi G, Ricciardi E, Pietrini P. Evidence of a direct influence between the thalamus and hMT+ independent of V1 in the human brain as measured by fMRI Neuroimage 2012; 60(2): 1440-7.

Gao Y, Choe AS, Stepniewska I, Li X, Avison MJ, Anderson AW. Validation of DTI tractography-based measures of primary motor area connectivity in the squirrel monkey brain. PLoS One. 2013; 8(10): e75065.

Gazzaley, A. and D'Esposito, M. Considerations for the application of BOLD fMRI to neurologically impaired populations. In: Hillary, F.G., DeLuca, J Functional Neuroimaging in Clinical Populations. 2005; Guilford Press; Chapter 4.

Gennari F. 1782; Francisci Gennari Parmensis Medicinae Doctoris Collegiati de Peculiari Structura Cerebri Nonnullisque Eius Morbis-Paucae Aliae Anatom. Observat. Accedunt. Parma, Italy: Regio Typographeo

Gilbert CD, Sigman M, Crist RE. The neural basis of perceptual learning. Neuron. 2001; 31: 681–697.

Gilhotra J, Mitchell P, Healey P, Cumming RG, Currie J. Homonymous Visual Field Defects and Stroke in an Older Population. Stroke. 2002; 33: 2417-2420.

Girard P, Salin PA, Bullier J. Response selectivity of neurons in area MT of the macaque monkey during reversible inactivation of area V1. J Neurophysiol 1992; 67(6): 1437-46.

Goebel R, Muckli L, Zanella FE, Singer W, Stoerig P. Sustained extrastriate cortical activation without visual awareness revealed by fMRI studies of hemianopic patients. Vision Res. 2001; 41: 1459-74.

Goodale MA, Milner AD. Separate visual pathways for perception and action. Trends Neurosci. 1992; 15 (1): 20–5.

Gray C, French J, Bates D, Cartlidge N, Venables G, James O. Recovery of Visual Fields in Acute Stroke: Homonymous Hemianopia Associated with Adverse Prognosis. Age and Ageing. 1989; 18: 419-421.

Grill-Spector K, Kushnir T, Hendler T, Edelman S, Itzchak Y, Malach R. A sequence of object-processing stages revealed by fMRI in the human occipital lobe. HBM. 1998; 6 (4): 316–328.

Grill-Spector K, Knouf N, Kanwisher N. The fusiform face area subserves face perception, not generic within-category identification. Nat Neurosci. 2004; 7(5): 555-62.

Gross CG. Representation of visual stimuli in inferior temporal cortex. Philos Trans R Soc Lond B Biol Sci. 1992; 335(1273): 3-10.

Haerer AF. Visual Field Defects and the Prognosis of Stroke Patients. Stroke. 1973; 4: 163-168.

Hallum LE, Landy MS, Heeger DJ. Human primary visual cortex (V1) is selective for second-order spatial frequency. J Neurophysiol 2011; 105: 2121–2131.

Handel B, Lutzenberger W, Thier P, Haarmeier T. Opposite dependencies on visual motion coherence in human area MT+ and early visual cortex. Cereb Cortex 2007; 17(7): 1542-9.

Hankey GJ. Stroke: how large a public health problem, and how can the neurologist help? Arch Neurol. 1999; 56: 748-54.

Hardiess G, Papageorgiou E, Schiefer U, Mallot HA. Functional compensation of visual field deficits in hemianopic patients under the influence of different task demands, Vision Res. 2010; 50: 1158–1172.

Harris RJ, Young AW, Andrews TJ. Morphing between expressions dissociates continuous from categorical representations of facial expression in the human brain. Proc Natl Acad Sci U S A. 2012; 109(51): 21164-9.

Harrison LM, Stephan KE, Rees G, Friston KJ. Extra-classical receptive field effects measured in striate cortex with fMRI. Neuroimage 2007; 34(3): 1199-208.

Harting JK, Huerta MF, Hashikawa T, van Lieshout DP. Projection of the mammalian superior colliculus upon the dorsal lateral geniculate nucleus: organization of tectogeniculate pathways in nineteen species. J Comp Neurol. 1991; 304(2): 275-306.

Hawken MJ, Parker AJ. Contrast sensitivity and orientation selectivity in lamina IV of the striate cortex of Old World monkeys. Exp Brain Res. 1984; 54(2): 367-72.

Haxby JV, Hoffman EA, Gobbini MI. The distributed human neural system for face perception. Trends Cogn Sci. 2000; 4(6): 223-233.

Haynes JD, Rees G. Decoding mental states from brain activity in humans. Nat Rev Neurosci. 2006; 7(7): 523-34.

Haynes JD, Rees G. Predicting the stream of consciousness from activity in human visual cortex. Curr Biol. 2005; 15(14): 1301-7.

He S, Cavanagh P, Intriligator J. Attentional resolution and the locus of visual awareness. Nature. 1996; 383(6598): 334-7.

Heeger DJ, Boynton GM, Demb JB, Seidemann E, Newsome WT. Motion opponency in visual cortex. J Neurosci. 1999; 19(16): 7162-74.

Hendry SH, Reid RC. The koniocellular pathway in primate vision. Annu Rev Neurosci. 2000; 23: 127-53.

Hendry SH, Yoshioka T. A neurochemically distinct third channel in the macaque dorsal lateral geniculate nucleus. Science. 1994; 264(5158): 575-7.

Henriksson L, Raninen A, Nasanen R, Hyvarinen L, Vanni S. Training-induced cortical representation of a hemianopic hemifield. J Neurol Neurosurg Psychiatry. 2007; 78: 74–81.

Hess RF, Pointer JS. Spatial and temporal contrast sensitivity in hemianopia. A comparative study of the sighted and blind hemifields. Brain. 1989; 112(4): 871-94.

Heuer HW, Britten KH. Linear responses to stochastic motion signals in area MST. J Neurophysiol 2007; 98(3): 1115-24.

Hochstein S, Ahissar M. View from the top: hierarchies and reverse hierarchies in the visual system. Neuron 2002; 36: 791-804.

Holliday IE, Anderson SJ, Harding GF. Magnetoencephalographic evidence for non-geniculostriate visual input to human cortical area V5. Neuropsychologia. 1997; 35(8): 1139-46.

Honey C, Kirchner H, VanRullen R. Faces in the cloud: Fourier power spectrum biases ultrarapid face detection. J Vis. 2008; 8(12):1-13.

Horton JC, Landau K, Maeder P, Hoyt WF. Magnetic Resonance Imaging of the Human Lateral Geniculate Body. Arch Neurol. 1990;47(11):1201–1206.

Horton JC. Vision restoration therapy: confounded by eye movements. Br J Ophthalmol. 2005; 89: 792–794.

Hubel DH, Wiesel TN. Laminar and columnar distribution of geniculo-cortical fibres in macaque monkey. J Comp Neurol. 1972; 146:421-450.

Hubel DH, Wiesel TN. Receptive fields and functional architecture of monkey striate cortex. J Physiol. 1968; 195(1): 215-43.

Huk AC, Dougherty RF, Heeger DJ. Retinotopy and functional subdivision of human areas MT and MST. J Neurosci 2002; 22(16): 7195-205.

Huk AC, Heeger DJ. Pattern-motion responses in human visual cortex. Nat Neurosci 2002; 5(1): 72-5.

Humphrey NK. Vision in a monkey without striate cortex: A case study. Perception. 1974; 3(3): 241–255.

Huxlin K, Martin T, Kelly K, Riley M, Friedman D, Burgin WS et al. Perceptual relearning of complex visual motion after V1 damage in humans. J Neurosci. 2009; 29: 3981-91.

Huxlin KR, Pasternak T. Training-induced recovery of visual motion perception after extrastriate cortical damage in the adult cat. Cerebral Cortex. 2004; 14: 81–90.

Huxlin KR. Perceptual plasticity in damaged adult visual systems. Vision Res. 2008; 48(20): 2154-66.

Ishiai S, Furukawa T, Tsukagoshi H. Eye-fixation patterns in homonymous hemianopia and unilateral spatial neglect. Neuropsychologia. 1987; 25: 675–9.

Itti L, Koch C. A saliency-based search mechanism for overt and covert shifts of visual attention. Vision Res. 2000; 40 (10-12):1489-506.

Jacquin-Courtois S, Bays PM, Salemme R, Leff AP, Husain M. Rapid compensation of visual search strategy in patients with chronic visual field defects, Cortex. 2012; doi: 10.1016/j.cortex.2012.03.025

Jagadeesh B, Chelazzi L, Mishkin M, Desimone R. Learning increases stimulus salience in anterior inferior temporal cortex of the macaque. J Neurophys. 2001; 86: 290–303.

Jayakumar J, Roy S, Dreher B, Martin PR, Vidyasagar TR. Multiple pathways carry signals from short-wavelength-sensitive ('blue') cones to the middle temporal area of the macaque. J Physiol. 2013; 591(1): 339-52.

Jenkinson M, Bannister P, Brady JM, Smith SM. Improved Optimisation for the Robust and Accurate Linear Registration and Motion Correction of Brain Images. NeuroImage 2002; 17(2): 825-841.

Jenkinson M, Smith SM. A global optimisation method for robust affine registration of brain images. Medical Image Analysis 2001; 5(2): 143-156.

Jiang Y, He S. Cortical responses to invisible faces: dissociating subsystems for facial-information processing. Curr Biol. 2006; 16(20): 2023-9.

Johansen-Berg H. Behavioural relevance of variation in white matter microstructure. Curr. Opin. Neurol. 2010. 23, 351–358.

Jones DK, Knösche R, Turner R. White matter integrity, fiber count, and other fallacies: The do's and don'ts of diffusion MRI. NeuroImage. 2013; 73: 239–254.

Jones DK, Lythgoe D, Horsfield MA, Simmons A, Williams SC, Markus HS. Characterization of white matter damage in ischemic leukoaraiosis with diffusion tensor MRI. Stroke. 1999; 30(2):393-7.

Jones, DK. Challenges and limitations of quantifying connectivity in the human brain in vivo with diffusion MRI. Imaging Med. 2010; 2: 341–355.

Kamitani Y, Tong F. Decoding the visual and subjective contents of the human brain. Nat Neurosci. 2005; 8(5): 679-85.

Kanwisher N, McDermott J, Chun MM. The fusiform face area: a module in human extrastriate cortex specialized for face perception. J. Neurosci. 1997; 11, 4302–4311.

Kaplan E. The M, P and K pathways of the Primate Visual System revisited. Chapter in: New Visual Neuroscience, (Werner J and Chalupa L, Eds), 2012, MIT Press

Kasten E, Sabel BA. Visual field enlargement after computer training in brain-damaged patients with homonymous deficits: an open pilot trial. Restor Neurol Neurosci. 1995; 8: 113-27.

Kasten E, Strasburger H, Sabel BA. Programs for diagnosis and therapy of visual field deficits in vision rehabilitation, Spat Vis. 1997; 10: 499-503.

Kasten E, Wüst S, Behrens-Baumann W, Sabel BA. Computer-based training for the treatment of partial blindness. Nat Med. 1998; 9: 1083-7.

Kastner S, O'Connor DH, Fukui MM, Fehd HM, Herwig U, Pinsk MA. Functional imaging of the human lateral geniculate nucleus and pulvinar. J Neurophysiol. 2004; 91(1):438-48.

Kato R, Takaura K, Ikeda T, Yoshida M, Isa T. Contribution of the retino-tectal pathway to visually guided saccades after lesion of the primary visual cortex in monkeys. Eur J Neurosci 2011; 33(11): 1952-60.

Kay K, Winawer J, Mezer A, Wandell B. Compressive spatial summation in human visual cortex. J Neurophysiolog 2013; 110, 481-494.

Kentridge RW, Heywood CA, Weiskrantz L. Attention without awareness in blindsight. Proc Biol Sci. 1999a; 266(1430): 1805-11.

Kentridge RW, Heywood CA, Weiskrantz L. Effects of temporal cueing on residual visual discrimination in blindsight. Neuropsychologia. 1999b; 37(4): 479-83.

Kentridge RW, Heywood CA, Weiskrantz L. Residual Vision in Multiple Retinal Locations within a Scotoma: Implications for Blindsight. J Cogn Neurosci. 1997; 9(2): 191-202.

Kentridge RW, Heywood CA. The status of blindsight. Near-threshold vision, islands of cortex, and the Riddoch phenomenon. J Conscious. Studies. 1999, 6(5): 3–11

Keshavan MS, Diwadkar VA, DeBellis M, Dick E, Kotwal R, Rosenberg DR, Sweeney JA, Minshew N, Pettegrew JW. Development of the corpus callosum in childhood, adolescence and early adulthood. Life Sci. 2002; 70(16): 1909-22.

Kleiner M, Brainard DH, Pelli D. What's new in Psychtoolbox-3? Perception 2007; 36, ECVP Abstract Supplement.

Kruggel F, von Cramon DY. Temporal properties of the hemodynamic response in functional MRI. Hum Brain Mapp. 1999; 8(4): 259-71.

Kwong KK, Belliveau JW, Chesler DA, Goldberg IE, Weisskoff RM, Poncelet BP, Kennedy DN, Hoppel BE, Cohen MS, Turner R, et al. Dynamic magnetic resonance imaging of human brain activity during primary sensory stimulation.

Proc Natl Acad Sci U S A. 1992; 89(12): 5675-9.

Lachica EA, Casagrande VA. The morphology of collicular and retinal axons ending on small relay (W-like) cells of the primate lateral geniculate nucleus. Vis Neurosci. 1993; 10(3): 403-18

Lane AR, Smith DT, Ellison A, Schenk T. Visual exploration training is no better than attention training for treating hemianopia. Brain. 2010; 133: 1717–1728.

Le Bihan D, and Johansen-Berg H. Diffusion MRI at 25: Exploring brain tissue structure and function. Neuroimage. 2012; 61(2): 324–341.

Le Bihan D, Breton E. Imagerie de diffusion in vivo par résonance magnétique nucléaire. C R Acad Sci Paris. 1985; T.301, II:1109–1112.

Lee BB, Creutzfeldt OD, Elepfandt A. The responses of magno- and parvocellular cells of the monkey's lateral geniculate body to moving stimuli. Exp Brain Res. 1979; 35(3): 547-57.

Leh SE, Chakravarty MM, Ptito A. The connectivity of the human pulvinar: a diffusion tensor imaging tractography study. Int J Biomed Imaging. 2008; doi: 10.1155/2008/789539.

Leh SE, Johansen-Berg H, Ptito A. Unconscious vision: new insights into the neuronal correlate of blindsight using diffusion tractography. Brain. 2006; 129: 1822–1832.

Leh SE, Ptito A, Schönwiesner M, Chakravarty MM, Mullen KT. Blindsight mediated by an S-cone-independent collicular pathway: an fMRI study in hemispherectomized subjects. J Cogn Neurosci. 2010; 22(4): 670-82.

Leopold DA. Primary visual cortex: awareness and blindsight. Annu Rev Neurosci 2012; 35, 91-109.

Lin C, Wagor E, Kaas JH. Projections from the pulvinar to the middle temporal visual area (MT) in the owl monkey (Aotus trivirgatus). Brain Res 1974; 76, 145-149.

Lin Z, He S. Seeing the invisible: the scope and limits of unconscious processing in binocular rivalry. Prog Neurobiol. 2009; 87(4): 195-211.

Liu Z. Perceptual learning in motion discrimination that generalizes across motion directions. PNAS USA. 1999; 96: 14085–14087.

Livingstone MS, Hubel DH. Thalamic inputs to cytochrome oxidase-rich regions in monkey visual cortex. Proc Natl Acad Sci. 1982; 79(19):6098-101.

Logothetis NK, Schall JD. Neuronal correlates of subjective visual perception. Science. 1989; 245(4919): 761-3.

Lyon DC, Nassi J, Callaway EM. A Disynaptic Relay from Superior Colliculus to Dorsal Stream Visual Cortex in Macaque Monkey. Neuron. 2010; 65(2): 270–279.

Maier A, Logothetis NK, Leopold DA. Context-dependent perceptual modulation of single neurons in primate visual cortex. Proc Natl Acad Sci. 2007;104(13):5620-5.

Malikovic A, Amunts K, Schleicher A, Mohlberg H, Eickhoff SB, Wilms M, Palomero-Gallagher N, Armstrong E, Zilles K. Cytoarchitectonic analysis of the human extrastriate cortex in the region of V5/MT+: a probabilistic, stereotaxic map of area hOc5. Cereb Cortex. 2007; 17(3): 562-74.

Marcel AJ. Blindsight and shape perception: deficit of visual consciousness or of visual function? Brain. 1998; 121 (8): 1565-88.

Marrocco RT, Li RH. Monkey superior colliculus: properties of single cells and their afferent inputs. J Neurophysiol. 1977; 40(4): 844-60.

Martin T, Riley ME, Kelly KN, Hayhoe M, Huxlin KR. Visually-guided behavior of homonymous hemianopes in a naturalistic task. Vision Res. 2007; 47: 3434–3446.

Marzi CA, Tassinari G, Aglioti S, Lutzemberger L. Spatial summation across the vertical meridian in hemianopics: a test of blindsight. Neuropsychologia. 1986; 24(6): 749-58.

Maunsell JH, Nealey TA, DePriest DD. Magnocellular and parvocellular contributions to responses in the middle temporal visual area (MT) of the macaque monkey. J Neurosci. 1990; 10(10):3323-34.

Maunsell JH, Van Essen DC. The connections of the middle temporal visual area (MT) and their relationship to a cortical hierarchy in the macaque monkey. J Neurosci 1983; 3(12): 2563-86.

Mazaika P. Percent Signal Change for fMRI calculations. 2009. Unpublished Tech Report. http://cibsr.stanford.edu/documents/FMRIPercentSignalChange.pdf

Mazzi C, Mancini F, Savazzi S. Can IPS reach visual awareness without V1? Evidence from TMS in healthy subjects and hemianopic patients. Neuropsychologia. 2014; 64C: 134-144.

McCarthy G, Puce A, Gore JC, Allison T. Face-specific processing in the human fusiform gyrus. J. Cogn. Neurosci. 1997; 5, 605–610.

McKeefry DJ, Watson JD, Frackowiak RS, Fong K, Zeki S. The activity in human areas V1/V2, V3, and V5 during the perception of coherent and incoherent motion. Neuroimage 1997; 5(1): 1-12.

Meienberg O, Zangemeister WH, Rosenberg M, Hoyt WF, Stark L. Saccadic eye movement strategies in patients with homonymous hemianopia. Ann Neurol. 1981; 9: 537–44.

Millington RS, Yasuda CL, Jindahra P, Jenkinson M, Barbur JL, Kennard C, Cendes F, Plant GT, Bridge H. Quantifying the pattern of optic tract degeneration in human hemianopia. J Neurol Neurosurg Psychiatry. 2014; 85(4):379-86.

Milner AD, Goodale MA. The visual brain in action. 1995. Oxford University Press.

Mohler CW, Wurtz RH. Role of striate cortex and superior colliculus in visual guidance of saccadic eye movements in monkeys. J Neurophysiol. 1977; 40(1): 74-94.

Morland AB, Jones SR, Finlay AL, Deyzac D, Le S, Kemp S. Visual perception of motion, luminance and colour in a human hemianope. Brain. 1999; 122: 1183–1198.

Morland AB, Lê S, Carroll E, Hoffmann MB, Pambakian A. The role of spared calcarine cortex and lateral occipital cortex in the responses of human hemianopes to visual motion. J Cogn Neurosci. 2004; 16(2): 204-18.

Morris JS, DeGelder B, Weiskrantz L, Dolan RJ: Differential extrageniculostriate and amygdala responses to presentation of emotional faces in a cortically blind field. Brain 2001, 124:1241-1252.

Movshon JA, Newsome WT . Visual response properties of striate cortical neurons projecting to area MT in macaque monkeys. J Neurosci. 1996; 16:7733–7741.

Mumford J. A guide to calculating percent change with featquery. 2007. Unpublished Tech Report. http://mumford.bol.ucla.edu/perchange_guide.pdf

Nakamura H, Kashii S, Nagamine T, Matsui Y, Hashimoto T, Honda Y et al. Human V5 demonstrated by magnetoencephalography using random dot kinematograms of different coherence levels. Neurosci Res 2003; 46(4): 423-33.

Nelles G, de Greiff A, Pscherer A, Forsting M, Gerhard H, Esser J et al. Cortical activation in hemianopia after stroke. Neurosci Lett 2007; 426(1): 34-8.

Nelles G, Esser J, Eckstein A, Tiede A, Gerhard H, Diener H. Compensatory visual field training in recovery from hemianopia after stroke. Neurosci Lett. 2001; 306:192–198.

Nelles G, Widman G, de Greiff A, Meistrowitz A, Dimitrova A, Weber J, Forsting M, Esser J, Diener HC. Brain representation of hemifield stimulation in poststroke visual field defects. Stroke. 2002; 33(5):1286-93.

Newsome WT, Paré, EB. A selective impairment of motion perception following lesions of the middle temporal visual area (MT). J Neurosci 1988; 8(6): 2201-11.

Ong Y-H, Brown MM, Robinson P, Plant GT, Husain M, Leff AP. Read-Right: a ‘‘web app’’ that improves reading speeds in patients with hemianopia. J Neurol. 2012; 259(12): 2611-5.

Oosterhof NN, Todorov A. The functional basis of face evaluation. Proc Natl Acad Sci U S A. 2008; 105(32): 11087-92.

Pambakian ALM, Mannan SK, Hodgson TL, Kennard C. Saccadic visual search training: a treatment for patients with homonymous hemianopia. J Neurol Neurosurg Psychiatry. 2004; 75: 1443–1448.

Pambakian ALM, Wooding DS, Patel N, Morland AB, Kennard C, Mannan SK. Scanning the visual world: a study of patients with homonymous hemianopia. J Neurol Neurosurg Psychiatry. 2000; 69: 751–759.

Panagiotaropoulos TI, Deco G, Kapoor V, Logothetis NK. Neuronal discharges and gamma oscillations explicitly reflect visual consciousness in the lateral prefrontal cortex. Neuron. 2012; 74(5):924-35.

Park S, Chun MM. Different roles of the parahippocampal place area (PPA) and retrosplenial cortex (RSC) in panoramic scene perception. Neuroimage. 2009 ; 47(4): 1747-56.

Pasik P, Pasik T, Schilder P. Extrageniculostriate vision in the monkey: discrimination of luminous flux-equated figures. Exp Neurol. 1969; 24:421–437.

Payne BR, Lomber SG, Macneil MA, Cornwell P. Evidence for greater sight in blindsight following damage of primary visual cortex early in life. Neuropsychologia. 1996; 34(8): 741-774.

Pegna AJ, Khateb A, Lazeyras F, Seghier ML: Discriminating emotional faces without primary visual cortices involves the right amygdala. Nat Neurosci 2005, 8:24-25.

Peli E. Field Expansion for Homonymous Hemianopia by Optically Induced Peripheral Exotropia. Opt and Vision Sci. 2000; 77: 453-64.

Perenin MT, Rossetti Y. Grasping without form discrimination in a hemianopic field. Neuroreport. 1996; 7(3):793-7.

Perez C, Peyrin C, Cavézian C, Coubard O, Caetta F, Raz N, Levin N, Doucet G, Andersson F, Obadia M, Gout O, Héran F, Savatovsky J, Chokron S. An FMRI investigation of the cortical network underlying detection and categorization abilities in hemianopic patients. Brain Topogr. 2013; 26(2):264-77.

Perry VH, Oehler R, Cowey A. Retinal ganglion cells that project to the dorsal lateral geniculate nucleus in the macaque monkey. Neuroscience. 1984; 12:1101–1123.

Pestilli F, Yeatman JD, Rokem A, Kay KN, Wandell BA. Evaluation and statistical inference for human connectomes. Nat Methods. 2014; 11(10):1058-63.

Peters A, Payne BR, Budd J. A numerical analysis of the geniculocortical input to striate cortex in the monkey. Cereb Cortex. 1994; 4(3):215-29.

Pierpaoli C, Basser PJ. Toward a quantitative assessment of diffusion anisotropy. Magn. Reson. Med. 1996; 36, 893–906.

Polonara G, Salvolini S, Fabri M, Mascioli G, Cavola GL, Neri P et al. Unilateral visual loss due to ischaemic injury in the right calcarine region: a functional magnetic resonance imaging and diffusion tension imaging follow-up study. Int Ophthalmol. 2011; 31: 129–134.

Powell HW, Parker GJ, Alexander DC, Symms MR, Boulby PA, Wheeler-Kingshott CA, Barker GJ, Koepp MJ, Duncan JS. MR tractography predicts visual field defects following temporal lobe resection. Neurology. 2005; 65(4): 596-9.

Previc FH, Liotti M, Blakemore C, Beer J, Fox P. Functional imaging of brain areas involved in the processing of coherent and incoherent wide field-of-view visual motion. Exp Brain Res 2000; 131(4): 393-405.

Priebe NJ, Lisberger SG, Movshon JA. Tuning for spatiotemporal frequency and speed in directionally selective neurons of macaque striate cortex. J Neurosci. 2006; 26(11):2941-50.

Raemaekers M, Bergsma DP, van Wezel RJ, van der Wildt GJ, van den Berg AV. Effects of vision restoration training on early visual cortex in patients with cerebral blindness investigated with functional magnetic resonance imaging. J Neurophysiol, 2011; 105: 872-82.

Raiguel S, Van Hulle MM, Xiao DK, Marcar VL, Orban GA. Shape and spatial distribution of receptive fields and antagonistic motion surrounds in the middle temporal area (V5) of the macaque. Eur J Neurosci 1995; 7(10): 2064-82.

Raninen A, Vanni S, Hyvarinen L, Nasanen R. Temporal sensitivity in a hemianopic visual field can be improved by long-term training using flicker stimulation. J Neurol Neurosurg Psychiatry. 2007; 78: 66–73.

Raposo N, Cauquil AS, Albucher JF, Acket B, Celebrini S, Pariente J et al. Poststroke

Conscious Visual Deficit: Clinical Course and Changes in Cerebral Activations. Neurorehabilitation and Neural Repair. 2011; 25: 703 –710.

Rees G, Friston K, Koch C. A direct quantitative relationship between the functional properties of human and macaque V5. Nat Neurosci 2000; 3(7): 716-23.

Reinhard J, Schreiber A, Schiefer U, Kasten E, Sabel BA, Kenkel S et al. Does visual restitution training change absolute homonymous visual field defects? A fundus controlled study. Br J Ophthalmol. 2005; 89: 30-5.

Reppas JB, Niyogi S, Dale AM, Sereno MI, Tootell RB. Representation of motion boundaries in retinotopic human visual cortical areas. Nature 1997; 388(6638): 175-9.

Riddoch G. On the Relative Perceptions of Movement and a Stationary Object in Certain Visual Disturbances due to Occipital Injuries. Proc R Soc Med. 1917; 10:13-34.

Rizzo M, Robin DA. Bilateral effects of unilateral visual cortex lesions in human. Brain. 1996; 119 (3):951-63.

Robinson DL, Petersen SE. The pulvinar and visual salience. Trends Neurosci. 1992; 15(4): 127-32.

Rodman HR, Albright TD. Coding of visual stimulus velocity in area MT of the macaque. Vision Res. 1987; 27(12):2035-48.

Rodman HR, Gross CG, Albright TD. Afferent basis of visual response properties in area MT of the macaque. I. Effects of striate cortex removal. J Neurosci. 1989; 9(6): 2033-50.

Rodman HR, Gross CG, Albright TD. Afferent basis of visual response properties in area MT of the macaque. II. Effects of superior colliculus removal. J Neurosci. 1990; 10(4): 1154-64.

Rodman HR, Gross CG, Albright TD. Responses of neurons in visual area MT after removal of the superior colliculus. Neurosci Abstr 1986; 12, 1369.

Rodman HR, Sorenson KM, Shim AJ, Hexter DP. Calbindin immunoreactivity in the geniculo-extrastriate system of the macaque: implications for heterogeneity in the koniocellular pathway and recovery from cortical damage. J Comp Neurol; 2001. 431(2):168-81.

Rossion B, de Gelder B, Pourtois G, Guérit JM, Weiskrantz L. Early extrastriate activity without primary visual cortex in humans. Neurosci Lett. 2000; 279(1): 25-8.

Rossion B, Pourtois G. Revisiting Snodgrass and Vanderwart's object pictorial set: the role of surface detail in basic-level object recognition. Perception. 2004; 33(2): 217-36.

Roth T, Sokolov AN, Messias A, Roth P, Weller M, Trauzettel-Klosinski S. Comparing explorative saccade and flicker training in hemianopia: A randomized controlled study. Neurology. 2009; 72: 324-31.

Rotshtein, P, Henson, RN, Treves, A, Driver, J, Dolan, RJ. Morphing Marilyn into Maggie dissociates physical and identity face representations in the brain. Nature Neuro; 2005; 8(1): 107–113.

Rottschy C, Eickhoff SB, Schleicher A, Mohlberg H, Kujovic M, Zilles K, Amunts K. Ventral visual cortex in humans: cytoarchitectonic mapping of two extrastriate areas. Hum Brain Mapp. 2007; 28(10):1045-59.

Rust NC, Mante V, Simoncelli EP, Movshon JA. How MT cells analyze the motion of visual patterns. Nat Neurosci 2006; 9(11): 1421-31.

Sahraie A, Macleod MJ, Trevethan CT, Robson SE, Olson JA, Callaghan P et al.

Improved detection following Neuro-Eye Therapy in patients with post-geniculate brain damage. Exp Brain Res. 2010; 206: 25-34.

Sahraie A, Trevethan CT, MacLeod MJ, Murray AD, Olson JA, Weiskrantz L. Increased sensitivity after repeated stimulation of residual spatial channels in blindsight. Proc Natl Acad Sci U S A. 2006; 103(40): 14971-6.

Sahraie A, Trevethan CT, Macleod MJ, Weiskrantz L, Hunt AR. The continuum of detection and awareness of visual stimuli within the blindfield: from blindsight to the sighted-sight. Invest Ophthalmol Vis Sci. 2013; 54(5): 3579-85.

Sahraie A, Trevethan CT, MacLeod MJ. Temporal properties of spatial channel of processing in hemianopia. Neuropsychologia. 2008; 46: 879–885.

Sahraie A, Trevethan CT, Weiskrantz L, Olson J, MacLeod MJ, Murray AD, Dijkhuizen RS, Counsell C, Coleman R. Spatial channels of visual processing in cortical blindness. Eur J Neurosci. 2003; 18(5):1189-96.

Sahraie A, Weiskrantz L, Barbur JL, Simmons A, Williams SC, Brammer MJ. Pattern of neuronal activity associated with conscious and unconscious processing of visual signals. Proc Natl Acad Sci. 1997; 94(17):9406-11.

Salat DH et al. Age-related alterations in white matter microstructure measured by diffusion tensor imaging. Neurobiol Aging. 2005; 26(8): 1215–1227.

Schadow J, Dettler N, Paramei GV, Lenz D, Fründ I, Sabel BA, Herrmann CS. Impairments of Gestalt perception in the intact hemifield of hemianopic patients are reflected in gamma-band EEG activity. Neuropsychologia. 2009; 47(2):556-68.

Schiller PH, Stryker M, Cynader M, Berman N. Response characteristics of single cells in the monkey superior colliculus following ablation or cooling of visual cortex. J Neurophysiol. 1974; 37(1): 181-94.

Schlegel D, Kolb SJ, Luciano JM, Tovar JM, Cucchiara BL, Liebeskind DS et al. Utility of the NIH Stroke Scale as a Predictor of Hospital Disposition. Stroke. 2003; 34: 134-137.

Schmid MC, Mrowka SW, Turchi J, Saunders RC, Wilke M, Peters AJ et al. Blindsight depends on the lateral geniculate nucleus. Nature. 2010; 466: 373-377.

Schmid MC, Panagiotaropoulos T, Augath MA, Logothetis NK, Smirnakis SM. Visually driven activation in macaque areas V2 and V3 without input from the primary visual cortex. PLoS One. 2009; 4(5):e5527.

Schmid MC, Schmiedt JT, Peters AJ, Saunders RC, Maier A, Leopold DA. Motion-sensitive responses in visual area V4 in the absence of primary visual cortex. J Neurosci. 2013; 33(48): 18740-5.

Schneider KA, Kastner S. Visual responses of the human superior colliculus: a high-resolution functional magnetic resonance imaging study. J Neurophysiol. 2005; 94(4):2491-503.

Schneider KA, Richter MC, Kastner S. Retinotopic organization and functional subdivisions of the human lateral geniculate nucleus: a high-resolution functional magnetic resonance imaging study. J Neurosci. 2004; 24(41):8975-85.

Schoenfeld MA, Noesselt T, Poggel D, Tempelmann C, Hopf JM, Woldorff MG, Heinze HJ, Hillyard SA. Analysis of pathways mediating preserved vision after striate cortex lesions. Ann Neurol. 2002; 52(6):814-24.

Schreiber A, Vonthein R, Reinhard J, Trauzettel-Klosinski S, Connert C, Schiefer U. Effect of visual restitution training on absolute homonymous scotomas. Neurology. 2006; 67: 143–145.

Schuett S, Heywood CA, Kentridge RW, Zihl J. The significance of visual information processing in reading: Insights from hemianopic dyslexia. Neuropsychologia. 2008; 46: 2445–2462.

Sclar G, Maunsell JH, Lennie P. Coding of image contrast in central visual pathways of the macaque monkey. Vision Res. 1990; 30(1):1-10.

Shadlen M, Carney T. Mechanisms of human motion perception revealed by a new cyclopean illusion. Science 1986; 232(4746): 95-7.

Sheinberg, DL, and Logothetis, NK. The role of temporal cortical areas in perceptual organization. Proc. Natl. Acad. Sci. USA. 1997; 94: 3408–3413.

Sherbondy AJ, Dougherty RF, Ben-Shachar M, Napel S, Wandell BA. ConTrack: Finding the most likely pathways between brain regions using diffusion tractography. J Vis. 2008; 8(9): 15.1–16.

Shostak Y, Ding Y, Mavity-Hudson J, Casagrande VA. Cortical synaptic arrangements of the third visual pathway in three primate species: Macaca mulatta, Saimiri sciureus, and Aotus trivirgatus. J Neurosci. 2002; 22(7):2885-93.

Siegel M, Donner TH, Oostenveld R, Fries P, Engel AK. High-frequency activity in human visual cortex is modulated by visual motion strength. Cereb Cortex 2007; 17(3): 732-41.

Silvanto J, Cowey A, Lavie N, Walsh V. Making the blindsighted see. Neuropsychologia. 2007; 45(14):3346-50.

Silvanto J, Cowey A, Lavie N, Walsh V. Striate cortex (V1) activity gates awareness of motion. Nat Neurosci 2005a; 8(2): 143-144.

Silvanto J, Lavie N, Walsh V. Double dissociation of V1 and V5/MT activity in visual awareness. Cereb Cortex 2005b; 15: 1736-1741.

Silvanto J, Walsh V, Cowey A. Abnormal functional connectivity between ipsilesional V5/MT+ and contralesional striate cortex (V1) in blindsight. Exp Brain Res. 2009; 193:645–650.

Simoncelli EP, Heeger DJ. A model of neuronal responses in visual area MT Vision Res 1998; 38(5): 743-61.

Sincich LC, Park KF, Wohlgemuth MJ, Horton JC. Bypassing V1: a direct geniculate input to area MT. Nat Neurosci. 2004; 7(10): 1123-8.

Smith AT, Wall MB, Williams AL, Singh KD. Sensitivity to optic flow in human cortical areas MT and MST. Eur J Neurosci 2006; 23(2): 561-9.

Smith J). Homonymous hemianopia, a review of one hundred cases. Amer. J. Ophthol. 1962; 54: 616- 623.

Smith SM, Jenkinson M, Johansen-Berg H, Rueckert D, Nichols TE, Mackay CE, Watkins KE, Ciccarelli O, Cader MZ, Matthews PM, Behrens TE. Tract-based spatial statistics: voxelwise analysis of multi-subject diffusion data. Neuroimage. 2006; 31(4):1487-505.

Smith SM. Fast robust automated brain extraction. Human Brain Mapping 2002; 17(3): 143-155.

Snow JC, Allen HA, Rafal RD, Humphreys GW. Impaired attentional selection following lesions to human pulvinar: evidence for homology between human and monkey. Proc Natl Acad Sci U S A. 2009; 106(10): 4054-9.

Snowden RJ, Treue S, Andersen RA. The response of neurons in areas V1 and MT of the alert rhesus monkey to moving random dot patterns. Exp Brain Res 1992; 88(2): 389-400.

Snowden RJ, Treue S, Erickson RG, Andersen RA. The response of area MT and V1 neurons to transparent motion. J Neurosci 1991; 11(9): 2768-85.

Sorenson JA, Wang X. Problems in estimating hemodynamic response parameters from fMRI data. Human Brain Mapping. 1996; 4(4): 265–272.

Spitzyna GA, Wise RJ, McDonald SA, Plant GT, Kidd D, Crewes H et al. Optokinetic therapy improves text reading in patients with hemianopic alexia: A controlled trial. Neurology. 2007; 68: 1922-30.

Sterling P, Wickelgren BG. Visual receptive fields in the superior colliculus of the cat. J Neurophysiol. 1969; 32(1): 1-15.

Sterzer P, Haynes JD, Rees G. Fine-scale activity patterns in high-level visual areas encode the category of invisible objects. J Vis. 2008; 8(15):10, 1-12.

Stoerig P, Barth E. Low-level phenomenal vision despite unilateral destruction of primary visual cortex. Conscious Cogn. 2001; 10(4): 574-87.

Stoerig P, Kleinschmidt A, Frahm J. No visual responses in denervated V1: high-resolution functional magnetic resonance imaging of a blindsight patient. Neuroreport. 1998; 9: 21-5.

Stoerig P. Blindsight, conscious vision, and the role of primary visual cortex. Prog Brain Res. 2006; 155: 217-34

Stoerig P. Functional rehabilitation of partial cortical blindness? Restor Neurol Neurosci. 2008; 26: 291-303.

Striemer CL, Chapman CS, Goodale MA. ‘‘Real-time’’ obstacle avoidance in the absence of primary visual cortex. PNAS. 2009; 106: 15996–16001.

Szmajda BA, Grunert U, Martin PR; Retinal ganglion cell inputs to the koniocellular pathway. J Comp Neurol. 2008; 510: 251–268.

Talairach J and Tournoux P. Co-Planar Stereotactic Atlas of the Human Brain. New York: Thieme, 1988.

Tamietto M, Pullens P, de Gelder B, Weiskrantz L, Goebel R. Subcortical connections to human amygdala and changes following destruction of the visual cortex. Curr Biol. 2012; 22(15): 1449-55.

Tanaka K, Hikosaka K, Saito H, Yukie M, Fukada Y, Iwai E. Analysis of local and wide-field movements in the superior temporal visual areas of the macaque monkey. J Neurosci 1986; 6(1): 134-44.

Tiel K, Kolmel H. Patterns of recovery from homonymous hemianopia subsequent to infarction in the distribution of the posterior cerebral artery. Neuro-ophthalmology. 1991; 11: 33-39.

Tinelli F, Cicchini GM, Arrighi R, Tosetti M, Cioni G, Morrone MC. Blindsight in children with congenital and acquired cerebral lesions. Cortex. 2013; 49(6): 1636-47

Tomaiuolo F, Ptito M, Marzi CA, Paus T, Ptito A. Blindsight in hemispherectomized patients as revealed by spatial summation across the vertical meridian. Brain. 1997; 120 (5): 795-803.

Tong F. Primary visual cortex and visual awareness. Nat Rev Neurosci. 2003; 4(3): 219-29.

Tootell RB, Hamilton SL, Switkes E. Functional anatomy of macaque striate cortex. IV. Contrast and magno-parvo streams. J Neurosci. 1988; 8(5):1594-609.

Tootell RB, Reppas JB, Kwong KK, Malach R, Born RT, Brady TJ, Rosen BR, Belliveau JW. Functional analysis of human MT and related visual cortical areas using magnetic resonance imaging. J Neurosci. 1995; 15:3215–3230.

Tournier JD, Calamante F, Connelly A. MRtrix: diffusion tractography in crossing fibre regions. Int J Imag Sci Technol 2012;22:53-66.

Trauzettel-Klosinski S. Current Methods of Visual Rehabilitation. Dtsch Arztebl Int. 2011; 108: 871–8.

Trauzettel-Klosinski S. Improving vision in a patient with homonymous hemianopia. J Neuroophthalmol. 2005; 25: 143-149.

Trevethan CT, Sahraie A, Weiskrantz L. Form discrimination in a case of blindsight. Neuropsychologia. 2007a; 45(9): 2092-103.

Trevethan CT, Sahraie A, Weiskrantz L. Can blindsight be superior to 'sighted-sight'? Cognition. 2007b; 103(3): 491-501.

Trobe JD, Lorber ML, Schlezinger NS. Isolated homonymous hemianopia. A review of 104 cases. Arch Ophthalmol. 1973; 89: 377-81.

Trojanowski J, Jacobson S. Areal and laminar distribution of some pulvinar cortical efferents in rhesus monkey. J Comp Neurol 1976; 140, 155-174.

Tsang JM, Dougherty RF, Wandell BA. Tract alignment errors decrease detection power in group analyses of diffusion data with TBSS. SfN. 2010; San Diego, CA.

Tsui JM, Pack CC. Contrast sensitivity of MT receptive field centers and surrounds. J Neurophysiol 2011; 106(4): 1888-900.

Turner BH, Mishkin M, Knapp M. Organization of the amygdalopetal projections from modality-specific cortical association areas in the monkey. Journal Comp. Neurol. 1990; 191: 515-543.

Ungerleider LG, Christensen CA. Pulvinar lesions in monkeys produce abnormal eye movements during visual discrimination training. Brain Res. 1977; 136(1): 189-96.

Ungerleider LG, Christensen CA. Pulvinar lesions in monkeys produce abnormal scanning of a complex visual array. Neuropsychologia. 1979; 17(5): 493-501.

Ungerleider LG, Desimone R, Galkin TW, Mishkin M. Subcortical projections of area MT in the macaque. J Comp Neurol. 1984; 223(3):368-86.

Ungerleider LG, Mishkin M. Two cortical visual systems. In Analysis of visual behaviour, (ed. Ingle DJ, Goodale MA, Mansfield RJW), pp. 549-586. 1982. MIT Press, Cambridge, MA.

Van Essen DC, Newsome WT, Bixby JL. The pattern of interhemispheric connections and its relationship to extrastriate visual areas in the macaque monkey. J Neurosci. 1982; 2(3): 265-83.

Van Essen DC, Newsome WT, Maunsell JH. The visual field representation in striate cortex of the macaque monkey: asymmetries, anisotropies, and individual variability. Vision Res. 1984; 24(5): 429-48.

Van Essen, DC. Functional organization of primate visual cortex. In: Jones, E.G. and Peters, A. (Eds), Cerebral Cortex, Vol. 3. 1985; Plenum Press, New York, pp. 259-329.

VanRullen R. On second glance: still no high-level pop-out effect for faces. Vision Res. 2006; 46(18):3017-27.

Wang HX, Heeger DJ, Landy MS. Responses to second-order texture modulations undergo surround suppression. Vision Res 2012; 62: 192–200.

Warner CE, Goldshmit Y, Bourne JA. Retinal afferents synapse with relay cells targeting the middle temporal area in the pulvinar and lateral geniculate nuclei. Front Neuroanat. 2010; 4(8):1-16.

Weiskrantz L, Barbur JL, Sahraie A. Parameters affecting conscious versus unconscious visual discrimination with damage to the visual cortex (V1). Proc Natl Acad Sci U S A. 1995; 92(13): 6122-6.

Weiskrantz L, Warrington EK, Sanders MD, Marshall J. Visual capacity in the hemianopic field following a restricted occipital ablation. Brain. 1974; 97: 709-28.

Weiskrantz L. Consciousness and commentaries. In: Hameroff, S., Kaszniak, A. and Scott, A. (Eds.), Towards a Science of Consciousness II—The Second Tucson Discussion and Debates. 1998; MIT Press, Cambridge, MA, pp. 371–377.

Weiskrantz L. Residual vision in a scotoma. A follow-up study of 'form' discrimination. Brain. 1987; 110 (1): 77-92.

Weiskrantz L. Roots of blindsight. Prog Brain Res. 2004; 144: 229-41.

Werring DJ, Toosy AT, Clark CA, Parker GJ, Barker GJ, Miller DH, Thompson AJ. Diffusion tensor imaging can detect and quantify corticospinal tract degeneration after stroke. J Neurol Neurosurg Psychiatry. 2000; 69(2):269-72.

White AJ, Wilder HD, Goodchild AK, Sefton AJ, Martin PR. Segregation of receptive field properties in the lateral geniculate nucleus of a New-World monkey, the marmoset Callithrix jacchus. J Neurophysiol. 1998; 80(4):2063-76.

Xu X, Ichida JM, Allison JD, Boyd JD, Bonds AB, Casagrande VA; A comparison of koniocellular, magnocellular and parvocellular receptive field properties in the lateral geniculate nucleus of the owl monkey (Aotus trivirgatus). J Physiol. 2001; 531(1):203-18.

Yeatman JD, Dougherty RF, Myall NJ, Wandell BA, Feldman HM. Tract Profiles of White Matter Properties: Automating Fiber-Tract Quantification. PLoS One. 2012; 7(11): e49790.

Zeki S, ffytche DH. The Riddoch syndrome: insights into the neurobiology of conscious vision. Brain. 1998; 121: 25–45.

Zeki S, Watson JDG, Frackowiak RSJ. Going beyond the information given: The relation of illusory motion to brain activity. Proc R Soc Lond B Biol Sci. 1993; 252:215–222.

Zeki S. A vision of the brain. 1993. Blackwell Scientific Publications.

Zhang X, Kedar S, Lynn MJ, Newman NJ, Biousse V. Homonymous hemianopias. Clinical–anatomic correlations in 904 cases. Neurology. 2006a; 66: 906–910.

Zhang X, Kedar S, Lynn MJ, Newman NJ, Biousse V. Natural history of homonymous hemianopia. Neurology. 2006b; 66: 901–905.

Zihl J, von Cramon D. Registration of light stimuli in the cortically blind hemifield and its effect on localization. Behav Brain Res. 1980; 1(4):287-98.

Zihl J, von Cramon D. Restitution of visual field in patients with damage to the geniculostriate visual pathway. Hum Neurobiol. 1982; 1: 5-8.

Zihl J, Von Cramon D. Visual field recovery from scotoma in patients with postgeniculate damage. A review of 55 cases. Brain. 1985; 108: 335-365.

Zihl J. Visual scanning behavior in patients with homonymous hemianopia. Neuropsychologia. 1995; 33: 287-303.

Appendix A

Visual field perimetry.

Humphrey automated visual field perimetry results are presented for patients 1-11, and 13-16. For patient 12, the Goldman perimetry report is included.

1.

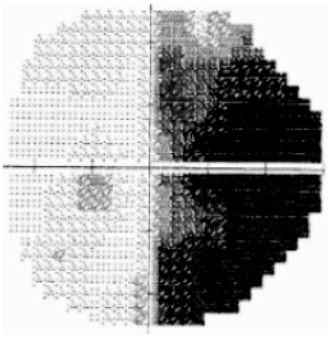

5.

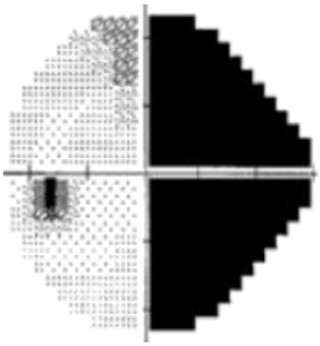

2.

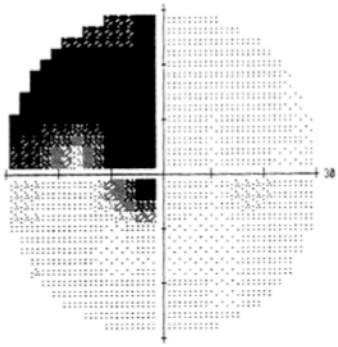

6.

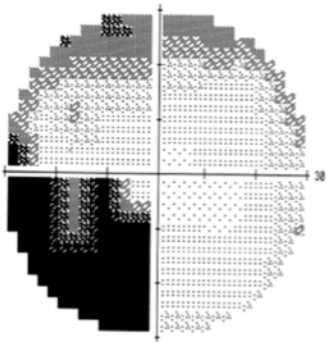

3.

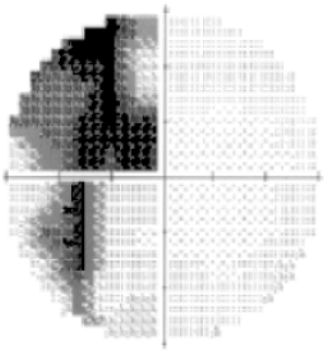

7.

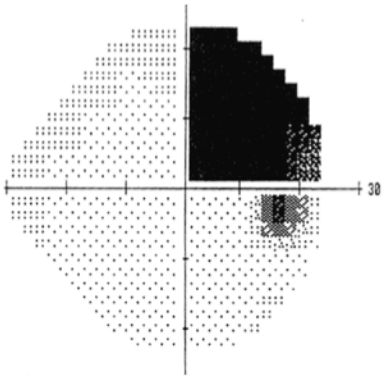

4.

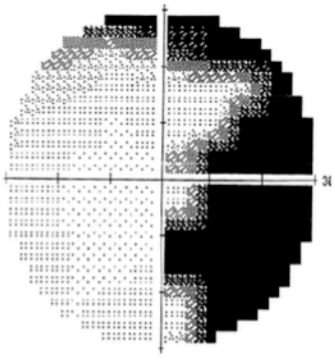

8.

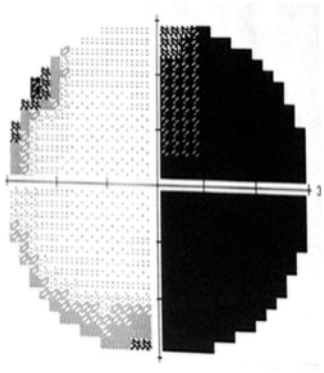

9.

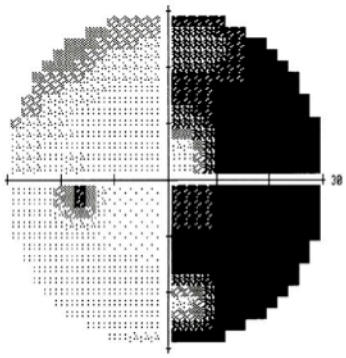

13.

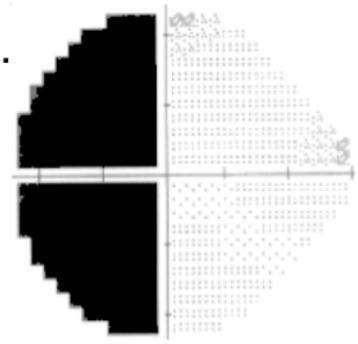

10.

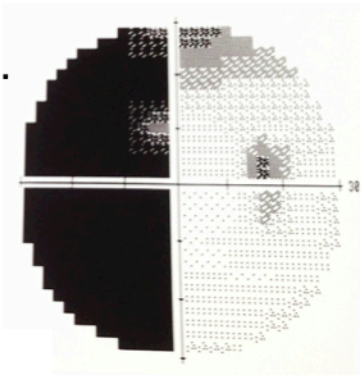

14.

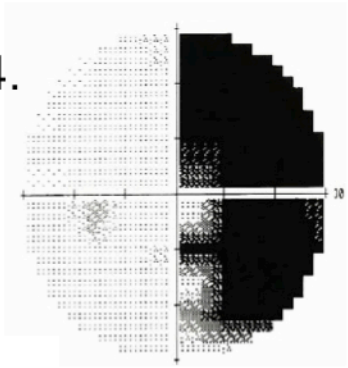

11.

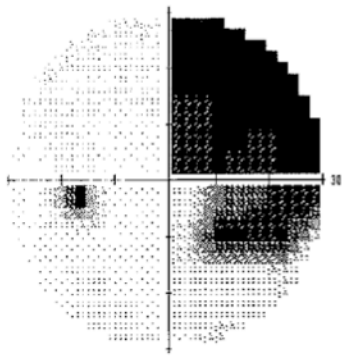

15.

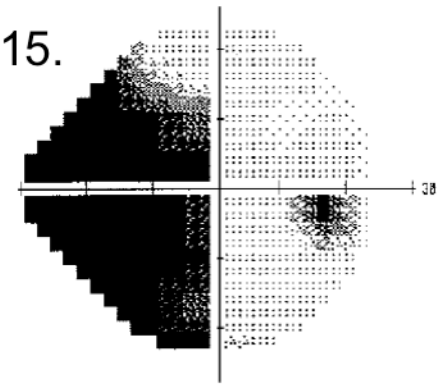

12.

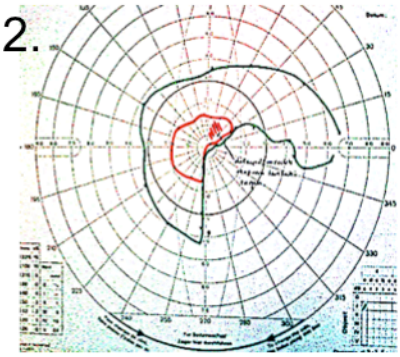

16.

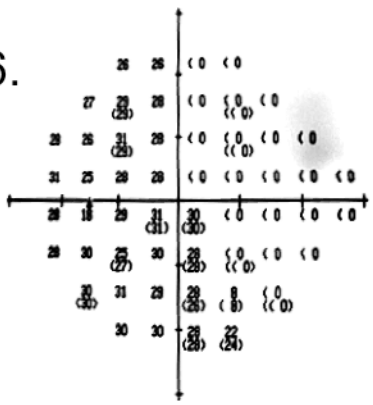

Appendix B

Additional patient details.

1. This patient underwent surgical resection of a benign meningioma in the left occipital lobe, resulting in a right homonymous hemianopia. The resection spared the lateral regions of the occipital lobe, including extrastriate cortex. Surgery was performed age 55 years, 21 years prior to taking part in this study. The patient took part in experiments described in Chapters 4 – 7.

2. This patient sustained a right occipito-temporal haemorrhage, resulting in a left homonymous hemianopia particularly affecting the upper quadrant. The damage occurred age 67 years, 6 months prior to first taking part in the study. This patient took part in experiments described in Chapters 3 – 8. For the rehabilitation study in Chapter 8, the patient (P4) was 18 months post-stroke at the start of training, and was assessed immediately pre and post-training.

3. This patient sustained a right posterior cerebral artery infarct, resulting in a left homonymous hemianopia particularly affecting the upper quadrant. The damage was mostly restricted to the right lingual gyrus, including a small portion of surrounding white matter. This occurred age 67 years, 16 months prior to taking part in the study. This patient took part in experiments described in Chapters 3 – 7.

4. This patient sustained a left posterior cerebral artery infarct extending to the left cerebellum, resulting in a right homonymous hemianopia but no other neurological deficit. The damage occurred age 54 years, 18 months prior to taking part in the study. This patient took part in experiments described in Chapters 3 – 8. For the rehabilitation study in Chapter 8, the patient (P1) was 23 months post-stroke at the start of training, and was assessed immediately pre and post-training.

5. This patient sustained an iatrogenic large left posterior circulation stroke, resulting in a right homonymous hemianopia but no other neurological deficit. The damage encompasses medial and ventral occipital cortex, and extends into the temporal lobe, with sparing of dorsolateral regions. The damage occurred age 41 years, 7 years prior to taking part in the study. This patient took part in experiments described in Chapters 5 – 7.

6. This patient sustained a small right posterior cerebral artery infarct, resulting in a left homonymous hemianopia. This damage is restricted to the grey matter in the medial portion of the right occipital lobe. This occurred age 61 years, 6 months prior to taking part in the study. This patient took part in experiments described in Chapters 3 – 8. For the rehabilitation study in Chapter 8, the patient (P2) was 7 months post-stroke at the start of training, and was assessed immediately pre and post-training.

7. This patient sustained a left posterior circulation stroke, resulting in a right homonymous hemianopia particularly affecting the upper quadrant. The damage

encompasses an area of white matter and cortex in the medial left temporal and occipital lobes. The damage occurred age 69 years, 19 months prior to taking part in the study. This patient took part in experiments described in Chapters 5 – 7.

8. This patient is believed to have sustained a large left posterior circulation infarct, resulting in a right hemianopia. The damage was restricted to the medial portion of the left occipital lobe. This is believed to have occurred age 18 years, and largely went unnoticed at the time. The patient took part in the study 13 years later, and took part in experiments described in Chapters 3, 5 – 7.

9. This patient sustained a left posterior circulation infarct, resulting in a right homonymous hemianopia. The damage was restricted to grey matter, in the medial portion of the left occipital lobe. This occurred age 45 years, 7 months prior to taking part in the study. This patient took part in experiments described in Chapters 4 – 7.

10. This patient sustained a right posterior cerebral artery haemorrhage, causing a left homonymous hemianopia. The damage encompasses quite an extensive area of white matter, as well as grey matter in the right occipital lobe and a small region of the right parietal lobe medially. The damage occurred at age 72 years, 6 months prior to taking part in the study. This patient took part in experiments described in Chapters 5 – 7.

11. This patient sustained a left posterior circulation infarct, resulting in a right homonymous hemianopia. The damage was restricted to the medial aspect of the

left occipital lobe. This occurred age 38 years, 7 months prior to taking part in the study. This patient took part in experiments described in Chapters 5 and 7.

12. This patient sustained a left posterior cerebral artery infarct, causing a right homonymous hemianopia. The damage was restricted to the posterior-medial left occipital lobe. This occurred at age 52 years, 8 years prior to taking part in the study. This patient took part in experiments described in Chapters 3, 5 – 7.

13. This patient sustained radiation induced necrosis of the medial portion of the right occipital lobe, following surgical resection and post-surgical radiotherapy for a Grade II occipital haemagipoericytoma. The damage occurred age 35 years, 3 years prior to taking part in the study. This patient took part in experiments described in Chapters 3 – 4, 7.

14. This patient sustained a left posterior cerebral artery infarct, causing a right homonymous hemianopia. The damage was isolated to the medial aspect of the left occipital lobe. This occurred age 36 years, 6 months prior to taking part in the study. This patient took part in experiments described in Chapters 3, 5 – 7.

15. This patient sustained a large right posterior cerebral artery infarct, causing a left homonymous hemianopia after emergency surgical repair of an aortic dissection. The stroke encompassed a large portion of the medial occipital lobe, extending to the medial parietal and temporal lobes, with probable extension to the subcortex around the lateral geniculate nucleus and pulvinar. This occurred age 53 years, 3 years prior to taking part in the study. This patient took part in experiments

described in Chapter 7. He underwent additional tests to rule out visual neglect in view of the right parietal lobe involvement (Appendix D).

16. This patient sustained a left posterior cerebral artery infarct, causing a right homonymous hemianopia. The damage included the medial and inferior portions of the left occipital lobe. This occurred age 41 years, 6 months prior to taking part in the study. This patient took part in experiments described in Chapters 3, 5 – 8. For the rehabilitation study in Chapter 8, the patient (P3) was 13 months post-stroke at the start of training, and was assessed immediately pre and post-training.

17. This patient sustained a left posterior cerebral artery infarct, causing a right homonymous hemianopia. The damage encompassed the medial aspect of the left occipital lobe, with slight extension to the nearby white matter. The damage occurred age 65 years, 8 months prior to taking part in the study. This patient took part in experiments described in Chapters 4 – 7.

18. This patient sustained a right posterior cerebral artery infarct, causing a left homonymous hemianopia. The damage was restricted to the calcarine cortex in the right occipital lobe. This occurred age 29 years, 18 months prior to taking part in the study. This patient took part in experiments described in Chapter 6.

Appendix C

Diffusion MRI tractography. Uncleaned results tables for the number of streamlines tracked between each region of interest.

C1. Ipsilateral streamlines between the LGN and hMT+ in (A) Blindsight positive patients; (B) Blindsight negative patients.

A

Patient no.	Uncleaned tracts		Cleaned tracts	
	LGN>MT ipsilesional	LGN>MT Intact hemi	LGN>MT ipsilesional	LGN>MT Intact hemi
PB1	568	726	75	115
PB2	72	1470	19	196
PB3	348	490	50	67
PB4	55	2918	19	315
PB5	871	538	93	83
PB6	59	571	12	64
PB7	2952	144	397	17
PB8	825	558	87	37
PB9	4309	442	635	53
PB10	310	128	32	29
PB11	1716	186	291	47
PB12	1443	98	194	17

B

Patient no.	Uncleaned tracts		Cleaned tracts	
	LGN>MT ipsilesional	LGN>MT Intact hemi	LGN>MT ipsilesional	LGN>MT Intact hemi
PN1	1831	80	157	19
PN2	85	1585	17	226
PN3	2928	590	351	89
PN4	0	741	no	101
PN5	25	1037	15	122

C2. Ipsilateral streamlines between the LGN and hMT+ in control participants.

A

Subject	Uncleaned tracts		Cleaned tracts	
	LGN>MT left	LGN>MT right	LGN>MT left	LGN>MT right
C1	2713	3174	308	339
C2	4406	2186	619	269
C3	559	369	57	59
C4	1640	1111	176	114
C5	778	189	84	30
C6	562	191	57	19
C7	736	474	78	46
C8	4742	1786	498	182
C9	5793	391	653	62

C3. Crossing interhemispheric streamlines between hMT+ bilaterally in control participants.

A

Subject	Uncleaned tracts		Cleaned tracts	
	LMT>RMT	RMT>LMT	LMT>RMT	RMT>LMT
C1	159	148	19	14
C2	7	7	no	no
C3	17	28	8	16
C4	15	14	8	6
C5	17	14	no	(8)
C6	5	4	no	no
C7	3	5	no	no
C8	30	34	19	14
C9	936	940	57	52

C4. Crossing interhemispheric streamlines between hMT+ bilaterally in (A) Blindsight positive patients; (B) Blindsight negative patients.

A

Patient no.	Uncleaned tracts		Cleaned tracts	
	LMT>RMT	RMT>LMT	LMT>RMT	RMT>LMT
PB1	12	10	(9)	no
PB2	11	9	(6)	no
PB3	352	360	24	24
PB4	7	6	no	no
PB5	13	41	7	19
PB6	26	33	13	15
PB7	0	2	no	no
PB8	27	29	12	16
PB9	9	5	no	no
PB10	0	0	no	no
PB11	37	34	9	18
PB12	32	41	17	13

B

Patient no.	Uncleaned tracts		Cleaned tracts	
	LMT>RMT	RMT>LMT	LMT>RMT	RMT>LMT
PN1	0	0	no	no
PN2	145	151	13	15
PN3	8	6	no	no
PN4	0	0	no	no
PN5	0	0	no	no

C5. Ipsilateral streamlines between the superior colliculus (SC) and hMT+ in (A) Blindsight positive patients; (B) Blindsight negative patients.

A

Patient no.	Uncleaned tracts		Cleaned tracts	
	SC>hMT+ ipsilesional	SC>hMT+ Intact hemi	SC>hMT+ ipsilesional	SC>hMT+ Intact hemi
PB1	40	35	12	12
PB2	5	78	no	18
PB3	35	37	17	17
PB4	1	80	no	15
PB5	100	61	14	14
PB6	5	149	no	17
PB7	34	12	16	8
PB8	62	28	20	17
PB9	160	10	16	no
PB10	3	1	no	no
PB11	18	9	12	no
PB12	46	4	15	no

B

Patient no.	Uncleaned tracts		Cleaned tracts	
	SC>MT ipsilesional	SC>MT Intact hemi	SC>MT ipsilesional	SC>MT Intact hemi
PN1	182	12	15	8
PN2	11	126	7	21
PN3	33	108	19	16
PN4	0	123	no	19
PN5	0	62	no	13

C6. Ipsilateral streamlines between the SC and hMT+ in control participants.

A

Subject	Uncleaned tracts		Cleaned tracts	
	SC>MT left	SC>MT right	SC>MT left	SC>MT right
C1	88	69	14	18
C2	357	182	39	17
C3	112	10	no	no
C4	133	40	18	16
C5	113	30	17	16
C6	47	46	15	16
C7	17	3	9	no
C8	438	36	35	14
C9	299	13	31	9

Appendix D

Line bisection test for visual neglect. This test was carried out by patient 15, who sustained additional involvement of the right parietal lobe.